A11101 888370

NAT'L INST OF STANDARDS & TECH R.I.C.

A11101888370

/Circular of the National Bureau of Stan
QC100 .U555 C521;1952 C.1 NBS-PUB-R 1934

Gravity Waves

U. S. Department of Commerce
National Bureau of Standards
Circular 521

UNITED STATES DEPARTMENT OF COMMERCE • Charles Sawyer, *Secretary*
NATIONAL BUREAU OF STANDARDS • A. V. Astin, *Director*

Gravity Waves

Proceedings of the NBS Semicentennial Symposium on Gravity Waves Held at the NBS on June 18–20, 1951

National Bureau of Standards Circular 521
Issued November 28, 1952

For sale by the Superintendent of Documents, U. S. Government Printing Office
Washington 25, D. C. - Price $1.75 (Buckram)

National Bureau of Standards
DEC 16 1952
7854.1
QC100
.U555
cop. 1

Foreword

The Symposium on Gravity Waves was the third of twelve symposia held as part of the scientific program of the National Bureau of Standards in the year 1951, which marked the fiftieth anniversary of its establishment. The subjects represented scientific fields of considerable current interest in which the National Bureau of Standards is active.

The papers presented at this symposium cover some of the results, both experimental and theoretical, in the study of gravity waves from many leading institutions both in the United States and abroad. The program was planned and conducted by the Bureau's Mechanics Division, in particular by K. Hilding Beij and Garbis H. Keulegan, who were co-chairmen of the committee on arrangements.

The cooperation of the Office of Naval Research in making possible this symposium is gratefully acknowledged.

A. V. Astin, *Director,*
National Bureau of Standards.

Contents

Page

Foreword III

1. Discrete and continuous spectra in the theory of gravity waves, by F. Ursell .. 1
2. Reflection of water waves from floating ice in water of finite depth, by Mortimer Leon Weitz (abstract only) 7
3. Laboratory study of breakers, by H. W. Iversen 9
4. Mechanics of sand movement by wave action, by Joseph M. Caldwell (abstract only) 33
5. Theory of floating breakwaters in shallow water, by J. J. Stoker (abstract only) 33
6. On the limiting clapotis, by Pierre Danel 35
7. Observations of internal tidal waves, by Jonas Ekman Fjeldstad 39
8. Motion of water due to breaking of a dam, and related problems, by Frederick V. Pohle 47
9. Symmetrical, finite amplitude gravity waves, by T. V. Davies 55
10. On the complex nature of ocean waves and the growth of the sea under the action of wind, by Gerhard Neumann 61
11. Results of exact wave measurements (by stereophotogrammetry) with special reference to more recent theoretical investigations, by A. Schumacher 69
12. Steady-state characteristics of subsurface flow, by Arthur T. Ippen and Donald R. F. Harleman 79
13. Wave intensity along a refracted ray, by W. H. Munk and R. S. Arthur 95
14. Diffraction of water waves by breakwaters, by John H. Carr and Marshall E. Stelzriede 109
15. Scattering of water waves treated by the variational method, by Joseph B. Keller (abstract only) 127
16. The diffraction of a swell. A practical approximate solution and its justification, by H. Lacombe 129
17. The criterion for the possibility of roll-wave formation, by A. Craya 141
18. Waves and seiche in idealized ports, by John S. McNown 153
19. The propagation of gravity waves from deep to shallow water, by Carl Eckart 165
20. On the propagation of waves from a model fetch at sea, by Willard J. Pierson, Jr. 175
21. On the theory of short-crested oscillatory waves, by Robert A. Fuchs 187
22. The present status of the resonance theory of atmospheric tides, by C. L. Pekeris 201
23. Analysis of sea waves, by G. E. R. Deacon 209
24. Some observations of breaking waves, by Martin A. Mason 215
25. Fourier analysis of wave trains, by Garrett Birkhoff and Jack Kotik 221
26. Water waves over sloping beaches, by A. S. Peters (abstract only) 235
27. Stability of uniform flow and roll-wave formation, by Robert F. Dressler 237
28. Study of wave propagation in water of gradually varying depth, by F. Biesel 243
29. Methods used at the National Hydraulic Laboratory of Chatou, France, for measuring and recording gravity waves in models, by J. Valembois 255
30. The slope of lake surfaces under variable wind stresses, by Bernhard Haurwitz (abstract only) 265
31. The tide in an enclosed basin, by W. B. Zerbe 267
32. The characteristics of internal solitary waves, by Garbis H. Keulegan (abstract only) 279
33. Growth of wind-generated waves and energy transfer, by J. Th. Thijsse 281

1. Discrete and Continuous Spectra in the Theory of Gravity Waves[1]

By F. Ursell[1]

It is shown how systems with discrete and continuous spectra differ in their physical behavior. It has generally been assumed that waves in an infinite canal have a continuous spectrum; examples are here given to show that the spectrum is mixed on a sloping beach and when there are internal boundaries. The corresponding oscillations are three-dimensional. The relation of the theory of spectra to the problem of uniqueness is discussed.

1. Introduction

This paper deals with properties of wave motion in an infinite canal of constant width; these may have important applications and should be more widely known. The discussion given here, applicable in the first place to an ideal inviscid fluid, will show how the general theory of eigenvibrations and their spectral frequencies links up with the determination of resonances and with the problem of uniqueness, particularly with the radiation condition of Sommerfeld [1],[2] which ensures uniqueness in many cases of forced periodic motion. But the Sommerfeld condition cannot be directly applied when the spectrum is mixed, as will be seen.

To illustrate the definition and physical significance of the spectrum we shall discuss examples of wave motion in a canal, first, of finite length and uniform depth; second, of infinite length and uniform depth; and third, of infinite length and nonuniform depth. Their spectra are, respectively, discrete, continuous, and mixed. Mixed spectra seem to be uncommon in physics, and attention is here called to their existence. It will be assumed throughout that the linear theory given by Lamb [2, chapter 9] is applicable. Let the x-axis be taken along the length of the canal, the y-axis vertically downward, and the z-axis across the canal. In the first two cases, it will also be assumed that the canal is of infinite depth. This assumption has no influence on the character of the spectrum.

2. Canal of Finite Length and Uniform Depth

In a canal of infinite depth, bounded by the vertical planes $x=0$, $x=a$; $z=0$, $z=b$; the normal modes are given by the velocity potentials [3, p. 75]

$$\phi_{m,n}\,(x,y,z)e^{i\sigma_{m,n}t}=C_{m,n}\cos\frac{m\pi x}{a}\cos\frac{n\pi z}{b}\exp\left[-\pi y\sqrt{\frac{m^2}{a^2}+\frac{n^2}{b^2}}\right]e^{i\sigma_{m,n}t},$$

[1] Trinity College, Cambridge, England.

[2] Figures in brackets indicate the literature references on p. 5.

where m,n are integers, $C_{m,n}$ is a complex constant,

$$\sigma_{m,n}^2 = g\pi\sqrt{\frac{m^2}{a^2}+\frac{n^2}{b^2}}, \tag{1}$$

and the real part of the expression on the right is to be taken. The frequencies given by (1) form a *discrete* enumerable set tending to infinity, and it is easily verified that

$$0 < \sigma_{m+1,n}^2 - \sigma_{m,n}^2 \leq g\pi/a, \tag{2}$$

independent of b. The frequencies $\sigma_{m,n}/2\pi$ derived from (1) are called the spectral frequencies of the system, or simply the *spectrum*. The spectrum is important in describing both free and forced motion.

The *free motion*, generated by an external agency that is no longer acting, is known to be of the form

$$\phi[x,y,z;t] = \sum_m \sum_n \phi_{m,n}[x,y,z] e^{i\sigma_{m,n}t}, \tag{3}$$

and so a frequency analysis leads to the spectral frequencies. To define a periodic *forced motion*, we suppose that there is a simple harmonic forcing agency, of frequency $\sigma/2\pi$ not belonging to the spectrum. The motion is known to consist of free modes, together with a simple harmonic motion of frequency $\sigma/2\pi$. The latter component is here called the periodic forced motion, its amplitude at any point depends only on the forcing agency, not on the initial conditions. For similar agencies differing only in the values of σ, a frequency-amplitude diagram can be drawn that has infinities [resonances] at the frequencies of the spectrum (1).

3. Canal of Infinite Length and Uniform Depth

Suppose the length of the canal becomes infinite, $a \to \infty$. The relation (2) suggests that the spectrum becomes *continuous* and this is easily verified. The normal modes are

$$\phi_n(x,y,z;k)e^{i\sigma_n(k)t} = C_n(k) \cos kx \cos \frac{n\pi z}{b} \exp\left[-y\sqrt{k^2+\frac{n^2\pi^2}{b^2}}\right] e^{i\sigma_n(k)t},$$

where

$$\sigma_n^2(k) = g\sqrt{k^2+(n\pi/b)^2},$$

and k is any positive number. For two-dimensional modes ($n=0$) all real values of σ are eigenvalues, for three-dimensional modes ($n>0$) all real $\sigma > \sqrt{(gn\pi/b)}$. When n is given, there is thus a lower limit (cut-off frequency) below which normal modes are impossible.

The free motion is now of the form

$$\phi(x,y,z;t) = \sum_n \cos \frac{n\pi z}{b} \int_0^\infty C_n(k) \cos kn \exp\left[-y\sqrt{k^2+\frac{n^2\pi^2}{b^2}}\right] e^{i\sigma_n(k)t} dk. \tag{3a}$$

When the variable in each integral is changed to σ, it becomes a Fourier integral in t for fixed values of x,y,z. Therefore, each integral $\to 0$ for fixed finite x,y,z as $t \to \infty$ [4, p. 11]. So the amplitude at all finite points tends to zero, and the whole energy is ultimately transferred to infinity by radia-

tion. As for the periodic forced motion, we can now define this either as in the first case or alternatively as the periodic motion which is approached asymptotically as $t \to \infty$. It can be determined uniquely from the motion of the boundaries together with the radiation condition discussed in detail by Sommerfeld [1]. Resonances no longer occur at all spectral frequencies but only at the cut-off frequencies, as can be seen from the Green's function [5, p. 350, eq 10]. Near a cut-off frequency $\sigma_1/2\pi$ the amplitude is $0(|\sigma-\sigma_1|^{-\frac{1}{2}})$, while near a discrete frequency $\sigma_2/2\pi$ in the first case it was $0(|\sigma-\sigma_2|^{-1})$. Resonances of this type also occur in the theory of electromagnetic wave-guides [6, p. 541].

4. Canal of Infinite Length and Non-Uniform Depth

The continuity of the spectrum in the second case depended ultimately on the relation (2), and for other boundaries there is no obvious reason why the corresponding spectrum should not tend to a *mixed*,—partly discrete and partly continuous—, spectrum as the longest dimension of the canal tends to infinity. It is the aim of this paper to emphasize that mixed spectra occur quite naturally in the theory of gravity waves, and to point out the consequences. To the discrete frequencies in a mixed spectrum there correspond modes of finite energy $\phi_{m,n} \exp(i\sigma_{m,n}t)$, with $\int |\text{grad } \phi_{m,n}|^2 d\tau < \infty$, and the free motion is the sum of a double series (3) and a series of integrals (3a). That part of the energy which has gone into (3a) is ultimately radiated to infinity, while the energy in (3) remains in the finite part of space, although our prejudices, derived from the second case suggest that the whole energy goes to infinity whenever there is a way left open for it. The discrete modes are also relevant to the discussion of *uniqueness*, for they satisfy the homogeneous boundary conditions and also the radiation condition (trivially since each mode is small at infinity). Thus uniqueness implies a continuous spectrum, and conversely; if there are discrete modes the radiation condition is insufficient to exclude them or determine the amplitude of the ultimate (inviscid) motion as distinct from the periodic forced motion. As for the latter, resonances occur at the discrete frequencies and at the cut-off frequences.

It is believed that all vessels of finite dimensions have a discrete spectrum, although published proofs seem to be somewhat defective. It would be very desirable to have a rigorous proof of the discreteness and completeness of the normal modes.

5. Examples of Mixed Spectra

All known examples relate to three-dimensional motion and can be written

$$\phi(x,y,z)e^{i\sigma t} = F(x,y)\cos kze^{i\sigma t}, \text{ with } \sigma^2 < gk,$$

where $2\pi/k$ is the wavelength across the canal, and $F(x,y)$ satisfies

$$F_{xx}(x,y) + F_{yy}(x,y) - k^2F(x,y) = 0$$

and the boundary conditions

$$\partial F/\partial n = 0 \text{ at fixed boundaries,} \tag{4}$$

and

$$\sigma^2 F + g\frac{\partial F}{\partial y} = 0 \qquad \text{on} \qquad y = 0, \tag{5}$$

given by Lamb [2, p. 364].

The best-known example is the edge-wave of Stokes [2, p.447], $F(x,y) = e^{-k(x\cos\alpha + y\sin\alpha)}$, satisfying (4) on the sloping beach, $x \sin\alpha = y\cos\alpha$, and (5) if $\sigma^2 = gk\sin\alpha$, and clearly of finite total energy. This was discovered in 1846, but Stokes and after him Lamb failed to realize the theoretical and practical applications. In fact, it is only one of the more general class

$$F(x,y) = e^{-k[x\cos\alpha + y\sin\alpha]} + \sum_{m=1}^{n} A_{m,n}[e^{-k[x\cos(2m-1)\alpha - y\sin(2m-1)\alpha}$$

$$+ e^{-k[x\cos(2m+1)\alpha + y\sin(2m+1)\alpha]}],$$

$$\text{where } \sigma^2 = gk\sin(2n+1)\alpha,\ \alpha < \pi/2(2n+1),$$

$$A_{m,n} = (-1)^m \prod_{r=1}^{m} \frac{\tan(n-r+1)\alpha}{\tan(n+r)\alpha}.$$

There is also a continuous spectrum $gk < \sigma^2 < \infty$. These modes were suggested to the author by C. Eckart's approximate theory [8, p. 93] based on the paper that Eckart communicated to this symposium. It has been suggested, by Eckart and others, that edge-waves excited by linear or nonlinear resonance may be observed as surf-beats on beaches; the foregoing theory may make a detailed discussion possible, although for small α the number of modes is large. Further discrete modes may emerge from the work that A. S. Peters described at this symposium, but which has not yet been studied in detail.

Discrete modes are not confined to sloping beaches. This significant point was established by the author [5]. (For an approximate theory see Eckart [8].) It was shown that discrete modes occur along the outside of the submerged circular cylinder,

$$x^2 + (y-f)^2 = a^2, a < f,$$

which is fixed right across a canal infinite in both directions along its length $(-\infty < x < \infty)$. The motion is symmetrical about the plane $x = 0$. Discrete modes occur when a convergent infinite determinant vanishes, and it is shown that this occurs when ka is small, and

$$\sigma^2 = gk\left[1 - \frac{9}{2}\pi^2(ka)^4 e^{-4kf} + \ldots\right].$$

The previous example suggests that further modes appear as ka increases.

No two-dimensional discrete modes are known. Their possible occurrence is limited by a uniqueness theorem due to F. John [7, p. 71], applicable to bodies intersecting the surface, and such that no vertical line intersects both the body and the free surface. A case not dealt with by John, the two-dimensional motion round a submerged circular cylinder, was studied by the author, who showed that there are no discrete modes [9]. But a fundamental question remains: Do two-dimensional discrete modes exist? More generally, are there any examples of discrete frequencies embedded in continuous spectra? The answer to this question will throw much light on the general theory of gravity waves.

6. References

[1] A. Sommerfeld: Die Greensche Funktion der Schwingungsgleichung. Jahresbericht d. deutschen Math.-Vereinigung. 21 (1912) 309–353.

[2] H. Lamb: Hydrodynamics. Sixth Edition. Cambridge 1932.

[3] C. A. Coulson: Waves. Fourth Edition. Oliver and Boyd, Edinburgh 1947.

[4] E. C. Titchmarsh: Fourier Integrals. Second Edition. Oxford 1948.

[5] F. Ursell: Trapping modes in the theory of surface waves. Proc. Cambridge Phil. Soc. 47 (1951), 347–358.

[6] J. A. Stratton: Electromagnetic Theory. First Edition. McGraw-Hill, New York 1941.

[7] F. John: On the motion of floating bodies, II. Simple harmonic motions. Comm. Pure and Appl. Maths. 3 (1950) 45–101.

[8] C. Eckart: Surface waves on water of variable depth. Scripps Inst. of Oceanography Lecture Notes, Fall Semester 1950–51. Ref. 51–12. Wave Report No. 100. August 1951.

[9] F. Ursell: Surface waves on deep water in the presence of a submerged circular cylinder. II. Proc. Cambridge Phil. Soc. 46 (1950), 153–158.

2. Reflection of Water Waves from Floating Ice in Water of Finite Depth[1]

By Mortimer Leon Weitz[2]

Abstract

The reflection of water waves that occurs when half the surface is covered by floating material (such as ice particles, for example) of uniform surface density, and the other half is free, was discussed. The waves may strike the straight line of separation between the two regions at any angle of incidence, and the water may have arbitrary finite but constant depth. The linear water-wave theory is employed.

The problem is first formulated as a boundary-value problem. By using Green's theorem and a suitably chosen Green's function, an integral equation is obtained for the velocity potential at the surface. This integral equation is practically of the Wiener-Hopf type and is solved by a slight modification of the procedure used by A. E. Heins.[3]

---

[1] Based on an article of the above title by Mortimer Weitz and Joseph B. Keller, Communications on Pure and Applied Mathematics, vol. III, No. 3, Sept. 1950, pp. 305–318.

[2] Institute for Mathematics and Mechanics, New York University, New York, N. Y.

[3] A. E. Heins, Water waves over a channel of finite depth with a dock, American Journal of Mathematics **70**, 1948, pp. 730–748.

3. Laboratory Study of Breakers

By H. W. Iversen [1]

The phenomena of breakers have been studied in the laboratory to determine the geometry and kinematics of breakers for various initial periodic wave conditions and for various beach slopes. The results so obtained, while limited in scope and restricted to uniform wave trains on impervious smooth bottoms of constant slope, show relationships of breaker heights, depths at breaking, breaker shapes, velocity fields, and other details of the breaker.

The size of the laboratory channel limited the investigation to beach slopes steeper than 1:50 and to waves which, for the most part, were not generated as deep-water waves. Data on the wave-height transformation as a function of depth, from the generating area to the breaker point, resulted in information that shows that the usual application of small amplitude theories to obtain the deep-water wave steepness from wave height and depth is not a reasonable approximation for waves of finite height. The effect is also apparent in the correlations of the geometric features of the breaker.

Breaker results of height, depth, crest elevation, surface shape, and velocity field were obtained for beach slopes of 1:10, 1:20, 1:30, and 1:50. A marked beach slope effect is shown by the results. For example, breaker heights for the same incident wave on the 1:10 beach slope averaged 30 percent higher than those on the 1:50 beach slope. Other results show features of the breaker which indicate the nature of the breaking action and of the effect of the bottom slope.

1. Introduction

In view of the limited knowledge of a complete description of breaker action, a laboratory study was made to obtain evidence of the geometry and kinematics of breakers for a range of incident wave characteristics, and for various beach slopes. During the course of the breaker study some questions were raised regarding the transformation of wave heights on shoaling bottoms prior to the breaker point. Laboratory information on this latter phenomena was obtained also.

An attempt has been made to describe breakers for the limited range of initial wave characteristics and the limited range of beach slopes that could be placed in the available laboratory wave channel. Due to the varied asymmetrical shapes of breakers such a description is limited. The summary results as herein presented point out enough of the salient features of breaker action to permit comparison of effects of the prime variables of initial wave characteristic and of beach slope.

2. Definitions of Terminology and Symbols

The description of breakers involves the use of terminology which may not be consistent in all wave and breaker studies. In order to avoid misinterpretation or confusion, the terminology and symbols as shown

[1] University of California, Berkeley, Calif.

on figure 1 are adopted for this discussion. Subscripts are used with the symbols to designate particular locations of the variables. Subscript 0 refers to deep water wherein the wave form is not affected by the proximity of the bottom. Subscript b refers to the breaker point.

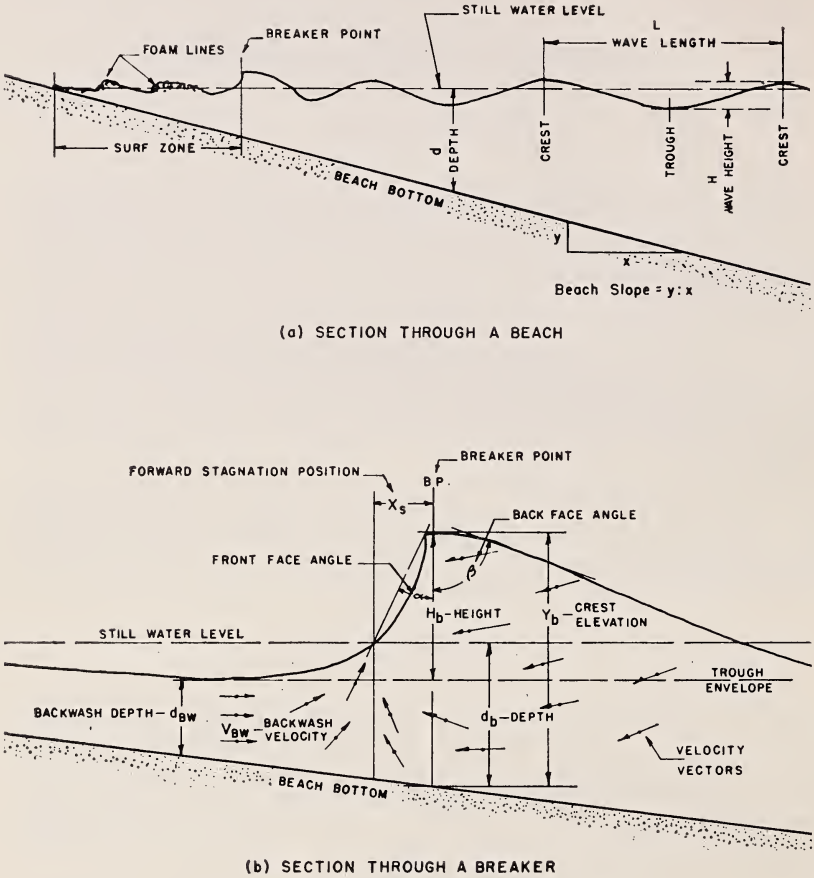

FIGURE 1. *Wave and breaker terminology.*

3. Experimental Procedure

Two sets of experiments were performed, one in which the breaker details were examined, the other in which wave-height transformation in shoaling water was obtained. Both were made in the same laboratory wave channel, figure 2, which consists of a 1-foot-wide by 3-feet-deep rectangular cross section of smooth side walls and smooth bottom with a working length of 54 feet. Smooth, impervious plane sloping bottoms of reinforced plywood or metal sheeting were placed in the channel to give desired beach slopes. In some arrangements a seaward toe was used with a steeper slope than the normal beach to give a longer constant depth portion of the channel. All beaches were sealed at the junction of the beach bottom and side walls.

Waves were generated as a continuous periodic train by a hinged plane flap oscillated with a constant period. The period and amplitude of the flap were adjustable to enable a range of initial wave conditions. For the breaker studies the flap was driven through top and bottom independently adjustable cranks to permit a closer approximation of a shallow water wave at the wave generator.

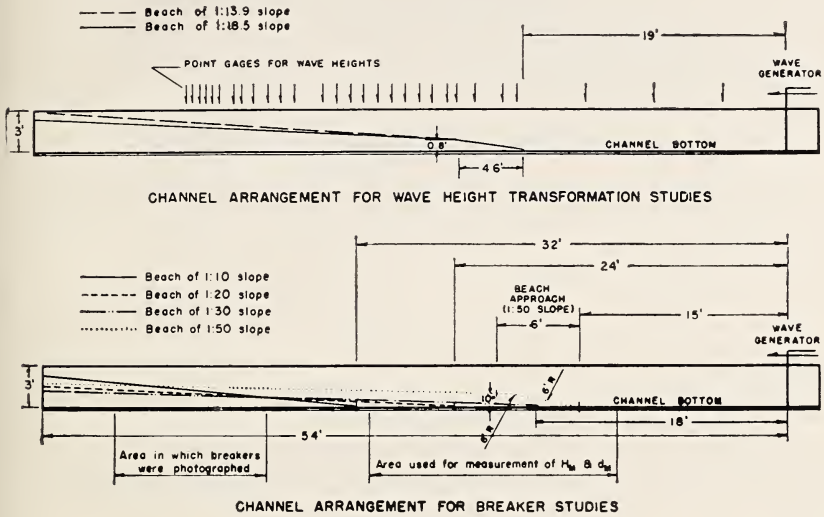

FIGURE 2. *Channel arrangements.*

Measurements were made as follows: (1) Wave-height transformation studies. Crest and trough positions at various stations as diagrammed in figure 2(a) were obtained with vertical point gages. Depth readings at each of the stations also were obtained. The wave period was obtained from the timed oscillations of the wave generator. (2) Breaker studies. Wave heights in the constant depth portion of the channel were obtained from point gage readings of crest and trough elevation. Movies of the breaker region were taken through the glass walls of the channel with the camera axis at the still water level. To obtain the kinematics of the water movement in the breaker, particles of a mixture of xylene and carbon-tetrachloride, with zinc oxide for coloring, with a specific gravity corresponding to that of the water, were introduced in the breaker region. The point to point movement of the particles was then recorded on the movies, from which each particle velocity was obtained by superposition of the projected movie frames to give distance moved and time interval of movement. Complete velocity fields were mapped for each wave for successive positions before and during breaking. The breaker surface profile transformation was also obtained by this procedure.

The limitation of the length of the laboratory wave channel restricted the investigation to beach slopes of 1:50 or steeper. In addition, in order to cover a range of characteristic waves with appreciable heights for reasonable measurements of vertical displacements, the majority of the waves were not generated as deep water waves due to the depth limitations of the channel. The defining incident waves, characterized by the

deep water wave steepness, the ratio of the deep water wave height to the deep water wave length, were evaluated from the wave heights measured in the constant depth portion of the channel with application of wave height transformation information to obtain deep water wave heights.

4. Results—Wave-Height Transformation on Shoaling Bottom

A brief review of oscillatory wave theory is necessary to establish certain arguments of this discussion.

4.1 Waves of Small Steepness

Wave theories are presented in Lamb [1][1] for waves of small steepness (wave height small as compared to the wave length). Pertinent relationships are

(a) *Wave velocity*:

$$C=\left[\frac{gL}{2\pi}\ \text{anh}\ \frac{2\pi d}{L}\right]^{1/2}. \tag{1}$$

From which,

$$C/C_0=\left[\frac{L}{L_0}\tanh\frac{2\pi d}{L}\right]^{1/2}. \tag{2}$$

The wave velocity is uniquely determined from the period and the wave length.

$$T=\frac{L_0}{C_0}=\frac{L}{C}. \tag{3}$$

Combining equations 2 and 3 results in

$$\frac{C}{C_0}=\frac{L}{L_0}=\tanh\left(\frac{2\pi d}{L}\right). \tag{4}$$

At values of L/L_0 corresponding to d/L from equation 6, the product

$$\frac{L}{L_0}\cdot\frac{d}{L}=\frac{d}{L_0} \tag{5}$$

is obtained. This is unique and results in d/L, C/C_0, and L/L_0 as functions of d/L_0.

(b) *Wave height.* Wave-height transformations result from a consideration of the energy contained in a wave and the redistribution of this energy as the wave travels into shoaling water. Energy dissipation due to internal or bottom friction is neglected.

$$\frac{H}{H_0}=\left[\frac{1}{2}\frac{1}{n}\frac{C_0}{C}\right]^{1/2}, \tag{6}$$

where

$$n=\frac{1}{2}\left[1+\frac{4\pi d/L}{\sinh\ (4\pi d/L)}\right]. \tag{7}$$

[1] Figures in brackets indicate the literature references on p. 29.

The factor, n, enters since one-half the wave energy travels with the wave in deep water, but in shallow water, with $d \ll L$, all the energy travels with the wave velocity. Since d/L is a function of d/L_0, it follows that n and H/H_0 are functions of d/L_0. Equations 4, 6, and 7 are shown in figure 3.

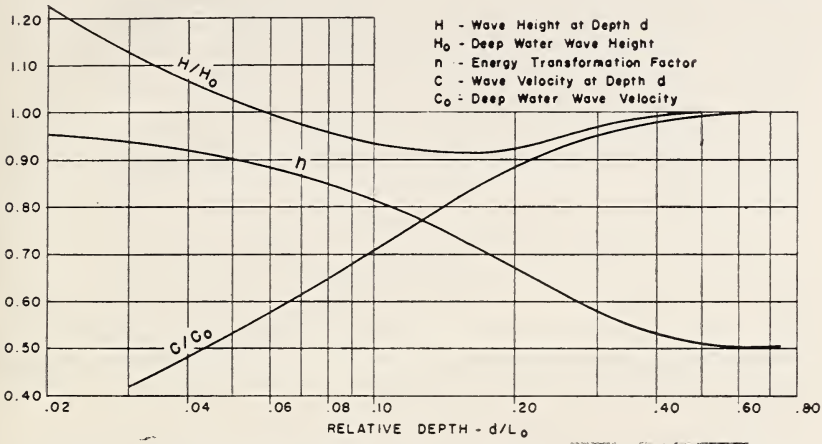

FIGURE 3. *Wave transformations as function of depth from small amplitude theory.*

4.2 Waves of Finite Amplitude

Stokes [2] developed a solution for wave velocity in deep water that included a wave-height parameter. Struik [3] expanded the analysis to include finite waves in any depth. To the third approximation in the analysis:

$$C=\left[\frac{gL}{2\pi}\tanh\frac{2\pi d}{L}\right]^{1/2}\left\{1+\left(\frac{\pi H}{L}\right)^2 B\right\}^{1/2}, \tag{8}$$

where

$$B=\left[\frac{2(\cosh 4\pi d/L)^2+2(\cosh 4\pi d/L)+5}{8(\sinh 2\pi d/L)^4}\right]. \tag{9}$$

For waves of small amplitude, $H \ll L$, equation 8 reduces to equation 1.

The question arises as to the effect of the inclusion of the finite wave height on the transformation relationship, equation 6, to predict wave heights as a function of depth from a given deep water wave in a periodic train of waves. The analytical theory of the energy transformation for this case has not been solved. The assumption is made that the energy transformation development is of the same nature as that of the small amplitude theory. That is, the velocity ratio and an energy conversion factor, n, will apply.

From equation 8

$$\frac{C}{C_0}=\left\{\frac{L}{L_0}\tanh\frac{2\pi d}{L}\right\}^{1/2}\left\{\frac{1+\left(\frac{\pi H}{L}\right)^2 B}{1+\left(\frac{\pi H_0}{L_0}\right)^2}\right\}^{1/2}. \tag{10}$$

The velocity ratio is a function of the wave steepness as well as the relative depth. The factor, B, becomes increasingly important as the depth ratio becomes smaller. For example, at $d/L=0.5$, $B=1.01$ and at $d/L=0.1$, $B=10.0$. In addition, the decrease in the wave length, if somewhat on the order of the small amplitude transformation, affects the ratio H/L more markedly than any change in height. Thus, the numerator of the right-hand term of equation 10 increases as the depth becomes smaller. The magnitude is not negligible for small values of d/L and finite values of H/L.

Since n, from the small amplitude theory, is a function of d/L, as was C/C_0, it is reasonable to assume that n, in finite waves, will be a function of d/L and H/L, with more dependence upon the wave height as the depth becomes smaller.

One factor that has not been included in either theory is the effect of the bottom slope upon the transformation. The assumption is made that the wave character at a specified depth on a sloping bottom is the same as that developed for the relationships at a corresponding constant depth. On steep beaches this assumption is open to question. On shallow beaches, where the depth gradient is small, it may be reasonable, although frictional effects will become increasingly important and should be included.

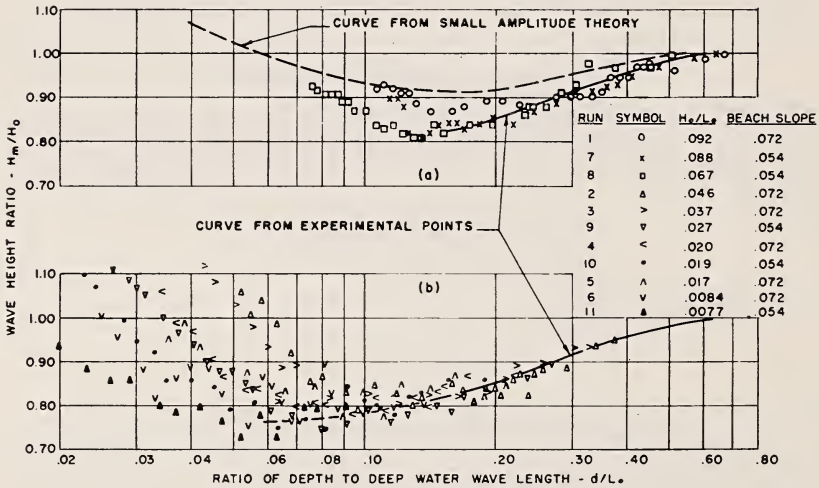

FIGURE 4. *Experimental wave-height transformations.*

H_m, Measured wave height at depth, d; H_0, deep-water wave height; L_0, deep-water wave length.

The experimental investigation [4] covered two beach slopes and a range of wave heights and period. Table 1 includes the defining variables for each investigated condition. Table 2 presents the measurements of one run as a sample of the data obtained from the wave-height transformation. The deep water wave length, L_0, was computed from the measured period from a combination of equations 1 and 3, which reduce to $L_0=5.12T^2$ for d large as compared to L (L_0, in feet; T, in seconds).

TABLE 1. *Summary of test conditions for transformation of waves on a sloping bottom*

[For runs 1, 7, and 8, $H_0 = H'_m$. For all other runs, H_0 computed from curve of figure 4]

Run	Beach slope	Period, T	Deep-Water wave length, L_0	Wave height in constant depth region of channel, $H'm$	Depth in constant depth region of channel, d	Deep-water wave height, H_0	Deep-water wave steepness, H_0/L_0
		Seconds	*Feet*	*Feet*	*Feet*	*Feet*	
1	0.072 (1:13.9)	0.865	3.83	0.351	2.55	0.351	0.092
2		1.15	6.73	.290	2.55	.308	.046
3		1.22	7.63	.262	2.55	.284	.037
4		1.50	11.53	.195	2.55	.226	.020
5		1.54	12.16	.182	2.55	.214	.017
6		1.97	19.89	.135	2.55	.169	.0084
7	0.054 (1:18 5)	0.86	3.80	.333	2.44	.333	.088
8		.965	4.77	.320	2.44	.320	.067
9		1.34	9.20	.219	2.44	.248	.027
10		1.50	11.53	.190	2.44	.223	.019
11		1.97	19.89	.123	2.44	.154	.0077

TABLE 2. *Sample summary of measured results of the transformation wave heights on a sloping bottom*

Run 1. Beach slope=0.072; wave period, T=0.865 second; deep-water wave length, L_0=3.83 feet; deep-water wave height, H_0=0.351 feet

Station	Measured values		Computed ratios	
	Depth d	Wave height H_m	Relative depth d/L_0	Relative height H_m/H_0
	Feet	*Feet*		
50	2.550	* 0.353	0.665	1.00
45	2.545	* .343	.662	0.98
40	2.545	* .360	.662	1.02
36	2.548	* .347	.665	0.99
34	2.31	.347	.602	.99
32	1.97	.337	.515	.96
30.78	1.727	.343	.451	.98
30	1.675	.339	.437	.97
29	1.616	1.338	.422	.97
28	1.551	0.335	.405	.96
27	1.485	.332	.388	.95
26	1.412	.332	.369	.95
25	1.349	.319	.352	.91
24	1.282	.315	.335	.90
23	1.215	.317	.317	.90
22	1.149	.317	.300	.90
21	1.078	.316	.281	.90
19	0.930	.308	.243	.88
18	.872	.308	.228	.88
17	.796	.311	.208	.89
16	.727	.312	.190	.89
15	.649	.308	.169	.88
14.5	.613	.306	.160	.87
13.5	.541	.304	.141	.87
13	.504	.314	.132	.89
12.8	.488	.319	.127	.91
12.5	.464	.321	.121	.91
12.3	.449	.322	.117	.92
12	.427	.325	.111	.92
11.8	.412	† .324	.108	.92

* Average H'_m=0.351, in constant depth portion of channel.
† Breaker point.

In this, and the following, the effect of the wave steepness on L_0, as shown by equations 3 and 8,

$$L_0=\frac{gT^2}{2\pi}\left[1+\left(\frac{\pi H_0}{L_0}\right)^2\right]=5.12T^2\left[1+\left(\frac{\pi H_0}{L_0}\right)^2\right] \tag{11}$$

is not included. The small values of H_0/L_0 of the majority of the experimental waves, plus the fact that the gradient of the experimental results with respect to L_0 is small, justifies the approximation.

When the transformation results of figure 3 were applied to each measured wave height at the corresponding depth, the deep-water wave heights did not result in the expected same value. An experimental wave-height transformation as a function of d/L_0 was then defined. The runs were selected in which the ratio d/L_0 in the constant-depth portion of the channel was greater than 0.5, for which equations 2 and 10 reduce to $C=C_0$ for all practical purposes. Hence, the average of the measured heights in the constant-depth portion of the channel was taken as the deep-water height. At other depths, the ratios of the measured height to deep-water height, H_m/H_0, were then plotted as a function of the corresponding relative depth d/L_0, figure 4a. Within the experimental error, the points define a single curve for the larger values of d/L_0. Regular deviation trends are noted at the lower values of d/L_0.

For the conditions with the ratio d/L_0 in the constant-depth portion of the channel less than 0.5, the curve established in figure 4a was used to obtain H'_m/H_0. H_0 was computed from the measured H'_m in the constant-depth portion of the channel. The extension of figure 4a by this artifice is shown in figure 4b.

As has been shown from the theories, the wave-height transformation, for waves of finite amplitude, is a function of both d/L and H/L. For small values of H/L, the finite amplitude velocity, and presumably the energy transformation factor, n, reduces to the small amplitude theory. Hence, H/L, or (H_0/L_0), is a parameter in the wave-height transformation and the single experimental curve of figure 4, based upon the laboratory experiments, is not a true representation of the situation. Thus, the method of extension of figure 4a into figure 4b is questionable. A series of wave-height transformation curves should result with H_0/L_0 as a parameter. For small values of H_0/L_0 and large values of d/L_0, the small amplitude theory gives a limiting relationship as shown.

Positive confirmation of the effects of the deep water steepness parameter, H_0/L_0, over a wide range of values can be accomplished with similar transformation experiments of the nature of those reported by which figure 4 was established. A deeper laboratory wave channel than that now available is needed in order to generate deep water waves over a larger range of H_0/L_0 for an extension of the results.

The deviation of results of each wave condition from the experimental curve at the smaller values of d/L_0 results from two conditions: (1) the finite wave-height theory predicts an increasingly appreciable effect of wave steepness at small values of d/L_0; and (2) when the wave approaches the breaking stage it is no longer the theoretical symmetrical wave, but is steeper on the front face than on the back face.

5. Breaker Studies

Data obtained from the breaker studies included the complete geometry of the wave transformation in the region of breaking, and also the complete velocity field from the water surface to the beach bottom at increments of the wave and breaker position in the region of breaking. The complex nature of the transformation of a wave into a breaker, with the dependence of the transformation upon initial wave steepness and beach slope, precludes any simple presentation of the experimental results. Certain features pertaining to the breaker point can be correlated. These include the variables as listed on figure 1b. Correlations are made as a function of deep water wave steepness and beach slope. Results of measured values are listed in tables 3, 4, 5, and 6 for the four beach slopes that were investigated, namely, 1:10, 1:20, 1:30, and 1:50. Correlations are shown on included figures, which will be discussed in turn.

The same limitation was present in the breaker experiments as was present in the wave-height transformation experiments, i.e., most of the waves that were generated were not deep-water waves in the constant depth portion of the channel. Deep water wave-heights were computed from measured wave-heights in the constant-depth portion of the channel, using the transformation results from small amplitude theory, figure 3, and using the laboratory results, figure 4.

Breaker-height correlations, based upon evaluation of H_0 from small-amplitude theory, and results based upon evaluation of H_0 from the experimental wave-height transformation established in figure 4, are shown in figures 5, 6, 7, and 8 for the four beach slopes investigated. The breakers are segregated into groups based upon the absolute breaker height. An apparent scale effect is noted. Application of the experimental transformation results lowers the breaker-height index, since larger deep-water wave-heights are predicted than those predicted from small-amplitude theory. While some rectification of the breaker results is evident, the scale effect still appears.

In view of the deductions made relative to the results of figure 4, neither the theoretical small-amplitude transformation results nor the laboratory experimental curve of figure 4 should be used in all cases to evaluate deep-water wave-heights from measured wave-heights in the constant-depth portion of the channel. The breaker results substantiate this conclusion.

For given deep-water waves of a fixed steepness, H_0/L_0, the wave train is defined. In the absence of frictional effects, the breaker geometry, in this case H_b/H_0, should be uniquely defined and not a function of the absolute height of the wave. If so, all the breaker results for one beach should produce a single relationship of $H_b/H_0=\phi(H_0/L_0)$. Since H_b and L_0 were measured directly (L_0 computed from the measured period), the only other variable to investigate is that of H_0.

An argument is proposed as follows: Consider one beach slope in the laboratory channel. Two waves are investigated with the following conditions:

$d_1'=d_2'$ (The constant depth portion of the channel. This corresponds to laboratory experimental condition.)

$L_{01}=L_{02}$

$H_{m1}>H_{m2}$ (This corresponds to the larger and smaller sets of waves based upon absolute height.)

TABLE 3. *Summary of Data—Beach Slope 1:10*

Run	Deep water wave steepness,* H_0/L_0	Period, T	Wave height,† H_m	Still water depth † (at H_m), d_m	Breaker height, H_b	Depth at breaking, d_b	Crest height at breaking, Y_b	Backwash depth at breaking, d_{BW}	Front face angle at breaking, α	Back face angle at breaking, β	Stagnation point location, X_s	Backrush velocity at breaking, V_{BW}	Crest velocity at breaking, V_c
		Seconds	*Feet*	*Feet*	*Feet*	*Feet*	*Feet*	*Feet*	*Degrees*	*Degrees*	*Feet*	*Feet/second*	*Feet/second*
4	0.0774	1.00	0.391	2.30	0.40	0.41	0.75	.....	.....	.....	.....	.....	.....
5	.0774	1.00	.391	2.30	.40	.41	.75	.....	46	.....	.....	.....	.....
22	.0206	1.51	.220	2.23	.37	.30	.56	0.18	40	74	0.46	0.148	4.65
15	.0165	1.73	.231	2.25	.36	.32	.60	.....	46	76	.....	.....	.....
25	.0797	1.00	.400	2.33	.35	.45	.72	.27	40	.....	.53	.....	3.55
18	.0581	0.92	.250	2.23	.26	.33	.52	.18	39	.....	.....	.....	3.10
2	.0076	1.98	.140	2.24	.31	.30	.51	.....	.....	.....	.....	.....	.....
23	.0071	1.98	.131	2.23	.29	.26	.46	.12	39	83	.33	.133	3.55
17	.0614	0.80	.200	2.23	.21	.21	.44	14	42	75	.....	.....	2.74
16	.0280	1.11	168	2.23	.22	.22	.39	.10	45	78	.....	.....	3.40
10	.0167	1.27	.129	2.17	.22	.18	.38	.....	.....	78	.....	.....	.....
7	.0150	1.26	.114	2.17	.19	.16	.32	.....	43	82	.....	.....	.....
8	.0125	1.45	123	2.17	.20	.18	.32	.....	.....	84	.....	.....	.....
27	.0112	1.26	.085	2.15	.16	.14	27	.08	42	82	.....	.150	.....
20	.0054	2.10	.113	2.22	.23	.28	.47	.....	.....	80	.....	.....	.....
24	0038	2.50	.111	2.23	.24	.24	.38	.12	.....	85	.26	.....	3.45

* L_0 from $5.12T^2$; H_0 from H_m and d_m/L_0, using small-amplitude theory.
† Constant-depth portion of channel.

TABLE 4. *Summary of Data—Beach Slope 1:20*

Run	Deep water wave steepness,* H_0/L_0	Period, T	Wave height,† H_m	Still water depth† (at H_m), d_m	Breaker height, H_b	Depth at breaking, d_b	Crest height at breaking, Y_b	Backwash depth at breaking, d_{BW}	Front face angle at breaking, α	Back face angle at breaking, β	Stagnation point location, X_s	Backrush velocity at breaking, V_{BW}	Crest velocity at breaking, V_c
		Seconds	*Feet*	*Feet*	*Feet*	*Feet*	*Feet*	*Feet*	*Degrees*	*Degrees*	*Feet*	*Feet/second*	*Feet/second*
31	0.0360	1.40	0.330	1.80	0.42	0.53	0.86	0.33	.....	.....	.....	.....	.....
34	.0280	1.50	.298	1.60	.40	.46	.76	.....	.....	.....	.....	.....	.....
30	.0210	1.59	.256	1.60	.40	.48	.77	.30	.....	.....	.....	.....	.....
29	.0130	1.89	.225	1.57	.38	.44	.72	.28	.....	.....	.....	.....	.....
28	.0076	2.24	.193	1.57	.36	.39	.65	.22	.....	.....	.....	.....	.....
46	.0730	1.04	.383	1.75	.35	.54	.79	.35	54	71	.....	0.79	4.35
45	.0480	1.15	.305	1.60	.31	.39	.61	.23	.....	.....	.....	.....	.....
42	.0350	1.26	.260	1.57	.33	.34	.59	.24	50	72	0.51	.75	3.13
44	.0290	1.33	.238	1.60	.30	.34	.56	.24	50	76	.48	.65	2.60
43	.0220	1.41	.202	1.56	.27	.33	.53	.22	50	77	.47	.58	3.20
47	.0130	1.67	.178	1.51	.27	.29	.49	.18	52	78	.38	.74	3.00
48	.0079	1.93	.144	1.49	.25	.25	.45	.16	50	77	.41	.60	2.90
36	.0767	0.74	.214	1.55	.19	.29	.42	.20	.....	.....	.33	.60	3.40
37	.0480	0.93	.206	1.50	.21	.27	.44	.19	55	75	.33	.64	3.17
40	.0360	.03	.185	1.50	.18	.25	.38	.18	52	75	.32	.60	3.20
39	.0270	1.12	.165	1.50	.19	.23	.38	.16	.....	70	.28	.64	2.50
38	.0220	1.17	.145	1.50	.20	.21	.36	.12	.....	.....	.....	.....	.....
35	.0130	1.34	.110	1.50	.14	.16	.27	.....	.....	.....	.....	.....	.....
41	.0083	1.55	.094	1.47	.15	.18	.29	.12	51	78	.25	.64	3.03

* L_0 from $L_0 = 5.12T^2$; H_0 from H_m and d_m/L_0, using small-amplitude theory.
† Constant-depth portion of channel.

TABLE 5. *Summary of Data—Beach Slope 1:30*

Run	Deep water wave steepness,* H_0/L_0	Period, T	Wave height,† H_m	Still water depth† (at H_m), d_m	Breaker height, H_b	Depth at breaking, d_b
		Seconds	*Feet*	*Feet*	*Feet*	*Feet*
8	0.0665	1.05	0.356	1.65	0.350	0.480
7	.0080	2.37	.230	1.64	.415	.510
9	.0353	1.24	.255	1.58	.275	.365
4	.0214	1.46	.214	1.55	.285	.350
3	.0099	1.87	.169	1.50	.262	.373
5	.0084	2.03	.173	1.49	.253	.335
6	.0043	2.67	.164	1.52	.290	.370
10	.0138	1.49	.144	1.44	.225	.270
11	.0093	1.60	.112	1.40	.175	.260
12	.0074	1.79	.115	1.40	.180	.260
14	.0052	2.10	.115	1.44	.215	.275
2	.0042	2.29	.116	1.43	.230	.280
16	.0035	2.52	.117	1.43	.200	.265
15	.0027	2.52	.093	1.42	.190	.230
1	.0025	2.65	.097	1.41	.180	.244

* L_0 from $5.12T^2$; H_0 from H_m and d_m/L_0, using small-amplitude theory.
† Constant-depth portion of channel.

$$\frac{d_1}{L_{01}}=\frac{d_2}{L_{02}}<0.5 \quad \text{(The waves were not measured as deep water waves.)}$$

then

$$\frac{H_{m1}}{L_{01}}>\frac{H_{m2}}{L_{02}}$$

Hence the second wave more nearly approximates a small-amplitude wave. The breaker-height index, H_b/H_0, would then be based upon a computed H_0, from H_m and d/L_0, from a transformation relationship that more nearly approximates the small-amplitude transformation. Likewise, the first wave more nearly approximates a finite wave and the experimental transformation results.

As can be noted in figures 5, 6, 7, and 8 the net result would be to lower the breaker index values of the larger waves (or breakers) to a greater extent than the smaller waves (or breakers). Thus, all data would be brought into a greater conformity than is shown on either of the two presentations on each of figures 5, 6, 7, and 8 and would be approximated by the curves that are shown on figures 5, 6, 7, and 8.

Figure 9 presents all the results of figures 5, 6, 7, and 8 to show the beach slope effect upon the breaker-height index. Curves have not been drawn in figure 9 in order to preserve the relative comparison of the points without the influence of the curves. Whichever evaluation of deep-water wave-height is made, a definite beach-slope effect is noted with higher breakers on the steeper beaches for the same initial wave train.

The other discernible relations of wave geometry, if specified on a dimensionless basis, can be correlated in a number of different ways. All geometrical relationships, such as the depth at breaking, can be referred to the deep-water wave-heights, e.g., d_B/H_0. Since the deep-water wave-heights have not been determined with a desired reliability, all variables are related to the breaker height that was measured directly. Results are presented for the beach slopes of 1:10, 1:20, and 1:50. Data with the 1:30 beach slope were obtained for breaker heights only. All variables

TABLE 6. *Summary of Data—Beach Slope 1:50*

Run	Deep water wave steepness,* H_0/L_0	Period, T	Wave height† H_m	Still water depth† (at H_m), d_m	Breaker height, H_b	Depth at breaking, d_b	Crest height at breaking, Y_b	Backwash depth at breaking, d_{BW}	Front face angle at breaking, α	Back face angle at breaking, β	Stagnation point location, X_s	Backwash velocity at breaking, V_{BW}	Crest velocity at breaking, V_c
		Seconds	*Feet*	*Feet*	*Feet*	*Feet*	*Feet*	*Feet*	*Degrees*	*Degrees*	*Feet*	*Feet/second*	*Feet/second*
78	0.0074	2.43	0.232	1.54	0.353	.....	.....	.....	57	.....	.....	.....	.....
81	.0065	2.65	.243	1.54	.398	0.513	0.840	0.436	60	75	0.68	0.11	2.30
58	.0718	1.00	.348	1.54	.303	.403	.633	.322	59	72	.....	.....	3.00
70	.0465	1.13	.282	1.54	.297	.350	.585	.292	58	68	.57	.16	2.80
63	.0376	1.17	.243	1.54	.274	.321	.554	.274	62	72	.49	.11	3.50
68	.0190	1.62	.228	1.54	.268	.306	.522	.251	63	73	.....	.....	3.50
66	.0130	1.74	.190	1.54	.283	.334	.565	.262	57	72	.46	.19	2.85
82	.0049	2.65	.186	1.54	.320	.422	.691	.360	59	74	.57	.07	.....
62	.0907	0.81	.301	1.54	.250	.....	.555	.292	.....	.....	.....	.....	.....
61	.0706	.90	.279	1.54	.222	.326	.497	.261	60	72	.39	.18	3.90
74	.0504	.95	.222	1.54	.191	.228	.394	.183	57	70	.....	.....	2.75
59	.0474	1.00	.230	1.54	.218	.....	.455	.236	63	.....	.....	.....	.....
60	.0376	1.00	.182	1.54	.185	.....	.....	.....	63	75	.....	.....	.....
73	.0305	1.30	.241	1.54	.248	.328	.538	.262	.....	.....	.....	.....	3.50
77	.0223	1.35	.190	1.54	.199	.231	.406	.191	61	72	.....	.....	3.00
71	.0092	2.00	.180	1.54	.208	.222	.406	.175	59	79	.....	.....	3.75
83	.0074	1.90	.129	1.54	.181	.212	.362	.173	.....	.....	.....	.....	.....
80	.0065	2.25	.168	1.54	.217	.....	.517	.276	60	75	.....	.....	3.50

* L_0 from $L_0 = 5.12T^2$; H_0 from H_m and d_m/L_0, using small amplitude theory.
† Constant-depth portion of channel.

were related to the deep-water steepness with evaluation of the deep-water wave-height and length from the small amplitude theory. A curve has been drawn through compatible results in each representation wherein agreement of the results indicates a definite trend.

Results are presented in a series of figures (see fig. 1 for definition of terminology). Figure 10. Depth; crest elevation; Figure 11, Backwash depth; forward stagnation point; Figure 12. Front face angle; Back face angle; Figure 13. Backwash velocity; crest velocity.

Some comments should be made relative to the evaluation of the results that appear in the above figures. The breaker point is, to a certain degree,

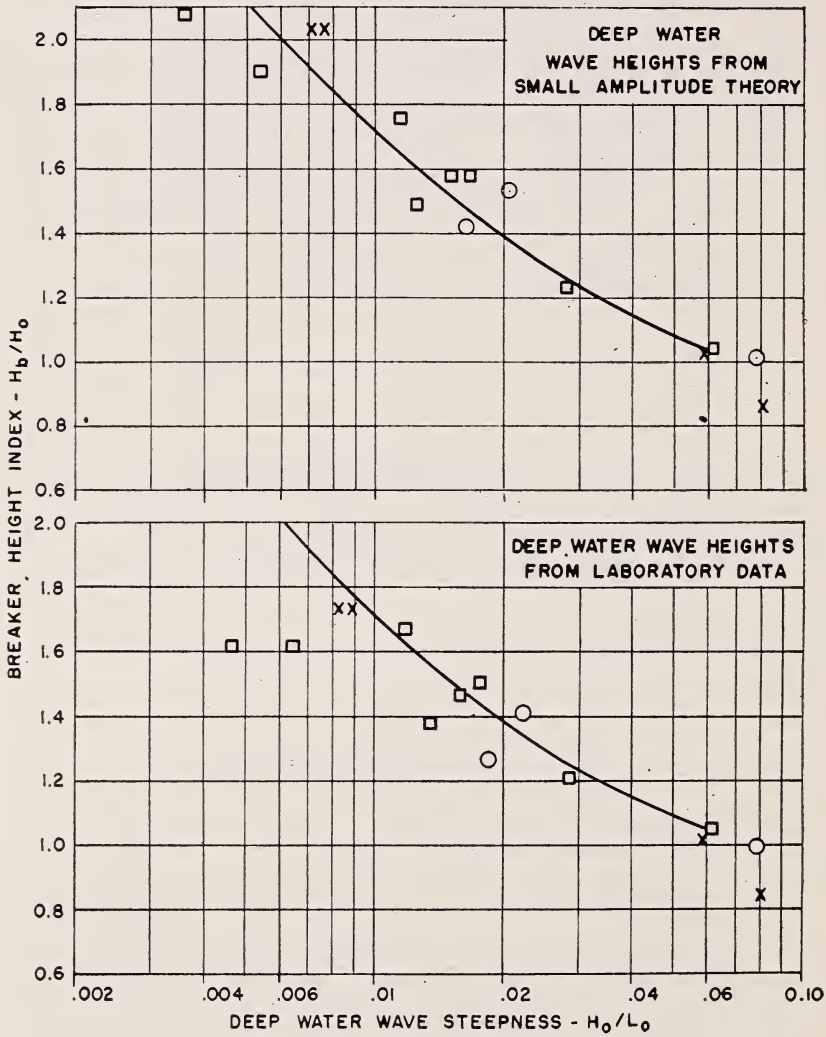

FIGURE 5. *Breaker heights from laboratory data.*

Beach slope, 1:10. ○, $0.40 > H_b > 0.36$; ×, $0.35 > H_b > 0.25$; □, $0.24 > H_b > 0.16$.

a matter of judgment, which depends upon the type of breaker that is formed. For "spilling" breakers, in which the crest became unstable in a mild fashion with the appearance of "white water" at the crest, which expanded down the front face of the breaker, the picture preceding that in which the first white water appeared was taken as the breaker point. For "plunging" breakers, in which the crest overshot the body of the wave to project ahead of the wave face, the picture in which the front face at the crest was vertical was taken as the breaker point. For "surging" breakers, in which the front face of the wave became unstable over the major portion of the face in a large-scale turbulent fashion, the picture preceding this action was taken as the breaker point. The movies, from

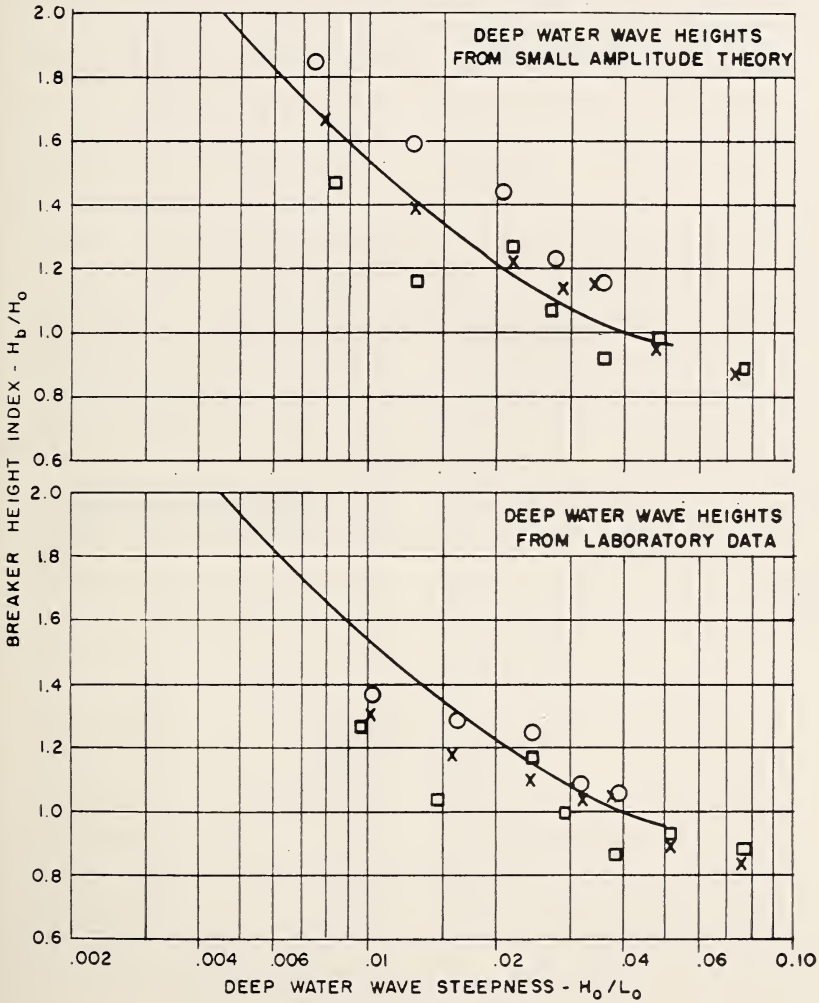

FIGURE 6. *Breaker heights from laboratory data.*

Beach slope, 1:20. ○, $0.42 > H_b > 0.36$; ×, $0.35 > H_b > 0.25$; □, $0.21 > H_b > 0.14$.

which the results were obtained, were taken at approximately 60 frames per second. The time interval of one-sixtieth of a second permitted a reasonable approximation of the breaker point.

The depth, crest elevation, backwash depth, and front and back face angles were easily determined from the selected pictures. The forward stagnation point, which was determined from the particle movements, was noted to occur at approximately the intersection of the still water line and the front face of the wave. Backwash velocities were obtained by averaging all particle velocities in the region of minimum depth in the

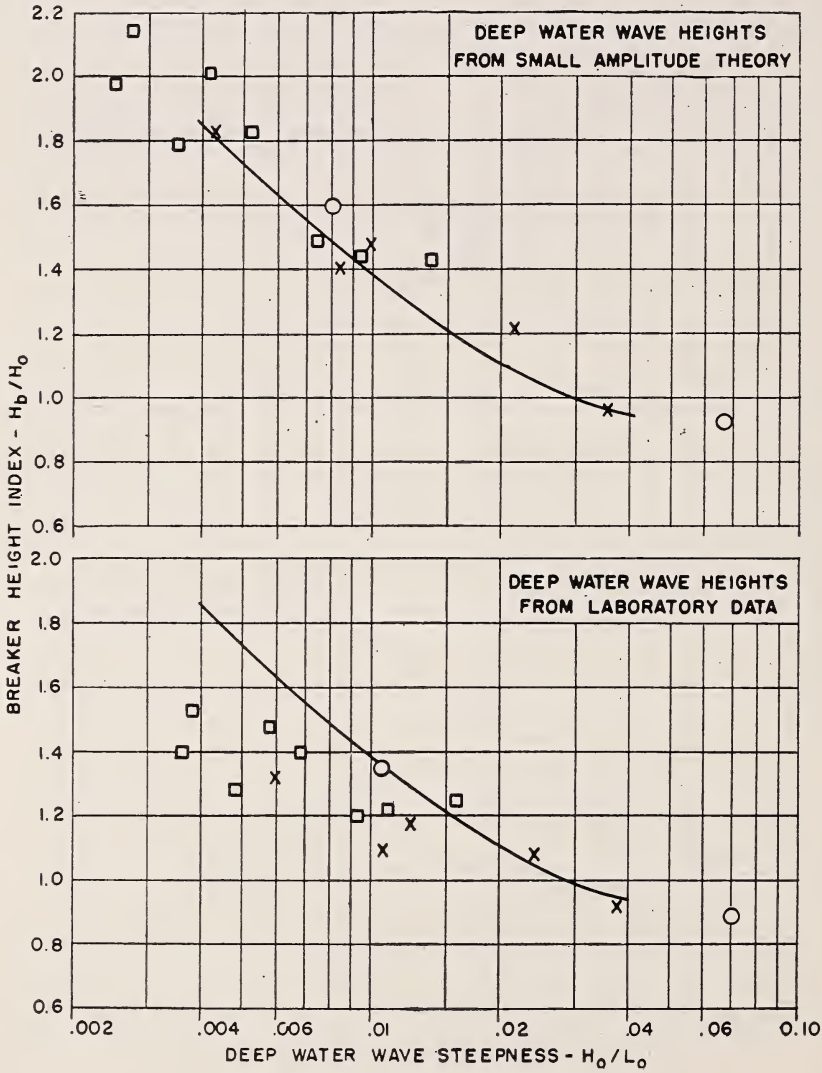

FIGURE 7. *Breaker heights from laboratory data.*

Beach slope, 1:30. ○, $0.41 > H_b > 0.35$; ×, $0.29 > H_b > 0.25$; □, $0.23 > H_b > 0.17$.

backwash. Crest velocities were obtained from the gradient of the crest position-time history. Small surface irregularities influenced the selection of the crest position in any one picture.

Relative comparison of beach slope effect in terms of a given wave train is difficult from figures 10 and 11. If the curves shown in figures 5, 6, 7, and 8, for the breaker height as a function of initial steepness and slope, are accepted, then cross-computations may be made to obtain ratios with the deep-water height as the denominator. Results so obtained are shown in figure 14 for the 1:10 and 1:50 slopes.

For a given wave train defined by the deep-water wave height and length, on a steep beach as compared to a flat beach, the breaker is higher,

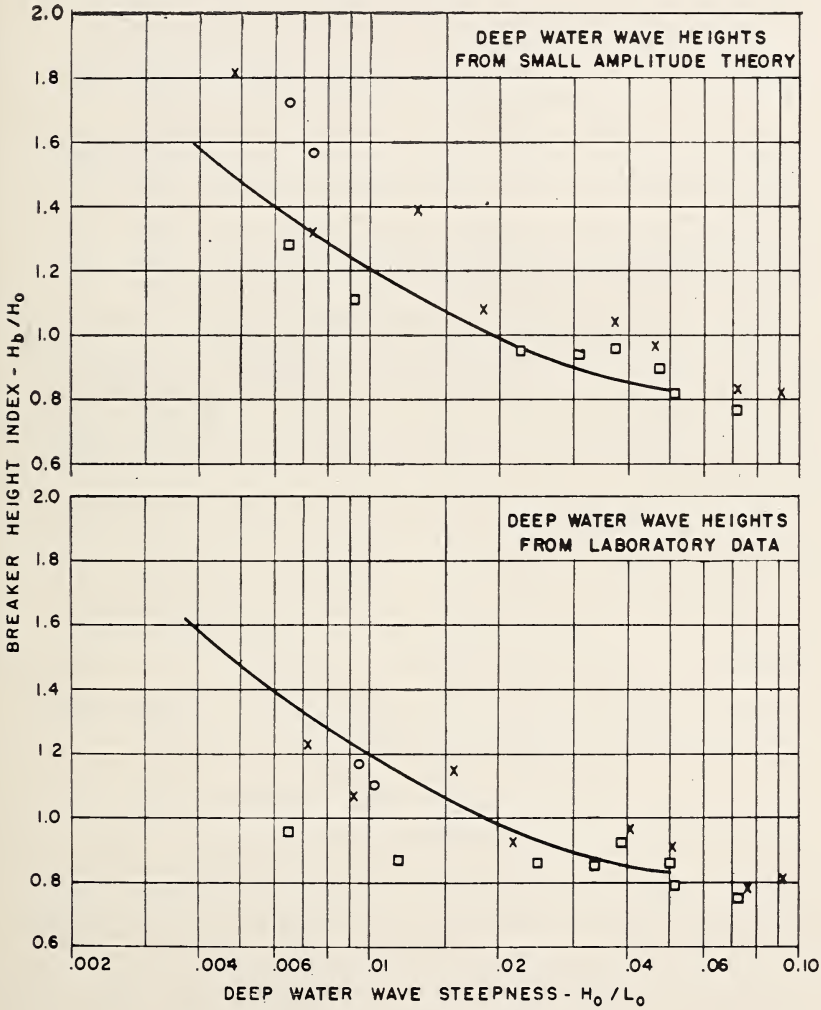

FIGURE 8. *Breaker heights from laboratory data.*

Beach slope, 1:50. ○, $0.39 > H_b > 0.36$; ×, $0.33 > H_b > 0.25$; □, $0.24 > H_b > 0.17$.

breaks in deeper water with a higher crest elevation, has a flatter back face and a steeper front face, and has a smaller depth in the backwash with a higher backwash velocity.

The backwash, which is a function of events preceding a particular breaker, is a factor in the breaking action. High backwash velocities retard the base of the wave with a consequent tendency to promote a "plunging" breaker. At large values of deep-water steepness, the breakers on all beaches were "spilling." At smaller values of deep-water steepness the waves tend to plunge with greater tendencies on the steeper slopes. At the extreme lower values of the deep-water wave steepness, particularly on the 1:10 slope, the breaker tended to "surge."

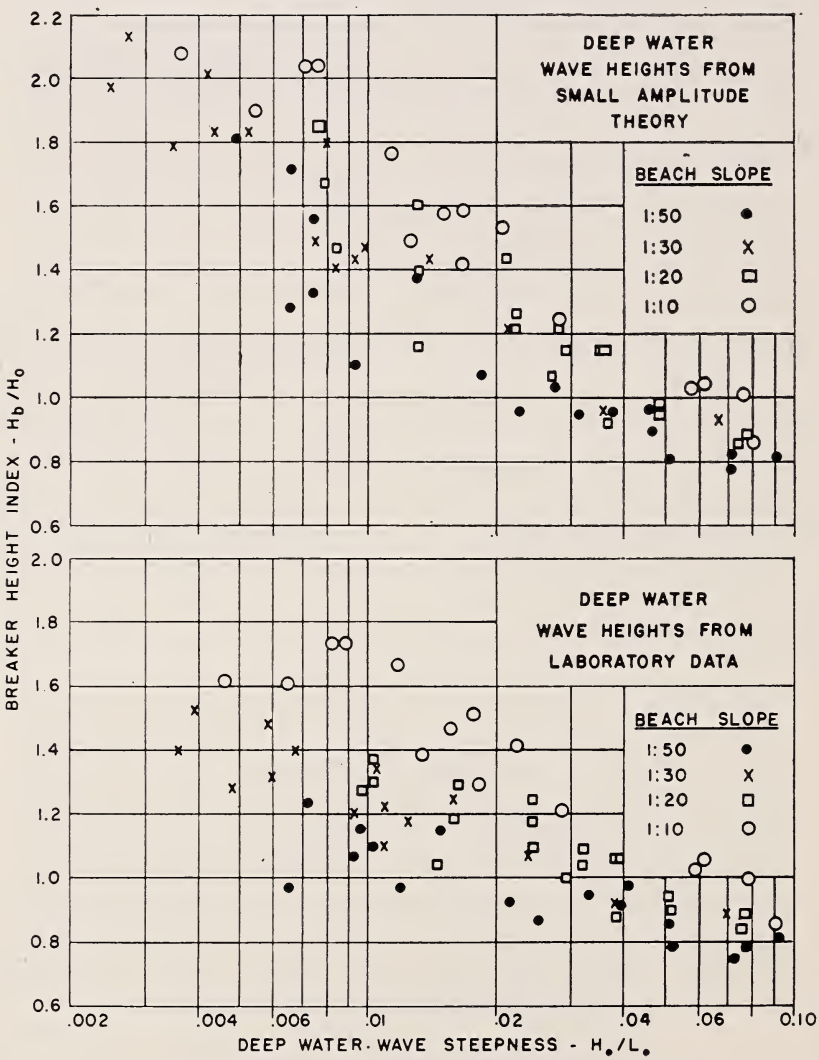

FIGURE 9. *Effect of beach slope on breaker heights.*

Other features of the breaker, particularly the kinematic field, may be noted in figures 15a and 15b. All the breakers studied showed essentially the same general kinematic field, except for the differences as noted in the fore part of the breaker in terms of the backrush and forward stagnation point.

The laboratory waves were of uniform period and geometry. Natural waves seldom correspond to this condition. What effect the previous and following wave histories have upon a single wave under consideration, if the wave train is irregular, is not known. The effect of bottom friction and percolation should be included for waves on natural beaches.

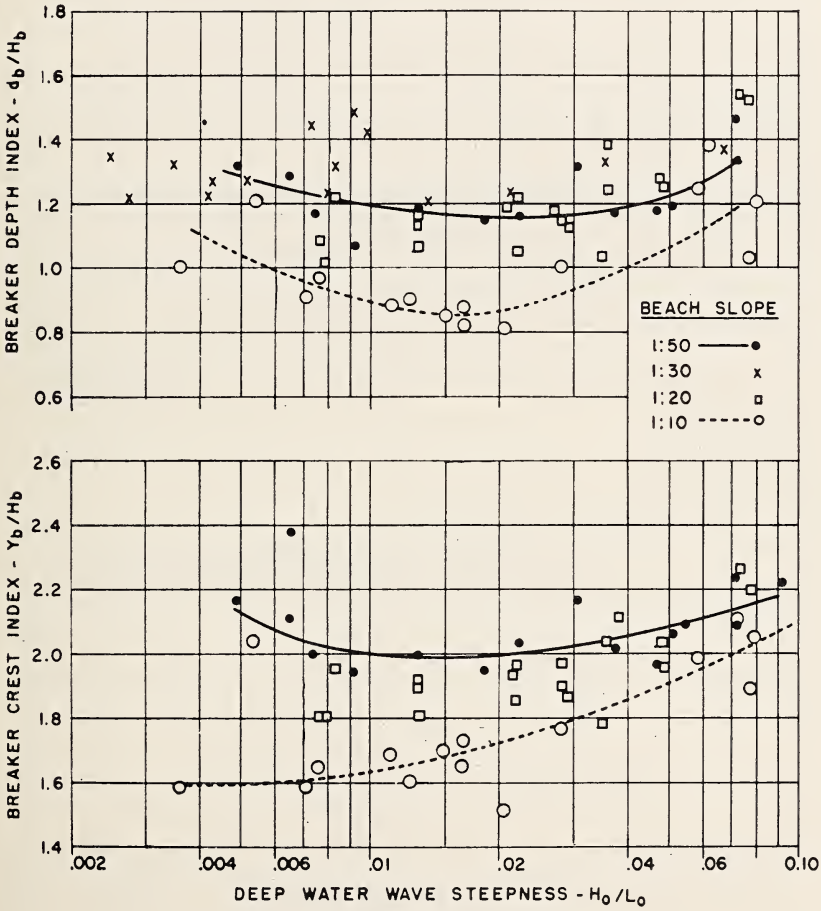

FIGURE 10. *Breaker crest and depth indexes.*

6. Summary

1. Laboratory results are presented for the transformation of wave heights as a function of depth in a wave system in a steady state of oscillation. The small amplitude theory is shown to be inadequate for laboratory wave channel work to enable evaluation of the true deep-water wave from a shallow-water wave-height measurement.

2. Breaker geometrical relationships are established for plane impervious beaches with slopes from 1:10 to 1:50. In this range, the beach slope has a marked effect upon the breaker in that, for a given wave train, the breaker is approximately 40 percent higher on a 1:10 slope as compared to a 1:50 slope. The breaker is also steeper in front and flatter in back, with a greater tendency to plunge.

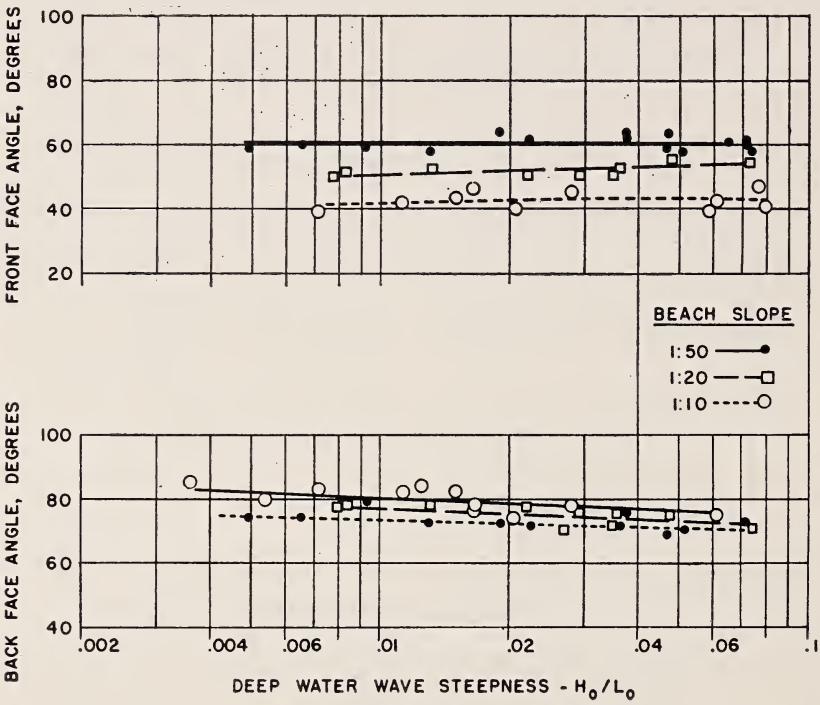

FIGURE 11. *Breaker face angles.*

7. Acknowledgments

This investigation was made by the Department of Engineering, University of California, Berkeley, under contracts with the Bureau of Ships, U. S. Navy, and the Office of Naval Research.

8. References

[1] H. Lamb: Hydrodynamics. Cambridge University Press. 6th Edition. 1932. Chapter IX.

[2] G. G. Stokes: On the theory of oscillatory waves. Trans. Cambridge Phil. Soc. vol. 8. 1847, and Supplement. Scientific Papers. Vol. 1.

[3] D. J. Struik: Determination rigoureuse des ondes irrotationelles periodiques dans un canal à profondeur finie. Mathematische Annalen. Vol. XCV. 1926. pp. 595–634 (Corrected by F. Wolf. University of California, Berkeley. Private Communication. 1944).

[4] J. A. Putnam and A. J. Chinn: Report on model studies on the transition of waves in shallow water. University of California. HE116–106. BuShips Contract NObs 16290. May 1945.

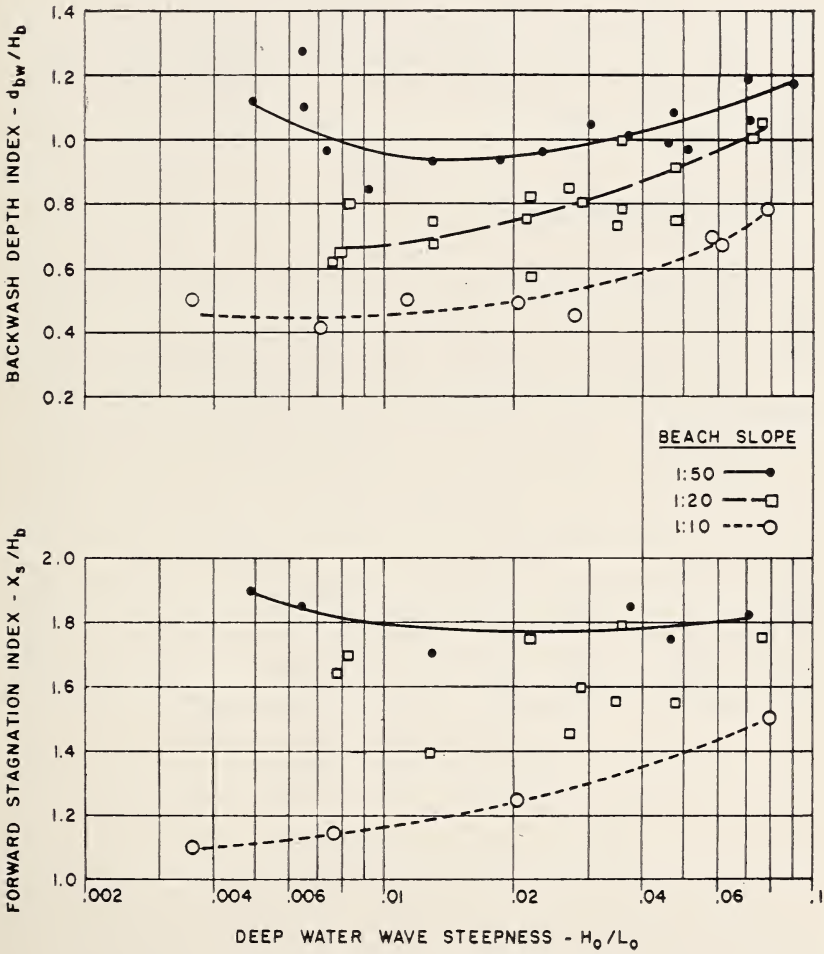

FIGURE 12. *Breaker backwash depth and forward stagnation indexes.*

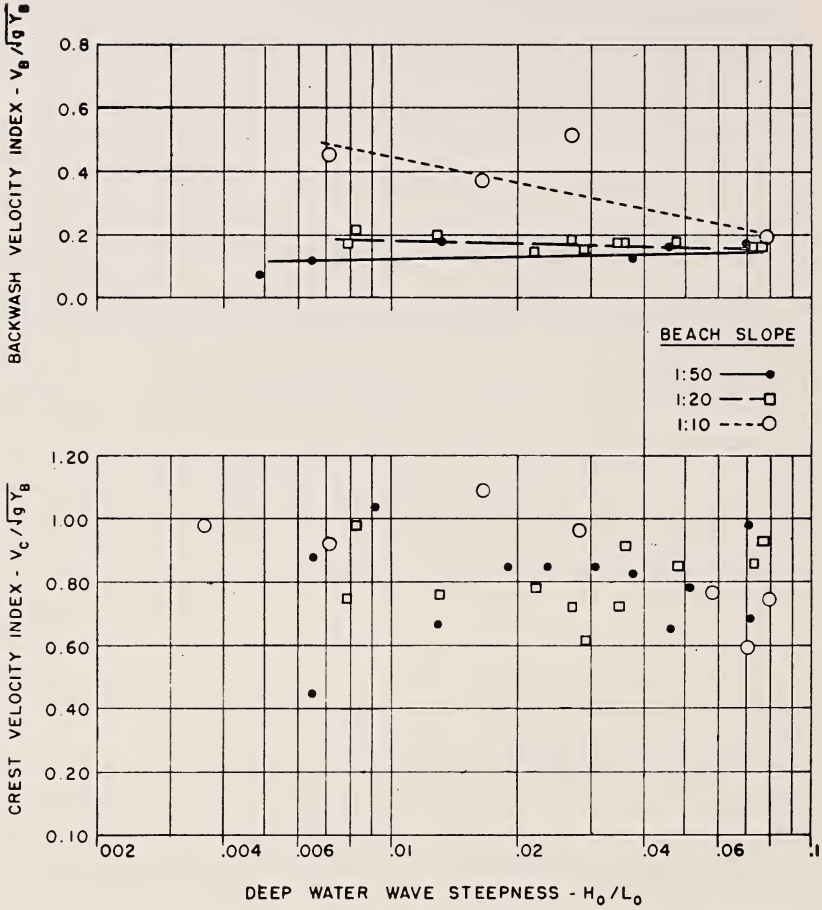

FIGURE 13. *Breaker velocities.*

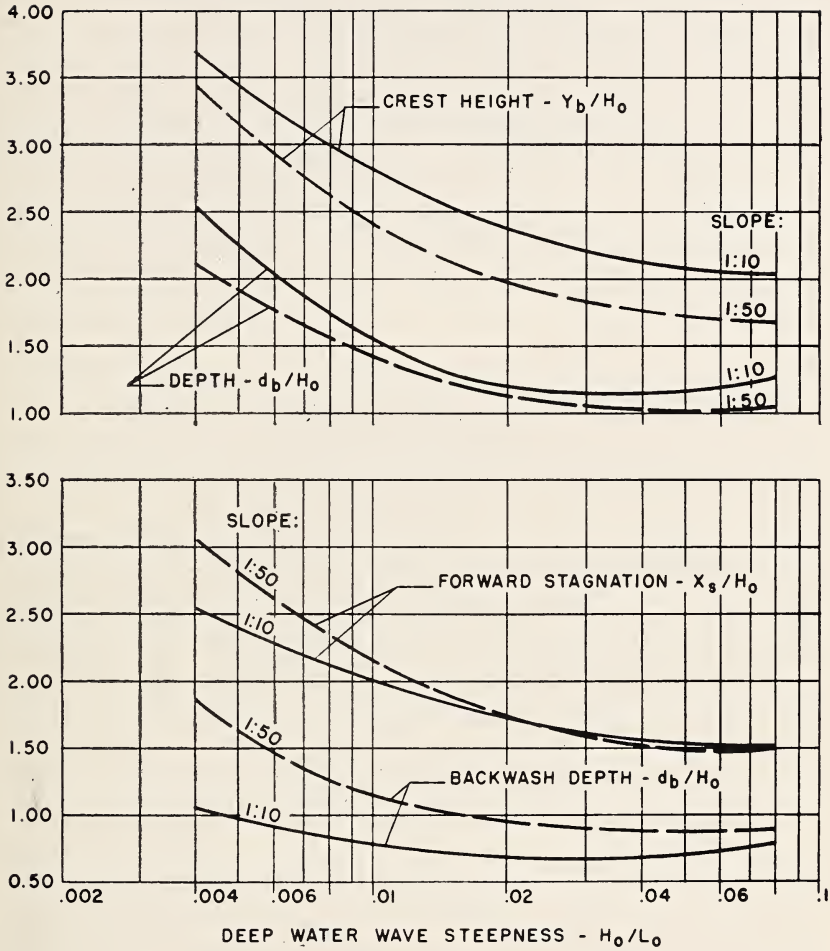

FIGURE 14. *Breaker geometries based on deep-water height.*

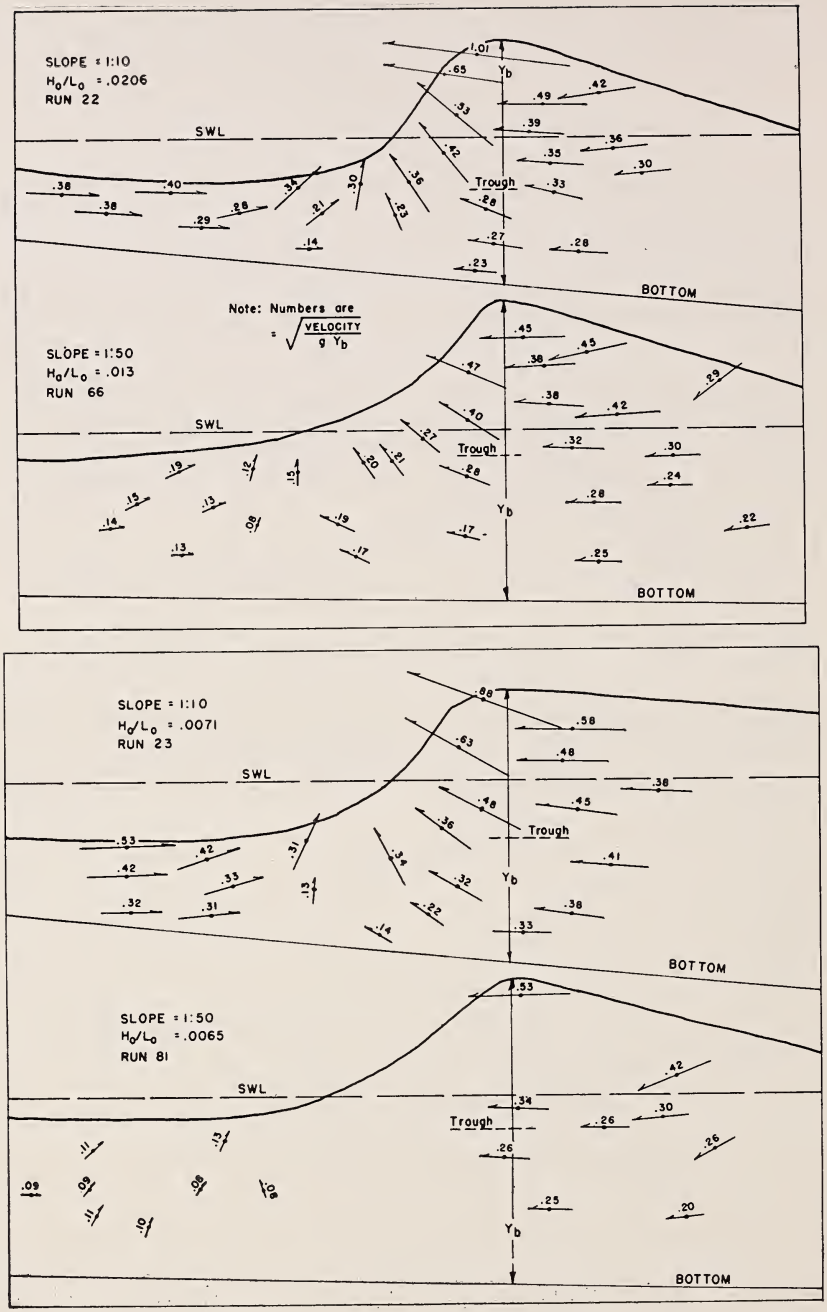

FIGURE 15. *Kinematics at breaker point.*

Equal breaker heights.

4. Mechanics of Sand Movement by Wave Action

By Joseph M. Caldwell [1]

Abstract

The results of a high-speed moving-picture study of the movement of beach sand by wave action in a laboratory flume were presented. The growth and progression of sand ripples was described, and the manner in which these ripples affect the movement of the sand was discussed. Results were presented showing that ripple forms move shoreward even while net sand movement is seaward from the beach. Hypotheses as to the cause of the observed sand transportation and the resulting sorting of the sand were presented.

[1] Beach Erosion Board, Washington, D. C.

5. Theory of Floating Breakwaters in Shallow Water

By J. J. Stoker [1]

Abstract

The exact theory for the interaction between floating bodies and water waves of small amplitude has been derived and discussed recently by F. John (On the motion of floating bodies, Communications on Pure and Applied Mathematics, vol. III, No. 1, 1950). F. John, in the same paper, also derived an approximate theory for rigid bodies floating in shallow water. The term "shallow water" means that the depth of the water should be small compared to the wave length of the surface waves.

The theory of floating breakwaters, which are not necessarily rigid bodies, in shallow water, was discussed. The theory was rederived in a sufficiently general way to apply to floating structures, which might, for example, be flexible beams, stretched membrances, floating ice particles, or also rigid bodies.

The mathematical formulation of the theory leads to the linear wave equation in places where the water surface is not covered by an obstacle, to a modification of the equation of the vibrating beam for a place where the surface is covered by a beam, and to other appropriate equations when the surface is covered by other obstacles. In addition, transition conditions at the junctures of regions of different properties must be derived, and appropriate conditions at ∞ must be prescribed. The result is a linear problem of a rather complicated type for which, however, methods of solution are known.

Special cases were then discussed in which the reflection and transmission coefficients, which measure the efficiency of a floating breakwater, were calculated. It is felt that this theory should form a reasonable basis for the design of structures to serve as breakwaters in shallow water.

[1] Institute for Mathematics and Mechanics, New York University, New York, N. Y.

6. On the Limiting Clapotis

By Pierre Danel [1]

Several examples are known of structures which, having stood for years under heavy storms, were destroyed fairly rapidly by a much milder one.

Hence the idea, borne out by model experiments, that certain waves may be actually worse than others of even greater magnitude, this depending also on the design of the structure itself and bottom topography.

This discussion is a short summary of research made in Grenoble to determine the wave characteristics that, for a given location and design of structure, give the heaviest pounding.

It is shown that this ties in with the determination of the limiting clapotis, or standing, wave, depending on the amount of wave energy reflected by the structure.

Experience with most types of breakwaters and maritime structures has shown that the greatest destructive effect is generally produced by the heaviest waves that reach effectively the structure. These may sometimes coincide with the largest incoming waves, but that is not always the case. Quite often the effect of bottom topography is such that the largest waves, under the influence of the shallowing of the bottom combined with the effects of local refraction and diffraction, already lose most of their energy by breaking or, at least a fair amount of it, by combing in various ways.

This dissipation of energy well ahead of the structure itself may also be enhanced by the waves reflected from the structure itself. The amount of reflection, in terms of energy, may vary from 100 percent for a good reflector such as a vertical wall to only a few percent for a good dissipator.

Although the problem of predicting the heaviest waves that can physically reach a given structure is of prime importance to the engineer, a glance through the literature seems to indicate that so far it has been very little studied, not so much because its importance was not recognized but because theoretically it appeared very difficult to tackle properly (and in all likelihood still does), and also because its experimental study by means of model or flume experiment was not an easy matter either.

In the last few years most of the experimental difficulties have disappeared one after the other and laboratory technique has progressed by leaps and bounds very rapidly indeed not only by the wonderful achievements in instrumentation but also by many new experimental techniques. One of the most outstanding is that of the wave-filter devised by Mr. Biesel, and its many recent improvements.[2]

In this short note however we shall not dwell at length on the many difficulties met with in experimenting on various types of waves and clapotis especially close to the breaking point. A special paper on experimental technique is now being prepared to be published at a later date.

---

[1] Laboratoire Dauphinois d'Hydraulique, Ets. Neyrpic, Grenoble, France.

[2] F. Biesel, Filtre à houle, La Houille Blanche 3, 276 (1948); 373, (A1949).

We will content ourselves in this first paper on this subject to present some of the experimental results so far obtained to date by the Neyrpic Laboratory of Grenoble (France).

The problem that faces the designing engineer, as already mentioned, is to be able to predict the heaviest wave that will actually reach the structure and which, by its incessant pounding during big storms, may bring havoc to the structure if it is not properly designed.

Let us then suppose that the largest waves in the open sea and coming toward the structure can be predicted either from local statistics or from reasonably adapted fetch formulae. These waves have then to be "routed" to the structure by known means of ascertaining the "wave pattern" taking into account both refractional and diffractional effects. In this routing it will be often found that some of the heaviest waves already break and lose energy before reaching the structure. But close to the structure, as already mentioned, account has to be taken in the "wave routing" of the waves reflected from the structure. The combined effect of the incoming waves with the reflected waves causes a wave pattern, which, with increased intensity of the incoming wave, reaches a limit above which some breaking or combing will occur. It is then essential for the designing engineer to ascertain properly this limiting condition.

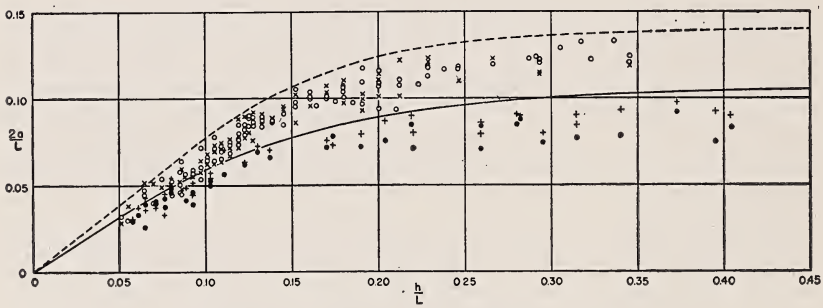

FIGURE 1. *Limiting wave and limiting clapotis.*

$2a$ = amplitude of the incident wave at depth, h; L = wave length; h = water depth.

Progressive wave {before breaking, ○. after breaking, ×. Clapotis {before breaking, ● after breaking, +.

In figure 1 a plot is given as a solid curve for the limiting pure clapotis, that is, for a total reflection. In other words, the amount of energy reflected is equal to the incoming energy, the structure being parallel to the wave crests.

As conditions depend on both wave characteristics and local depth, the plot, in dimensionless numbers, has for abscissa the ratio of depth to wave length and for ordinates the ratio of the total amplitude, $2a$, to that of the wave length. $2a$ is the amplitude the waves would have at the local depth were they not altered by the reflected waves.

Experience has shown that, with the limitations due to surface tension, the limiting clapotis is practically cuspidal as had been already suggested by some approximate theory (although it seems to still be a moot question among theoreticians).

This cuspidal condition is naturally very unstable and difficult to produce accurately experimentally. To get quick results as a first approximation we have plotted, as solid circles, clapotis that have not

reached the limiting condition and, as vertical crosses, the experimental points where slight breaking or combing was noticed, which may happen either because the pure clapotis would actually be above the limiting condition we are now looking for, or on the other hand because for one reason or other the incoming wave is not "pure" enough as any harmonics will induce some early combing.

In spite of these difficulties, we feel that the solid curve given is fairly representative of the real limit.

For this first paper on the subject we had not the time to carry on experiments with various percentages of reflection. However we present on the same graph experimental data for the limiting wave, that is when there is no reflection at all.

The limiting condition in deep water has been known theoretically for quite some time giving the asymptotic limit $2a/L=0.14$ for the dotted curve representing the condition for the limiting wave on the graph.

In fairly shallow waters it has been pointed out already by various authors that a good approximation is given by the solitary wave theory. The straight portion of the dotted curve from the origin corresponds to the condition of the limiting solitary wave.

For intermediate conditions in medium depth the approximations, as given by Miche, are quite close to our curve.

Here again, as for the limiting clapotis, plots are given of points before breaking and after breaking or combing. The limiting wave is not cuspidal but is angular at 120° as already known theoretically. When the experimental waves are free from harmonics or out of phase components, they come very close to the shape of the theoretical limiting wave displaying almost the 120° angle, save for a slight rounding up of the apex due to surface tension.

Although the case of the limiting wave was better known theoretically than that of the limiting clapotis, to our knowledge the problem had not been covered experimentally before. Of course for the limiting wave the amplitude, as plotted on the graph, corresponds not only to the incoming wave but also to the limiting wave itself as in this case it is all one and the same thing.

It must be noted here that the characteristics of the incoming waves that correspond to the limiting condition at the structure with no reflection (limiting wave) and for total reflection (pure clapotis) are not so far apart as might be supposed.

For a partial reflection (partial clapotis) the limiting conditions will correspond to a curve in between the two given curves, and from lack of a better tool the designing engineer can already interpolate between the two curves according to the reflection coefficient of the structure.

This may not seem a very accurate procedure. However, it must be borne in mind that the characteristics of the incoming waves at sea are more or less just a little better than guessed from fetch formulae or local statistics: this flavours the uncertainties of flood prediction for rivers. Just the same, although easier to ascertain, the reflection coefficient of most structures is not accurately known.

Another engineering aspect of the problem is that of the safety coefficient of the structure. If the structure is studied along the line here discussed, the first thing is to ascertain which waves are the most dangerous, and generally it is found they are just close to the limiting waves; then and then only, to check approximately from fetch formulae and "local wave routing" whether they are likely to occur and how often. If the predicted heavy waves are just slightly under the limiting waves

here discussed, the structure should be designed, in our opinion, for the limiting condition with enough safety in view of the uncertainty of the "predicted waves." In this way almost 100-percent-safe structures could be designed, and most of the money spent annually on heavy maintenance could be saved.

It must be noted that a totally reflecting structure, such as a vertical wall, cannot be reached and pounded upon by as heavy waves as perfectly absorbing structures. This advantage, however, is often more than counterbalanced by many inconveniences, such, for instance, as inducing a very choppy condition at sea nearby, rendering navigation more hazardous.

A full discussion of the advantages and disadvantages of the various profiles used or proposed would be out of place here. In this short note we just wanted to show by an example that by the proper blending of theory and modern experimental technique the designing of maritime works is becoming more and more an exact science and that really safe structures will be designed leaving the mystery of the insuperable pounding of raging seas to the realm of literature where they should belong.

7. Observations of Internal Tidal Waves

By Jonas Ekman Fjeldstad [1]

In 1933 a theory was given of internal waves in a sea where the density varied continuously with depth. It was shown that an infinite number of solutions could be found, corresponding to waves of the same period but different velocities of propagation. To test this theory measurements were made in 1934 of temperature and salinity at different depths, and at the same time current measurements to determine the tidal currents. The temperature and the salinity showed quite large variations of tidal period which could be explained satisfactorily by assuming that they were composed of four internal waves. The amplitudes of these waves could be calculated from the density variations. The theory made it possible to calculate also the current, for comparison with the observed values. From the theoretical velocities of propagation it was then possible to compute vertical oscillations and tidal currents also and compare the results with the observations. It was found that the phase angles computed in this way corresponded fairly well with those observed. Since the observations at the three different stations were not simultaneous it was impossible to ascertain if the diminution of the amplitudes was caused by the configuration of the fjord only or if the friction also should be taken into account.

In 1949 the observations were repeated with two vessels simultaneously. Conditions were much the same as in 1934 and a similar program was carried through. The two vessels were anchored about 11 km apart. It was found that the tidal currents were small, except in the upper 15 to 20 m. The variation of temperature and salinity indicated large internal waves of a progressive type. The phase differences between the two stations amounted to some 5 hours, corresponding to a velocity of propagation of 60 cm/sec. This is also the theoretical value found for the first-order internal wave. The theory makes it possible to give a more detailed analysis of the wave phenomenon.

In 1933 I gave a theory of internal tidal waves in a sea where the density is a continuous function of depth.[2] I shall briefly recall some theoretical considerations.

If ρ be the density and $w=d\zeta/dt$ the vertical component of velocity, then w is a solution of the second-order differential equation

$$\frac{d}{dz}\left(\rho\frac{dw}{dz}\right)-\lambda^2\left(g\frac{d\rho}{dz}+\sigma^2\rho\right)w=0,$$

subject to the boundary conditions $w=0$, $z=0$, (bottom); and $dw/dz-\lambda^2gw=0$, $z=h$, (surface).

The equation has ordinarily an infinite number of solutions. These correspond to internal waves of the same period but different velocities of propagation. We shall designate these waves as waves of the first order, second order, and so on. The wave of zero order is then the ordinary tidal wave.

The horizontal velocity is connected with the vertical elevation of a particle from its equilibrium position by the equation

$$u=c\frac{d\zeta}{dz}\cdot$$

---

[1] Oseanografisk Institutt, Universitetet, Oslo, Norway.

[2] J. E. Fjelstad, Observations of internal tidal waves, *Geof. Publ.* (Oslo) X:6, 1933.

λ is a parameter that is connected with the velocity of propagation c. When the influence of the earth's rotation can be neglected, we have simply $\lambda = 1/c$.

To test the theory some observations were made in the summer of 1934 in Herdlafjord, near Bergen, Norway. One end of the fjord is nearly closed by an island and a ridge with a maximum depth of some 20 m. The other end opens into a larger fjord system. The depths vary between 200 and 300 m.

Observations were made at three different stations. Station 1 was occupied for 88 hours, and temperature measurements were made every half hour at the depths 0, 5, 10, 15, 20, 30, and 100 m. Water samples for determination of salinity were taken at the same depths every hour. At the same time, current measurements were made at the surface and at 5-, 10-, 15-, 35-, 50-, and 100-m. depths. At the two other stations the time intervals covered by the observations were 33 and 36 hours.

In table 1 we give the results of the harmonic analysis of the density variations and the corresponding amplitudes of the vertical oscillations at Station 1.

TABLE 1

Depth	σ_T	k	ζ
m		*Degrees*	*cm*
5	0.344	14	59
10	.306	50	130
15	.272	42	220
20	.158	43	283
30	.057	44	222
100	.009	18	680

The computed values of the amplitude of the vertical oscillations at 30- and 100-m depth are naturally rather uncertain because the gradient of density is very small at these depths.

The results of the current measurements are given in table 2.

TABLE 2

Depth	v	k
m	*cm/sec*	*Degrees*
5	8.7	245
10	11.1	242
15	6.8	242
35	3.7	242
50	0.9	216
100	1.2	121

From the mean density distribution the theoretical internal waves could be found by a numerical integration process, and from the observed density variations the coefficients of the different internal waves could be computed. When trying to represent the observed vertical oscillations by four internal waves, the result was

$$\zeta = 13.88 \cos(\sigma t - k_1 x - 42°) w_1 + 6.90 \cos(\sigma t - k_2 x - 242°) w_2 + 2.85 \cos(\sigma t - k_3 x - 291°) w_3 + 3.64 \cos(\sigma t - k_4 x - 268°) w_4.$$

For $x=0$ we get the values in table 3.

TABLE 3

Depth	ζ	k	ζ_{obs}	k_{obs}
m	*cm*	*Degrees*	*cm*	*Degrees*
5	58	19	59	14
10	184	55	130	50
15	246	51	220	42
20	290	45	283	43
30	367	41	222	44
100	503	50	680	18

For comparison the observed values are entered in the same table. On the assumption that the waves are progressive, we may with the same set of coefficients compute the corresponding velocities, which may then be compared with the observed values. The results are given in table 4.

TABLE 4

Depth	v	k	v_{obs}	k_{obs}
m	*cm/sec*	*Degrees*	*cm/sec*	*Degrees*
5	13.8	237	8.7	245
10	10.2	232	11.1	242
15	6.7	222	6.8	242
35	2.3	227	3.7	242
50	0 9	241	0.9	216
100	1.4	42	1.2	121

The approximate agreement between computed and observed values confirm the assumption of free progressive waves.

The theory gives the velocities of propagation to be 62, 33, 23.4 and 17.4 cm/sec for the four internal waves. We are then able to calculate the values which are to be expected at the two other stations. We shall only reproduce the results for Station 3.

Putting $x=12.3$ km in the formula, we find the values in table 5.

TABLE 5

Depth	ζ	k	$0.44\,\zeta$	ζ_{obs}	k_{obs}
m	*cm*	*Degrees*	*cm*	*cm*	*Degrees*
5	166	202	70	78	179
10	252	207	106	106	200
15	273	198	115	111	181
20	257	191	108	94	198
30	168	194	71	69	(241)
100	137	287	57	.....	.....

As will be seen, the computed amplitudes are much larger than the observed. In the fourth column we give the computed amplitudes multiplied by a common factor 0.44. These reduced amplitudes agree very nearly with the observed values. To explain the reduction of amplitude, we have to take into account that the breadth of the fjord at Station 3 is about double that at Station 1, but we have also to bear in mind that the observations are not simultaneous.

The reduced amplitudes and the phase angles correspond fairly well with the observed values, and this may be taken as a confirmation of the theory.

In the summer of 1949 I had an opportunity to repeat the observations in the same fjord, and this time I had two vessels at my disposal so that the observations were simultaneous. For Station 1 the *Armauer Hansen* was anchored at the same place as at Station 1 in 1934, and for Station 2 the *Johan Hjort* was anchored at a distance of 11 km from Station 1.

The final analysis is not yet finished, but I can give some preliminary results.

Temperature measurements were taken every half hour at 0, 5, 10, 20, 30, 50, and 100 m, and water samples were collected at the same depths every hour. On board the *Armauer Hansen*, current measurements were made at the surface and at 5-, 10-, 15-, 20-, 30-, 40-, and 60-m depths. At Station 2, the *Johan Hjort*, current meters were used at 5-, 10-, 15-, 20-, and 30-m depths.

The results of the harmonic analysis of the density oscillations and different depths are given in table 6.

TABLE 6

Depth	Station 1		Station 2	
	σ_T	k	σ_T	k
m		*Degrees*		*Degrees*
5	0.423	78	0.333	210
10	.304	56	.139	213
20	.189	74	.094	191
30	.138	80	.041	185
50	.048	68	.021	211
100	.006	61	.002	168

As will be seen, there is a large phase difference between the two stations. The mean value is 127 degrees, corresponding to 4.38 hours. As the distance is 11 km, we find a velocity of propagation of 70 cm/sec.

The results of the harmonic analysis of the tidal currents are given in table 7.

TABLE 7

Depth	Station 1		Station 2	
	v	k	v	k
m	*cm/sec*	*Degrees*	*cm/sec*	*Degrees*
0	11.3	260	.....	.....
5	14.5	280	6.6	29
10	13.2	275	6.6	51
15	12.4	265	6.6	65
20	5.5	254	5.3	80
30	3.4	204	.....	.....
40	4.0	231	.....	.....
60	1.3	171	.....	.....

The weather conditions during the measurements were very unfavorable with heavy rain and wind. This was unfortunate, not only because the observation work was disagreeable, but during more than a day the whole

surface layer was swept away, and thus the density distribution in the upper layer was changed, so that the conditions could not be regarded as stationary. The observations cover a time interval of 4½ days.

We have made numerical integrations corresponding to the mean density distribution during the first day at Station 1. Using the method of the least squares to determine the coefficients of four internal waves, we found

$$\zeta = 15.08 \cos(\sigma t - k_1 x - 71°) w_1 + 8.58 \cos(\sigma t - k_2 x - 249°) w_2$$
$$+ 0.82 \cos(\sigma t - k_3 x - 307°) w_3 + 2.86 \cos(\sigma t - k_4 x - 146°) w_4.$$

We have also tried to draw a curve for the observed vertical oscillation and determine the coefficients by numerical integrations. The result was then

$$\zeta = 15.58 \cos(\sigma t - k_1 x - 71°) w_1 + 8.48 \cos(\sigma t - k_2 x - 252°) w_2$$
$$+ 1.00 \cos(\sigma t - k_3 x - 276°) w_3 + 1.16 \cos(\sigma t - k_4 x - 152°) w_4.$$

The agreement is excellent for the two first internal waves, but for the third and fourth the agreement is only qualitative. However these waves have only small amplitudes. With the first set of coefficients we compute the values in table 8 for the vertical oscillations.

TABLE 8

Depth	ζ	k	ζ_{obs}	k_{obs}
m	*cm*	*Degrees*	*cm*	*Degrees*
5	43	77	43	78
10	150	59	153	56
20	370	73	378	74
30	524	78	507	80
50	628	73	668	68
100	520	53	495	61

The agreement between computed and observed values is satisfactory, indicating that four waves are sufficient to represent the observed internal oscillations.

Using the same set of coefficients, we can also calculate the corresponding horizontal velocities. The results, together with the observed values, are given in table 9.

TABLE 9

Depth	v	k	v_{obs}	k_{obs}
m	*cm/sec*	*Degrees*	*cm/sec*	*Degrees*
0	9.7	264	11.3	260
5	11.1	242	14.5	280
10	10.8	251	13.2	275
15	9.4	257	12.4	265
20	7.6	259	5.5	254
30	4.2	255	3.4	204
40	1.7	235	4.0	231
60	1.0	125	1.3	170

The velocities computed from the observed density variations give a more gradual decrease with depth than those observed, and there seems to be a systematic difference of phase. At present it is difficult to say whether this indicates that the waves are of a more complex nature than assumed, or if it may be attributed to casual errors. We have also to bear in mind that the ordinary tidal current has not been included in the values calculated, and that no corrections have been applied to account for the influence of the surface tide. By using Bessels functions for the solution one gets better agreement.

It would be tempting to make an analysis of the currents in the same manner as has been made with the densities, and so obtain independent values of the coefficients of the different internal waves. But the difficulty is that we have no current measurements in the deeper layers. The method of least squares breaks down in this case, because the determinant of the normal equations will be nearly zero. This is what might have been expected, since it is possible to represent a function which is constant in the upper layers by a sufficient number of eigenfunctions. One of the coefficients will therefore be arbitrary.

Using the theoretical velocities of propagation, which in this case are 60, 34, 22, and 17 cm/sec, we may calculate the values of the vertical oscillations and the corresponding tidal currents that would be expected at Station 2 if there were no decay of the waves. The results are given in tables 10 and 11.

TABLE 10

Depth	ζ	k	ζ_{obs}	k_{obs}
m	*cm*	*Degrees*	*cm*	*Degrees*
5	186	194	33	210
10	203	200	73	213
20	275	232	184	191
30	365	249	176	185
50	385	266	189	211

TABLE 11

Depth	v	k	v_{obs}	k_{obs}
m	*cm/sec*	*Degrees*	*cm/sec*	*Degrees*
5	10.8	30	6.6	20
10	6.1	73	6.6	51
15	5.8	88	6.6	65
20	5.1	96	5.3	80

As will be seen, there is an approximate agreement of phase, but the observed vertical amplitudes are much smaller than the calculated values. This is in accordance with the results of 1934. The amplitudes marked "obs." are computed from density amplitudes by means of the formula

$$\rho_1+\zeta\frac{d\rho_0}{dz}=0,$$

and consequently they are affected with relatively large errors in the deeper layers, where the gradient of density is small.

The large phase difference between the tidal currents at the two stations is a phenomenon worthy of attention, since it could not be explained without taking the internal waves into account. An ordinary tidal wave would have nearly the same phase at two places which are lying so near to each other. It shows that the internal waves may change the tidal currents very considerably.

As to the cause of the internal waves, it is clear that the tide producing potential of the moon is not able to create internal waves of noticeable magnitude. But when the tidal currents are distorted by the bottom configuration, this will set up internal waves such that the superposition of the ordinary tidal wave and the internal waves will give a variation of tidal currents with depth, which is necessary to satisfy the boundary conditions of the current.

8. Motion of Water Due to Breaking of a Dam, and Related Problems

By Frederick V. Pohle [1]

The two-dimensional hydrodynamical equations of motion, expressed in Lagrangian representation, are used to investigate the motion of an ideal fluid. This representation has the far-reaching advantage in problems with time-dependent free boundaries that the independent space variables (a,b) are the initial coordinates of the particles: the region occupied by (a,b) is thus a *fixed* region independent of t.

The displacements $X(a,b;t)$, $Y(a,b;t)$ and the pressure $P(a,b;t)$ are expanded in powers of the time, t. Equating to zero the coefficients of powers of t leads to a systematic procedure for the determination of the successive terms in the three expansions. Each term is a solution of the Poisson equation, in which the inhomogeneous terms are known functions of previously determined quantities. In all cases considered, higher approximations require determination of a Green's function, which is the same for all approximations.

The method is applied to the initial stages of the breaking of a dam.

Certain calculations for semicircular and hemispherical domains agree with similar calculations carried out independently by C. K. Thornhill, using other methods.

Calculations of the maximum pressure exerted on a dam during an earthquake agree with the previous work of H. M. Westergaard.

1. Introduction

The hydrodynamical equations of motion may be formulated in two different ways, which bear the names of Euler and Lagrange respectively. The more commonly used Eulerian representation takes the space coordinates (x,y,z) and the time (t) as independent variables; the dependent variables (pressure, density, velocity) are determined as functions of $(x,y,z;t)$. The Lagrangian representation, which will be used in this paper, introduces the initial particle displacements (a,b,c) as the independent variables in place of (x,y,z). The dependent variables are the particle displacements $(X,Y,Z,)$, the pressure (P), and the density (ρ).

The Eulerian representation concentrates upon a fixed point (x,y,z) and describes the motion of the fluid which streams past this point. In the Lagrangian representation one seeks to determine the motion of all particles at any time t. In many problems such specific information is not required, if the domain of (x,y,z) is known in advance or if a fixed, known domain may be obtained by a suitable linearization process, such as that used in the theory of surface waves.

The Lagrangian representation is suited to those hydrodynamical problems in which the domain of (x,y,z) must be determined as part of the problem, for example, the determination of a time-dependent free boundary. The important distinction between the Eulerian and Lagrangian representations were clearly pointed out by Dirichlet [1] [2],

---

[1] Polytechnic Institute of Brooklyn, Brooklyn, N. Y. This work was done while the author was on the research staff of the Institute for Mathematics and Mechanics, New York University.

[2] Figures in brackets indicate the literature references on p. 53.

who emphasized that (x,y,z) were not "independent variables" in the usual sense.

The Lagrangian representation has the far-reaching advantage that the independent space variables (a,b,c) are the initial coordinates of the particle: the region occupied by (a,b,c) is therefore a *fixed* region. The purpose of this paper is to develop an expansion scheme suitable for the treatment of time-dependent free boundary problems, for example, to the determination of the initial stages of the flow from a dam, the forward wall of which has been suddenly removed.

2. General Expansion Scheme for the Solutions of Hydrodynamical Problems in Lagrangian Representation

Since two dimensional problems alone will be considered, the necessary equations will be restricted to those cases. If the horizontal x-axis is taken as positive to the right and the vertical y-axis is taken as positive downward, the equations of motion are [2, p. 13]

$$\left.\begin{aligned} X_{tt}X_a+(Y_{tt}+g)Y_a+(1/\rho)P_a=0 \\ X_{tt}X_b+(Y_{tt}+g)Y_b+(1/\rho)P_b=0 \end{aligned}\right\} \tag{2.1}$$

In eq 2.1, ρ is the density, P is the pressure, and X,Y are the horizontal and vertical displacements, respectively; the independent variables are $(a,b;t)$. The only external force considered is the force due to gravity. Subscripts are used to denote partial differentiation.

The equation of continuity for an incompressible fluid is [2, p. 15]

$$X_aY_b-X_bY_a=1. \tag{2.2}$$

The condition for irrotational flow is

$$X_aX_{bt}+Y_aY_{bt}=X_bX_{at}+Y_bY_{at}. \tag{2.3}$$

Equation 2.3 may be obtained directly from the corresponding Eulerian condition [4, pp. 9–10]. If P is eliminated from the eq 2.1 by differentiation, the result is

$$(X_aX_{bt}+Y_aY_{bt})_t=(X_bX_{at}+Y_bY_{at})_t. \tag{2.4}$$

Integration of eq 2.4 with respect to t yields eq 2.3; an arbitrary function of (a,b) must be added. This function represents the vorticity at $t=0$, which is zero since the fluid is assumed to be irrotational at $t=0$. The arbitrary function is therefore zero and the flow remains irrotational for all time.

The assumption that X, Y, and P can be represented as analytic functions of t leads to the expansions

$$\left.\begin{aligned} &X(a,b;t)=\sum_{r=0}^{\infty}X^{(r)}t^r;\quad Y(a,b;t)=\sum_{r=0}^{\infty}Y^{(r)}t^r;\quad P(a,b;t)=\sum_{r=0}^{\infty}P^{(r)}t^r. \\ &X^{(0)}=a,\ Y^{(0)}=b;\ X^{(r)}=X^{(r)}(a,b),\ Y^{(r)}=Y^{(r)}(a,b);\ P^{(r)}=P^{(r)}(a,b). \end{aligned}\right\} \tag{2.5}$$

If the expansions for X and Y in eq 2.5 are substituted into the continuity eq 2.2 and the coefficients of t^n, $(n \geqq 1)$, are set equal to zero, one obtains

$$X_a^{(1)} + Y_b^{(1)} = 0,$$

$$X_a^{(n)} + Y_b^{(n)} = -\sum_{r=1}^{n-1} \frac{\partial(X^{(r)}, Y^{(n-r)})}{\partial(a,b)}. \qquad (n \geqq 2). \tag{2.6}$$

The usual notation for Jacobians has been used in eq 2.6.

The same substitution of X and Y from eq 2.5 into the irrotationality condition 2.3 yields the conditions $(n \geqq 2)$

$$X_b^{(n)} - Y_a^{(n)} = -\left(\frac{1}{n}\right)\sum_{r=1}^{n-1}(n-r)\left\{\frac{\partial(X^{(r)}, X^{(n-r)})}{\partial(a,b)} + \frac{\partial(Y^{(r)}, Y^{(n-r)})}{\partial(a,b)}\right\}. \tag{2.7}$$

The right-hand side of eq 2.7 is zero for $n = 1,2$.

Comparison of the sets of eq 2.6 and 2.7 shows that the left-hand sides, respectively, resemble the Cauchy-Riemann equations of function theory, Separate equations can therefore be found for $X^{(n)}$ and $Y^{(n)}$ in terms of $X^{(0)} \ldots X^{n-1}$; $Y^{(0)} \ldots Y^{n-1}$. Let Δ denote $\partial^2/\partial a^2 + \partial^2/\partial b^2$; then the equations for $X^{(1)}$ and $Y^{(1)}$ are $\Delta X^{(1)} = 0$, $\Delta Y^{(1)} = 0$. The equations for $X^{(2)}$ and $Y^{(2)}$ are

$$\Delta X^{(2)} = -\frac{\partial}{\partial a}\left[\frac{\partial(X^{(1)}, Y^{(1)})}{\partial(a,b)}\right]; \quad \Delta Y^{(2)} = -\frac{\partial}{\partial b}\left[\frac{\partial(X^{(1)}, Y^{(1)})}{\partial(a,b)}\right]. \tag{2.8}$$

The general equations for $\Delta X^{(n)}$, $\Delta Y^{(n)}$ will involve known functions of previously determined functions [4, p. 15]. These equations are all of the Poisson type for a fixed domain. Therefore the knowledge of the appropriate Green's function makes possible an explicit solution of the inhomogeneous equations, of which eq 2.8 are typical examples.

$X^{(1)}$ and $Y^{(1)}$ represent the initial components of velocity; a and b represent the initial displacements. These quantities and the necessary boundary conditions specify the general problem. The right hand sides of eq 2.8 are therefore known functions; $X^{(2)}$ and $Y^{(2)}$ can be determined when the appropriate boundary conditions have been imposed. The known values of $X^{(2)}$ and $Y^{(2)}$ can be inserted into the equations for $X^{(3)}$ and $Y^{(3)}$, and so on. The successive terms can be calculated in this way, but the inhomogeneous terms become extremely complicated.

The successive terms in the expansion of P must also be determined. The boundary condition for P along a free boundary is $P(a,b;t) = 0$; the quantities b and a are connected by their values at $t = 0$. This formulation of the free-surface condition is simpler than the corresponding formulation in the Euler representation. Other boundary conditions also enter; for example, along a fixed horizontal bottom, $b = 0$, the kinematical condition is $Y(a,0;t) = 0$ for all a and t. This condition implies that $Y^{(r)}(a,0) = 0$ for all r. The appropriate boundary conditions can therefore be imposed upon $X^{(r)}$, $Y^{(r)}$, and $P^{(r)}$ [4, pp. 22–25; p. 35].

The successive pressure terms $P^{(0)}$, $P^{(1)}$, ... are obtained from the eq 2.1 after the substitutions from eq 2.5 have been made. The general

results are obtained by setting the coefficient of t^n equal to zero in eq 2.1

$$\left.\begin{aligned}(n+2)(n+1)X^{(n+2)}+\sum_{r=0}^{n+1}r(r-1)\{X^{(r)}X_a^{(n+2-r)}+Y^{(r)}Y_a^{(n+2-r)}\}\\ +gY_a^{(n)}+\frac{1}{\rho}P_a^{(n)}=0,\\ (n+2)(n+1)Y^{(n+2)}+\sum_{r=0}^{n+1}r(r-1)\{X^{(r)}X_b^{(n+2-r)}+Y^{(r)}Y_b^{(n+2-r)}\}\\ +gY_b^{(n)}+\frac{1}{\rho}P_b^{(n)}=0.\end{aligned}\right\}\tag{2.9}$$

The general continuity equation of 2.6, with n replaced by $(n+2)$ is

$$X_a^{(n+2)}+Y_b^{(n+2)}=-\sum_{r=1}^{n+1}\frac{\partial(X^{(r)},Y^{(n+2-r)})}{\partial(a,b)}.\tag{2.10}$$

If the first of eq 2.9 is differentiated with respect to a and the second equation is differentiated with respect to b, the sum of the results will contain $X_a^{(n+2)}+Y_b^{(n+2)}$, which can be eliminated by eq 2.10. The result is an equation of the Poisson type for $P^{(n)}$; the inhomogeneous terms are known functions of $X^{(r)}$, $Y^{(r)}$ $(r=1,2,\ldots(n+1))$ [4, p. 18]. In the determination of $P^{(0)}$ only (a,b) and $(X^{(1)}, Y^{(1)})$ enter; thus the initial displacements and the initial velocity components alone determine the initial pressure distribution $P(a,b;0)$. Lichtenstein [3, p. 411] has commented upon this property of the Lagrangian equations in contrast to the Euler equations.

On a free boundary, $P^{(0)}=0$. If a fixed horizontal boundary is present, $P_b^{(0)}=\rho g$, which is the hydrostatic pressure gradient. Once $P^{(0)}$ is determined, $X^{(2)}$ and $Y^{(2)}$ are known from eq 2.9 with $n=0$. The known functions can then be inserted into the equation for $P^{(1)}$; if $P^{(1)}$ is known, $X^{(3)}$ and $Y^{(3)}$ can be determined from eq 2.9 with $n=1$. The successive terms of $P(a,b;t)$ can be calculated in this way.

3. The Initial Stages of the Breaking of a Dam

The water is assumed to occupy the region shown in figure 1.

The wall of the dam $(a=0, 0\leq b\leq h)$ is assumed to be removed instantaneously at $t=0$; the fluid is initially at rest everywhere. The mathematical conditions are:

$$X(a,b;0)=a,\qquad Y(a,b;0)=b,\tag{3.1}$$

$$X_t(a,b;0)=0,\qquad Y_t(a,b;0)=0,\tag{3.2}$$

$$P(a,h;t)=0,\qquad P(0,b;t)=0,\tag{3.3}$$

$$Y(a,0;t)=0.\tag{3.4}$$

The conditions 3.1 are satisfied by the expansions assumed in eq 2.5. The conditions 3.2 assert that all particles start from rest; in particular,

$$X^{(1)}=0;\quad Y^{(1)}=0.\tag{3.5}$$

The conditions 3.3 assert that the pressure is zero on the free surfaces $(b=h, a\geq 0)$ and $(a=0, 0\leq b\leq h)$. Since the pressure is hydrostatic everywhere for $t<0$, there will be a discontinuity in P at $t=0$, and a singularity in the pressure gradient must be expected. The condition 3.4 is the kinematic boundary condition on the bottom of the dam.

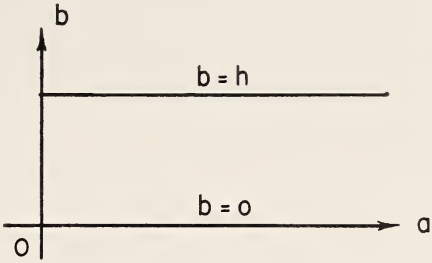

FIGURE 1. *Region occupied by water.*

The boundary condition for the terms of $X(a,b;t)$ and $Y(a,b;t)$ can now be determined from eq 3.3, 3.4, and 2.1. For example, $Y^{(2)}(a,0)=0$, $Y^{(2)}(0,b)=(\frac{1}{2})g$, and $X^{(2)}(a,h)=0$; these conditions have obvious physical interpretations. The boundary conditions for the higher terms are more complicated and need not be written here. The eq 2.6 and 2.7 show that $X^{(2)}$ and $Y^{(2)}$ are conjugate potential functions. The functions $Y^{(2)}$ and $X^{(2)}$ are determined as the real and the imaginary parts, respectively, of the complex function $Y^{(2)}+iX^{(2)}$. The usual methods of conformal mapping [4, pp. 26–29] determine these functions to be

$$X^{(2)}(a,b)=-\frac{g}{2\pi}\log\left\{\frac{\cos^2\left(\frac{\pi b}{4h}\right)+\sinh^2\left(\frac{\pi a}{4h}\right)}{\sin^2\left(\frac{\pi b}{4h}\right)+\sinh^2\left(\frac{\pi a}{4h}\right)}\right\};$$

$$Y^{(2)}(a,b)=-\frac{g}{\pi}\arctan\left(\frac{\sin\frac{\pi b}{2h}}{\sinh\frac{\pi a}{2h}}\right). \qquad (3.6)$$

The functions in eq 3.6 behave physically in a reasonable way [4, pp. 29–33].

The initial pressure distribution $P^{(0)}$ can be calculated from $P^{(0)}_a = -2\rho X^{(2)}$; this result follows from the first equation of 2.9 with $n=0$.

The boundary conditions for the higher terms of X and Y become too involved to be used directly. A more suitable formulation may be made in terms of the pressure, for $P(a,b;t)$ has the two *fixed* boundary conditions.

$$P^{(r)}(a,h)=0; \quad P^{(r)}(0,b)=0. (r=0,1,2,\ldots). \qquad (3.7)$$

The differential equations for $P^{(r)}$ are all of the Poisson type (or of the potential type for $P^{(0)}$), and the main problem is to determine the condi-

tions along $b=0$; for $P^{(0)}$ the condition on $b=0$ is $P^{(0)}_b=-\rho g$. The function $P^{(0)}$ may be determined as a Fourier series

$$P^{(0)}(a,b)=\rho g(h-b)-\frac{8\rho gh}{\pi^2}\sum_{n=0}^{\infty}\left\{\frac{1}{(2n+1)^2}e^{\frac{-(2n+1)\pi a}{2h}}\cos\left(\frac{2n+1}{2h}\right)\pi b\right\}. \tag{3.8}$$

The eq 2.9 may be used to determine the series representations of $X^{(2)}$, $Y^{(2)}$. Equation 3.8 shows, for fixed b, that the pressure rapidly becomes equal to the hydrostatic pressure $\rho g(h-b)$ as a increases. The same effect is observed for fixed a and decreased h, that is, as the water becomes shallower in the depth.

The differential equation for $P^{(2)}$ can now be determined to be [4, pp. 38–39], $(P^{(1)}=0)$,

$$\Delta P^{(2)}=\frac{-8\rho g^2}{h^2\left(\cosh\frac{\pi a}{h}-\cos\frac{\pi b}{h}\right)}. \tag{3.9}$$

The boundary conditions are

$$P^{(2)}(a,h)=0;\quad P^{(2)}(0,b)=0;\quad P^{(2)}_b(a,0)=\frac{\rho g^2}{2h}\cdot\frac{1}{\sinh(\pi a/2h)}. \tag{3.10}$$

The solution of eq 3.9 under the conditions 3.10 requires the determination of the appropriate Green's function. This function may be obtained in closed form by conformal-mapping methods [4, p. 42], but a more useful series representation is

$$\left.\begin{aligned} G(x,y;a,b)&=-\frac{4}{\pi}\sum_{n=0}^{\infty}\frac{1}{2n+1}\cos(\lambda_n y)\cos(\lambda_n b)\sinh(\lambda_n x)e^{-\lambda_n a}, \\ &\qquad 0\leq x\leq a, \\ G(x,y;a,b)&=-\frac{4}{\pi}\sum_{n=0}^{\infty}\frac{1}{2n+1}\cos(\lambda_n y)(\cos\lambda_n b)\sinh(\lambda_n a)e^{-\lambda_n x}, \\ &\qquad x\geqq a,\quad \lambda_n=\frac{(2n+1)\pi}{2h}. \end{aligned}\right\} \tag{3.11}$$

The result 3.11 is derived in [4, p 46].

The function $P^{(2)}$ may now be written in the usual way in terms of integrals of eq 3.11 and the functions appearing in eq 3.9 and 3.10.

4. Applications

The methods of section 2 can be applied to a wide variety of problems [4, part IV], of which two may be taken as representative.

(a) C. K. Thornhill, in a discussion at the Institute for Mathematics and Mechanics at New York University [3] discussed flow problems of this general nature by means of the Euler representation. In particular, a semicircular domain can be treated in the same way that the problem of the breaking of the dam was treated in section 3.

[3] September 1950. The results are to be published in the near future.

A cylindrical mass of water is assumed to be initially in the shape of a unit semicircle ($x^2+y^2=1$, $y \geqq 0$); at $t=0$, the boundary is removed and the initial stages of the flow are to be determined. Here $\Delta P^{(0)}=0$ in $x^2+y^2 \leqq 1$, $y \geqq 0$; $P^{(0)}=0$ on $x^2+y^2=1$, $y \geqq 0$, $P_b^{(0)}=-\rho g$ on $y=0$, $|x| \leqq 1$. The procedure outlined in section 3 may be used to determine $P^{(0)}$ explicitly [4, p. 49]. In particular, the pressure at the stagnation point (0,0) is $2\rho g/\pi$ for unit height; this value agrees with Thornhill's result, which was obtained numerically.

The same method can be applied to the spherical case, $x^2+y^2+z^2=1$, $y \geqq 0$, $z \geqq 0$ [4, pp. 50–51]. The pressure at (0,0,0) in this case is $\rho g/2$ for unit height.

(b) Westergaard [5] has treated the problem of a vertical oscillating wall and has determined the maximum dynamical pressure resulting from such a motion. The wall is the forward face of a dam, and it is assumed that the simple harmonic oscillations are caused by a sudden earthquake.

Figure 1 may be used to represent the dam; the wall ($a=0$, $0 \leq b \leq h$) is assumed to have a known acceleration, α, at $t=0$. The boundary conditions for $P^{(0)}$ are $P_b^{(0)}(a,0)=-\rho g$, $P_a^{(0)}(0, b)=-\rho\alpha$, $P^{(0)}(a,h)=0$; $\Delta P^{(0)}=0$ in $a \geqq 0$, $0 \leq b \leq h$. The pressure, $P^{(0)}$, may be found as a Fourier series [4, p. 54]. The result agrees with Westergaard's result.

5. References

[1] Dirichlet, P. L. Untersuchungen über ein Problem der Hydrodynamik. Journal für die reine und angewandte Mathematik. Bd. 58. 1861. pp. 181–216.

[2] Lamb, H. Hydrodynamics. Sixth edition. Cambridge University Press. 1932.

[3] Lichtenstein, L. Grundlagen der Hydromechanik. J. Springer, Berlin. 1929.

[4] Pohle, F. V. Thesis. New York University. 1950.

[5] Westergaard, H. M. Water pressure on dams during earthquakes. Transactions A.S.C.E. Volume 98. 1933. pp. 418–433.

9. Symmetrical, Finite Amplitude Gravity Waves

By T. V. Davies [1]

The problem of the steady propagation of gravity waves of finite amplitude in a tank with a horizontal base is a nonlinear problem of a special type. The stream function ψ satisfies a linear partial differential equation and the nonlinearity enters through the free surface boundary condition. The classical theory converts the nonlinear boundary condition into a linear condition using the perturbation method and is therefore restricted to infinitesimal amplitude waves. It is possible, however, to deal with the finite amplitude problems by replacing the exact nonlinear condition by a new nonlinear condition that is a close approximation and for which the exact solution may be determined. This enables one to discuss all waves up to and including the limiting case when breaking occurs at the crest. The Levi-Civita approach is used for this purpose, and the application of the method to the solution of the solitary wave problem is demonstrated.

1. Introduction

The essential difficulty and interest of the classical gravity wave problem lies in the fact that the boundary condition to be satisfied at the free surface of the fluid is nonlinear in the dependent variables. If we express

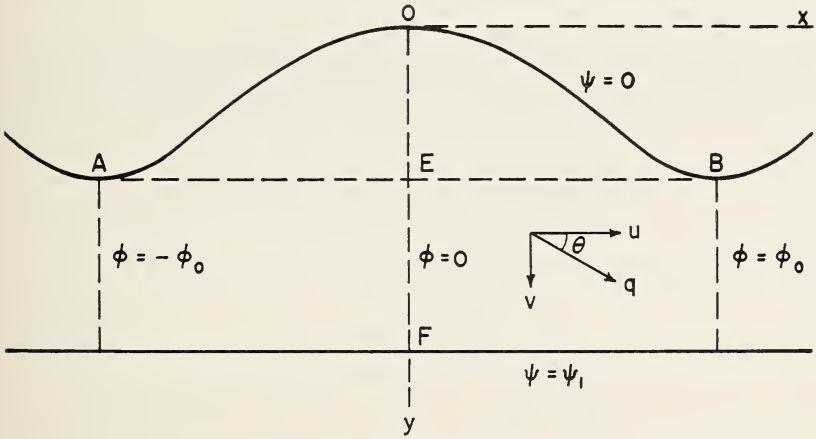

FIGURE 1. *Diagram of wave showing rotation.*
Wave length $=AB=\lambda$; $OE=a$; $AD=h$.

the problem in the Levi-Civita form [1] [2] in which the dependent variables are τ and $\theta(\xi=\tau-i\theta)$, and the independent variables are ϕ and $\psi(w=\phi+i\psi)$, the problem may be stated as follows:

[1] The Institute for Advanced Study, Princeton, N. J. Presently at King's College, London, England.
[2] Figures in brackets indicate the literature references on p. 60.

ξ is a regular function of w throughout the rectangle $-\phi_0 \leq \phi \leq \phi_0$, $0 \leq \psi \leq \psi_1$, and is periodic in ϕ with period $2\phi_0$. With the assumption of symmetry about $\phi = 0$, ξ must satisfy the following boundary conditions

$$\Im(\xi) = 0, \quad \psi = \psi_1; \tag{1}$$

$$\Im(\xi) = 0, \quad \phi = 0, \quad \phi = \pm\phi_0, \quad \ldots; \tag{2}$$

$$\frac{\partial\theta}{\partial\psi} = -\frac{g}{c^3} e^{-3\tau} \sin\theta, \quad \psi = 0. \tag{3}$$

The nonlinearity enters in condition eq 3, and in the first approximation we modify this condition though still preserving its nonlinear character. The aim of the present investigation is to deduce an approximate solution to the gravity wave problem that will be valid up to and including the wave that is on the point of breaking at the crest. We define this limiting wave, following Stokes, to be that one for which the particles of fluid at the wave crest are moving with exactly the velocity of propagation, c, of the wave (or waves). Relative to axes that are moving with the wave system (assumed above in the statement of the problem), the velocity of the particles at the wave crest is then zero. This has an important bearing upon the values of the symbols introduced above. The relative velocity components (u,v) are given in terms of τ and θ by the relation

$$u - iv = \frac{dw}{dz} = qe^{-i\theta} = ce^{\tau - i\theta} = ce^{\xi}, \tag{4}$$

where $q = ce^{\tau}$. Thus in the case of the limiting wave that is on the point of breaking at the crest, we have $q = 0$ or $\tau = -\infty$ at this point. In order, therefore, to be able to discuss the breaking wave, it is necessary to retain the term $e^{-3\tau}$ in eq 3, and we approximate instead to $\sin\theta$.

Stokes has shown that θ satisfies $-\pi/6 \leq \theta < \pi/6$, the equalities actually being attained in the breaking case, and we may, therefore, approximate to $\sin\theta$ in eq 3 by writing $\sin\theta = l \sin 3\theta$, where l is a suitable constant. Then eq 3 becomes approximately

$$\frac{\partial\theta}{\partial\psi} = -\frac{gl}{c^3} e^{-3\tau} \sin 3\theta, \quad \psi = 0, \tag{3'}$$

or

$$\Im\left\{i\frac{d\xi}{dw} + \frac{gl}{c^3} e^{3\xi}\right\} = 0, \quad \psi = 0 \cdot \tag{3''}$$

l may be chosen to be one-third, in which case our results will tend to coincide with the classical small-amplitude theory when θ becomes sufficiently small, or alternatively, l may be chosen so that $l \sin 3\theta$ is the best fit to $\sin\theta$ throughout the interval $0 \leq \theta \leq \pi/6$. The former is more useful if we wish to proceed to higher approximations (see eq 7).

2. Periodic Waves in a Channel of Infinite Depth

$(\psi_1=\infty,\ \phi_0=\frac{1}{2}c\lambda)$

The region occupied by one complete wave is now a semiinfinite strid in the w-plane, namely, $-\frac{1}{2}\ c\lambda \leq \phi \leq \frac{1}{2}\ c\lambda$, $0 \leq \psi \leq \infty$. Here we have assumed that there is a state of absolute rest at $\psi=\infty$,[3] or relative velocity $+c$ to axes moving with the waves. In this case we use the transformation (*v.* 1) $s=\exp(2\pi iw/c\lambda)$, which converts the semiinfinite strip into a circle $|s|\leq 1$. It then follows that eq 3″ is satisfied on $|s|=1$, and hence throughout the unit circle

$$i\frac{d\xi}{dw}+\frac{gl}{c^3}e^{3\xi}=\text{ constant }=\frac{gl}{c^3}=k,$$

the constant being evaluated at the center $s=0$ or $\psi=\infty$. Hence we obtain the solution

$$\chi=\left(\frac{u-iv}{c}\right)^3=e^{-3\xi}=1-Ae^{ikw}, \tag{5}$$

where A, the constant of integration, is a real parameter such that $0\leq A\leq 1$. The lower range of A gives small amplitude waves, and the upper limit is the breaking case. Since $k\phi_0=\frac{1}{2}kc\lambda=\pi$, it follows that

$$c^2=\frac{3gl\cdot\lambda}{2\pi}. \tag{6}$$

By using eq 4 we can return to the physical plane, and it is easily shown that the Stokes 120° angle is true for eq 5 at the breaking case. The method of proceeding to higher approximations consists in using $\sin\theta=\frac{1}{3}\sin 3\theta-\frac{4}{3}\sin^3\theta$ successively, so that we replace eq 3 by

$$\frac{\partial\theta}{\partial\psi}=-\frac{g}{c^3}e^{-3\tau}\left\{\frac{1}{3}\sin 3\theta+\frac{4}{81}\sin^3 3\theta+\frac{16}{729}\sin^5 3\theta+\ldots\right\}. \tag{7}$$

We then determine a solution of eq 7 in an ascending series in A, provided we assume that g/c^3 is also dependent upon A. We thus obtain the solution

$$e^{-3\xi}=1-Ae^{ikw}+\frac{1}{54}A^3e^{3ikw}+A^4\left(-\frac{1}{27}e^{2ikw}+\frac{1}{81}e^{4ikw}\right)+\ldots, \tag{8}$$

$$c^2=\frac{g\lambda/2\pi}{1-\frac{1}{9}A^2-\frac{5}{162}A^4+\ldots}. \tag{9}$$

It is easily shown that A is simply related to the ratio a/λ.

[3] No loss of generality is involved here.

3. The Solitary Wave $(\psi_1 = ch, \quad \phi_0 = \infty)$

We take the absolute velocity of the fluid at infinity to be zero or $+c$ relative to the moving system of axes. The fluid motion is now confined to the strip $0 \leq \psi \leq ch, -\infty \leq \phi \leq \infty$. If we choose $\chi = e^{-3\xi}$ as a new dependent variable, then the problem may be stated as follows: χ is a regular function of w in $0 \leq \psi \leq \psi_1$ and is such that

$$\left.\begin{aligned} &\Im(\chi) = 0, \quad \psi = \psi_1 = ch; && \text{(a)} \\ &\Im(\chi) = 0, \quad \phi = 0, \quad \phi = \pm\infty; && \text{(b)} \\ &\Im\left\{\left(i\frac{d\chi}{dw} - \frac{g}{c^3}\right)/\chi\right\} = 0, \quad \psi = 0, && \text{(c}^4\text{)} \\ &\chi \to 1, \quad \phi \to \pm\infty. && \text{(d)} \end{aligned}\right\} \tag{10}$$

The method consists in continuing χ analytically outside the strip $0 \leq \psi \leq ch$ and over the whole w-plane; the completed w-plane then appears as in figure 2. We show first that

$$\Im\left\{\left(i\frac{d\chi}{dw} + \frac{g}{c^3}\right)/\chi\right\} = 0$$

on $\psi = 2\psi_1$, but thereafter the method is tentative. On the analogy with the solution eq 5 for χ, which has zeros at the points $w = \pm mc\lambda + i/k \log_e A$, $(m = 0,1,2,\ldots)$ we introduce one zero of χ at $w = -i(\pi/k - 3\psi_1)$ and consider the successive images of this zero in $\psi = \psi_1$, $\psi = 2\psi_1$, and $\psi = 0$. We finally postulate periodicity of χ in the ψ direction with period $2k$. It then follows that $\Im(\chi) = 0$ around the perimeter of the semiinfinite strip $FGHK$, and we may, therefore, map this rectangle on the upper half of the χ-plane. The mapping is effected by the Schwarz-Christoffel theorem, and when the constants are suitably chosen we obtain

$$\chi = \left(\frac{u - iv}{c}\right)^3 = 1 - \sin^2 \kappa ch \operatorname{sech}^2 \frac{1}{2}\kappa(w - ich) \cdot \tag{11}$$

If we substitute eq 11 into eq 10c, we obtain the wave-velocity formula

$$\frac{g}{c^3} = \kappa \cot \kappa ch, \tag{12}$$

and from eq 11 it easily follows that the parameter κ must satisfy the inequality

$$0 \leq \kappa ch \leq \frac{\pi}{3} \cdot \tag{13}$$

As $\kappa \to 0$, the solitary wave tends to a uniform flow; the upper limit is the breaking case (obtained by writing $\chi = 0, w = 0$ in eq 11). The wave-velocity eq 12 is similar to McCowan's. To proceed to higher approxi-

[4] In eq 10c we use eq 3″ with $l = \frac{1}{3}$.

mations we again use eq 7, and the next approximation has been obtained by Brian Packham [3].

We may quote one result of interest that pertains to the limiting solitary wave. The equation of Bernoulli in the limiting case is $q^2=2gy$, and when we specialize this to the conditions at infinity, we obtain $c^2=2ga$. From eq 12, in the limiting case,

$$\frac{gh}{c^2}=\frac{\pi}{3}\cot\frac{\pi}{3},$$

hence

$$\frac{a}{h}=\frac{3\sqrt{3}}{2\pi}=0.827\cdot \tag{14}$$

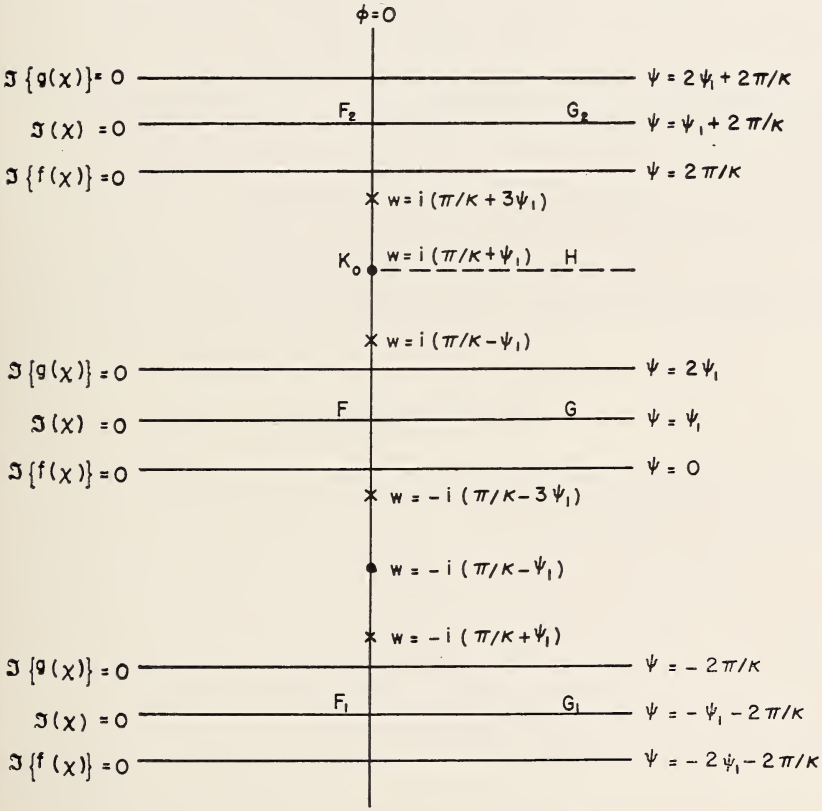

FIGURE 2. *Diagram of complex w-plane.*

× indicates zero of χ; ● indicates pole of χ; $f(\chi)=\left(i\frac{d\chi}{dw}-\frac{g}{c^3}\right)/\chi$; $g(\chi)=\left(i\frac{d\chi}{dw}+\frac{g}{c^3}\right)/\chi$.

This must be compared with McCowan's value 0.78. The result eq 14 is modified when we proceed to higher approximations and details may be found in eq 3.

Finally, we may quote the result for the drift of a fluid element at the base $\psi=\psi_1$. This is given by

$$\mathfrak{D}=\frac{1}{c}\int_{-\infty}^{\infty}\left\{1-(1-\sin^2\kappa\psi_1\operatorname{sech}^2\frac{1}{2}\kappa\phi)^{-\frac{1}{3}}\right\}d\phi, \tag{15}$$

and hence we have the approximate formula

$$\frac{\mathfrak{D}}{h}=-\frac{4\sin^2\kappa\psi_1}{3\kappa\psi_1}\left\{1+\frac{4}{9}\sin^2\kappa\psi_1+\frac{56}{405}\sin^4\kappa\psi_1+\ldots\right\}. \tag{16}$$

The drift is in the direction of propagation of the wave.

4. References

[1] T. Levi-Civita. Math. Annalen. 1925.
[2] T. V. Davies. Proc. Roy. Soc. (in press).
[3] B. Packham. Quart. Journal Mechanics and App. Maths. (in press).

10. On the Complex Nature of Ocean Waves and the Growth of the Sea Under the Action of Wind

By Gerhard Neumann [1]

The results of recent observations in the North Atlantic, the Caribbean Sea, and the Gulf of Mexico are given. The state of the sea in its fully developed form represents a wave system of two or three principle components which, with the secondary compons ents, yields the complex picture of the rough sea surface. Observed wave dimension- are compared with values derived from theory. Another phenomenon is the characteristic wave groups resulting from interference.

The growth of the "sea" in relation to the complex nature of the ocean waves for given wind velocities is dealt with. The analysis starts from the energy equation in a form which equates the time variation of the wave energy to the difference between the energy supplied and the dissipation. The energy dissipated plays a large role in the energy balance. The dissipation coefficients, or the coefficients of eddy viscosity of the complex wave motion with its turbulence, depend on the wind intensity and the conditions of the sea. Their order of magnitude is comparable with the known values of the "Austausch" coefficients for the upper layers.

For a given wind intensity are developed the differential relations between the wave characteristics (velocity, wave length, wave height) and the fetch and wind duration. The integrations are carried out numerically. A satisfactory agreement between theory and observations is obtained.

1. Introduction

The question of the manner in which waves of the sea arise when the wind blows over the water has not yet been clearly explained physically. Even the many attempts to discover empirical relations between the dimensions of ocean waves and wind velocity by statistical treatment of systematically collected observations led to few explanations, in part even to contradictory results. The ideas regarding the translation velocity of fully developed wind waves diverged very greatly. The same holds even for wave lengths and periods, although these characteristics of waves in deep water are simply related to each other according to the Gerstner formula. Some observers and theoretical workers support the view that the translation velocity of fully developed wind waves in the sea (phase velocity) is greater than the wind velocity, while others energetically oppose this.

According to the theory of H. U. Sverdrup and W. H. Munk [1] [2] the ratio "translation velocity to wind velocity", $\sigma/v=\beta$, for "significant waves" for end conditions with sufficiently long action by the wind and sufficiently great sea-room (fetch) is about $\beta=1.37$. These waves make themselves evident by their great wave length λ and small steepness $\delta=H/\lambda$ (H=wave height). With the value $\delta=0.022$, which these waves

[1] Geophysikalischen Institut der Universität, Hamburg, Germany.
[2] Figures in brackets indicate the literature references on p. 68.

reach under final conditions, $H/\lambda = 1/46$. Thus in this case we are concerned with mildly rounded waves of the swell type, which are never the characteristic features shown by sea waves that are under the direct influence of the wind. The wind agitated sea is covered with shorter and steeper waves, which, however, in their entire picture can present a quite irregular appearance.

The reason for the deficiencies in our empirical knowledge of the dimensions of sea waves for different wind speeds is to be sought neither in misconceptions nor in unexact observations; it lies more in the nature of the sea-wave phenomenon in itself, because "irregularity is the conspicuous feature of the sea surface". (H. Jeffreys).

In a sea waves of different heights and lengths approach each other and come together. Hence the sea obtains its so-called "rough" appearance, especially in certain stages of complex wave formation. But the longer the wind acts and the more the sea rises, that is to say, the more it approaches its maximum conditions, the more distinctly "characteristic" waves corresponding to the wind strength appear out of the wave mixture; at the same time, the originally more hill-like wave masses coalesce in increasing mass into long combers. As the sailor says, the "sea" builds up. With continuing development of the sea waves there comes into being a category of longer but considerably flatter waves; yet the steeper "sea," breaking from time to time remains as partial waves. This characteristic picture is impressed on the sea at all wind intensities, but shows great fluctuations and irregularities in its appearance.

Another characteristic feature of fully developed sea waves is the typical group phenomenon. If one tries to follow the "seas" individually for a considerable time, one recognizes that sooner or later they diminish in height and disappear in the wave mixture, while others rise up, which later likewise die away. These wave groups are a consequence of certain interference phenomena. The sea waves for a given wind intensity in a completely or nearly completely developed condition are not only recognizable by the characteristic "sea," although this stands out most strikingly, but also by a system of two or three principal waves, which in turn overlay the waves of secondary size, making up the apparently irregular picture of the rough sea surface. The sea waves are thus a complex phenomenon and only as such to be explained in their entirety.

The first principal wave in complex sea waves is the above-mentioned distinctly recognizable "sea." It has a phase velocity, σ, which is always smaller than the wind velocity, v. If the wind blows long enough, the second principal wave builds up, of which the phase velocity becomes greater than the wind velocity. This wave the author [2] has named "long wave." Its steepness is considerably less than that of the "sea," which is continually being overrun by the "long waves." With diminishing winds or when spreading out into a calmer region (dispersion) the "long waves" come into appearance as swells. The dimensions of these two principle waves and their interaction in a complex sea have previously been discussed elsewhere [2].

2. Results of Recent Observations

In the autumn of 1950 and the winter 1950-51 the author had the opportunity of making special studies of sea waves in the North Atlantic Ocean, the Caribbean Sea, and the Gulf of Mexico, and to collect voluminous observational data on sea waves for different wind intensities in different

stages of development, as well as on group phenomena in complex sea waves. The primary feature of the observation program was the measurement of individual "periods" (time intervals between succeeding crests). Whenever possible the periods of characteristic waves immediately following each other in the sea were determined with simultaneous wind measurements made with the aid of cupanemometers. From 70 to 150 (or more) single observations of periods were assembled in "series," together with the corresponding wind velocity. In total some 27,000 single measurements were assembled into about 250 series, which include wind intensities in the range from 2 to 22 m/sec.

The observations of each series were represented in the form of frequency diagrams for the "period" values (period-spectra). Two examples taken from this extensive material are shown in figure 1a and 1b for wind velocities of $V=16$ m/sec and $V=13.5$ m/sec, respectively. The individually measured periods according to the wind intensity cover a more or less large period interval, which in the range of short periods in nearly all cases is sharply bounded. This means that at the lower end of a certain period range only waves of secondary magnitude appear, which do not yet perceptibly influence the characteristic form of the sea. Separate "bands" in the period spectrum clearly show as accumulation points of measured values in definite class intervals. The vertical arrows with the

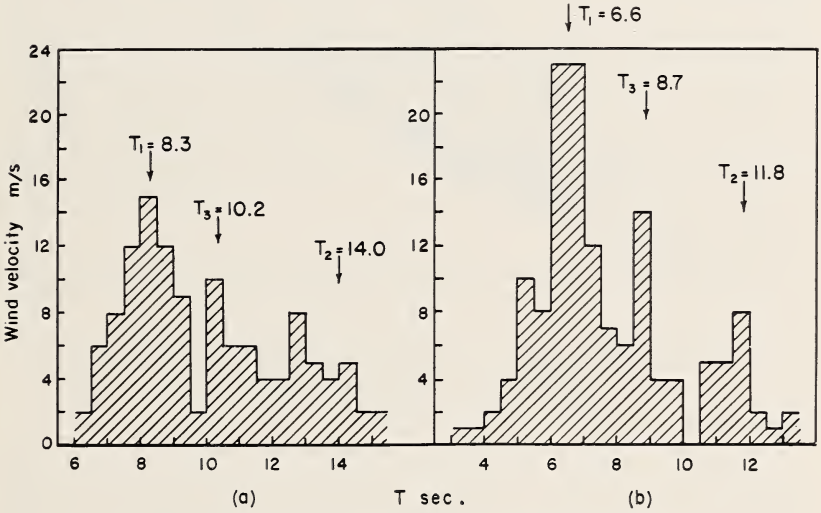

FIGURE 1. *Frequency distribution of measured period values.*

a, For $v=16$ m/s; b, for $v=13.5$ m/s.

notations T_1 and T_2 give the computed periods, which should stand out as characteristic in the sea for the corresponding wind intensity according to previous results [2]. T_1 is the theoretical period for the "sea," T_2 for the "long wave." At a wind velocity of 16 m/sec (fig. 1a) an accumulation of measured values in the class interval from about 7.5 to 9.5 seconds clusters about the expected period of $T_1=8.3$ seconds. At 13.5 m/sec we find a corresponding cluster of observations about the computed value $T_1=6.6$ seconds. Similarly, although not in all cases so clearly marked, frequency maxima can be found in the region of "long waves."

Worthy of notice is the accumulation of period values in a class interval *between* the previously mentioned principle waves. For $V=16$ cm/sec this intermediate maximum appears with periods from 10.0 to 11.5 seconds, for a wind velocity of $V=13.5$ cm/sec with periods from 8.5 to 9.0 seconds. Since period values for such "intermediate waves" were determinable in nearly all the observation series, it appears that here we have to do with a third characteristic wave in the complex sea motion. These intermediate waves seemly have a translation velocity which corresponds to the wind velocity. In the figure, T_3 marks a period that applies to a wave whose phase velocity is equal to the wind velocity.

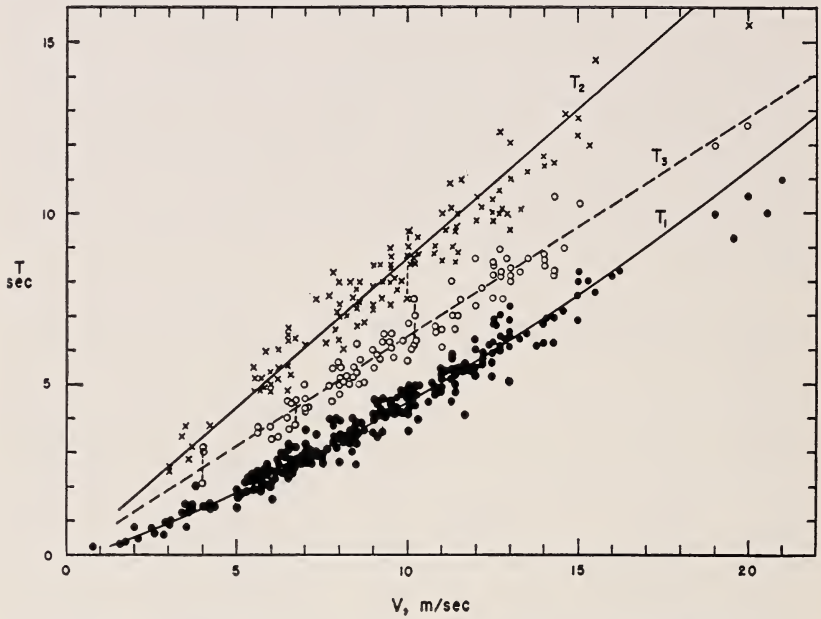

FIGURE 2. *Dependence of the periods T_1, T_2, and T_3 on the wind velocity v.*
The curves give the theoretical relations $T=f(v)$.

The results of the period measurements are expressed in a summary presentation in figure 2. For each observation series the characteristic periods were taken from the frequency diagram and plotted as function of the wind velocity. The observations arrange themselves in this presentation in a clear relationship under each other and in correspondence with the wind intensity. The curves drawn give the computed relations $T=f(v)$; that is,

$$T_1=f(v) \quad \text{(according to [2] or formula 4)},$$

$$T_2=(2\pi/g)\ 1.37v=0.877v,$$

$$T_3=(2\pi/g)v=0.64v.$$

In the period spectra (see figs. 1a and 1b) the frequency maximum is spread out to a "period band." This scatter of the individual measurements in the region of the period maxima is not to be attributed to the

unavoidable errors alone, but also in great measure is real and a very natural consequence of interference of the three principle waves in the sea movement.

In this paper the phenomenon of interference at different wind intensities can only be briefly discussed. Concerning the investigations of the time and space fluctuations of the complex sea conditions, which have been treated more completely elsewhere [3], only one example will be given here for the fully developed sea motion at a wind intensity of $v=16$ m/sec. At this wind velocity three principal waves are to be expected with periods of $T_1=8.3$ sec, $T_2=14.0$ sec, and $T_3=10.2$ sec. In figure 3 the time fluctuations of the sea motion are constructed, which were derived theoretically from the combined action of the three principle waves at a fixed place. The amplitude of the waves are $a_1=3.0$ m, $a_2=3.4$ m, and $a_3=3.0$ m.

The upper wave record (a) shows the waves following each other in time at the location $x=0$ for the time interval $t=0$ to $t=260$ sec (theoretical "wave record"). The lower wave record (b) gives the corresponding fluctuations for the same time interval at a location $x=550$m, that is, a place about one-third nautical mile from $x=0$ in the direction of travel of the waves. These constructed sea-level fluctuations show that pronounced wave groups are to be expected only *occasionally* at a given place. At $x=0$ they are to be found in the beginning of the observation period, where they occur at intervals of about 45 sec; at $x=550$ m they appear clearly at the end of the observation period. In these groups single wave masses rise to considerably greater heights, so that apparently in nature they do not quite reach their full heights because in passing a certain maximum steepness they become unstable and break. On account of the time and space regularity in their appearance a certain law is to be expected in the case of the high "breakers." The thought that the "law of breakers" is connected with the interference phenomena thus suggest itself.

Between the groups three smaller waves are to be observed whose heights change greatly with time and space. Also a wave called "double-wave"—a phenomenon often seen in the sea movement—appears at certain intervals. Following the passage of a succession of pronounced groups, the picture of the sea movement at a fixed place changes after a given time. The striking difference between especially high waves and the smaller waves between the groups gradually equalizes in time, as the upper curve in figure 3 shows. The typical group character then occurs

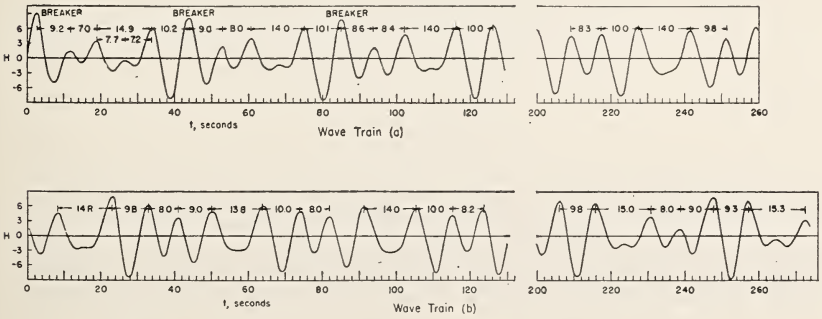

FIGURE 3. *Superposition of the three principal waves for $v=16$ m/s.*

Wave train (a): Fluctuations of the complex "sea" at a fixed point a during the time $t=0$ to $t=260$ sec.
Wave train (b): Corresponding fluctuations during the same time at a point b 550 m distant from a.

in another portion of the sea surface. During this time and space change striking interference phenomena characterize the complex picture of the wave disturbed sea surface, and only through the combined action of the principle waves can the characteristic features of the actual sea structure be made understandable.

The horizontal lines drawn in figure 3 between the individual wave peaks identify, with the figures written in, the periods of waves which were measured at the corresponding wind intensities in a fairly complex sea, for example, from aboard a ship. The periods of successive waves fluctuate—as the observations also have shown—within wide limits. So it is understandable that no satisfactory results can be obtained on the basis of some single, more detailed wave measurements in a complex sea taken at random. The wave curves of theoretical construction in figure 3 for the periods drawn are to be compared directly with the observations in figure 1a.

3. The Growth of the "Sea"

Along with the question concerning the appearance and the dimensions of fully developed waves in a complex sea stands the problem of the *generation of the sea movement.* A brief discussion will be given here of the attempt to calculate the growth of the "sea" with consideration of the complex nature of the wave-disturbed sea surface at different wind velocities [3]. The starting point of these theoretical considerations, like that of Sverdrup and Munk [1], is the energy equation, however in the form that the time change in the energy of the wave motion is equal to the *difference between the supplied* (A) *and the dissipated* (D) *energies.*

In the cited work [3] an investigation was made to determine the magnitude $A-D$, which is important for the growth of the sea. The dissipation plays a great role in the energy balance in turbulent seas. For the dissipation coefficient M (cm^{-1} g sec^{-1}) or the eddy viscosity coefficient of the turbulent wave-motion values were obtained which were of the same order of magnitude as the well-known "austausch" coefficient. The coefficient was determined empirically in this investigation; its relation to the wind intensity and the actual state of the sea motion (called the "age" β of the sea motion) can be expressed by the formulas

$$M\ (\beta)=Me^{-2r\left(\frac{\beta_m^*-\beta}{\beta_m}\right)} \text{ for } 1\leq\beta\leq\beta_m^*. \tag{1}$$

$$M\ (\beta)=M(1)e^{-2r(1-\beta)} \text{ for } 0.1\leq\beta\leq 1, \tag{2}$$

where

$$M=1.825\times 10^{-5}V^{5/2} \tag{3}$$

β_m is the ratio σ/v for the fully developed "sea", and $\beta_m^*=1.37$ (cm^{-1} g sec^{-1}). In addition, the empirical condition $H/\lambda=\delta=0.215e^{-r\beta}$, $\frac{1}{3}\leq\beta\leq 1.37$, was used. The quantity r has the value 1.667. If the supplied energy is equal to that dissipated ($A=D$), then there follows a relation between the translation velocity of the "sea" and the wind velocity, v,

$$\beta_m=\frac{2r(\beta_m^*-1)}{ln\ 182.5-ln\sqrt{v}},$$

For the fully developed "sea" this formula, in agreement with previous computations [2], gives the values in the table 1 below.

TABLE 1

V(m/sec)	4	6	8	10	12	14	16	20	24
β_m	0.56	0.61	0.66	0.70	0.74	0.78	0.81	0.88	0.94
T_1(sec)	1.43	2.35	3.4	4.5	5.7	7.0	8.3	11.3	14.6
λ (m)	3.2	8.6	18.0	31.5	51.0	75.0	107.0	198.0	327.0
H (m)	0.27	0.67	1.3	2.1	3.2	4.4	5.9	9.8	14.6

The periods T_1 and the wave lengths, λ, follow from the Gerstner formulas, and H from the empirical relation $H/\lambda = f(\beta)$. The periods T_1 here computed are to be compared with the values given by the curve T_1 in figure 4.

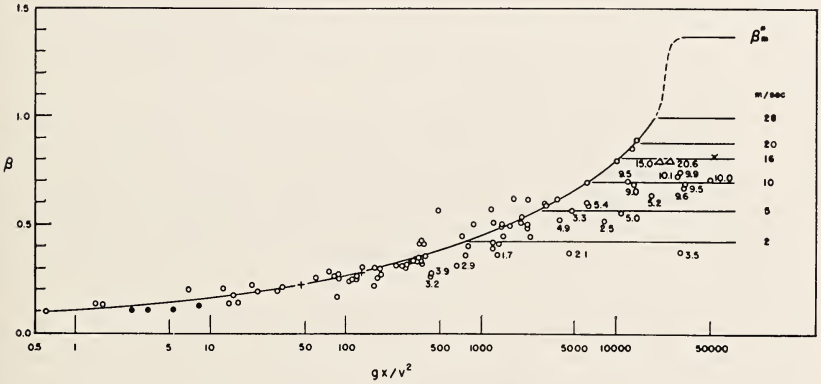

FIGURE 4. *Fetch diagram.*

Observed and computed values of β as functions of the distance of wave travel, x, and the wind velocity, v. $\beta = \phi(gF/v^2)$; ○, observations (1950/51, M. S. *Heidberg*); +, Gibson; ×, U. S. Engineers; △, Cornish; ●, Stanton.

From the energy equation the differential equations relating to the age of the waves, β, to the length of the fetch, F, or the time, t, that the wind acts for a given wind velocity, v, were developed. The numerical integration of the equation leads to expressions of the form

$$\beta = \phi(gF/v^2),$$

or

$$\beta = f(gt/v),$$

which Sverdrup and Munk have also employed. From these solutions the wave periods, the wave lengths, and the translation velocities of the "seas" in the various stages of development of the sea motion are also obtained. With help of the empirical relationship $\delta = f(\beta)$, the wave height can be determined for various wind intensities as a function of F and t.

For the generation of sea waves, shorter fetches, or times required for action by the wind, are derived than Sverdrup and Munk computed in

their well-known work. In figure 4, as an example of the results, the $\beta=\phi(gF/v^2)$ diagram for the growth of the sea for different wind intensities is given. For comparison with the computed curve are given, in addition to some older observations, the measurements made by the author in the autumn and winter of 1950–51 near the coast of the island San Miguel (Azores) and in West Indian waters.

From the diagram we observe, for example, that for a wind velocity $v=10$ m/sec the "sea," that is to say, the waves with $\beta_m=0.7$ and a height $H=2.1$ m, has arisen after passage over a fetch of about 62 km. This relationship remains constant for the "sea" for increasing fetches, as is expressed in the diagram by the horizontal line for $\beta=0.7$. The straight lines for other wind velocities are to be interpreted in a similar manner. Thus in the region of the horizontal lines to the right of the curve fully developed "seas" are to be expected. Here naturally for larger fetches of any given magnitudes the values of β_m for the corresponding wind intensities are constant. To illustrate this fact in the diagram, the wind intensities in meters per second corresponding to the observations in the region of the horizontal lines have been written in.

The length of the shortest fetch that is necessary for the development of the "sea" increases rapidly with increasing wind intensity. For $v=20$ m/sec, a fetch of 670 km is required to generate the waves; for $v=28$ m/sec, a fetch of 2,000 km.

For the time of generation, that is for the shortest duration of wind action for generation of the fully developed "sea" in an unlimited fetch, the computation gives a duration of $t=6.5$ hours for $v=10$ m/sec, 27.5 hours for $v=20$ m/sec, and about 55 hours for $v=28$ m/sec. After the development of the "sea," a certain amount of energy in the difference "supplied minus dissipated energy" is left over, which is used in the generation of longer waves in the disturbed sea. The process of generating the complex motion of the sea is thus no continuous action.

The extensive computations and the results of the analysis will be published in the near future as a report on a wave project dealing with the generation and the growth of complex ocean surface waves, conducted in the Meteorology Department of New York University under the sponsorship of the Office of Naval Research.

4. References

[1] H. U. Sverdrup and W. H. Munk, Wind, sea, and swell: theory of relations for forecasting, H. O. Publ. No. 601, Hydrographic Office, Washington, 1947.

[2] G. Neumann, Über Seegang, Dünung und Wind, Deutsche Hydrographische Zeitschrift, Band 3, Heft 1/2, Hamburg, 1950.

[3 G. Neumann, Über die komplexe Natur des Seeganges. I. Teil: Neue Seegangsbeobachtungen im Nordatlantischen Ozean, in der Karibischen See und in Golf von Mexiko (M. S. "Heidberg," Okt. 1950–Feb. 1951). II. Teil: Das Anwachsen der Wellen unter dem Einfluss des Windes. (To appear in the Deutsche Hydrographische Zeitschrift, Hamburg.)

11. Results of Exact Wave Measurements (by Stereophotogrammetry) with Special Reference to More Recent Theoretical Investigations

By A. Schumacher [1]

After some short remarks on the technique of wave stereophotogrammetry (single stereo photos and stereo pictures of rapid sequence) it is pointed out what kind of information on surface waves may be gained from wave plans in addition to dimensional and morphological data (length and height, steepness, angles formed by the crests, mass of waves). Topographic wave charts and profiles are discussed and qualitatively analyzed with special regard to the problem of the co-existence of the well-known wind-waves (the "sea" in the sailor's nomenclature) and the longer waves (with phase velocities greater than the respective wind velocities), a problem which, proceeding from Sverdrup's and Munk's investigations, G. Neumann has recently discussed anew. Examples supporting these ideas are given as well as some contradicting them. Especially with regard to these problems, the superiority of cine-stereophotogrammetry is obvious. It is the only quantitative (or nearly quantitative) method that gives an insight into the development of the waves with regard to space as well as to time, thus supplying a clear perception and eventually numerical information on interference phenomena. Therefore, a plea is made for continuation of cine-stereophotogrammetric wave research (although it must be admitted that this way of investigation is expensive and even somewhat uneconomical).

As far as I am aware, stereophotogrammetry has not yet been applied to wave research by American oceanographers. Therefore, on the following pages a brief review is given of the technique of wave stereophotogrammetry and, in addition, it is pointed out in what way this method may help to check and verify some results of more recent theoretical research.

Table 1 briefly recapitulates the various attempts at stereophotogrammetric wave research. With the exception of the last entry, all statements refer to German work. There are also Russian wave stereophotograms (obtained on the Black Sea), and a French attempt at wave cine-stereophotogrammetry was made on the jetty of Algiers, but unfortunately technical details are not available.[2]

The principal merit of the first three attempts is to have shown the applicability of the method; however, they could not yet sufficiently fulfill the two fundamental demands which must be met in stereophotogrammetry, viz, a base line of suitable length at a sufficient height above the sea surface. Later on a greater amount of freedom in handling the apparatus aboard ship was obtained, thanks to the most remarkable progress in measuring apparatus (especially by the invention of the stereoplanigraph). With the apparatus constructed for the Atlantic

---

[1] Deutsches Hydrographische Institut, Hamburg, Germany.

[2] Moreover, only some years ago there have been successful attempts by the French Navy (carried out on the coast of Morocco) to obtain cine-stereophotograms of swell and surf by airborne cameras with a base line of 300 or 600 m (the two planes flying at a height of 1,000 or 2,000 m above the sea surface). The author is indebted to M. Lacombe, Ingenieur Hydrographe en Chef de la Marine, for details of these attempts.

cruise of the *Meteor* 1925, it was no longer necessary to have the two cameras unalterably connected with, or adjusted to, each other, but it was sufficient to insure that the reciprocal position of the cameras could be reconstructed for each shot. This was done by the aid of an auxiliary camera rigidly fixed to each of the main cameras and facing the opposite pair of cameras (fig. 1). On the rather small R. S. *Meteor* conditions were not too favourable; however, thanks to the long duration of the cruise, it was, for the first time, possible to bring home a number of stereophotograms comprising at least one wave length. Up to 1934, this apparatus was used aboard four other ships, either with the tube bearing the cameras lengthened or with the cameras installed without any rigid

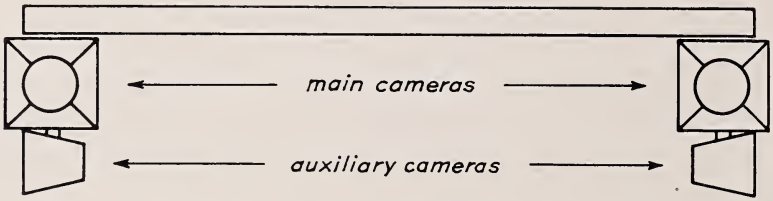

FIGURE 1. *Diagram of arrangement of cameras.*

connection and adjusted by aid of the auxiliary cameras with open shutters and focussing screens. The most successful installations were on the liner *Deutschland* where two or three consecutive lengths of storm waves could be caught, and on the liner *San Francisco* where G. Weinblum was fortunate enough to obtain a stereophotogram of a wave of a medium height of 16.5 m (50 feet), the maximum difference between crest and trough being 18.5 m (56 feet).

The amounts of inaccuracy computed for a distance of 200 and 500 m from the cameras refer to the minor and medium steps of the sea scale where the water surface can still be distinctly defined, but they must not be exactly applied to stereopictures of the sea in a full gale, when the surface is a rather thick layer of foam and salty spray.

It must be admitted that the apparatus of the *Meteor* Expedition was often somewhat troublesome to work with since for each snapshot *four* plateholders had to be prepared and four plates had to be simultaneously and correctly exposed, each of them having to catch the horizon as the only line of reference. However, it is indispensable to continuously check the reciprocal position of the cameras.

In 1938 it was possible to tackle the problem of wave stereophotogrammetry anew, now with rapid succession of pictures. The well-known firm of Zeiss, who had also furnished the apparatus of the *Meteor* Expedition, constructed an implement mainly consisting of two cameras for aerial photogrammetry and enabling consecutive stereosnapshots (up to 30 in one sequence) to be taken every second. In figure 2 the right-hand camera is shown as photographed by the auxiliary apparatus of the left-hand camera. There were no proper auxiliary cameras, but by the aid of a lens and a prism (left side of fig. 2, in the tube pointing toward the reader) the picture of the other camera and especially that of a mark-lamp (shown as No. 7 in fig. 2) was projected on that portion of the wave film where the sky appeared. In fig. 2 the optical axis of the wave camera points toward the left, the film holder—for 60 m of film, allowing about 300 exposures—is on the right side of the picture.

As for wave stereophotogrammetry from aboard ships it may be pointed out that the conditions aboard the liner *Europa* will hardly be surpassed for some time to come.[3]

The only disadvantage was the ship's high speed of 26 to 27 knots, or 13.5 m/sec, whereby the identical space on the consecutive plans was unpleasantly diminished. (The stereophotograms obtained aboard the *Europa*, which are discussed below belong to a reduced speed of 12.5 knots or 6.4 m/sec.)

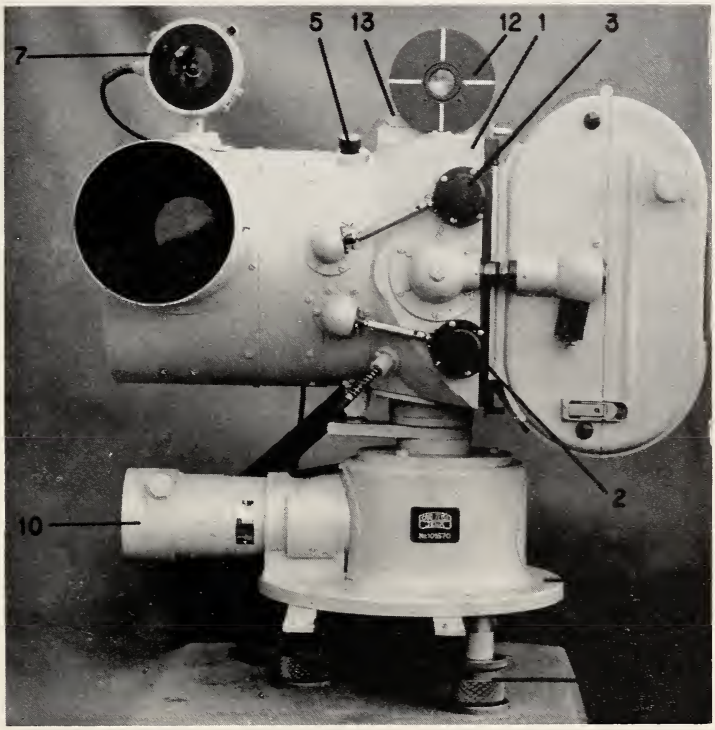

FIGURE 2: *Right-hand camera, shown as photographed by the auxiliary apparatus of the left-hand camera.*

Obviously the material about waves which can be derived from wave charts is to a large extent of purely statistical and morphological character. (Length and height, steepness, angles of crest profiles, mass of waves, and eventually enlargement of the sea surface by seaway, e.g., for considerations on evaporation.) This holds good, above all, if single wave charts are analyzed; consecutive charts in rapid succession will certainly also yield valuable evidence of nonstatistical character. Among the problems discussed in more recent theoretical research there is especially one to which the discussion of topographical wave charts may contribute, viz., that of the coexistence of the "normal" and "longer" waves originated at the same step of the Beaufort scale of wind force. The coexistence of

[3] An aggregate almost equal to that used aboard the *Europa* was installed on the island of Heligoland about 55 m above the sea surface, the base line being about 70 m long. In this way, topographic charts covering a rather large section of the sea surface could be obtained, one of them comprising 12 consecutive wave lengths, each of them more than 100 m long, with lengths of crests up to 1,500 m.

two such orders of magnitude has been already conjectured by Vaughn Cornish and Graf Larisch-Moenich, both of whom are well known as most careful observers [8].[4] Sverdrup and Munk, in their endeavours to provide foundations for forecasting sea and swell, also point in this direction, speaking of the larger waves present and, later of the one-third highest waves as their "significant" waves. The familiar formula of the classic wave theory are not applicable to the "significant waves" [9].

Recently, Gerhard Neumann [8] has discussed the problem of wave generation by wind. In principle, Neumann agrees with Sverdrup's and Munk's conception of longer waves, but he assumes that there are two distinct maxima of wave length in the wave spectrum belonging to each step of the Beaufort scale of wind force. The first "main wave" in the complex sea-way is the rather steep "sea" in the sailor's usual nomenclature with phase velocities smaller than the wind velocities. When the wind blows long enough, a second "main wave" becomes more and more conspicuous (though often hidden by the normal "sea") with phase velocities greater than the wind velocities and of lesser steepness than the "sea." This second category of "main waves" is called the "long waves" by Neumann, the symbols referring to it are λ^*, H^*, c^*, etc. They become

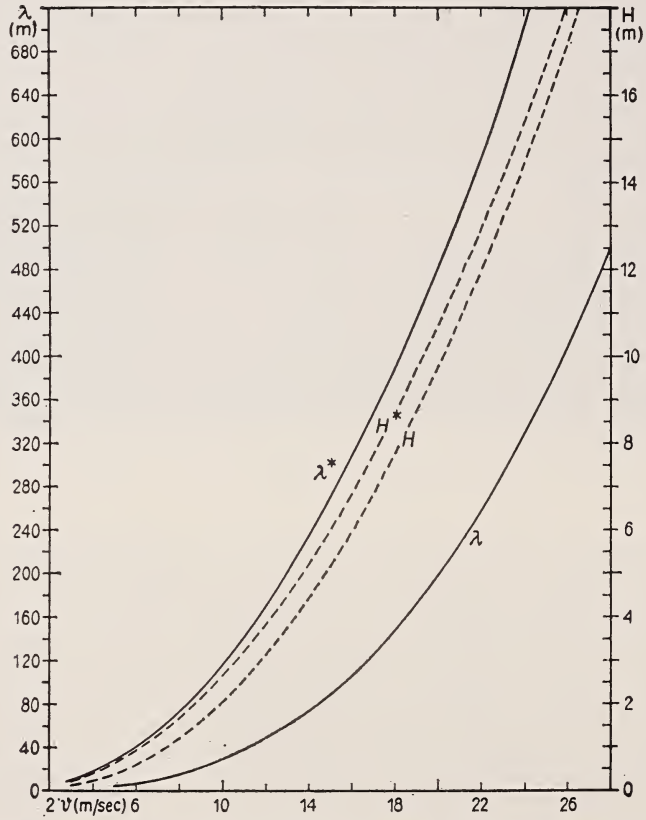

FIGURE 3: *Lengths and heights of "sea" and "long waves" as dependent on wind velocity.* (After G. Neumann).

[4] Figures in brackets indicate the literature references on p. 78.

obvious as swell after leaving the storm region or when the shorter and steeper "sea" is abating with easing wind. It is impossible to give an abstract of Neumann's theoretical considerations; only a diagram representing lengths and heights of the "sea" (λ,H) and of the "long waves" (λ^*,H^*) as a function of wind velocity is reproduced (fig. 3) in order to enable the reader to check the statements in tables 2 and 3.

By a large number of measurements of wave periods (about 27,000) obtained during a recent winter voyage to the Carribean Sea and the Gulf of Mexico, G. Neumann [10, 11] has found that for almost all steps of the Beaufort scale the wave periods corresponding to the "sea" and to the "long waves" have distinct maxima of frequency, and that between these two maxima there is often a third maximum recognizable, which remains to be discussed thoroughly.

Besides the evidence gained by G. Neumann from his observations it seemed to be useful to look for further though by far more scanty evidence in the topographical wave charts, especially of the *Meteor* work. Obviously, the most suitable objects of such a review are charts of trade-wind waves, since in these regions one may expect to find rather uniform conditions (G. Neumann himself has already referred to one of these charts).

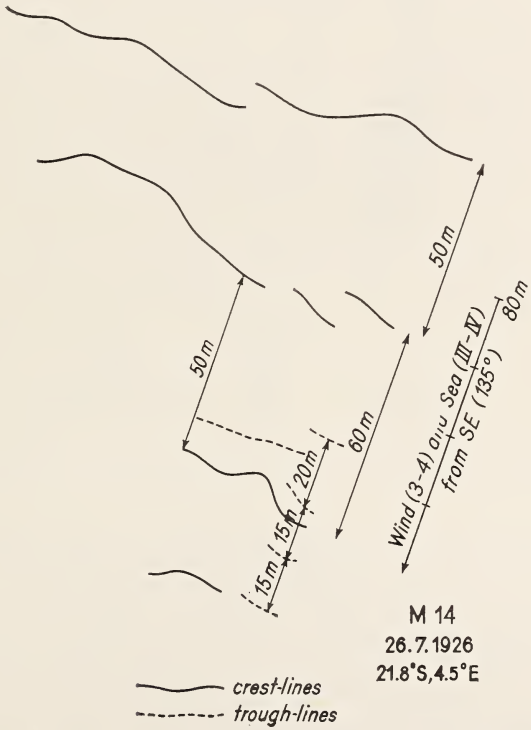

FIGURE 4. *Plan of wave crests and troughs taken from wave chart.*

It is to be regretted that altogether only seven serviceable wave plans from the trade regions are available. They are published in [3] and [4]; in figures 4 and 5 two samples are given in a very simplified manner merely showing the crests and troughs in order not to suppress the rather

small amount of evidence that can be obtained from wave charts of this extent.[5]

In table 2 the column "observations and measurements" contains the observations of wind, sea, and swell made during the wave photographs (the directions of wind and "sea" are in accordance with each other, the roman numerals indicating the state of the sea) and the wave dimensions are taken from the wave charts. The "sea" is the "wind sea" in the sailor's nomenclature, "swell" has in the former discussions of the wave charts (e.g., in the *Meteor* work [3]) mostly been taken in the usual sense, although not without hesitation. In the column "wave dimensions etc." the wind in meters per second corresponds with the Beaufort step in the left column, and the dimensions of the sea and the long waves belong to this wind velocity according to Neumann's paper quoted above (cf. fig. 3). In six of the seven wave charts the length of the "swell" is in a rather good agreement with the length of the "long waves" which are to be expected after Neumann; as for the wave heights the accordance is somewhat less.

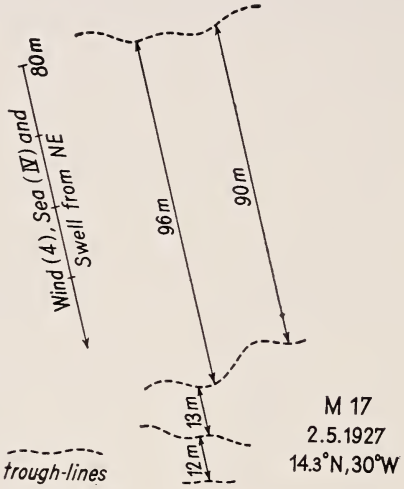

FIGURE 5. *Plan of wave crests and troughs taken from wave chart.*

Another group of wave charts representing a rough winter sea in the North Atlantic (table 3) also yields wave lengths corresponding with Neumann's "sea" as well as with his long waves (cf. fig. 6).

The second example in table 3 (photographs taken aboard S.S. *Europa* on 3/4/1939) is based on four wave charts of a fully developed storm sea; here only the "sea" is caught with a wave length of 350 m and a height of 13 m, which is in good agreement with the calculation after Neumann. The extent of the chart is not large enough to comprise the "long wave," which in this case would be 675 m long.

These four wave charts, the last two of which are reproduced in figures 7 and 8, represent the state of the sea every second. Thanks to the long rolling period of the *Europa* (20 to 25 seconds) and to the installation of the photo-apparatus not too far from the ship's longitudinal, or rolling,

[5] In the original publication the isohypses have a distance of only 20 cm, or 7.5 inches.

axis, the differences in the height of the apparatus above the sea surface are rather small. Therefore, corresponding wave profiles taken from the charts under consideration of the ship's speed will give a quasiquantitative representation of propagation of waves within 4 seconds. In figure 9 this process is shown by the development of four profiles which are shifted over the four wave charts according to the ship's speed. (The profiles

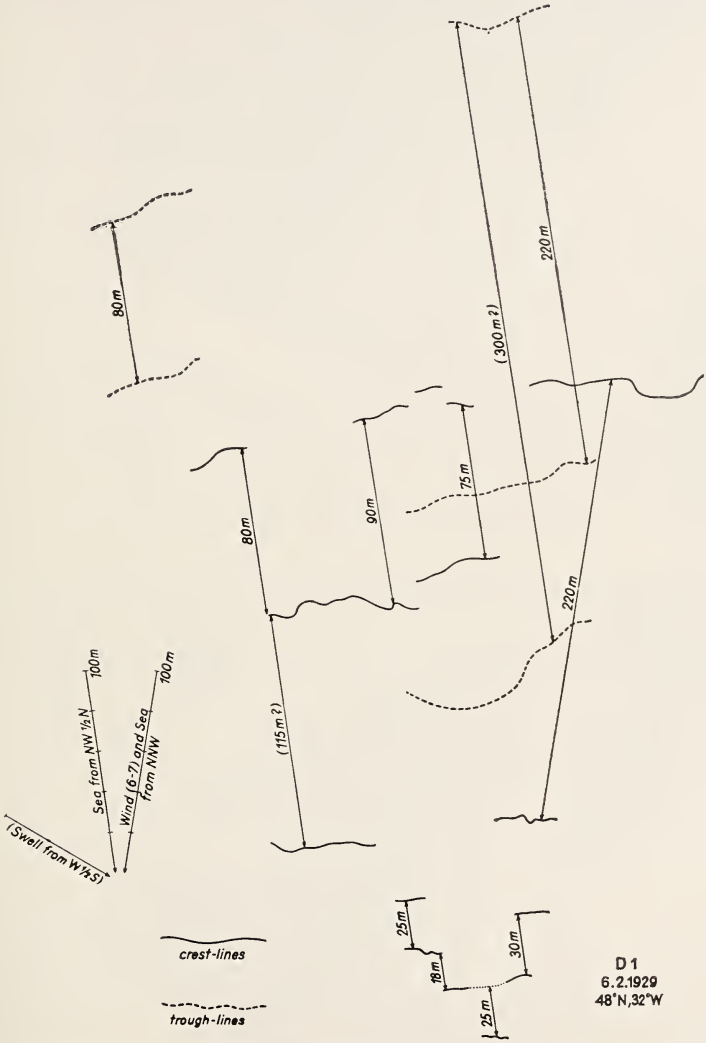

FIGURE 6. *Plan of wave crests and troughs taken from wave chart from North Atlantic Ocean.*

are confined to the foreground and the center of the charts.) By the way, the main wave crest is advancing at an average speed of 15 m/sec from wave charts 1 to 4, or at 11 m/sec between charts 3 and 4. As for the order of magnitude, these two values are in good agreement with the value

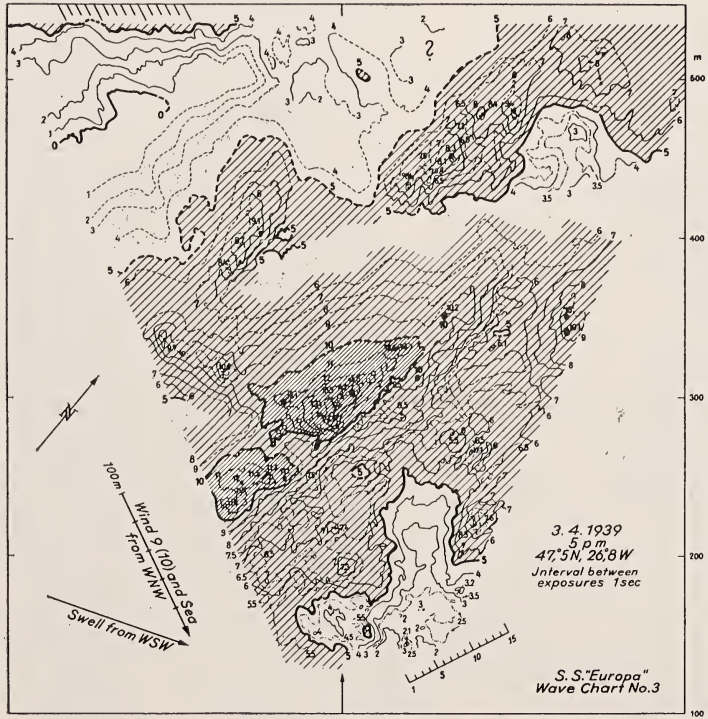

Fig. 7

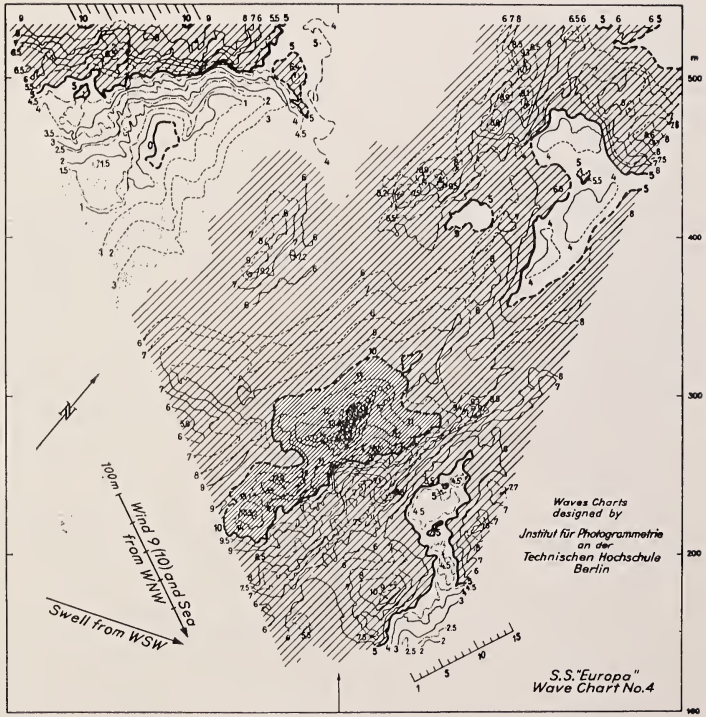

Fig. 8

Jn both charts the plane of reference for isohypses is 33,5 m below the left object lens

FIGURES 7 and 8. *Wave chart from photographs taken from S. S. Europa.*

of group velocity, u, (about 12 cm/sec) which, after Stokes' formula $u=\frac{1}{2}c$, results from a wave length of 360 m ($c=1.25\sqrt{\lambda}$).

Finally, I should like to add some general and rather simple remarks on exact wave measurements. Certainly, all methods and apparatus of wave investigation have merits and disadvantages of their own: probably most of them either surface wave recorders or pressure recorders [12 to 15] while yielding comparatively much more observational material, are not so expensive as stereophotogrammetry.

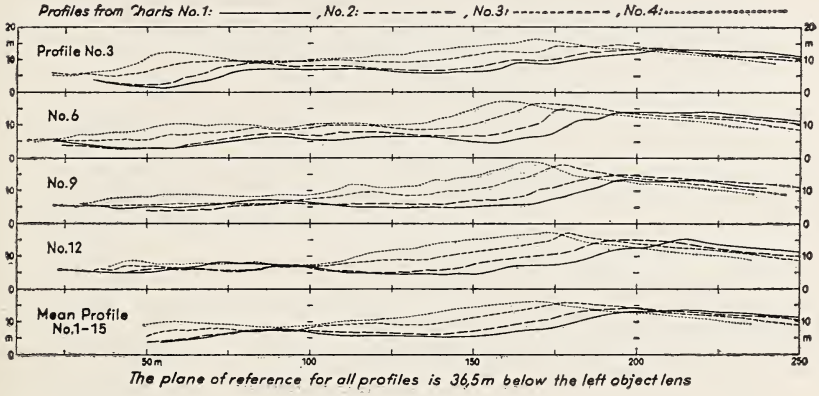

FIGURE 9. *Wave profiles taken from wave charts.*

However, from theoretical, practical, and didactic view points it seems not only useful but necessary to have exact *three*-dimensional representations of waves. For instance, it is probably a matter of makeshift (and in the course of time it may prove to be insufficient) that the steepness of waves is indicated by $H:\lambda$ without referring to the different lengths of the two wave slopes. Furthermore, e.g., the relation of crest lengths to wave lengths can be studied only in this way. Certainly, the cinestereophotogrammetrical method is much more effective than the method of single shots, since it enables the time to be combined with the three dimensions of space at least in a quasiquantitative way. At any rate the simple chance that a number of consecutive films will be realizable, even if full wave periods have not always been covered, greatly helps to diminish the risk of a wave-research voyage with a stereophotogrammetric apparatus of rapid sequence of pictures. As for the apparent costs of wave cinestereophotogrammetry, I may just refer to a remark of Mr. Mason [16] concerning "potential savings" in more efficient design of maritime structures which may be as well applied to naval architecture. The possibility of such savings should cause ideas of uneconomical research to be set aside. In Germany the above quoted cine-stereophotogrammetric investigations will hardly be resumed for a long time to come, but it is hoped that one day it will be possible to continue the evaluation of the films obtained in the spring of 1939. I should like to conclude with the hope that American oceanographers, naval architects, and maritime engineers, will become interested in this method of wave research, ship- or shore-borne, as well as air-borne.

References

[1] Laas, W., Die photographische Messung der Meereswellen. Veröff. Inst. f. Meereskunde. N. F. A. Heft 7. Berlin 1921.

[2] Kohlschütter, E., Stereophotogrammetrische Arbeiten. Forschungsreise S. M. S. "Planet". 3, 135. Berlin 1909.

[3] Schumacher, A., Stereophotogrammetrische Wellenaufnahmen. Wiss. Erg. Dtsch. Atlant. Exped. "Meteor" 1925/7, 7, Heft 2, Lfg. 1 (with atlas) Berlin 1939.

[4] Schumacher, A., Untersuchung des Seegangs mit Hilfe der Stereophotogrammetrie. Jahrbuch 1936 Lilienthal-Ges. f. Luftfahrtforschung. Berlin 1936, 239.

[5] Weinblum, G., and Block, W., Stereophotogrammetrische Wellenaufnahmen. Schiffbautechn. Ges. 36. ord. Hauptvers. Berlin 1935.

[6] Schumacher, A., Stereophotogrammetrische Wellenaufnahmen mit schneller Bildfolge. Dtsch. Hydrogr. Z. 3, 1950, 78.

[7] Hidaka, Koji, A stereophotogrammetric survey of waves and swells in the ocean. Me. Imp. Mar. Obs. Kobe 1941, 7, Nr. 3 231–368.

[8] Neumann, G., Über Seegang, Dünung und Wind. Dtsch. Hydrogr. Z. 3, 1950, 40, (53, footnote).

[9] Sverdrup, H. U. and Munk, W. H., Sea and swell: Theory of Relations for Forecasting. H. O. Pub. No. 601, U. S. Navy Dept. Hydrogr. Off. 1947.

[10] Neumann, G., On the complex nature of ocean waves and the growth of the sea under the action of wind. Symposium on Gravity Waves. Washington. June 18–20, 1951. This volume page.

[11] Neumann, G., Über die komplexe Natur des Seeganges I, II. Will be published in Dtsch. Hydrogr. Z.

[12] Pabst, W., Über ein Gerät zur Messung und Aufzeichnung des Seeganges. DVL-Jahrbuch 1933, II, 13.

[13] Joseph, J., Meereskundliche Messgeräte. Geophysik II. Naturforschung u. Medizin in Deutschland 1939-46. 18, Wiesbaden.

[14] Seiwell, H. R., Sea Surface roughness measurements in theory and practice. Ocean surface waves. Annals of the New York Academy of Science 51, Art. 3, S. 483.

[15] Ewing, M., and Press, Fr. Notes on surface waves. Ibid. S. 453.

[16] Mason, M. A. Ocean wave research and its engineering applications. Ibid. S. 523 (531).

12. Steady-State Characteristics of Subsurface Flow

By Arthur T. Ippen [1] and Donald R. F. Harleman [1]

Some analytical and experimental observations concerning steady state characteristics of subsurface flows or density currents are presented.

(a) The uniform flow of a density current in the laminar and transition region is investigated experimentally by varying the channel slope, rate of flow, and density difference. Vertical velocity distributions in the subsurface flow and across the interface are obtained from motion pictures of falling droplets. From these data a general coefficient C in the modified Chezy equation is determined for laminar flow conditions. The influence of the ratio of depth to an adjusted hydraulic radius taking account of shear at the interface is generalized for the range of experimental data.

(b) The interfacial waves, which in breaking give rise to mixing of the dense liquid with the clear liquid above, are investigated according to the various criteria for wave stability. These criteria are shown to be inter-related by a wave length fundamental to the critical regime of flow. The influence of depth upon such wave motion is shown to be negligible and interfacial waves may therefore be dealt with by "deep-water" relationships.

(c) The front of a subsequent density current in uniform motion is defined by a characteristic head or initial surge of larger depth moving with essentially constant shape and velocity. Measurements obtained from motion pictures of the transit of these fronts through the experimental flume result in a dimensionless representation of their shapes. The assumption of a particular potential flow that fits the experimentally determined shapes permits the calculation of dynamic pressures acting on the surge fronts.

1. Introduction

Since 1947, experiments have been conducted at the Hydrodynamics Laboratory of MIT on the characteristics of flows stratified due to density differences. These flows demonstrate various open channel problems in slow motion due to the greatly reduced influence of the gravitational forces. While laminar flow conditions prevail, these phenomena are subject to theoretical solution.

The following problems are to be dealt with at this time:

1. A steady uniform density current having a depth d is produced along the bottom of an inclined rectangular tank. The depth, d, is small in comparison with the depth of the lighter fluid above. The driving force due to the small density difference between the fluid of the subsurface flow and that of the supernatant fluid is in equilibrium with the shear forces exerted by the stationary walls and by the moving interfacial boundary. The independent variables are velocity, depth to width ratio, channel slope, and density difference. The interface between the two fluids is distinct and smooth up to the point of mixing. The problem is to determine the general relationship between the above variables when laminar flow conditions are maintained.

[1] Massachusetts Institute of Technology, Cambridge, Mass.

2. The steady uniform flow conditions of these subsurface currents are adjusted until interfacial waves appear. The ultimate breaking of these waves leads to mixing of the denser fluid with the supernatant layer. The experimental flow and wave characteristics in this critical region are compared to various criteria for wave stability.

3. Upon releasing an underflow into the channel and maintaining thereafter a constant rate of flow an initial head or surge of larger than uniform depth is built up at the front of the stream. This head moves with essentially constant shape and velocity. The characteristic shape of this frontal surge is presented in dimensionless form.

The experimental difficulties are considerable due to the small density differences involved and the consequent low velocities which are encountered. Therefore, special techniques had to be developed in order to produce measurements of sufficient accuracy.

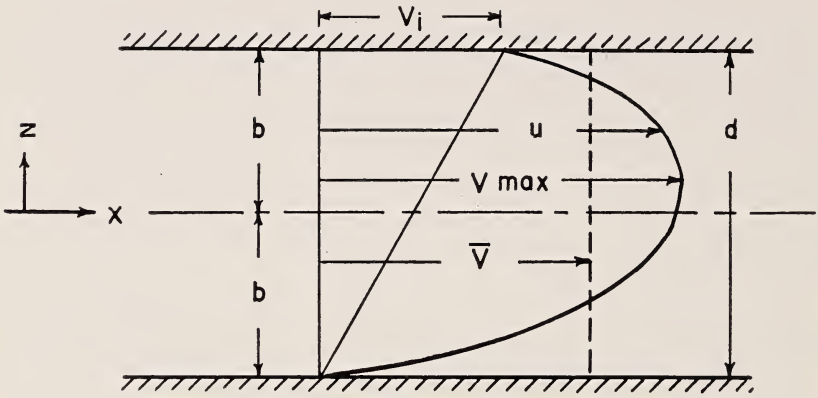

FIGURE 1. *Laminar flow between parallel boundaries.*
Upper boundary in motion.

2. Uniform Subsurface Flow

2.1 Laminar Flow Theory-Velocity Distribution

The equation of motion for the laminar flow of an incompressible fluid underneath a lighter fluid may be obtained by analogy to the case of laminar flow between parallel plates, the upper one of which is in motion relative to the lower stationary plate. Let the channel bottom be represented by the lower plate and the interface by the moving upper plate, then following the notation of figure 1, the equation of motion for two-dimensional conditions may be written as

$$u = V_i\left(\frac{b+z}{2b}\right) + \frac{z^2-b^2}{2\mu}\frac{\partial}{\partial x}(p+\gamma h)\cdot \tag{1}$$

The parabolic distribution curve is displaced by an amount varying directly with the velocity of the moving boundary, and thus the mean velocity, $\bar{V}$, in the x-direction has the magnitude

$$\bar{V} = \frac{V_i}{2} - \frac{b^2}{3\mu}\frac{\partial}{\partial x}(p+\gamma h)\cdot \tag{2}$$

Equation 1 may be applied to the subsurface flow in the following manner. Let $d=2b$ be the depth of the underflow; γ and γ' be the specific weights of the lower and upper fluids, respectively; and S be the slope of the energy gradient. Therefore, $\partial h/\partial x=-S$ is the elevation change; $\partial p/\partial x=\gamma' S$ is the pressure change; and $\partial/\partial x(p+\gamma h)=-\Delta\gamma S=-\Delta\rho g S$ with $\Delta\gamma=\gamma-\gamma'$ and $\nu=\mu/\rho$.

Equation 1 may then be rewritten as

$$u=V_i\left(\frac{1}{2}+\frac{z}{d}\right)-\frac{\Delta\rho}{\rho}gS\frac{d^2}{2\nu}\left(\frac{z^2}{d^2}-\frac{1}{4}\right). \tag{3}$$

Substituting for V_i in terms of $\bar{V}$ from eq 2, the dimensionless velocity distribution law can be stated as follows:

$$\frac{u}{\bar{V}}=1+2\left(\frac{z}{d}\right)-\frac{1}{2J}\left[\left(\frac{z}{d}\right)^2+\frac{1}{3}\frac{z}{d}-\frac{1}{12}\right]. \tag{4}$$

In this equation, the parameter $\bar{V}\nu/\left(\frac{\Delta\rho}{\rho}gSd^2\right)$ has been replaced by J, indicating the ratio of viscous forces to gravity forces. This parameter, J is readily shown to be equivalent to

$$J=\frac{\bar{V}\nu}{\frac{\Delta\rho}{\rho}gSd^2}=\frac{F^2}{N_R S}, \tag{5}$$

where

N_R = Reynolds number, defined as $\bar{V}d/\nu$,

F = Froude number, defined as $\bar{V}\Big/\sqrt{\frac{\Delta\rho}{\rho}gd}$.

The interface velocity, V_i, results by substituting $z=+d/2$,

$$\frac{V_i}{\bar{V}}=2-\frac{1}{6J}. \tag{6}$$

The location of the maximum velocity, V_m, is obtained by setting the derivative of eq 3 with respect to z equal to zero

$$\frac{z_m}{d}=2J-\frac{1}{6}. \tag{7}$$

Substituting this value in eq 4, the relation between the maximum and mean velocities is obtained

$$\frac{V_m}{\bar{V}}=\frac{2}{3}+2J+\frac{1}{18J}. \tag{8}$$

If eq 6 is divided by eq 8, the relation between the interface and maximum velocity is obtained

$$\frac{V_i}{V_m}=\frac{12J-1}{12J^2+4J+\frac{1}{3}}. \tag{9}$$

It should be noted that the velocity distribution given by eq 4 has two limiting conditions that are of interest here.

(a) Parallel flow between stationary plates; therefore, $V_i=0$, and from eq 6 $Js=1/12=0.083$.

(b) Parallel flow with upper surface free, or laminar flow in an open channel; therefore the maximum velocity occurs at $z_m/d=+0.5$, and from eq 7 $J_f=1/3=0.333$.

Therefore, the value of J for all uniform two dimensional subsurface flows must lie between 1/12 and 1/3. While the value of J may vary between these limits, it can be shown that the ratio V_i/V_m must be a constant if the region near the interface is treated as a problem of laminar boundary layer development between parallel streams. This problem was investigated first by Keulegan [1] [2] in 1944, and again by Lock [2] in 1951. Both determined the velocity distribution and the growth of the laminar boundary layer for the steady flow of a stream of viscous incompressible fluid in contact with a parallel stream of different velocity, density, and viscosity. Both streams are assumed to be of *infinite* extent in the direction normal to the interface. For the case in which the heavier fluid is in motion with a velocity V_m and the lighter fluid is at rest, Keulegan and Lock have shown that the ratio of interface to maximum velocity is a constant depending only on the density and viscosity ratios of the two fluids. For the range of densities and viscosities encountered in the flows of the present investigation, these fluid property ratios may be taken as unity with negligible error and the corresponding velocity ratio is $V_i/V_m=0.59$, in accordance with table II of [1]. Substituting this value in eq 9, J is found equal to 0.138. However, for cases of widely differing fluid properties, this constant obviously varies from the value given, and the following treatment must be adjusted accordingly.

For the problem under investigation, the case of indefinitely growing zones of flow near the interface must be combined with the limitation imposed by the bottom boundary. In the initial phase of establishing the underflow, a laminar boundary layer will grow upward from the bottom, as well as downward from the interface. Beyond the point where these two boundary layers meet, the velocity distributions must remain fixed in a manner analogous to the cases of channel and pipe inlets. There seems little question that this is the case (see fig. 4). It follows that the ratio of energy dissipated in the underflow to that dissipated in the supernatant fluid is also constant, since the interfacial shear is constant as soon as these equilibrium conditions are established. The influence of the underflow remains confined to a relatively narrow zone in the upper fluid. With $J=0.138=$ constant, it follows from definition that in the two dimensional flow

$$S=\frac{1}{J}\frac{\bar{V}d\nu}{d^3\frac{\Delta\rho}{\rho}g}=7.25\frac{\mu}{\Delta\gamma}\frac{q}{d^3}. \tag{10}$$

In a given channel, therefore, and with the fluid properties fixed, the depth, d, varies with the third root of the discharge, q. Also, for a constant discharge, the depth will vary inversely with $S^{\frac{1}{3}}$ as the slope changes along the course of the undercurrent.

[2] Figures in brackets indicate the literature references on p. 93.

2.2 Generalized Resistance Function for Laminar Underflows

(a) Two-dimensional case

For comparison with established relations for free surface and for closed conduit flow, it is desirable to express the parameter, J, in its relation to the familiar resistance coefficient, c_f. The latter coefficient is useful for laminar as well as turbulent flow conditions and is defined usually from

$$\tau = c_f \cdot \frac{\rho \bar{V}^2}{2}, \tag{11}$$

where τ is the shear on the fixed boundary, and $\bar{V}$, as before, represents the average velocity of the flow. Assuming a uniform steady underflow on a sloping bottom, the driving gravity force over a unit area is in equilibrium with the shear stresses

$$\Delta\rho g d S = \tau_0 + \tau_i, \tag{12}$$

where S equals the sine and approximately the tangent of the channel inclination, τ_0 is the bottom shear, and τ_i the interfacial shear.

At this point, the effective hydraulic radius, R_e, is introduced. The hydraulic radius is commonly defined as the ratio of cross-sectional area to wetted perimeter; i.e., it represents a purely geometric property of the channel. For subsurface flows, however, the interface shear is less than the fixed boundary shear. The shear varies linearly from a maximum τ_0 to zero at the point of maximum velocity to $\tau_i < \tau_0$ at the interface. Letting $\tau_i = \alpha\tau_0$, the total shear at the interface may be replaced by its equivalent; i.e., a shear stress, τ_0, applied over a width reduced from unit width to α. Shear on lateral boundaries is not considered for the present. Thus the effective hydraulic radius is simply

$$R_e = \frac{d}{1+\alpha}. \tag{13}$$

The ratio α can also be defined in terms of z_m/d (eq 7)

$$\alpha = \frac{1 - \dfrac{2z_m}{d}}{1 + \dfrac{2z_m}{d}} = \frac{\dfrac{1}{3} - J}{\dfrac{1}{6} + J}. \tag{14}$$

For open channel flow, $\alpha = 0$, and $R_e = d$, while for flow between stationary plates, $\alpha = 1$ and $R_e = d/2$. Eliminating τ_i in terms of α

$$\tau_0 = \Delta\rho g R_e S. \tag{15}$$

With the definition of τ from eq 11

$$\bar{V} = \sqrt{\frac{2g}{c_f}} \sqrt{\frac{\Delta\rho}{\rho}} R_e S. \tag{16}$$

From eq 5, J may be related to the resistance coefficient, c_f

$$\frac{1}{c_f} = \frac{1+\alpha}{2} J N_R = \frac{1+\alpha}{2} \frac{F^2}{S}. \tag{17}$$

Since for underflows with small differences of viscosity and of density J has been shown to have a constant value of 0.138, α has a corresponding value of 0.64 (eq 14). Thus the laminar resistance law for these cases becomes

$$\frac{1}{c}=0.114N_R. \tag{18a}$$

For comparison, the equation for flow between stationary plates becomes

$$\frac{1}{c_f}=0.083N_R=\frac{N_R}{12}, \tag{18b}$$

and for free surface flow

$$\frac{1}{c_f}=0.167N_R=\frac{N_R}{6}. \tag{18c}$$

It is clear that the differences in the constants in eq 18a and 18c are inherent entirely in the definition of N_R and J. If the velocities in the Reynolds number and in the parameter J were expressed as maximum velocities and the lengths by the effective hydraulic radii, the coefficient of N_R would be reduced to a single value.

(b) Corrections for end effects

In establishing the validity of the laminar resistance law (eq 18a) by experimental means, it is necessary to investigate the influence of the three dimensional conditions existing in the tank. Specifically, the effect of the side-wall resistance or depth-to-width ratio, which is neglected in

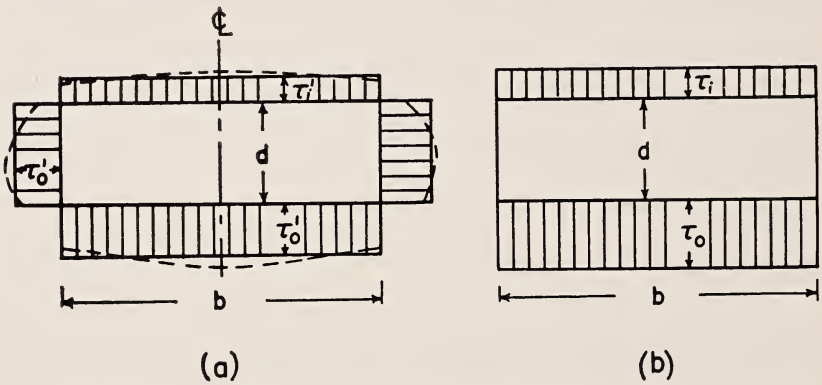

FIGURE 2. *Comparison of assumed shear distributions in* (a) *three-, and in* (b) *two-dimensional channels.*

eq 12, is to be developed by assuming the shear distribution in figure 2 as the most convenient one. Three dimensional quantities will be distinguished by primes, thus $\bar{V}'=Q/A$. Equation 12 therefore becomes

$$\Delta\rho g dS=\tau_0'(1+2d/b)+\tau_i', \tag{19}$$

where τ_0' and τ_i' are the bottom and interface shears introduced as average shears over the width and sides. Assuming the ratio of τ_i'/τ_0' again as α

and comparing it to the two dimensional case of figure 2b, the value of τ_0' may be expressed in terms of τ_0, representing the bottom shear for the equivalent two dimensional flow and therefore also the maximum value of the bottom shear for the three dimensional flow.

From symmetry it follows that the centerline mean velocity of the three dimensional case equals the mean velocity of the two dimensional case. Therefore, the ratio $\bar{V}/\bar{V}'$ is the same as τ_0/τ_0'.

$$\frac{\tau_0}{\tau_0'}=\frac{\bar{V}}{\bar{V}'}=\frac{[1+\alpha+2d/b]}{1+\alpha}. \tag{20}$$

Thus the resistance, eq 17, can be modified to contain the mean velocity $\bar{V}'$ rather than $\bar{V}$ in the JN_R parameter and can be written

$$\frac{1}{c_f}=\frac{(1+\alpha+2d/b)^2}{2(1+\alpha)}\cdot J'N_R'. \tag{21}$$

This equation is the basis for calculating the two dimensional friction coefficient from experimental three dimensional quantities with $N_R'=\bar{V}'d/\nu$ and

$$J'=(\bar{V}'\nu)\Big/\left(\frac{\Delta\rho}{\rho}gd^2S\right).$$

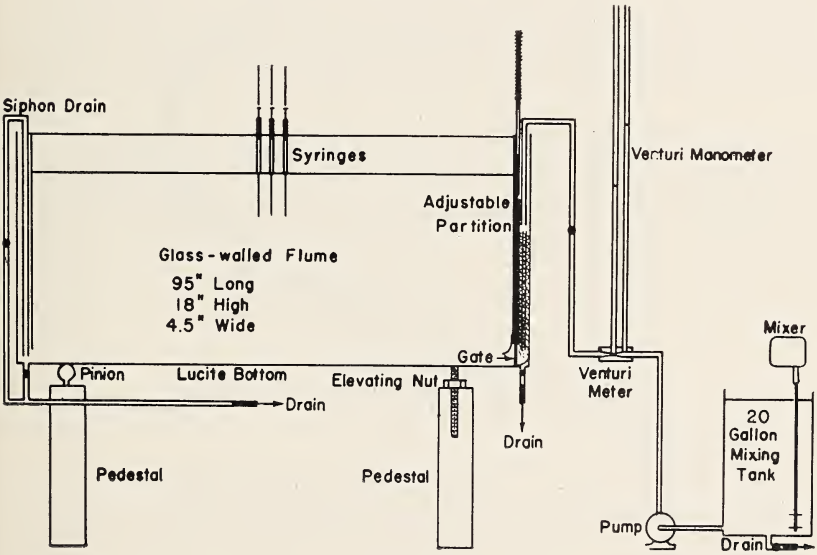

FIGURE 3. *Schematic diagram of density-current flume.*

2.3 Experimental Results

The essential components of the experimental apparatus are shown in figure 3. The glass walled flume is initially filled with clear water. The heavier liquid for the underflow is produced in a mixing tank by adding salt to give the required density difference. This salt solution is pumped through the Venturi meter to the extrance chamber. A quick-opening

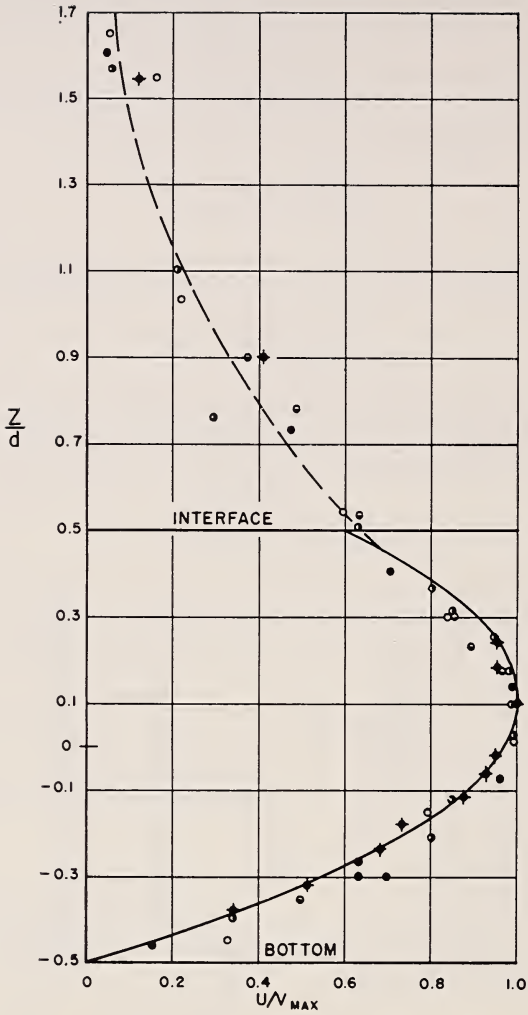

FIGURE 4. *Velocity distribution in uniform underflow.*

Symbol	Slope	$\Delta\rho/\rho$	$\overline{V}$	d	J
			ft/sec	*ft*	
◐	0.005	0.0075	0.044	0.062	0.121
◑	.005	0107	.064	.058	.158
⊗	.010	.0132	.062	.042	.151
●	.015	.0035	.074	.062	.130
○	.015	.0090	.096	.046	.143
Average					0.140

gate releases the mixture into the flume. It proceeds along the bottom to the far end where a siphon drain removes the underflow from the exit chamber. After a uniform depth has been established along the length of the flume, the discharge and depth are measured. The entire channel can be tilted by raising the upper end, and slopes greater than 15 percent can be obtained. For each run the variables are discharge, depth, slope, and density difference, and, in addition, temperatures are recorded. For 5 runs of a total of 64, actual velocity distributions were obtained during the period in which the flow was uniform. To obtain the velocity distributions, hypodermic syringes are used to inject periodically small globules of butyl phthalate and xylene dyed red. The mixture can be readily adjusted to produce a density slightly in excess of that of the two liquids in the flume and thus the globules settle slowly through the upper and lower strata to the bottom. The paths of the spheres are recorded by means of a motion-picture camera. By projecting frame by frame, the successive lateral positions of the drops are analyzed to give the velocities at various points.

The velocity distribution curves for the five runs are plotted in dimensionless form in figure 4, using the depth of the underflow and the maximum velocity as reference quantities. The experimental points are compared to the theoretical velocity distribution given by eq 4 with $J=0.138$, as described in section 1. The experimental data were obtained on the centerline of the channel, and therefore two dimensional conditions (as required by the theory) should be approximated. The value of J as calculated from the experimental data is given for each run in the table in figure 4 and varies from a minimum of 0.121 to a maximum of 0.158, with an average for all runs of $J=0.140$, which agrees with the predicted value.

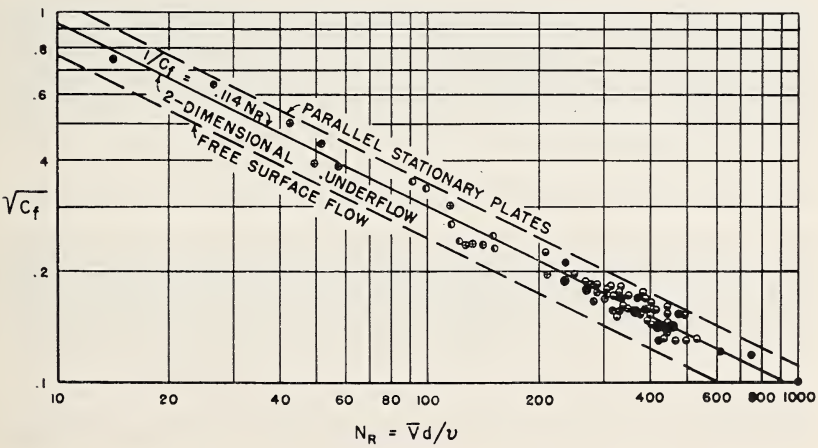

FIGURE 5. *Laminar resistance law for uniform underflow.*

⊕, Kuiper; ○, Noble and Podufaly; ◒, Braucher; ●, two-dimensional runs.

Figure 5 presents the experimental values of the resistance coefficient as calculated from eq 21, for convenience represented as $\sqrt{c_f}$ and plotted against N_R. To obtain the two dimensional N_R, the value of N_R' was corrected as per eq 20. This method gave the best agreement between

experimental and analytical results. Five points were calculated on the basis of measured two dimensional velocity distributions along the center line and fit the theoretical line very closely. An indication of the experimental range covered by Kuiper [5], Noble and Podufaly [6], and Braucher [7] is given in table 1. In all, 64 runs are represented in the plot of figure 5.

TABLE 1

All results for constant width of channel: $b = 4.5$ inches

Investigator	$\frac{\Delta\rho}{\rho}$		Slope S		Depth, d in inches	
	max	min	max	min	max	min
Kuiper	0.024	0.0017	0.188	0.0060	1.19	0.14
Noble Podufaly	.024	.005	.058	.029	1.12	.22
Braucher	.013	.0021	.015	.005	1.44	.50

3. Instability of the Interface

By increasing the rate of underflow, undulations eventually appeared at the initially smooth interface, which with further increases in flow develop to the breaking point. Figure 6 shows this phenomenon. As near to the breaking point as could be determined, observations of wave length, discharge, and depth were made to define it.

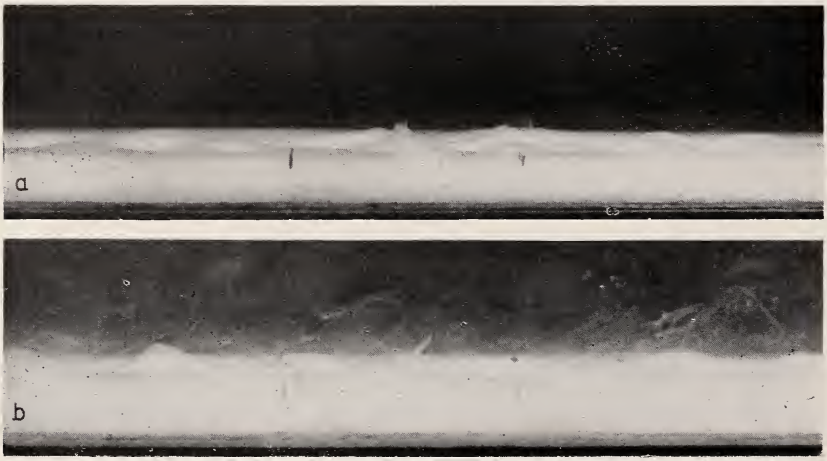

FIGURE 6. *Waves at interface of underflow.*

a, Before mixing; b, mixing with upper layer.

3.1 Stability on Basis of Inertia and Gravity Forces

On this basis, with viscous damping neglected, the limit for stable interfacial waves is the condition for which the wave celerity becomes imaginary [3, 4].

For layers of infinite thickness the relative velocity of the layers becomes critical, and waves of length λ begin to break when

$$\frac{\bar{V}_c}{\sqrt{g\frac{\Delta\rho}{\rho}\frac{\lambda}{\pi}}}=1. \tag{22}$$

With both layers finite, h being the thickness of the supernatant layer and d the depth of the underflow, this critical velocity is

$$\frac{\bar{V}_c}{\sqrt{g\frac{\Delta\rho}{\rho}\frac{\lambda}{\pi}}}=\sqrt{\frac{1}{2}\left(\tanh\frac{2\pi d}{\lambda}+\tanh\frac{2\pi h}{\lambda}\right)}. \tag{23}$$

Both equations have been plotted in figure 7, employing

$$F=\frac{\bar{V}_c}{\sqrt{g\frac{\Delta\rho}{\rho}d}} \quad \text{and} \quad \frac{2\pi d}{\lambda}$$

as convenient parameters.

It is seen that the ratio h/d is of negligible effect on d/λ until $F>1$. Therefore, for values of F lower than unity, eq 22 and 23 give the same result. The parameter F was chosen in preference to the one employing the wave length for its significance in free surface flow, the celerity $\sqrt{g\frac{\Delta\rho}{\rho}d}$ denoting the speed of propagation of small gravity waves on the underflow. When the analogous celerity, $\sqrt{gd}$ for free surface flow becomes equal to the velocity of flow, and therefore $F_c=1$, large undulations are known to appear and the flow is denoted as critical. This condition is coincident with the minimum value of the "specific head," obtained by taking the derivative of the specified head H_s with respect to d from

$$H_s=\frac{\Delta\rho}{\rho}d+\frac{V^2}{2g}=\frac{\Delta\rho}{\rho}d+\frac{q^2}{2gd^2}. \tag{24}$$

Combining this critical value of $F_c=1$ with the stability criterion of eq 22, the critical wave length becomes

$$\lambda=\pi d. \tag{25}$$

Indeed, plotting the wave lengths λ in figure 7 in terms of πd from experimental observations for incipient mixing, i.e., at the breaking point, it is seen that the points lie close to these critical values of $F=1$ and $\lambda=\pi d$. The scattering must be attributed to observational difficulties in defining consistently the point of incipient mixing. The experimental points seem to exhibit in general slightly larger values of F than given by the theory, which neglects viscous damping.

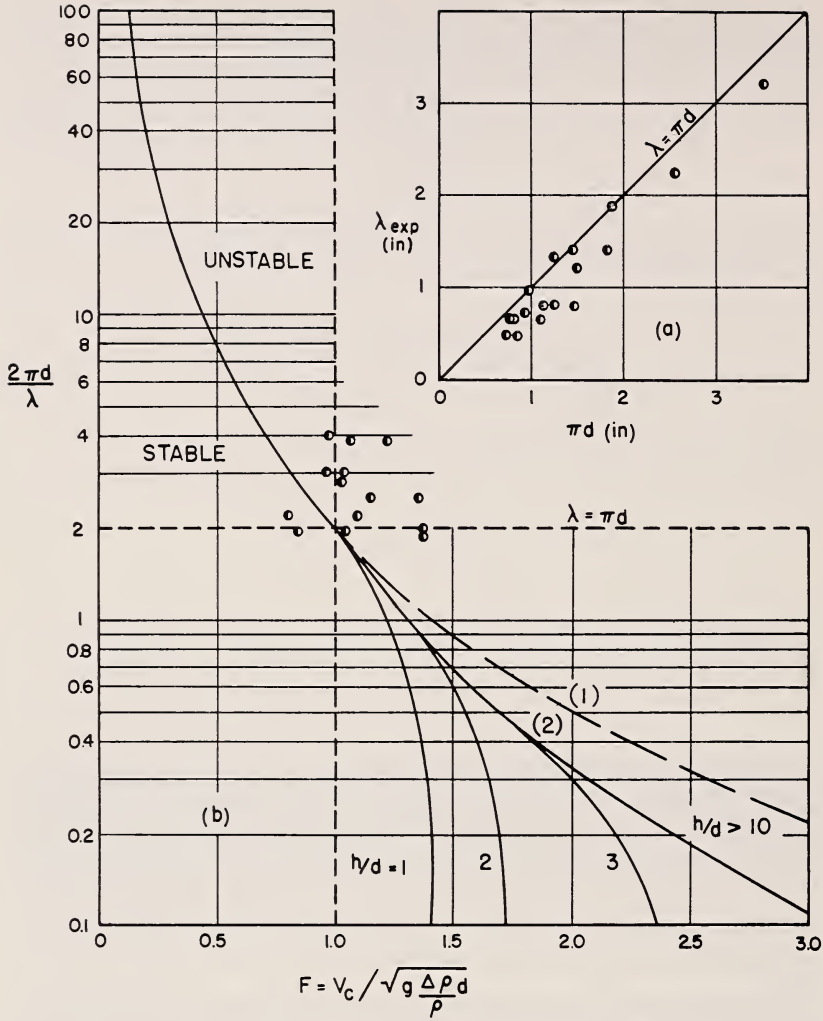

FIGURE 7. *Stability criteria for interfacial waves.*

$$(1) \quad F = \frac{V_c}{\sqrt{g\frac{\Delta\rho}{\rho}d}} = \sqrt{\frac{\lambda}{\pi d}}$$

$$(2) \quad F = \sqrt{\frac{\lambda}{\pi d}\frac{1}{2}\left(\tanh\frac{2\pi d}{\lambda} + \tanh\frac{2\pi h}{\lambda}\right)}$$

3.2 Stability on Basis of Gravity and Viscous Forces

Keulegan [8] has defined a stability parameter or criterion for mixing under these conditions as

$$\theta = \frac{\nu g \frac{\Delta\rho}{\rho}}{\bar{V}^3}, \tag{26a}$$

which is readily transformed for the case in question into the form

$$\theta=\frac{1}{F^2N_R}\cdot \tag{26b}$$

If, as postulated in the preceding section, the surface disturbances become unstable for a critical value of $F_c=1$, the critical value of θ at which mixing begins is simply

$$\theta_c=\frac{1}{N_R}\cdot \tag{27a}$$

From eq 18a, it is seen that θ_c is related to a critical friction factor c_f as long as laminar flow exists

$$\theta_c=0.114c_{fc}. \tag{27b}$$

Equations 16 and 17 imply that again for $F_c=1$ and for $\alpha=0.64$, this critical value of θ_c is established for a critical slope

$$S_c=7.2\theta_c=0.82c_{fc}. \tag{28}$$

Since the Reynolds number N_R depends only on the rate of flow per unit width $q=\bar{V}d$ and the viscosity of the fluids involved, the values of the instability criterion θ_c and of the critical slope S_c are immediately obtained. For all values of $F<1$, and thus with θ values larger than θ_c (see eq 26b), no mixing should occur.

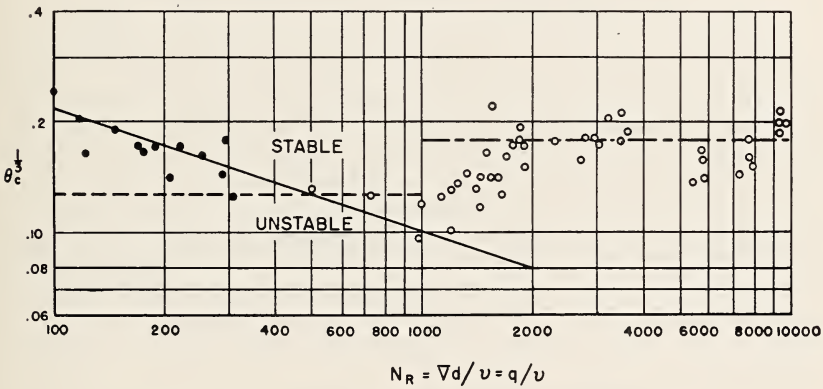

FIGURE 8. *Instability criterion for two-dimensional flow.*

● ———— $\theta_c=1/N_R$, laminar range, M.I.T.
○ – – – – – $\theta_c=0.127$, laminar range, Keulegan.
○ —·—·— $\theta_c=0.178$, turbulent range, Keulegan.

Figure 8 presents the data obtained during the present investigation, together with Keulegan's data [8], which for convenience are stated here in terms of $\theta_c^{\frac{1}{3}}$ to conform to his definition of θ, with Reynolds numbers adjusted from his definition of

$$\frac{V_cR}{\nu}=\frac{V_cd}{4\nu} \quad \text{to} \quad N_R=\frac{V_cd}{\nu}\cdot$$

It is seen that instability in the laminar range occurs essentially as specified by eq 27 and not in accordance with a constant value of $\theta_c^{\frac{1}{3}} = 0.127$. The variations of the experimental results from the theoretical line are as in figure 7 and are due to the difficulty in defining the experimental point of instability and in determining accurate values of $\Delta\rho/\rho$ for the small density differences employed. Table 2 lists the results of the experiments of Noble and Podufaly [6] on incipient mixing.

TABLE 2. *Summary of runs at mixing*

$\frac{\Delta\rho}{\rho}$	S	d	λ	F	N_R
		in.	*in.*		
0.001	0.029	1.13	3.2	0.79	290
.001	.087	0.44	1.4	1.37	122
.003	.029	.56	1.4	1.35	304
.005	.029	.56	1.8	1.08	287
.005	.058	.38	1.3	1.37	207
.005	.087	.30	1.0	0.83	100
.010	.029	.44	0.7	.97	252
.010	.058	.34	.7	1.06	190
.0145	.029	.38	.8	0.95	220
.0145	.058	.28	.7	1.15	174
.0145	.087	.27	.5	1.22	169
.024	.058	.25	.55	1.03	147
.024	.087	.22	.5	1.01	117

4. Initial Head of the Underflow

When first released into the channel, the front portion of the moving underflow has been observed to have a characteristic "head," or bulge, of greater thickness than the uniform current following. The shape of this head is of considerable interest and it has been pointed out that this phenomenon has its counterpart in certain meteorological events of which the moving cold front is perhaps the most familiar.

A qualitative analysis of the flow conditions at the head of the underflow shows that as the current moves along the channel it displaces the lighter fluid upward. A force must be provided to accelerate the fluid initially at rest and to overcome the interfacial as well as the fixed boundary resistance. This initial force is obviously larger than the gravity forces maintaining the subsequent uniform motion. Therefore, this increased driving force for the head calls for an increase of the initial depth of the underflow to $d_2 > d$.

The shape of the front was obtained by Braucher [7] experimentally by taking motion pictures of the flow at certain positions along the flume. The pictures were projected by single frames and the shape was traced directly. By comparing the same head at various positions, it was found that the front moved with essentially constant form and velocity. For the range of variables involved in these experiments, it was found that the shape could be presented as a single dimensionless curve, using the maximum thickness d_2 as the reference quantity. This curve, with readings indicated from the various experimental profiles, is shown in figure 9. Of interest is the lifting of the nose of the surge above the channel bottom in the front, its relatively short length, and rather abrupt change in the rear to the depth of uniform flow.

The experimental data employed in confirmation of the analytical treatment presented were taken from theses for the degree of M.S. carried on under the supervision of the authors by Kuiper, Noble, and Podufaly, and Braucher, which are acknowledged in the references.

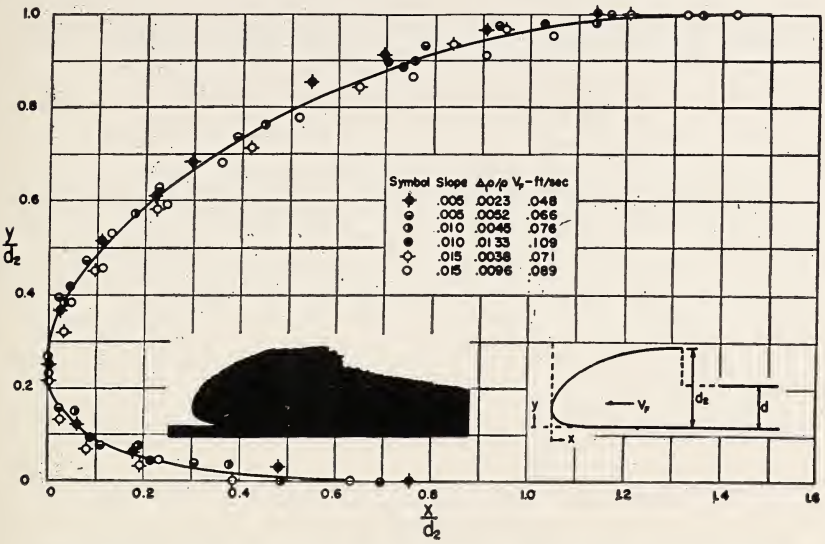

FIGURE 9. *Shape of density-current surge front moving with constant velocity.*

5. References

1] Keulegan, G. H., Laminar flow at the interface of two liquids, Journal of Research National Bureau of Standards 32, 303 (1944) RP1591.

[2] Lock, R. C., The velocity distribution in the laminar boundary layer between parallel streams, Quart. J. Mech. and Applied Math. March 1951.

[3] Lamb, H., Hydrodynamics, 6th Edition, Dover Publications, New York 1945.

[4] Harleman, D. R. F., Characteristics of density currents, M.I.T. thesis (S.M.) 1947.

[5] Kuiper, E., Sedimentation in storage reservoirs, M.I.T. thesis, (S.M.) 1947.

[6] Noble, C. and Podufaly, E., Investigation of mixing criteria for density currents, M.I.T. thesis (S.M.) 1948.

[7] Braucher, E., Initial characteristics of density current flow, M.I.T. thesis (S.M.) 1950.

[8] Keulegan, G. H., Interfacial instability and mixing in stratified flows, Journal of Research, National Bureau of Standards 43, 487 (1949) RP2040.

13. Wave Intensity Along a Refracted Ray [1,2]

By W. H. Munk [3] and R. S. Arthur [3]

This paper is concerned with the application of ray theory to the calculation of the intensity of waves refracted in an arbitrary, two-dimensional velocity field, $c(x,y)$. A *ray* equation determines the path of the rays (orthogonals), and an equation of *ray separation* expresses the convergence or divergence along a ray. These two equations are combined into an equation of *wave intensity*, from which the intensity *along* a ray can be determined given only the ray path and the wave velocity both on and near the ray. This procedure has advantages over the usual method of computing intensity from measurements of the distance *between* adjacent rays.

Application is made to special types of velocity fields. It is demonstrated that periodic convergences of rays with associated maxima of intensity occur along the axes of certain types of symmetrical underwater ridges (or of any comparable channel of minimum velocity). Along the axes of symmetrical underwater troughs the rays diverge and the intensity diminishes exponentially. Numerical and graphical methods for obtaining solutions over a complex bottom are outlined.

1. Introduction

Observed changes in the height of waves entering shallow water have been accounted for on the basis of the change in group velocity and the effect of refraction. For a wave train of given period the group velocity is a function of depth only, and any variation in wave height along a fixed depth contour is, therefore, the result of refraction. The *refraction factor*, K, is a linear measure of this effect.

Wave rays (or orthogonals) are defined as lines which are everywhere perpendicular to the wave fronts. They may be visualized as the wakes behind surfboards which are always oriented normal to the crests, that is, in the direction of wave motion. Let l_0 designate the distance between adjacent rays at some initial depth, l the distance between the same rays at an arbitrary depth, and $\beta = l/l_0$ the *ray separation factor*. Then

$$K = |\beta|^{-\frac{1}{2}}, \quad K_b = |\beta|^{-\frac{1}{5}}, \tag{1.1}$$

depending on whether the arbitrary depth is outside or within the breaker zone (Munk and Traylor, 1947).

Over a complex bottom, β can be determined by graphical methods. One technique (Hydrographic Office, 1944) consists of constructing the wave fronts by a method analogous to Huygen's and then drawing the rays. Another method (Johnson, O'Brien, and Isaacs, 1948) makes it possible to draw rays immediately. In either method the refraction factor is obtained by measuring the distance *between* adjacent rays. Here it will be shown how the refraction factor *along* a ray can be determined

[1] Contributions from the Scripps Institution of Oceanography, New Series, No. 000.

[2] Sponsored by the U.S. Navy Office of Naval Research, Project NR-083-005, Contract N6ori-111, Task VI, and the U.S. Army Beach Erosion Board, Contract W-49-055 eng 3.

[3] University of California, Scripps Institution of Oceanography.

directly. The latter procedure alone appears to be feasible in the case of extreme convergence, such as occurs near focal points and caustics (Pierson, 1951), or in the case of extreme divergence. However, these are precisely the conditions for which the approximations underlying any of these methods, including ours, must be critically examined.

In the construction of refraction diagrams it is assumed that the expression

$$c^2 = \frac{g}{k} \tanh kh$$

for the velocity c of a wave of length $2\pi/k$ at constant depth h is an adequate approximation in the case of sloping bottoms. This assumption is supported by observations as well as theoretical investigations of certain special cases (Lewy, 1946; Stoker, 1947; Lowell, 1949). The computation of intensity from these refraction diagrams is based on ray theory. For very shallow water Lowell (1949) has shown this procedure to be justified, except in regions of strong convergence or divergence of rays. No attempt to justify ray theory is intended in the development that follows.

2. The Ray Equation

Starting from Fermat's principle, according to which the ray is a path of minimum travel time, it can be shown that the expressions for parametric representation of the ray, $x = x(t)$ and $y = y(t)$, satisfy the equations

$$\frac{dx}{dt} = c \cos \alpha; \quad \frac{dy}{dt} = c \sin \alpha; \quad \frac{d\alpha}{dt} = -\frac{Dc}{Dn}, \qquad (2.1a,b,c)$$

where t is the travel time, α the angle between the ray and the x-axis, and D/Dn denotes differentiation with respect to arc length n along the wave front (fig. 1). The derivation of eq 2.1 requires that the wave velocity, c, be a *given* function of x,y which, along with the necessary partial derivatives, is continuous. An even more general form of eq 2.1 is valid for waves refracted in the presence of a current as long as the conditions on c obtain (Arrow, 1949; Arthur, 1950).

Elimination of α from eq 2.1a,b yields

$$dt = (1/c)\sqrt{(dx)^2 + (dy)^2} = (1/c)Ds,$$

where s is the arc length along the ray. Substitution in eq 2.1c gives the ray equation[4]

$$\frac{D\alpha}{Ds} = -\frac{1}{c}\frac{Dc}{Dn}, \qquad (2.2)$$

which states that the curvature of the ray is equal to the logarithmic velocity gradient along the wave front and that the ray bends toward the direction of lower velocity.

[4] Equation 2.2 can be derived directly from the eikonal equation, which is the fundamental equation of the wave fronts. Frank, Bergmann, and Yaspan (1946, pp. 42–46) give a complete development. Equation 2.2 follows immediately from eq 22 of their paper when specialized to two dimensions. See also, eq 3.5 of Lowell (1949, p. 283), which is identical with eq 2.2.

3. The Equation of Ray Separation

The variation of β in terms of the arc length s along a ray is derived from elementary considerations using figure 1. If α denotes the angle between the ray and the x-axis at point P, the corresponding angle of a ray through A, an infinitesimal distance l removed, is $\alpha + D\alpha$, where

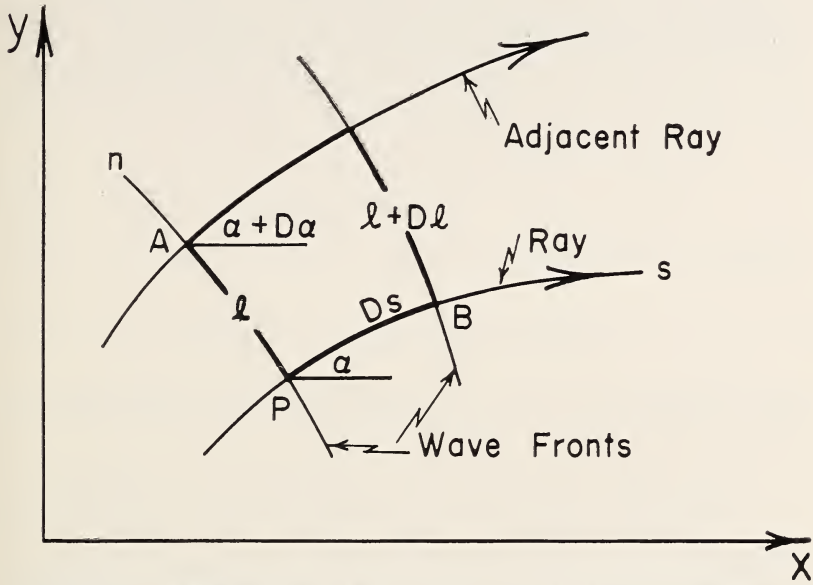

FIGURE 1. *Definition of terms used in derivation of ray equation and equation of ray separation.*

$D\alpha = (D\alpha/Dn)l$. The ray separation at B is $l + Dl$, where $Dl = D\alpha \cdot Ds$. Hence

$$\frac{1}{l}\frac{Dl}{Ds} = \frac{D\alpha}{Dn}. \tag{3.1}$$

In terms of $\beta = l/l_0$, the equation of ray separation

$$\frac{1}{\beta}\frac{D\beta}{Ds} = \frac{D\alpha}{Dn} \tag{3.2}$$

is obtained. According to eq 3.2 the logarithmic change in the separation factor along the way is equal to the curvature of the wave front. Lowell (1949, p. 286) has derived this equation in a more systematic manner, using the Gauss integral theorem.

It is to be emphasized that differentiation with respect to arc length s and n is accomplished by use of the special operators

$$\frac{D}{Ds} = (\cos\alpha)\frac{\partial}{\partial x} + (\sin\alpha)\frac{\partial}{\partial y},$$

$$\frac{D}{Dn} = -(\sin\alpha)\frac{\partial}{\partial x} + (\cos\alpha)\frac{\partial}{\partial y}. \tag{3.3a,b}$$

The arc lengths s and n do not constitute a set of curvilinear coordinates. If a set of curvilinear coordinates r for the rays and w for the wave fronts were to be introduced, a more complete notation would be

$$(\partial/\partial s)_r \text{ for } D/D_s, \text{ and } (\partial/\partial n)_w \text{ for } D/Dn.$$

It is useful to derive a modified version of the ray-separation equation by eliminating α from the ray eq 2.2 and the ray separation eq 3.2. Because the operators 3.3 involve α, which varies differently along ray and wave front, the order of differentiation is not immaterial in the mixed second derivatives. For example, the difference of the mixed second derivatives of α, as computed from repeated use of eq 3.3 is not zero but

$$\frac{D}{Dn}\left(\frac{D\alpha}{Ds}\right)-\frac{D}{Ds}\left(\frac{D\alpha}{Dn}\right) \quad \left(\frac{\partial\alpha}{\partial x}\right)^2+\left(\frac{\partial\alpha}{\partial y}\right)^2=\left(\frac{D\alpha}{Ds}\right)^2+\left(\frac{D\alpha}{Dn}\right)^2. \tag{3.4}$$

Substitution from eq 2.2 and 3.2 gives

$$\frac{D}{Dn}\left(\frac{D\alpha}{Ds}\right)-\frac{D}{Ds}\left(\frac{D\alpha}{Dn}\right)=\frac{1}{c^2}\left(\frac{Dc}{Dn}\right)^2+\frac{1}{\beta^2}\left(\frac{D\beta}{Ds}\right)^2. \tag{3.5}$$

Differentiating eq 2.2 and 3.2 with respect to s and n, respectively, and adding, yields

$$\frac{D}{Dn}\left(\frac{D\alpha}{Ds}\right)-\frac{D}{Ds}\left(\frac{D\alpha}{Dn}\right)=-\frac{1}{c}\frac{D^2c}{Dn^2}+\frac{1}{c^2}\left(\frac{Dc}{Dn}\right)^2-\frac{1}{\beta}\frac{D^2\beta}{Ds^2}+\frac{1}{\beta^2}\left(\frac{D\beta}{Ds}\right)^2. \tag{3.6}$$

If the right-hand members of eq 3.5 and 3.6 are equated, the elimination of α from eq 2.2 and 3.2 is completed, and the final result is the modified equation of ray separation,

$$\frac{D^2\beta}{Ds^2}+k^2\beta=0, \tag{3.7}$$

where

$$k^2=\frac{1}{c}\frac{D^2}{Dn^2}. \tag{3.8}$$

Equation 3.7 relates changes in the ray separation factor along the ray to changes in wave velocity along the wave front. The solution $\beta(s)$ to this second-order equation involves two arbitrary constants that can be evaluated in terms of the initial conditions $\beta=\beta_0$ and $D\beta/Ds=K_0\beta_0$ at $s=0$. Here

$$\frac{1}{\beta}\frac{D\beta}{Ds}=\frac{D\alpha}{Dn}=\kappa \tag{3.2}$$

represents the curvature of the wave front, which is taken positive if the wave front is convex as viewed from the direction of increasing s.

Either form of the equation of ray separation contains in a compact manner the law governing the variation of intensity in a two-dimensional velocity field, according to ray optics. The simplicity of eq 3.2 and 3.7 is, however, somewhat misleading. Their application involves the con-

struction of wave fronts[5] and rays on the refraction diagram, but it is desirable to construct only rays. We shall therefore derive an equation of wave intensity that is less compact but better adapted to calculations. This equation of wave intensity will eliminate the need for constructing the wave fronts, and will allow the determination of β given only a ray path and the wave velocity everywhere, i.e., both on and near the ray.

4. Derivation of an Equation of Wave Intensity

Differentiation of c with respect to n gives

$$\frac{Dc}{Dn}=-(\sin\alpha)\frac{\partial c}{\partial x}+(\cos\alpha)\frac{\partial c}{\partial y}, \tag{4.1}$$

and

$$\frac{D^2c}{Dn^2}=-(\sin\alpha)\left\{-(\sin\alpha)\frac{\partial^2 c}{\partial x^2}-\left[(\cos\alpha)\frac{\partial c}{\partial x}+(\sin\alpha)\frac{\partial c}{\partial y}\right]\frac{\partial\alpha}{\partial x}+(\cos\alpha)\frac{\partial^2 c}{\partial x\partial y}\right\}$$

$$+(\cos\alpha)\left\{(\cos\alpha)\frac{\partial^2 c}{\partial y^2}-\left[(\cos\alpha)\frac{\partial c}{\partial x}+(\sin\alpha)\frac{\partial c}{\partial y}\right]\frac{\partial\alpha}{\partial y}-(\sin\alpha)\frac{\partial^2 c}{\partial x\partial y}\right\}. \tag{4.2}$$

If eq 4.2 is simplified and substitutions are made for groups of terms equal to Dc/Ds and $D\alpha/Dn$, the result is

$$k^2=\frac{1}{c}\frac{D^2c}{Dn^2}=\frac{1}{c}\left[\sin^2\alpha)\frac{\partial^2 c}{\partial x^2}-2(\sin\alpha\cos\alpha)\frac{\partial^2 c}{\partial x\partial y}+(\cos^2\alpha)\frac{\partial^2 c}{\partial y^2}-\frac{Dc}{Ds}\frac{D\alpha}{Dn}\right]. \tag{4.3}$$

The term $D\alpha/Dn$, the curvature of the wave front, cannot be evaluated, given only the ray path and $c=c(x,y)$. However, the equation of ray separation 3.2 shows that

$$\frac{D\alpha}{Dn}=\frac{1}{\beta}\frac{D\beta}{Ds},$$

and this result, together with eq 4.3 and 3.8, gives an equation of wave intensity

$$\frac{D^2\beta}{Ds^2}+p\frac{D\beta}{Ds}+q\beta=0, \tag{4.4}$$

where

$$p(s)=-(\cos\alpha)\left[\frac{1}{c}\frac{\partial c}{\partial x}\right]-(\sin\alpha)\left[\frac{1}{c}\frac{\partial c}{\partial y}\right],$$

$$q(s)=(\sin^2\alpha)\left[\frac{1}{c}\frac{\partial^2 c}{\partial x^2}\right]-2(\sin\alpha\cos\alpha)\left[\frac{1}{c}\frac{\partial^2 c}{\partial x\partial y}\right]+(\cos^2\alpha)\left[\frac{1}{c}\frac{\partial^2 c}{\partial y^2}\right]. \tag{4.5a,b}$$

As indicated, the coefficients p and q in eq 4.5 are functions of the arc length s along a ray only, and the wave fronts are not required for their evaluation. Equation 4.4 offers, therefore, a practical basis for the determination of wave intensity, and considering the high development

[5] In eq 3.2 the curvature of the wave front enters explicitly; in eq 3.7 the evaluation of k^2 at a point on the ray involves the second derivative of c along the curvilinear wave front. One may think that a sufficient approximation could be attained by evaluating the derivative along a straight-line tangent to the wave front, but it is easy to select examples that show that this is not the case.

of ray optics, it is surprising that this equation is not familiar. An explanation might be that this law governing-wave intensity is adapted to a continuous velocity field, whereas the development of ray optics has been primarily concerned with discontinuous changes involved in the design of lens systems.

The quantities in square brackets depend on c and its partial derivatives with respect to the fixed coordinates x,y. The values of p and q are readily determined at each point of the ray in terms of a local coordinate system that has its origin on the ray at the point of determination and some specified orientation at that point. Two obvious, special cases

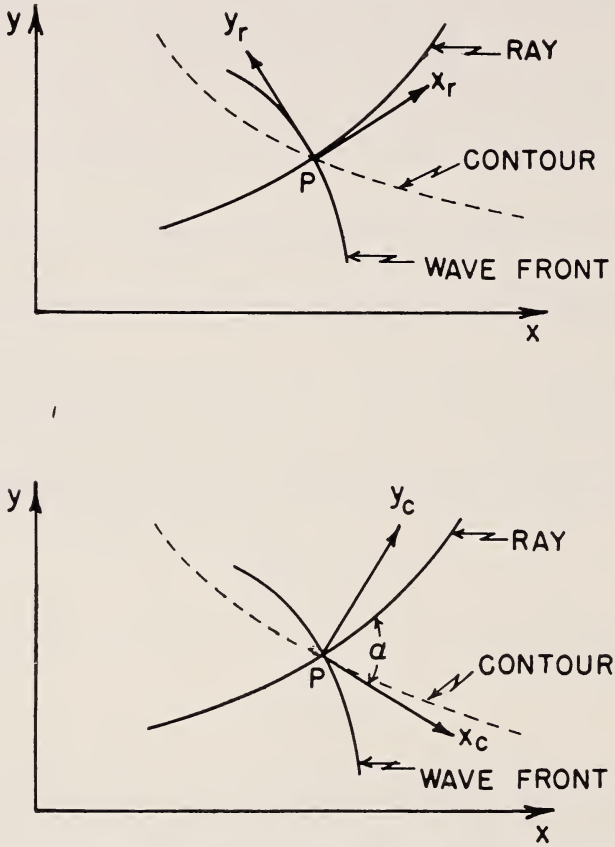

FIGURE 2. *Local coordinate systems oriented with respect to ray and depth contours.*

are a system (x_r,y_r) oriented with respect to the rays (fig. 2, upper) and a system (x_c,y_c) oriented with respect to the contours (fig. 2, lower).

For the ray system, $\alpha=0$ and

$$p(s)=-\frac{1}{c}\frac{\partial c}{\partial x_r},$$

$$q(s)=\frac{1}{c}\frac{\partial^2 c}{\partial y_r^2}. \qquad (4.5c,d)$$

For the contour system, $\partial c/\partial x_c=0$ and $\partial^2 c/\partial x_c^2=-\kappa_c(\partial c/\partial y_c)$, where κ_c is the curvature of the contour at the point of intersection with the ray. Consequently,

$$p(s)=-(\sin\alpha)\left[\frac{1}{c}\frac{\partial c}{\partial y_c}\right],$$

$$q(s)=(\cos^2\alpha)\left[\frac{1}{c}\frac{\partial^2 c}{\partial y_c^2}\right]-2(\sin\alpha\cos\alpha)\left[\frac{1}{c}\frac{\partial^2 c}{\partial x_c\partial y_c}\right]-(\sin^2\alpha)\left[\frac{\kappa c}{c}\frac{\partial c}{\partial y_c}\right]. \quad (4.5e,f)$$

Forms 4.5c,d appear to be simpler. However, a possible advantage of forms 4.5e,f is that the expressions in square brackets depend only on properties of the depth contours, and can be tabulated on charts of bottom topography along each contour, regardless of direction of wave approach, providing the wave period is specified. The dependence on direction enters entirely through the trigonometric functions of α in the parentheses. Equation 4.5f is simplified if the contours are parallel or have at most only slight convergence or divergence, for, then $|\partial^2 c/\partial x_c\partial y_c|\ll 1$, and the middle term is negligible.

5. Application to Special Types of Underwater Topography

5.1 Shelf of Uniform Depth

If the depth is constant, c is constant and p and q are zero. The equation of wave intensity, 4.4, reduces to

$$\frac{D^2\beta}{Ds^2}=0, \quad (5.1)$$

with solution

$$\beta=\beta_0(\kappa_0 s+1). \quad (5.2)$$

The two constants of integration (section 3) are evaluated in terms of the initial value, β_0, of the ray separation factor and the initial curvature, κ_0, of the wave front at the edge of the shelf, where $s=0$.

The depth being constant, there is no refraction over the shelf and the rays are straight. However, β remains constant along the ray only if the wave front is initially plane ($\kappa_0=0$). If the wave front is initially convex (diverging rays) as viewed from the positive s direction, then $\kappa_0>0$ and β increases linearly with s along the ray. The refraction factor 1.1 and wave intensity decrease. If the wave front is initially concave (converging rays), then $\kappa_0<0$ and $\beta=0$, where $s=-1/\kappa_0$. Therefore, at a distance $(-1/\kappa_0)$ along the ray the wave intensity becomes infinite on the basis of ray theory, i.e., a focal point, or caustic, is reached. This conclusion is in agreement with results obtained by Pierson (1951) in a detailed analysis of refraction over a semicircular ledge.

5.2 Straight, Parallel Contours

If the contours are parallel to the x-axis, then $c=c(y)$ and $\alpha=\alpha(y)$; the equation of wave intensity, 4.4, reduces to

$$\frac{D^2\beta}{Ds^2}-(\sin\alpha)\left[\frac{1}{c}\frac{dc}{dy}\right]\frac{D\beta}{Ds}+(\cos^2\alpha)\left[\frac{1}{c}\frac{d^2c}{dy^2}\right]\beta=0. \quad (5.3)$$

The known refraction relationships for this case, in terms of α, are (Hydrographic Office, 1944)

$$\left.\begin{aligned} \frac{c}{c_0} &= \frac{\cos\alpha}{\cos\alpha_0}, \\ \beta = \frac{l}{l_0} &= \frac{\sin\alpha}{\sin\alpha_0}. \end{aligned}\right\} \tag{5.4a,b}$$

The first relation is Snell's law. It can be verified that the second relation satisfies eq 5.3, but the details are tedious and uninteresting.

5.3 Ridge and Trough

It is instructive to consider in some detail the special cases of a ridge or trough for which the contours are symmetrical with respect to a straight axis. One ray is assumed to coincide initially with the axis, and eq 2.2 shows that this ray continues as a straight line. The variation in β along this axial ray is to be determined. The application to wave refraction along any channel of maximum or minimum velocity, e.g., the sound channel, is obvious.

Let the x-axis coincide with the axial ray and be directed in the direction of wave propagation. Since $\alpha=0$, then $D/Ds=d/dx$ and the coefficients of the equation of wave intensity, 4.4, are

$$\left.\begin{aligned} p(x) &= -\left(\frac{1}{c}\frac{\partial c}{\partial x}\right)_{y=0} = 2a, \\ q(x) &= \left(\frac{1}{c}\frac{\partial^2 c}{\partial y^2}\right)_{y=0} = b^2, \end{aligned}\right\} \tag{5.5a,b}$$

where a, which is dependent on the inclination of the ridge or trough along the axis, and b^2, which is dependent on the bottom curvature normal to the axis, are assumed constant along the axial ray. Along the axial ray the wave velocity, as determined by eq 5.5a, is

$$c/c_0 = e^{-2ax}, \tag{5.6}$$

where c_0 is the value of c at $x=0$. If $a=0$, the wave velocity and depth along the axis are constant, and the ridge or trough is level. More generally, the ridge or trough may be inclined upward ($a>0$) or downward ($a<0$) in the direction of the axis. From eq 5.5b it is apparent that for a ridge $b^2>0$ and for a trough $b^2<0$.

The resulting form of the modified equation of wave intensity is

$$\frac{d^2\beta}{dx^2} + 2a\frac{d\beta}{dx} + b^2\beta = 0, \tag{5.7}$$

a second-order, linear differential equation with constant coefficients. The solution in its various forms is particularly familiar because the same type of equation arises in the study of damped oscillatory systems. The solutions corresponding to overdamped, critically damped, and under-

damped oscillations are, respectively,

$$\beta=\beta_0 e^{-ax}\left[\cosh(\lambda x)+\left(\frac{a+\kappa_0}{\lambda}\right)\sinh(\lambda x)\right] \quad \text{for} \quad \lambda^2>0,$$

$$\beta=\beta_0 e^{-ax}[1+(a+\kappa_0)x] \quad \text{for} \quad \lambda^2=0, \qquad (5.8a,b,c)$$

$$\beta=\beta_0 e^{-ax}\left[\cos(i\lambda x)+\left(\frac{a+\kappa_0}{i\lambda}\right)\sin(i\lambda x)\right] \quad \text{for} \quad \lambda^2<0,$$

where $\lambda^2=a^2-b^2$. All arguments are real. The two constants of integration have been evaluated from the initial conditions (section 3) at $x=0$: $\beta=\beta_0$ and $(d\beta/dx)_0=\kappa_0\beta_0$, where κ_0 is the initial curvature of the wave front. For waves from a distant storm, $\kappa_0 \doteqdot 0$.

The various forms of the solutions are shown in figure 3. The simplest case is that of a level ridge or trough (fig. 3, upper). The results can be

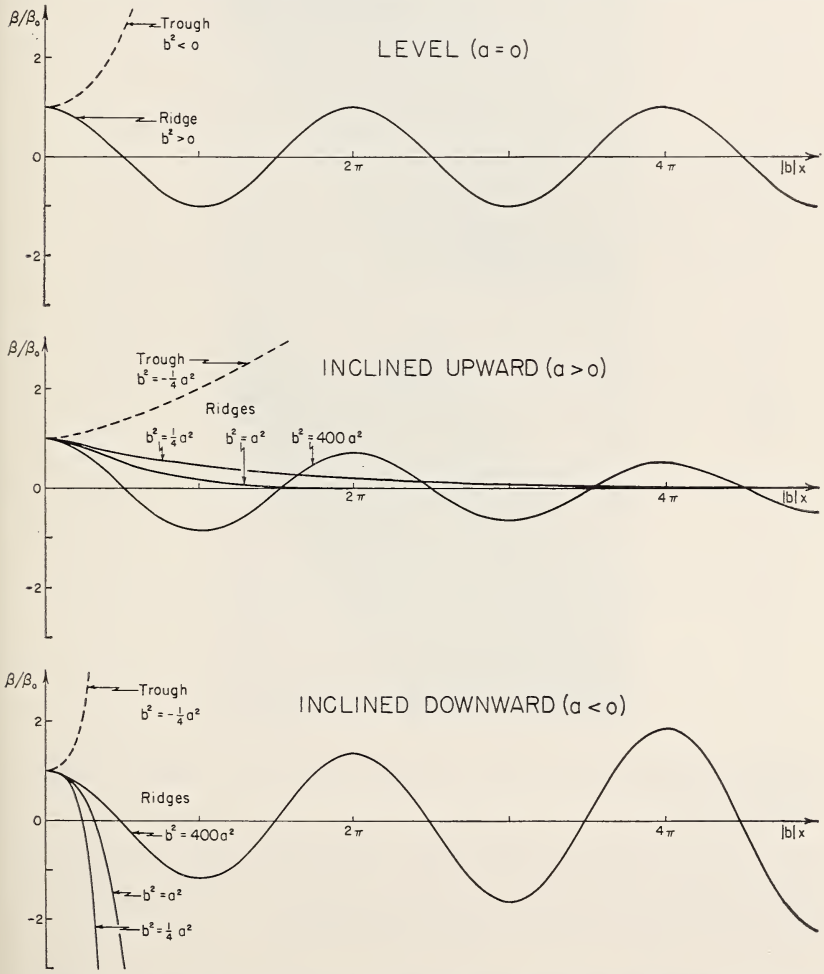

FIGURE 3. *The separation factor β as function of the nondimensional distance $|b|x$ along the axes of symmetrical ridges ($b^2>0$) and troughs ($b^2<0$), where $|b|=$ mod b.*

visualized easily in terms of Eckart's (1950) analogy between the rays and the paths of small balls rolling along suitably shaped surfaces with "inverse" bottom topography (fig. 4). The ray over the submarine ridge corresponds to the path of a ball rolling along a trough. If slightly disturbed, the ball will roll first somewhat to one side and then to the other side of the trough bottom, crossing the bottom at distances π/b. The zeroes of the β solution occur where the paths converge periodically to produce a focal point or a caustic with infinite wave intensity.[6] The

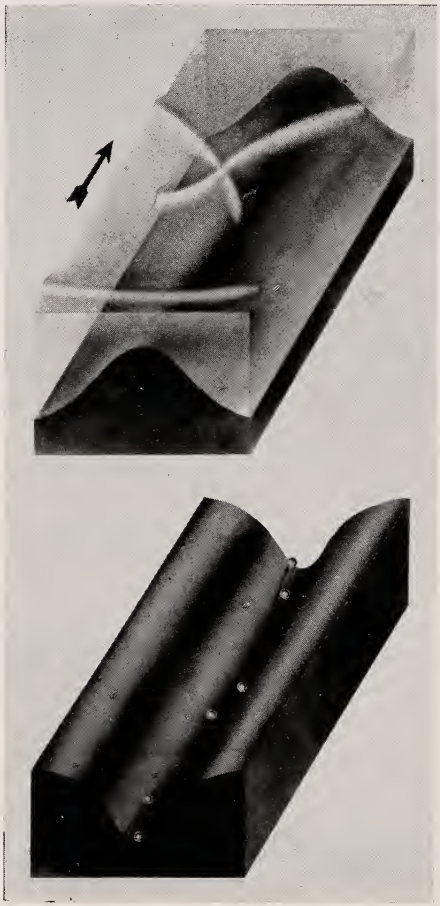

FIGURE 4. *Schematic view of wave refraction over a level, underwater ridge (upper), and the corresponding rays traced by small balls rolling along a surface of "inverse" topography (lower).*

ray over the trough, on the other hand, corresponds to the path of a ball moving along the very crest of a ridge. If slightly displaced, it will roll down one side or the other. The adjacent rays, therefore, diverge from the axial ray and the wave intensity diminishes.

[6] Allyn Vine of the Woods Hole Oceanographic Institution has called our attention to an unpublished manuscript by F. Brooks (1948) in which there is derived the distance π/b between focal points on the axis of a sound channel where the velocity varies parabolically with depth.

Tilting ridges have periodic convergences only if the lower sign holds in the inequality $a^2 \gtreqless b^2$. This condition stated in terms of the curvature of the contours, 4.5e,f, becomes

$$\left(\frac{1}{c}\frac{\partial c}{\partial x}\right)^2 \gtreqless (4\kappa_c)^2. \tag{5.9}$$

The critical case arises when the two members of the inequality are equal ($a^2 = b^2$). Setting

$$c/c_d = e^{-2ax}\cosh ay, \tag{5.10}$$

where c_d is the deep-water wave velocity, leads to the critical case. The nondimensional representation of the topography (see fig. 5) associated with eq 5.10 indicates that the "critical" ridge has a steep inclina-

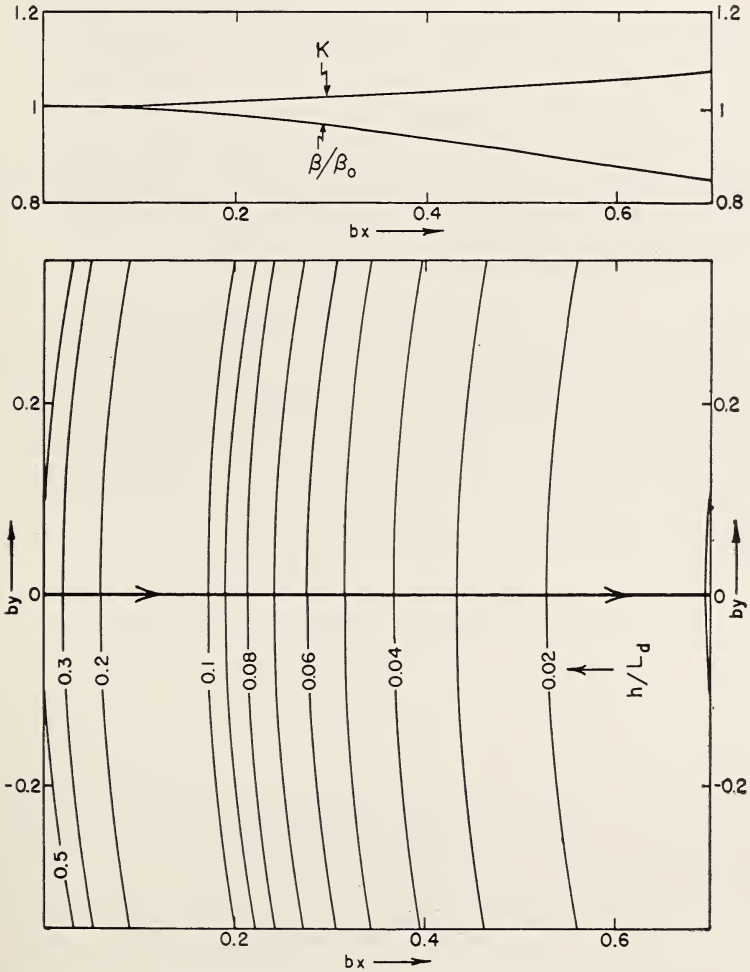

FIGURE 5. *An example of a submarine ridge corresponding to the "critically damped" case.*

tion and is relatively broad (contours have small curvature). If the inclination is less steep, periodic focal points, or caustics, occur along the axial ray.

6. Application to a Complex Bottom

It is assumed that the rays have been constructed directly (Johnson, O'Brien, and Isaacs, 1948) and that p and q along the rays have been evaluated from the contour charts by some suitable method. Such methods will be discussed in a forthcoming paper. It suffices to remark here that neither the term $p(s)D\beta/Ds$ or $q(s)\beta$ in the modified equation of wave intensity

$$\frac{D^2\beta}{Ds^2}+p(s)\frac{D\beta}{Ds}+q(s)\beta=0 \tag{4.4}$$

may, in general, be considered negligible, and to outline the following approximate methods for solution of the complete equation.

6.1 Constant Values of p and q

If the ray is divided into small intervals, and $p(s)$, $q(s)$ are replaced by average values within each interval, the solution appropriate to each interval is of the trigonometric or hyperbolic form discussed in section 5.3. The solutions are joined together by requiring $\beta(s)$ and $D\beta/Ds$ to be continuous from one interval to the next.

6.2 Kelvin's Method

This method involves approximating the integral curve of a second-order differential equation by fitting together circular arcs (Willers, 1948). Johnson, O'Brien, and Isaacs (1948) have derived an essentially similar technique for the construction of wave rays. Consider the construction of the integral curve $\beta=\beta(s)$ on a β,s-diagram, where the curvilinear coordinate s is now laid out rectilinearly. If the angle between the integral curve and the s-axis is θ, then the slope of the curve is $D\beta/Ds=\tan\theta$, and the curvature, using eq 4.4, is

$$\kappa_\beta=\frac{D^2\beta/Ds^2}{[1+(D\beta/Ds)^2]^{3/2}}=-(p\tan\theta-q\beta)\cos^3\theta. \tag{6.1}$$

The curvature is computed at the initial point $s=0$, where β, $D\beta/Ds$, p, and q are all known. The curvature is assumed constant over a small interval of s, and an arc of a circle of this curvature constructed from the initial point with the proper initial slope. The values of β and $D\beta/Ds$ at the end of the small interval are obtained, a new curvature computed, and the new arc laid off, keeping β and $D\beta/Ds$ continuous. Repetition of the process produces an approximation to the integral curve $\beta=\beta(s)$. This method has the advantage of employing similar procedures for computing the ray and the intensity.

6.3 WKB Method

The transformation

$$\beta=v(s)e^{-\frac{1}{2}\int pDs} \tag{6.2}$$

reduces the equation of wave intensity 4.4 to the normalized form

$$\frac{D^2v}{Ds^2}-\mu^2v=0, \tag{6.3}$$

where

$$\mu^2(s)=q-\frac{1}{4}p^2-\frac{1}{2}\frac{Dp}{Ds}. \tag{6.4}$$

Equation 6.3 has been studied intensively in quantum mechanics, and it is possible to adapt, with certain modifications, methods which have been developed for finding approximate solutions (see, for example, Condon and Morse, 1929, pp. 44-47, 111–114). An approximate solution, which constitutes the basis of the WKB method is,

$$\beta=\beta_0\sqrt{\frac{\mu_0}{\mu}}\left\{A\exp\left[-\int\left(\frac{1}{2}p+i\mu\right)Ds\right]+B\exp\left[-\int\left(\frac{1}{2}p-i\mu\right)Ds\right]\right\}, \tag{6.5}$$

where μ_0 is the value of μ at $s=0$, and the arbitrary constants A and B are to be evaluated from the initial conditions. The solution is trigonometric for $\mu^2>0$ and hyperbolic for $\mu^2<0$. The approximation becomes inadequate when μ^2 approaches zero, and through these "forbidden" regions solutions of type 6.5 have to be joined to other special solutions.

6.4 Analogue Computers

The modified equation of wave intensity is analogous to the equation of a damped oscillation. It is also analogous to the equation of an oscillatory voltage, V, in a RLC circuit, provided we identify p with R/L, and q with $1/LC$, β with V, and s with time. By changing resistance and capacitance with time in the required manner, the recorded voltage would give the desired solution. A more useful analogy is probably that of the telegraph equation. Bullard and Moon (1931) have discussed a method which depends on the equations of motion of a current-carrying coil, suspended in a magnetic field. Mechanical analogue computers, such as the differential analyzer, can also be used to obtain the solution.

Numerical methods which are capable of greater accuracy than any of the above outlined methods are available (Willers, 1948; Kamke, 1943). Greater precision is hardly warranted, however, in view of the fact that the bottom topography is known only approximately and that ray theory is at best only an approximate method for determining wave intensity.

Dr. Carl Eckart of the Marine Physical Laboratory; Dr. Sherman C. Lowell of the Office of Naval Research, London; and Dr. Willard J. Pierson, Jr. of the Department of Meteorology, New York University, have made many helpful comments. Dr. Pierson has undertaken experiments in a ripple tank for the purpose of checking the applicability of our ray theory results for underwater troughs and ridges. He will report his conclusions at a later date.

7. References

[1] Arrow, Kenneth J., 1949, On the use of winds in flight planning, J. Met. **6**, 150–159.

[2] Arthur, Robert S., 1950, Refraction of shallow water waves. . . . Trans., Amer. Geophy. Union, **31**, 549–552.

[3] Bullard, E. C., and Moon, P. B., 1931, A mechanical method for the solution of second-order linear differential equations. Proc. Cambr. Phil. Soc. **27**, 546–552.

[4] Condon, Edward U., and Morse, Phillip M., 1929, Quantum Mechanics. New York, McGraw-Hill.

[5] Eckart, Carl, 1950, The ray-particle analogy. J. Mar. Research **9**, 139–144.

[6] Frank P. G., Bergmann, P. G., Yaspan, A., 1946, Ray acoustics (Chap. 3 of Physics of sound in the sea), NDRC Summary Tech. Rep., Div. 6, **8**.

[7] Hydrographic Office, 1944. Breakers and surf. Hydrographic Off., Navy Dept., Pub. No. 234.

[8] Johnson, J. W., O'Brien, M. P., Isaacs, J. D., 1948, Graphical construction of wave refraction diagrams. Hydrographic Off., Navy Dept., Pub. No. 605.

[9] Kamke, E., 1943, Differentialgleichungen Lösungsmethoden und Lösungen. Leipzig, Akad. Verlagsgesellsch. . . . v. 1.

[10] Lewy, H., 1946, Water waves on sloping beaches. Bul. Amer. Math. Soc. **52**, 737–775.

[11] Lowell, Sherman Cabot, 1949, The propagation of waves in shallow water. Comm. on Pure and App. Math. **2**, 275–291.

[12] Munk, W. H., and Traylor, M. A., 1947, Refraction of ocean waves . . . J. Geol. **55**, 1–26.

[13] Pierson, Willard J., Jr., 1951, The interpretation of crossed orthogonals in wave refraction phenomena. Tech. Memo. No. 21, Beach Erosion Board, Corps of Engin.

[14] Stoker, J. J., 1947, Surface waves in water of variable depth. Quart. of App. Math. **5**, 1–54.

[15] Willers, Fr. A., 1948, Practical Analysis, New York, Dover.

14. Diffraction of Water Waves by Breakwaters

By John H. Carr[1] and Marshall E. Stelzriede[1]

Diffraction is an important factor in the determination of the distribution of wave energy within a harbor, and therefore is of importance in harbor design. Previous investigations in this field have made use of Sommerfeld's solution of the diffraction of waves by a semiinfinite screen to obtain results for semiinfinite breakwaters, and by superposition, approximate results for continuous breakwaters with openings large compared to the wave length. The investigation of this subject by the Hydrodynamics Laboratories of the California Institute of Technology has been guided by the theoretical solutions of Morse and Rubenstein for the diffraction of waves by ribbons and by slits with the two boundary conditions of zero wave function and zero normal gradient. Morse and Rubenstein separate the wave equation in elliptic cylinder coordinates and obtain the total transmission and the angular distribution of the scattered or diffracted waves in terms of Mathieu functions. This method bridges the gap between the method of Rayleigh for very small slits and the approximation based on Sommerfeld's solution, which is applicable for slit widths greater than three or four wave lengths, and is useful for any angle of wave approach.

The difficulties of computation of the required Mathieu functions have been overcome in recent years by the use of modern methods of machine computation. The Institute for Numerical Analysis of the National Bureau of Standards has recently completed the computation of the transmission and distribution of wave energy for openings of one-half, one, two, and three wave lengths, with wave approach angles from 0° to 90° in 15° increments. These data, in the form of polar plots of a dimensionless intensity factor, are compared with experimental measurements conducted to verify the theory, and the two results are found to be in good agreement. The experimental procedure has also been used to investigate a number of breakwater configurations for which theoretical solutions are not obtainable.

1. Introduction

Considered in the most general way, the disturbance level at a point in a harbor is a function of the amount of wave energy entering the harbor and the distribution of the energy within the harbor. Because the aim of the harbor designer is to provide specific regions within the harbor where the wave disturbances will always be less than some maximum, and thus guarantee an optimum level of usability for these regions, the design technique consists of the determination of disturbance levels in particular places for certain assumed harbor configurations and ocean conditions. The significance of diffraction in connection with the problems of harbor layout and design is that both the amount of energy entering the harbor and especially the distribution of wave energy within the harbor are conditioned by this phenomenon.

The amount of energy entering the harbor is determined largely by the size of the opening and the intensity and direction of the incident wave, but for small openings— less than one wave length in width—diffraction becomes an increasingly important modifying factor.

[1] California Institute of Technology, Pasadena, Calif.

The distribution of wave energy within a harbor is governed by three factors, diffraction, refraction, and reflection. Of these, diffraction and refraction account for the distribution of what may be called the primary wave disturbances—waves that have not yet reached a boundary and reflected. Secondary, or reflected, wave disturbances are determined by the character and alinement of the harbor boundaries, the distribution of the primary disturbances, and subsequent diffraction and refraction. Because the refraction of water waves is due to wave-velocity changes corresponding to depth changes, refraction is an important factor in the distribution of wave energy within a harbor only if the topography of the harbor bottom is irregular. Typical harbors on open coasts are characterized by fairly uniform water depths, especially as improved by peripheral bulkheading and dredging, hence in many cases the primary energy distribution, and as a consequence, the secondary distribution for a given set of boundary conditions, may be predicted with sufficient accuracy for engineering application by the consideration of diffraction effects alone.

The Hydraulic Structures Division of the Hydrodynamics Laboratories, California Institute of Technology, is engaged in a study of the application of the principles of wave behavior to harbor design. This study is sponsored by the Bureau of Yards and Docks of the Department of the Navy. The investigation of water-wave diffraction described herein is one result of this study.

2. Theory

2.1 General

There are two theoretical methods by which the general problem of water-wave diffraction through a breakwater gap may be most directly approached. The first mode of attack, which may be attributed to Penney and Price [1],[2] involves a solution by Sommerfeld [2] for diffraction of light waves by a semiinfinite screen, or a half plane. The procedure is extended by superposition to a breakwater with a gap. The resulting solution is reasonably accurate, however, only for gap widths of over two wave lengths.

The second method of approach may be credited largely to Morse and his associates at Massachusetts Institute of Technology [6 to 9]. This analysis, based on elliptic-cylinder coordinates and the associated Mathieu functions, was originally developed for the diffraction of sound and electromagnetic waves. At the Hydraulic Structures Laboratory it has been used with a high degree of success in water-wave diffraction studies, especially because the solution converges most rapidly for gap widths of the order of zero to three wave lengths.

2.2 Penney-Price Method

The principal features of the solution by Penney and Price have been verified experimentally by Putnam and Arthur [3], and by Blue and Johnson [4]. Although this theory did not serve as the primary basis of work done at this laboratory, there is sufficient agreement between it and the Morse-Rubenstein theory within certain areas, so that a brief discussion of it is warranted.

[2] Figures in brackets indicate the literature references on p. 125.

The solution is based on the following assumptions: (a) The water is an ideal, incompressible fluid. (b) Motion of the water is irrotational, and the velocity potential ϕ satisfies the Laplace equation,

$$\frac{\partial^2\phi}{\partial x^2}+\frac{\partial^2\phi}{\partial y^2}+\frac{\partial^2\phi}{\partial z^2}=0, \tag{1}$$

where x- and y-axes are in the plane of the undisturbed water surface, and z is the vertical coordinate. (c) The wave height is very small. (d) The pressure at the surface, $z=\eta(t)$, is constant. (e)The component of the fluid velocity normal to the surface equals the velocity of the surface normal to itself. (f) The velocity of the fluid normal to a fixed boundary surface is zero. (g) The depth of the water is constant.

Using these assumptions, the Laplace equation is solved for ϕ and an expression set up for the free water surface, by the method of Lamb [5]. These equations are, respectively,

$$\phi=Ae^{-ikct}\cosh k(z+h)\cdot F(x,y), \tag{2}$$

$$\eta=\frac{ikc}{g}Ae^{ikct}\cosh kh\cdot F(x,y), \quad \text{where} \tag{3}$$

$$\frac{\partial^2F}{\partial x^2}+\frac{\partial^2F}{\partial y^2}+k^2F=0, \tag{4}$$

and where $k=2\pi/\lambda$; c=wave celerity, or velocity; λ=wave length; h=water depth; and Akc/g cosh kh=amplitude. Progressive waves with straight crest alinement and traveling in the positive y-direction may be represented by the following solution of eq 4

$$F(x,y)=e^{-iky}. \tag{5}$$

Consistent with assumption (f), for a rigid barrier extending along the positive x-axis from the origin,

$$\frac{\partial\phi}{\partial y}=\frac{\partial F}{\partial y}=0, \quad \text{when} \quad y=0, x>0. \tag{6}$$

To study the diffraction of waves incident normally on a semiinfinite rigid breakwater, the xy-plane may be divided into the three regions (shown in fig. 1 for a general angle of approach). It can be shown [3] that the modulus and argument of F determine, respectively, the amplitude and phase of the diffracted wave, hence the problem reduces to that of finding a solution of eq 4, which satisfies the boundary condition of eq 6, and which reduces to eq 5 when x is large and negative.

Penney and Price show that eq 4, 5, and 6 are identical with those satisfied by Sommerfeld's solution for the diffraction of light waves polarized in a plane parallel to the edge of the semiinfinite screen. In Cartesian coordinates this equation may be written

$$F(x,y)=\frac{1+i}{2}\left\{e^{-iky}\int_{-\infty}^{\sigma}e^{-\frac{\pi}{2}iu^2}du+e^{iky}\int_{-\infty}^{\sigma'}e^{-\frac{\pi}{2}iu^2}du\right\}, \tag{7}$$

$$\sigma=\sqrt{\frac{4}{\lambda}(r-y)}, \quad \sigma'=\sqrt{\frac{4}{\lambda}(r+y)}, \quad r^2=x^2+y^2. \tag{8}$$

The signs of σ and σ' for a given point are determined by which of the three regions, Q, R, or S (fig. 1), contains the point. The form of this Sommerfeld equation is convenient, in that it lends itself to evaluation by means of tabulated values of Fresnel's integrals,

$$\int_0^u \cos\frac{\pi}{2}u^2du \quad \text{and} \quad \int_0^u \sin\frac{\pi}{2}u^2du, \tag{9}$$

or by Cornu's spiral. The behavior of the modulus and argument of F over the plane, determined from eq 7, presents a complete picture of the surface configuration in the three regions.

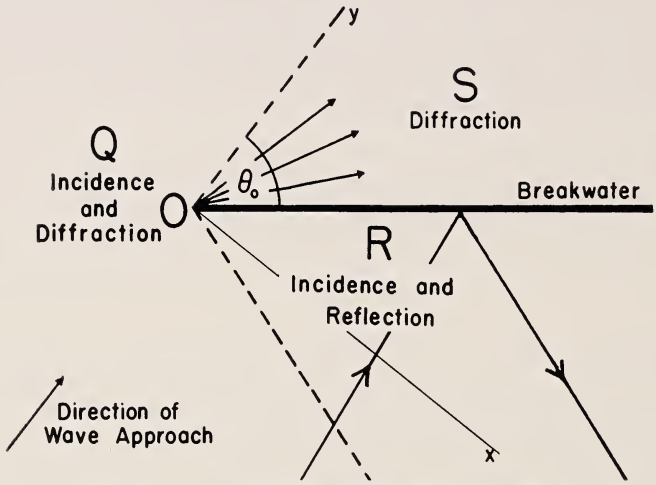

FIGURE 1. *Regions about semiinfinite breakwater.*

Replacing Cartesian by polar coordinates, the Sommerfeld solution may be generalized to the case of waves incident obliquely on a semi-infinite barrier. So far the solution is exact; the specified boundary conditions are satisfied exactly within the limits of certain approximations which were made for convenience. The procedure may be extended to a breakwater with a gap by superposing the solutions for one semi-infinite barrier to the right and one to the left, separated by a gap of width d, and with the origin at the center of the gap.

The resulting compound solution is discussed by Penney and Price for waves of normal incidence. The solution is no longer exact, for the boundary conditions at each barrier are not automatically satisfied by diffraction waves arising from incident waves on the other barrier. For openings of over two wave lengths, $\partial F/\partial y$ differs from zero by a relatively small amount at the boundaries, with the accuracy improving with increasing width of opening. For large gaps, therefore, the diffraction picture presented by the behavior of the modulus and argument of F is assumed to be reasonably accurate.

For angles of wave incidence other than normal, the determination of wave heights becomes somewhat more involved. That factor, together with the total unsuitability of the solution for small gaps, prompted the adoption of another theory to serve as the basis for evaluation of experimental data.

2.3 Morse-Rubenstein Solution

The unsatisfactory features of the Penney-Price method are largely avoided by the approach outlined by Morse and Rubenstein [6] for diffraction of sound and electromagnetic waves by a slit in an infinite plane. It is an exact solution for small gaps, and possesses the added feature of leading to direct expressions for angular distribution of energy transmitted through the opening, and for the total of such transmitted energy.

Application of the exact boundary conditions of zero potential gradient to the breakwater with a gap is expedited by the use of elliptic-cylinder coordinates,

$$\left.\begin{aligned} x &= \frac{d}{2}\cosh \xi \cos \phi, \\ y &= \frac{d}{2}\sinh \xi \sin \phi, \\ z &= z. \end{aligned}\right\} \tag{10}$$

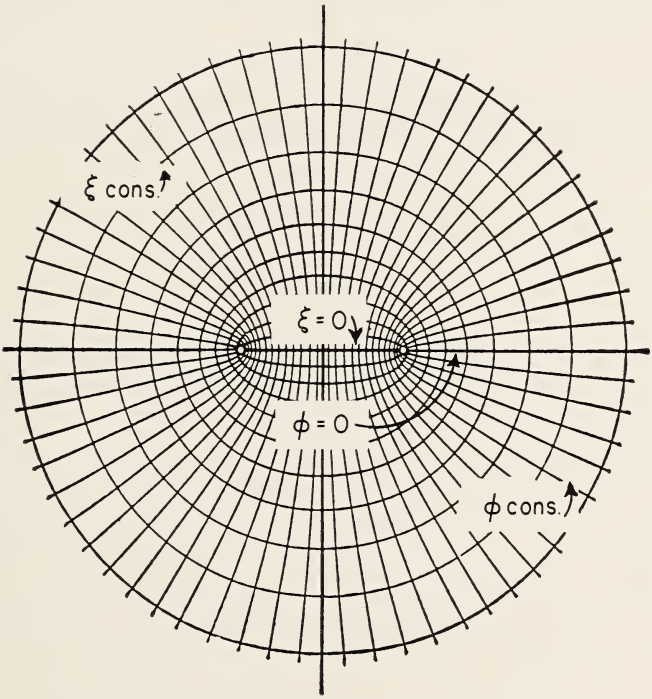

FIGURE 2. *Elliptic cylinder coordinates.*

For constant z, lines of constant ξ and ϕ become, respectively, confocal ellipses and hyperbolas of focal length d (fig. 2). The suitability of these coordinates for the expression of the desired boundary conditions lies in the fact that, for $\phi=0$, the hyperbolas degenerate into a straight line with a gap of width d. On the other hand, diffraction around both ends

of a barrier of finite length, the reciprocal case to the breakwater with a gap, could be investigated by using the degenerate ellipse, corresponding to $\xi=0$.

The three-dimensional wave equation is, in Cartesian coordinates,

$$\frac{\partial^2\psi}{\partial x^2}+\frac{\partial^2\psi}{\partial y^2}+\frac{\partial^2\psi}{\partial z^2}=\frac{1}{c^2}\frac{\partial^2\psi}{\partial t^2}, \tag{11}$$

where c is again the velocity of wave propagation. Substituting the new coordinates into eq 11 puts the wave equation in the ellyptic-cylinder form

$$\frac{2}{\left(\frac{d}{2}\right)^2(\cosh 2\xi-\cos 2\phi)}\left(\frac{\partial^2\psi}{\partial\xi^2}+\frac{\partial^2\psi}{\partial\phi^2}\right)+\frac{\partial^2\psi}{\partial z^2}=\frac{1}{c^2}\frac{\partial^2\psi}{\partial t^2}. \tag{12}$$

It is desirable to find solutions of the wave equation, which, in addition to possessing zero gradient at the two slit walls, disappear at infinity and remain finite in the gap.

The variables in eq 12 may now be separated in the standard manner, by assuming a product solution of the form

$$\psi=G(\xi)H(\phi)Z(z)\,e^{-2\pi i\nu t}, \tag{13}$$

ν being the wave frequency. Neglecting time and the z-coordinate, since the propagation vector is taken in the xy-plane, the following differential equations result

$$\frac{d^2H}{d\phi^2}+(b-s\cos^2\phi)H=0, \tag{14}$$

$$\frac{d^2G}{d\xi^2}+(s\cosh^2\xi-b)G=0, \tag{15}$$

where $s=(\pi d/\lambda)^2$, and b is a separation constant. Equations 14 and 15 are commonly known, respectively, as Mathieu's equation and Mathieu's modified equation, the second being derivable from the first by substituting $\phi=i\xi$.

Solutions of these equations, and linear combinations of such solutions are, of course, solutions of the wave equation from which eq 14 and 15 arise. Using a countably infinite number of values of the characteristic constant b results in an infinite number of solutions of the differential equations, not all of which are periodic. In particular, it is the solutions, or Mathieu functions, of periods π and 2π, which are of present interest.

Each equation possesses even and odd solutions, which, in the case of the angular functions, or solutions of eq 14, assume the form of Fourier series

$$Se_r(s,\phi)=\sum_{k=0}^{\infty}{}'De_k\cos k\phi, \tag{16a}$$

$$So_r(s,\phi)=\sum_{k=0}^{\infty}{}'Do_k\sin k\phi. \tag{16b}$$

That these functions form an orthogonal set can be easily shown. Even and odd solutions of the first kind of the modified equation are designated

$Je_r(s,\xi)$ and $Jo_r(s,\xi)$, and those of the second kind are $Ne_r(s,\xi)$ and $No_r(s,\xi)$. As their designations indicate, these radial Mathieu functions are normally expressed in terms of Bessel's functions of the first and second kinds. Computable factors of proportionality or joining factors, however, relate the radial functions to each other and to the angular functions.

The subscripts r in eq 16a and 16b are index numbers 0, 1, 2, 3, ... corresponding to increasing characteristic values of the parameter b that yield the desired periodic functions and identify the order of the solution. In practice, for a gate width of three wave lengths or less, convergence of the final equations is such that it is necessary to consider values of r up to a maximum of about five or six. The primed summation signs indicate that for even values of r, only even values of k are included in the summation, and for odd r only odd values of k are summed.

The Mathieu coefficients, De_k and Do_k, may be determined by substituting eq 16a or 16b into the Mathieu eq 14, using the series representation for trigonometric functions, and equating coefficients of like powers of ϕ to zero. The coefficients are then seen to satisfy certain recursion relationships that may be represented by continued fractions. The value of such fractions may be computed, provided the first coefficient is known. This first coefficient, where $k=0$ or 1, as the case might be, is effectively established by choosing

$$Se_m(s,0)=1, \tag{17a}$$

$$\frac{d}{d\phi}[Se_m(s,\phi)]_{\phi=0}=0, \tag{17b}$$

and

$$So_m(s,0)=0, \tag{18a}$$

$$\frac{d}{d\phi}[So_m(s,\phi)]_{\phi=0}=1. \tag{18b}$$

Normalizing in this manner also insures the vanishing of the wave-function gradient at the boundaries. Stratton, et al. [9] published a very limited table of even and odd coefficients with their associated characteristic values. The Institute for Numerical Analysis of the National Bureau of Standards is publishing an extensive table of coefficients, characteristic values and joining factors. This publication [10] may well serve as a handbook on Mathieu functions, as, in addition to the tables and an extensive bibliography, the introduction contains a summary of all important relations involving the functions.

Morse [8] demonstrates that the addition formula expressing the expansion of a plane, or in the case of water straight-crested, wave in terms of Mathieu functions is, exclusive of the time factor,

$$e^{ik(x\cos u+y\sin u)}=\sqrt{8\pi}\sum_m i^m\left[\left(\frac{1}{N_m}\right)Se_m(s,u)\right.$$

$$\left.\cdot Se_m(s,\phi)Je_m(s,\xi)+\left(\frac{1}{N_m'}\right)So_m(s,u)So_m(s,\phi)Jo_m(s,\xi)\right], \tag{19}$$

where N_m and N_m' are normalization factors, and u is the angle of incidence of the waves with the breakwater. The diffracted wave beyond the

rigid breakwater with a gap is expressed by the equation

$$\psi=\sqrt{8\pi}\sum_m \frac{i^{m-1}}{N_m}\sin\gamma_m e^{i\gamma_m} Se_m(s,u)Se_m(s,\phi)-[Je_m(s,\xi)+iNe_m(s,\xi)]. \tag{20}$$

Here γ_m is the phase angle of the partial wave, and ctn $\gamma_m=(Ne_m(s,0))/(J_{em}(s,0))$ is identical in value to the joining factors $f_{e,r}$ tabulated by the Institute for Numerical Analysis. The quantity in brackets bears the same relationship to the radial functions of the first and second kinds as Hankel functions bear to the Bessel functions, and represent diverging cylindrical waves which disappear at infinity but remain finite in the region of the gap. It may be shown that the gradient of the wave function of eq 20 is zero at the slit boundary, and that ψ and its gradient are continuous in the slit opening.

The modulus of eq 20 represents the amplitude of the diffracted wave. It may be shown [3] that at sufficient distance R from the center of the opening, the normal expression for the energy flux carried by a straight-crested wave may be applied with ample accuracy to a diverging circular wave. As a matter of fact, at points where the radius of curvature of the wave crest is as little as about three wave lengths, the error introduced by using this relationship is negligible. It is apparent, therefore, that the ratio of energy intensity at a point in the harbor to that in the open sea is $h^2_{\rho,\phi}/h^2_i$, where $h_{\rho,\phi}$ is the wave height at the point, and h_i is the incident wave height. Or, if the incident intensity is taken as unity, the intensity at a point is just $h^2_{\rho,\phi}$.

If the asymptotic forms of the radial functions

$$\left.\begin{aligned} Je_m(s,\xi)&\underset{\rho\to\infty}{\longrightarrow}\sqrt{\frac{1}{c\rho}}\cos\alpha,\\ Ne_m(s,\xi)&\underset{\rho\to\infty}{\longrightarrow}\sqrt{\frac{1}{c\rho}}\sin\alpha,\end{aligned}\right\} \tag{21}$$

where $\alpha=\left[c\rho-\left(\frac{2m+1}{4}\right)\pi\right]$, and $\rho=\cosh\xi$, be introduced into eq 20,

and the modulus squared, this expression results

$$I_{\rho,\phi}=h^2_{\rho,\phi}=\frac{8\pi}{\sqrt{s\rho}}\sum_{m,n}\frac{1}{N_mN_n}\sin\gamma_m\sin\gamma_n Se_m(s,u)Se_n(s,u)$$
$$\cdot Se_m(s,\phi)Se_n(s,\phi)\cos(\gamma_n-\gamma_m). \tag{22}$$

When R is sufficiently large,

$$x=\frac{d}{2}\rho\cos\phi=R\cos\phi,\text{ or }\rho=\frac{2R}{d}. \tag{23}$$

Then the intensity of the diffracted wave at (R,ϕ) resulting when a plane

[3] Proof that the plane-wave expression is valid for diverging waves of sufficiently large radius of curvature was communicated to the Hydraulic Structures Laboratory by L. I. Schiff, and is based on the rapidity of convergence of the Bessel's functions of the first and second kinds for a given radius of curvature of the wave crest.

wave of unit intensity is incident on the other side of the slit at an angle u to the plane of the slit, is

$$I_{R,\phi}=\frac{\lambda}{R}\cdot I, \tag{24}$$

$$I=\sum_{m,n}\frac{d}{\lambda}\cdot\frac{4\pi}{\sqrt{s}}\sin\gamma_m\sin\gamma_n Se_m(s,u)Se_n(s,u)$$
$$\cdot Se_m(s,\phi)Se_n(s,\phi)\cos(\gamma_n-\gamma_m). \tag{25}$$

Equation 25 is used to define an intensity factor corresponding to a point $(R=1\lambda, \phi=\phi_1)$, which is so close to the gap that the preceding analysis, of course, is not valid. The factor is tabulated in this form, however, only to serve as a number which may be divided by R_1/λ to yield the intensity at a point (R_1, ϕ_1), as eq 24 indicates.

Proceeding further, the total energy transmitted through the opening is obtained by integrating over ϕ, as follows:

$$T'=\int_0^{\pi} I_{R_1\phi}P_1 d\phi=\frac{d}{R_1}\cdot\frac{4\pi}{\sqrt{s}}\cdot\frac{R_1}{2}\int_0^{2\pi}\sum_{m,n}f_m(\phi)f_n(\phi)\cos(\gamma_n-\gamma_m)d\phi, \tag{26}$$

where

$$f_m(\phi)=\sum_m\frac{1}{N_m}\sin\gamma_m Se_m(s,u)Se_m(s,\phi),$$

$$f_n(\phi)=\sum_n\frac{1}{N_n}\sin\gamma_n Se_n(s,u)Se_n(s,\phi). \tag{27}$$

The integral and summation signs in eq 26 may be interchanged, because the series is uniformly convergent throughout the interval of integration. In addition, it may be noted that, because of the orthogonality of the Mathieu functions, all terms of eq 26 disappear except the ones in which $m=n$, and the cosine factor becomes unity.

Equation 26 becomes, therefore,

$$T'=Td=\frac{2d\pi}{\sqrt{s}}\sum_m\frac{1}{N_m^2}\sin^2\gamma_m[Se_m(s,u)]^2\int_0^{2\pi}[Se_m(s,\phi)]^2 d\phi. \tag{28}$$

Moreover, since the integrand in this equation is by definition identical in value to the normalizing factor, N_m, the final form of the equation for the total transmission factor is taken as

$$T=\frac{2\pi}{\sqrt{s}}\sum_m\frac{1}{N_m}\sin^2\gamma_m[Se_m(s,u)]^2. \tag{29}$$

T may be interpreted physically as the ratio of the energy actually transmitted through the slit to the energy which geometrical optics predicts would be transmitted at normal incidence. Equation 29, being relatively simple in form, could be computed manually without too much difficulty. Equation 25, however, which is by far the more important of the two relationships from a design standpoint, lends itself best to mechanical means of computation. Plots of the two factors as computed by the Institute for Numerical Analysis, appear in figures 3 and 4.

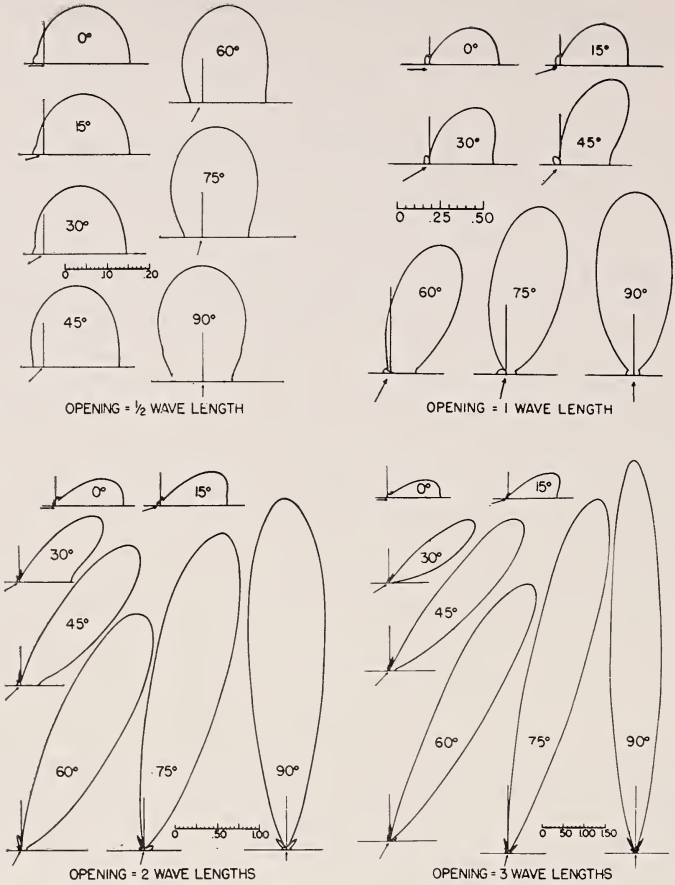

FIGURE 3. *Polar plots of intensity factor,*

$$I_{R,\phi} = \frac{(h_{R,\phi})^2}{(h)^2} \times \frac{R}{\lambda}$$

(Vertical face straight breakwaters.)

2.4 Comparison

While the Morse-Rubenstein solution appears to be of most direct value in harbor design, it should be pointed out that the Penney-Price solution, too, possesses certain valuable qualities. The wave crest alinement and phase relationships, for example, are more readily ascertained by the latter method, except for the small openings. For very large gap widths, say of the order of seven or eight wave lengths, the boundary condition of the Penney-Price solution approaches the desired value rather well, whereas the Mathieu functions converge much more slowly for large openings. For that reason, it may be more convenient for such large widths to determine the energy intensities by means of the Penney-Price approach.

It is interesting to note that there is a great deal of agreement between results of the two methods in their common domain. It has been found,

for example, that an intensity plot based on wave heights tabulated by Penney and Price for an opening of 2.5 λ shows a form strikingly similar in relative proportions to one for a 2λ opening based on the Morse-Rubenstein solution.

An important quantitative result developed by Penney and Price for the slit problem appears to apply reasonably well when compared with the Morse-Rubenstein curves of figure 3. For distances behind the gap greater than some minimum

$$I_{max}=\left(\frac{d}{\lambda}\right)^2, \tag{30}$$

or, the maximum intensity factor is approximately equal to the square of the opening in wave lengths.

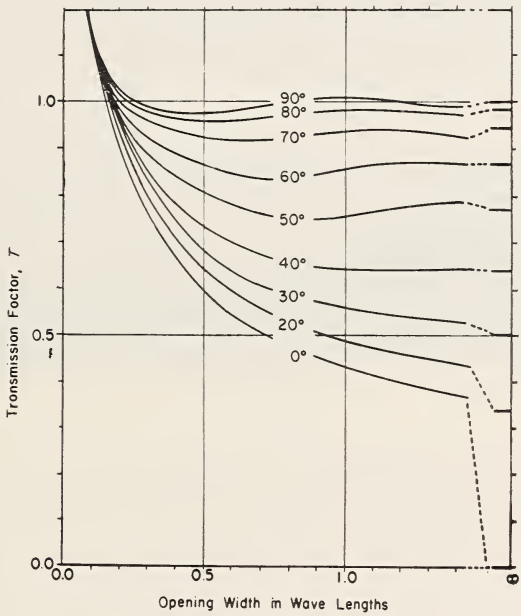

FIGURE 4. *Theoretical transmission factors.*

3. Experiments

3.1 Techniques

The primary purpose of the experimental program was to check the theoretical results of the *Morse* and *Rubenstein* solution for vertical face, straight breakwaters. This was especially important for small openings and for wave-approach angles less than 90°, since no experimental work covering this range of variables had come to the attention of the Laboratory. The development of equipment and techniques for this purpose made it possible to extend the experimental investigation to include some breakwater configurations of practical interest, which, because of their alinement, are not susceptible to theoretical analysis.

The experiments were conducted in an L-shaped basin (fig. 5), 20 feet wide by 60 feet long, with an offset portion 12 by 24 feet at the shallow end. The water depth at one end of the basin was made 12 inches to accommodate one of the standard laboratory pneumatic wave generators, with the bottom rising from this depth at a slope of 1 in 40 to a line where the depth is 3 inches. The remainder of the basin has a uniform depth of 3 inches. The breakwaters and "harbor" were located in the region of uniform water depth, thus eliminating refraction phenomena from the investigation. Pea gravel beaches around the periphery of the harbor effectively prevented reflection from the basin walls. Different angles of

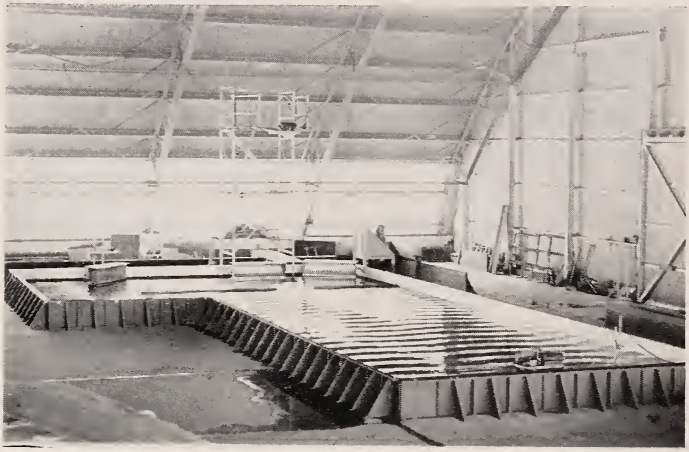

FIGURE 5. *Basin for experimental measurements.*

wave approach were obtained by rotating the breakwater, the wave machine remaining fixed. The offset portion of the basin provided space for a damping beach to prevent the reentry of waves reflected from the breakwater into the region near the breakwater opening, thus simulating a basin of infinite extent. For the cases where the breakwater was alined at 60° and 90° to the direction of wave approach, waves reflected from the breakwater were not intercepted by this side beach, but traveled the length of the basin, reflected from the wave machine and so could interfere with the incident wave train. Difficulties of this kind were prevented by providing sufficient distance from wave generator to breakwater so that measurements could be obtained before waves reflected from the breakwater reached the wave generator.

Incident wave height was measured in deep water, near the wave machine, to insure freedom from obscuring reflections. The data obtained was corrected to represent wave heights incident at the breakwater opening. Calculations based on the effect of shoaling indicated that the deep-water values should be reduced by 8 percent, but direct measurement of the change in incident wave height gave a value of 25 percent. The additional height reduction is assumed to be a fluid friction phenomenon.

The distribution of transmitted wave energy was obtained by wave-height measurements at 4° intervals on a semicircle of radius 5.76 wave

lengths centered on the opening. The intensity factor, $I_{R,\phi}$ in each direction ϕ can then be expressed as:

$$I_{R,\phi}=\frac{(h_{R,\phi})^2}{(h_i)^2}\cdot\frac{R}{\lambda}=5.76\frac{(h_{R,\phi})^2}{(h_i)^2},$$

where

$h_{R,\phi}$ = wave height measured at ϕ,R, inside the breakwater,

h_i = wave height incident at the breakwater,

R = radius of measuring circle,

λ = wave length.

The total transmission factor, T, is computed by a summation process

$$T=\frac{\int_0^{\pi}(h_{R,\phi})^2 R d\phi}{h_i^2 d},$$

where d is the gap width in the same units as R.

Wave heights were measured by means of sixteen channels of electrical-conductivity cells. Each cell consists of a pair of wire electrodes supported and spaced one-half inch apart by an insulating block at one end. The electrodes are immersed to a mean submergence of 1 inch, and a constant voltage is applied across the cell. The amount of current conducted by the cell is a linear function of the submergence, hence of wave height. The current signal from each cell corresponding to the wave motion past each cell is recorded on a galvanometer oscillograph.

3.2 Results

A comparison of theoretical with experimentally determined energy transmission for vertical face straight breakwaters is shown in figure 6. The theoretical solutions indicate that for projected widths of openings in the direction of wave approach greater than one-half wave length, the effect of diffraction on energy transmission is minor, but for smaller openings, the energy transfer is larger than would be expected from geometrical considerations. The experimental data are in fairly good agreement with the theoretical values with respect to these general conclusions, although the measured values are about 20 percent lower than theoretical. Because wave energy is proportional to the square of the wave height, the difference between theory and experiment on a wave-height basis — which is the measured quantity — is but 10 percent in most cases. These results are considered sufficient evidence of the validity of the theoretical approach, at least for engineering applications.

The most important application of diffraction considerations is in the analysis of wave-energy (or height) distribution in the lee of the breakwater gap. Figures 7, 8, and 9 present some results of experimental distribution measurements for three breakwater configurations: (1) straight arms in line with each other, (2) straight arms inclined symmetrically with respect to an axis consisting of the perpendicular bisector of the line of the opening, (3) straight arms at right angles to each other, the seaward arm parallel, and the leeward arm perpendicular to the incident wave crests. Three degrees of sheltering of the gap by the sea-

ward arm were studied, corresponding to projected openings in the direction of wave advance of $1/\sqrt{2}$ and zero gap widths, and a seaward arm overlap of $1/\sqrt{2}$ gap widths.

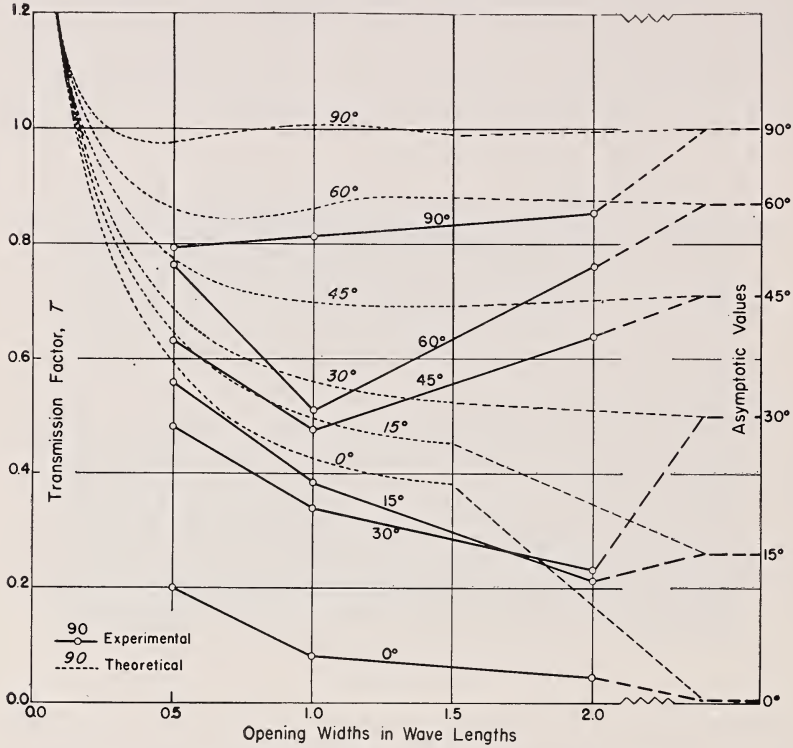

FIGURE 6. *Theoretical and experimental transmission factors.*
(Vertical face straight breakwaters.)

The experimental data for straight breakwater alinements, some of which are shown in figure 7, may be compared with the theoretical data of figure 3. The agreement between experiment and theory, while not exact, is reasonably close, and supports the important general conclusions of the theory. In particular, the experimental data verify that the maximum value of the intensity factor is proportional to the square of the gap width, and that the effect of reducing the gap width is to distribute the wave energy more uniformly in the region behind the breakwater.

Figures 8 and 9 present experimental data for the wave-energy distribution in the lee of some breakwater configurations that cannot be analyzed by the theoretical approach.

The data of figure 8 show the energy distribution resulting from normal wave approach for an important class of breakwater alinements — symmetrical arms converging seaward, or so-called "wave traps." The data show that, as the included angle between the breakwater arms is reduced from 180° (straight breakwater) to 90°, there is virtually no change in the energy distribution. This result is in agreement with the observations of

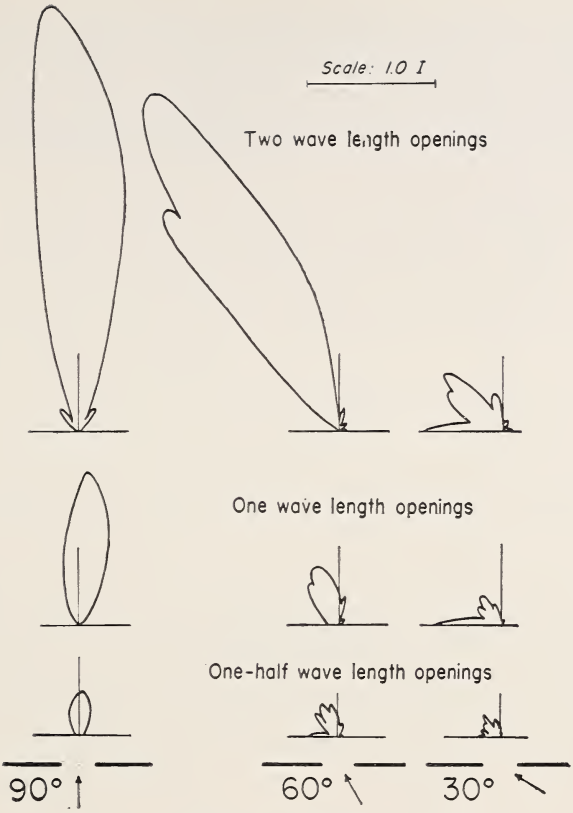

FIGURE 7. *Polar plots of energy distribution.*
(Vertical face straight breakwaters.)

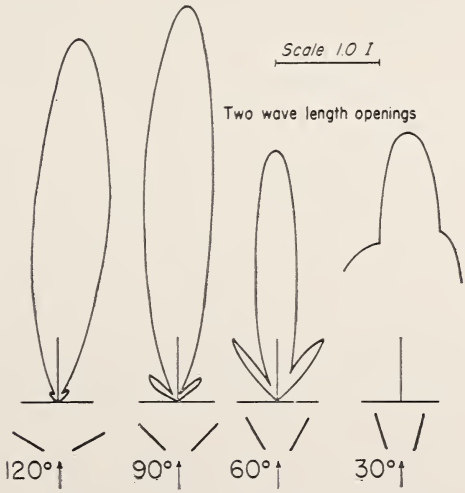

FIGURE 8. *Polar plots of energy distribution.*
(Vertical face symmetrically inclined breakwaters.)

Blue and Johnson [4]. For still smaller included angles, marked changes appear due to the partial frustration of the diffraction process, or prevention of free expansion of the wave crests. Thus, the 60° and 30° alinements are marked by a decrease in intensity along the axis of symmetry, and a build up of intensity along the breakwater arms. It should be noted that for such extreme cases as the 30° alinement the intensity

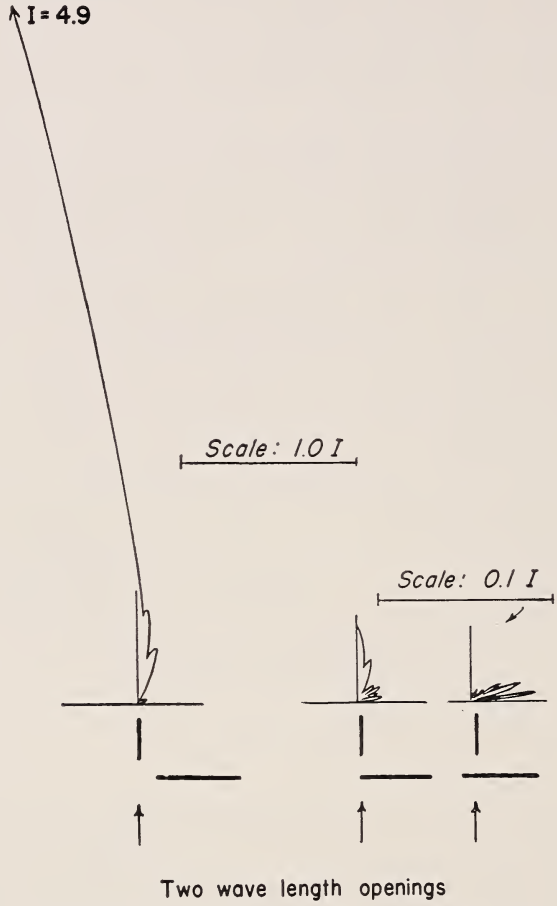

FIGURE 9. *Polar plots of energy distribution.*
(Vertical face right angle breakwaters.)

factor concept is not valid, and the data cannot be used to compute wave heights at other than the original measuring distance of 5.76 wave lengths from the opening. In the limiting case of parallel breakwater arms, there would be no diffraction at all, the wave heights remaining constant for the entire length of the channel; in the 30° case illustrated, the heights must decrease at some rate intermediate between the "zero rate" for a channel and the inverse square root of distance relation for complete diffraction. The data clearly indicate the transition in behavior between

60° and 30° enclosed angles, and so points out an important factor to be considered in the design of harbors with converging breakwaters.

The data of figure 9 are included as a purely experimental evaluation of types of energy distribution that may occur for typical asymmetrical breakwater alinements. The origin of the polar plots for these cases is not the center of the breakwater opening as in the other figures, but is the terminus of the breakwater arm oriented parallel to the incident wave crests.

The case in which the seaward arm does not shelter the opening may be regarded as a half-model of a straight breakwater with a gap width of $2\sqrt{2}\lambda$. The resulting intensity diagram, with allowance for the skewness resulting from the unsymmetrical locus of the plot, compares in general shape (although somewhat deficient in magnitude) with the corresponding data of figure 3 for a 3λ opening.

The intensity diagram for the case in which the seaward leg just shelters the gap is similar in shape and of the same order of magnitude as those for the straight breakwater with 0° wave approach. This observation is in agreement with the behavior observed for some of the symmetrically inclined breakwater alinements, that the diffraction process is more sensitive to the angle of wave approach with respect to the alinement of the opening than to the alinement of the breakwater arms which define the opening.

The diagram for the case in which the seaward arm overlaps the leeward arm not only shows the remarkable increase in sheltering obtained with such alinements, but also indicates a shift in direction of the maximum disturbance. The latter effect is easily explained: The wave crests after diffraction around the terminus of the seaward arm of the breakwater approach the leeward leg at nearly 90°, and the resulting intensity distribution is as would be expected after diffraction around the leeward terminus.

4. References

[1] Penney, W. G. and Price, A. T., Diffraction of sea waves by breakwaters, Directorate of Miscellaneous Weapons Development History No. 26—Artificial Harbors, Sec. 3D, 1944.

[2] Sommerfeld, A., Math. Annalen. Bd. **47**, p. 317 (1896).

[3] Putnam, J. A. and Arthur, R. S., Diffraction of water waves by breakwaters Transactions, American Geophysical Union **29**, No. 4, Aug. 1948.

[4] Blue, F. L. and Johnson, J. W., Diffraction of waves passing through a breakwater gap, Transactions American Geophysical Union **30**, No. 5, Oct. 1949.

[5] Lamb, H., Hydrodynamics, Sixth Edition, Dover Publications, 1945.

[6] Morse, P. M. and Rubenstein, P. J., The diffraction of waves by ribbons and by slits, Physical Review **54**, pp. 895–8, Dec. 1, 1938.

[7] Stratton, J. A., Spheroidal functions, Proceedings of National Academy of Sciences **21**, pp. 51–6, 1935.

[8] Morse, P. M., Addition formulae for spheroidal functions, Proceeding of National Academy of Sciences **21**, pp. 56–62, 1935.

[9] Stratton, Morse, Chu, Hutner, Elliptic cylinder and spheroidal wave functions, N. Y. Wiley, 1941.

10] Blanch, G., Introduction to tables of Mathieu Functions, Institute for Numerical Analysis, National Bureau of Standards. (Now being published—contains extensive bibliography on Mathieu functions.)

15. Scattering of Water Waves Treated by the Variational Method

By Joseph B. Keller [1]

Abstract

To describe the scattering (i.e., reflection, transmission, and diffraction) that occurs when water waves impinge upon a submerged or floating obstacle, a discontinuity of bump in the bottom contour, a change in width or depth of a channel, etc., requires the solution of a partial differential equation subject to specified boundary conditions. But generally the complete solution is not desired—only its behavior far from the obstacle is required. The far behavior of the solution (in the linear theory) can be obtained without solving the complete problem, by means of the variational method employed extensively by Schwinger and his coworkers to treat the corresponding electromagnetic problems.

The method depends upon the fact that the far field can generally be characterized by one number, the amplitude of a scattered wave, or sometimes by the amplitudes of several scattered waves. This fact can be deduced from the representation of the solution as an integral over the obstacle, which is obtained from Green's theorem. From this same representation both an integral equation and various variational problems for the solution can be obtained. The stationary values of these variational problems are just the amplitudes of the scattered waves. Thus good approximations to these amplitudes can be obtained by applying the Rayleigh-Ritz method (or any similar procedure) to the variational expressions. The method has been applied to several water-wave scattering problems: a small post in a channel or rectangular cross section, a change in depth of a channel[2] (e.g., "continental-shelf" problem), etc.

---

[1] Institute for Mathematics and Mechanics, New York University, New York, N. Y.

[2] This application was made by Mortimer L. Weitz and the author.

16. The Diffraction of a Swell. A Practical Approximate Solution and Its Justification

By H. Lacombe [1]

There is presented a practical approximate solution for the evaluation of the amplitude of a swell diffracted at any incidence whatever by a pass in a breakwater.

M. Schoemacher, of the Laboratory of Delft, has reported that the problem of the diffraction by a pass at any incidence whatever has been solved. But this solution involves the rather unusual Mathieu functions [2],[2] of which there exist few detailed tables. There is presented a solution easy to employ which, even though approximate, should suffice for most cases.

There is also presented a generalization of Huyghens principle for oblique incidence derived from the method advocated by Kirchhoff [3] to justify this principle for waves of three dimensions. The assumptions are examined in detail; because it is difficult to predict their effect, it is necessary to compare with the exact solution and, still better, with the results of model tests.

1. Generalization of Huyghen's Principle

Consider a swell moving in the unlimited plane xOy of water of depth h, Oz being positive upward. Its velocity potential is of the form

$$\phi=\frac{g}{\sigma}\frac{\mathrm{Ch}k(h+z)}{\mathrm{Ch}\,kh}ue^{i\sigma t},$$

$$\text{with}\quad \sigma=2\pi/T=gk\ \mathrm{Th}\ kh \quad\text{and}\quad k=2\pi/\lambda,$$

T the period, λ the wave length. u, a function of x and y, is the topography of the free surface at the instant $t=0$. As ϕ satisfies $\Delta\phi=0$, one has

$$\frac{\partial^2 u}{\partial x^2}+\frac{\partial^2 u}{\partial y^2}+k^2u=0.$$

Consider on the other hand, the function

$$\psi=\frac{\mathrm{Ch}\ k(h+z)}{\mathrm{Ch}\ kh}D_0(kr)e^{i\sigma t},$$

where r is the distance of a fixed point P from any point M, and $D_0(kr)\equiv v(kr)$. Following the notation of Lamb [4],

$$D_0(Z)=-Y_0(Z)-iJ_0(Z),$$

[1] Service Hydrographique de la Marine, Paris, France.

[2] Figures in brackets indicate the literature references on p. 139.

J_0 and Y_0 being the Bessel functions of order 0, of the first and second kinds, respectively. Retaining the real part one has

$D_0(kr)e^{i\sigma t}=J_0(kr)\sin\sigma t-Y_0(kr)\cos\sigma t$. ψ satisfies $\Delta\psi=0$, and one has

$$\frac{\partial^2 v}{\partial r^2}+\frac{1}{r}\frac{\partial v}{\partial r}+k^2 v=0.$$

ψ is the velocity potential of a surface wave created by oscillations in the small region enclosing the point P.

Consider then (fig. 1) a volume, V, formed by a vertical cylinder with horizontal cross section, l, in the interior of which is placed a second circular cylinder of radius ϵ whose cross section λ centers on the vertical through P. These cylinders are limited at the bottom where $z=-h$ and on the surface where $z\#0$.

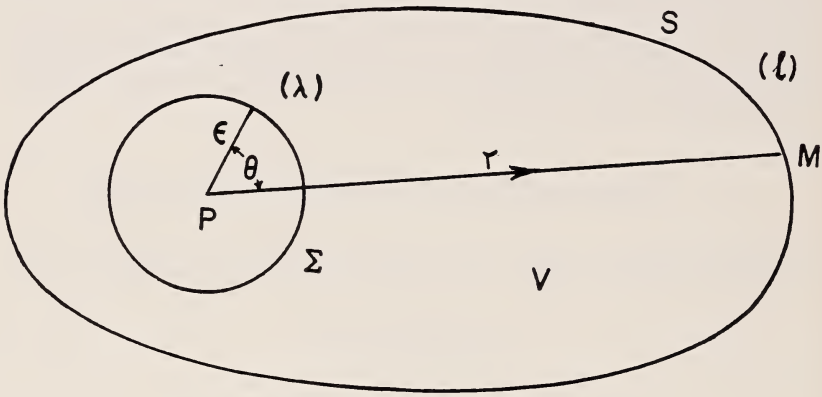

FIGURE 1. *Notation diagram.*

For the volume comprised between the two cylinders, where ψ and ϕ remain finite as well as their derivatives, we can write Green's theorem

$$\iiint_v(\phi\Delta\psi+\psi\Delta\phi)dv=\iint\left(\phi\frac{\partial\psi}{\partial n}-\psi\frac{\partial\phi}{\partial n}\right)ds. \tag{1}$$

The normal derivative is taken in the outward sense from V.

The triple integral is zero because $\Delta\phi=\Delta\psi=0$. The surface integral is taken over the whole surface of the volume V, that is to say, on the one hand over the surface of the exterior cylinder S and the surfaces of the bases diminished by the bases of the small cylinder, and on the other hand over the lateral surface Σ of the interior cylinder. Thus the formula reduces to

$$\iint_{(S)}\left(\phi\frac{\partial\psi}{\partial n}-\psi\frac{\partial\phi}{\partial n}\right)dS+\iint_{(\Sigma)}\left(\phi\frac{\partial\psi}{\partial n}-\psi\frac{\partial\phi}{\partial n}\right)d\Sigma=0. \tag{2}$$

Since at the surface and at the bottom the normal is directed according as Oz is positive or negative, one has

$$\frac{\partial\phi}{\partial n}=\pm\frac{\partial\psi}{\partial z},\quad \frac{\partial\psi}{\partial n}=\pm\frac{\partial\psi}{\partial z},$$

rigorously at the bottom where z is equal to $-h$, to the second order (approximately for a flat wave) near the surface.

The integrals relative to the bottom and to the surface are thus zero.

There remain the integrals relative to the lateral surfaces of the two cylinders; substituting the values of ϕ and ψ, they become

$$\frac{g}{\sigma}\int\int_S \frac{\mathrm{Ch}^2\, k(h+z)}{\mathrm{Ch}^2\, kh}\left(u\frac{\partial v}{\partial n}-v\frac{\partial u}{\partial n}\right)dS$$

$$+\frac{g}{\sigma}\int\int_\Sigma \frac{\mathrm{Ch}^2\, k(h+z)}{\mathrm{Ch}^2\, kh}\left(u\frac{\partial v}{\partial n}-v\frac{\partial u}{\partial n}\right)d\Sigma=0.$$

u and v depending not on z but only on l and λ, one can simplify and write

$$\int_{(l)}\left(u\frac{\partial v}{\partial n}-v\frac{\partial u}{\partial n}\right)dl+\int_{(\lambda)}\left(u\frac{\partial v}{\partial n}-v\frac{\partial u}{\partial n}\right)\epsilon d\theta=0$$

because on the circle λ one has $d\lambda=\epsilon d\theta$.

The second term of the second integral tends toward zero because $\partial_u/\partial_n=-\partial_u/\partial\epsilon$ has a finite limit and $\epsilon D_0(k\epsilon)$ tends toward zero, since for small z,

$$D_0(z)\#-\frac{2}{\pi}\log\frac{z}{2}\cdot$$

As to the first term, u tends toward u_p, $\epsilon\partial v/\partial n=-\partial v/\partial\epsilon$ tends toward $2/\pi$, and

$$\int_{\epsilon\to 0} u\frac{\partial v}{\partial n}\epsilon d\theta=\frac{2}{\pi}u_p\int d\theta=4u_p.$$

One thus has deduced the fundamental formula

$$\int_{(l)}\left(u\frac{\partial v}{\partial n}-v\frac{\partial u}{\partial n}\right)dl=-4u_p, \tag{3}$$

which relates the value u_p of u at a point P to the values supposedly known which the function ϕ has on the closed contour l.

Let there be an unlimited basin of constant depth referred to the two axes Ax and Ay. There is propagated in the direction of y positive a simple harmonic wave of the form

$$\frac{ga}{\sigma}\frac{\mathrm{Ch}\, k(h+z)}{\mathrm{Ch}\, kh}e^{-iky}e^{i\sigma t}.$$

Suppose one introduces in this basin a breakwater leaving a pass AB (fig. 2). Let AX and AY be the axes relating to the breakwater, and Ax

and Ay the axes relating to the direction of the swell. Let α be the angle between Ox and $\overline{AB}$, A being the first end of the pass reached by the swell. The coordinates of the point P where one seeks the motion are x,y and X,Y in the two systems of axes.

We apply Green's theorem to a closed contour l formed by the portion $X'A$ of the breakwater, the pass AB, the portion BX, and then a line to infinity represented schematically by the broken line in the figure.

We then suppose that (a) the functions u and $\partial u/\partial n$ are identically zero from X' to A, from B to X, and on the remainder of the contour l; (b) between A and B the function u *maintains on* AB the value that it would have in the absence of the obstacle; (c) in spite of the discontinuity thus introduced in u and $\partial u/\partial n$, we can apply Green's theorem.

Nothing can be said at this time as to whether the movement that we will deduce from eq 3 will coincide with the assumed movement at $Y=0$.

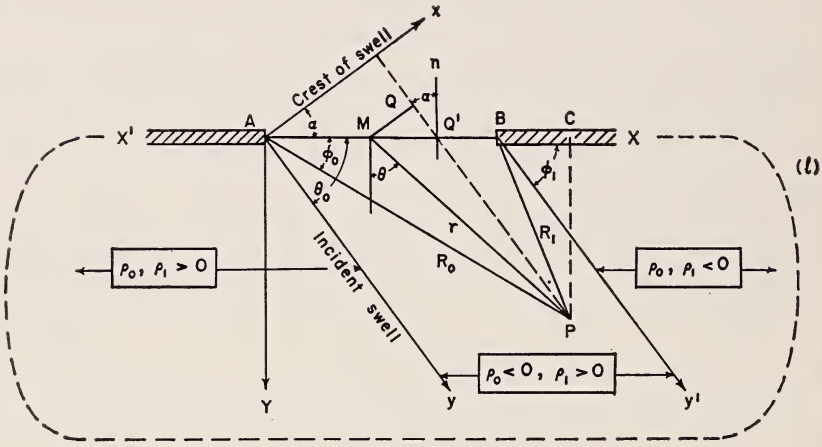

FIGURE 2. *Diagram of breakwater with pass, showing notation.*

Under these conditions, the function u on AB is taken equal to ae^{-ky} or $ae^{-ikl\sin\alpha}$, denoting by l the length AM (fig. 2). Let θ be the angle between the normal at M to AB directed toward Y negative, and the radius vector $PM=r$. Equation 3 gives

$$4u_p=-\int_{AB}\left[(ae^{-ikl\sin\alpha}\frac{\partial D_0(kr)}{\partial n}-D_0(kr)\frac{\partial}{\partial n}(ae^{-ikl\sin\alpha})\right]dl,$$

$$\frac{\partial u}{\partial n}=-\cos\alpha\frac{\partial u}{\partial y}=aik\cos\alpha e^{-iky}.$$

On the other hand, if r is sufficiently large, greater than two or three wave lengths, one has practically

$$D_0(kr)\#\frac{1}{\pi}\sqrt{\frac{\lambda}{r}}e^{-i(kr+\pi/4)}$$

by neglecting a term in $r^{-\frac{3}{2}}$. In the same manner, by neglecting a new term $r^{-\frac{3}{2}}$, one has practically

$$\frac{\partial v}{\partial n}=\cos\theta\frac{\partial v}{\partial r}=-\frac{\sqrt{\lambda}}{\pi}\frac{ik\cos\theta}{\sqrt{r}}e^{-i(kr+\pi/4)}.$$

By substitution, these become

$$4u_p=\frac{a}{\pi}k\sqrt{\lambda}\int_{AB}\frac{e^{-i[k(l\sin\alpha+r)-\pi/4]}}{\sqrt{r}}(\cos\theta+\cos\alpha)dl,$$

and, taking λ as the *unit of measure of horizontal lengths*

$$u_p=a\int_{AB}\frac{1}{\sqrt{r}}\frac{\cos\alpha+\cos\theta}{2}e^{-i[2\pi(l\sin\alpha+r)-\pi/4]}dl. \tag{4}$$

One passes to ϕ_p by multiplying by $\frac{\mathrm{Ch}\,k(z+h)}{\mathrm{Ch}\,kh}e^{i\sigma t}$. This formula, gives a *statement of Huyghen's principle* valid (within the limits of the assumptions made) for oblique incidence.

The motion at P can be considered as due to elementary sources distributed on AB, the phases being taken equal to those that exist on AB in the original motion, say $2\pi l\sin\alpha$, and which produce at M a motion inversely proportional to $\sqrt{r}$ and of which the phase is retarded by $2\pi r$ because of the trajectory MP. The term $(\cos\theta+\cos\alpha)/2$ expresses the effect of the *oblique incidence* and of a directivity of the sources.

For normal incidence, AB is a wave surface and the angular term becomes $(1+\cos\theta)/2$. If one refers to our study of diffraction at normal incidence [5], one sees that we arrive here at the average of two solutions, which we have believed should be considered and which are quite close, at least near the limit of the geometric shadow.

2. Practical Evaluation of the Motion

Displacing the phases by $\pi/4$ and taking in the following as origin of the phases those existing at the point P in the absence of an obstacle, that is to say, subtracting $2\pi y$, we have

$$u_p=\frac{a}{2}\int_{AB}\frac{1}{\sqrt{r}}(\cos\theta+\cos\alpha)e^{-i[2\pi(l\sin\alpha-y+r)]}dl.$$

The equation is valid in large part if $Y>2$.
Placing [3] then

$$l\sin\alpha-y+r=\rho^2/4=PM-PQ,$$

ρ has two values of opposite sign between which we will later make a choice. Eliminating l, this becomes

$$\overline{MC}^2=\overline{(l-x)}^2=r^2-Y^2,\quad dl=\frac{rdr}{\pm\sqrt{r^2-Y^2}}.$$

[3] This change of variables is that previously used by Fresnel for the study of optical diffraction.

Since $\cos\theta = Y/r$, u_p is equal to

$$u_p = \frac{a}{2}\int_{AB}\left(\sqrt{r}\cos\alpha + \frac{Y}{\sqrt{r}}\right)e^{-i\rho^2\pi/2}\frac{dr}{\pm\sqrt{r^2-Y^2}}, \tag{5}$$

and one easily obtains

$$\frac{\rho d\rho}{2} = dr + \frac{rdr\sin\alpha}{\pm\sqrt{r^2-Y^2}} \quad \text{and} \quad \frac{dr}{\pm\sqrt{r^2-Y^2}} = \frac{d\rho}{\mp 2\sin\alpha\sqrt{\frac{\rho^2}{16}+\frac{Y}{2}\sin\alpha}},$$

$$r = \frac{\rho^2+4Y\cos\alpha \pm \rho\sin\alpha\sqrt{\rho^2+8Y\cos\alpha}}{4\cos^2\alpha}.$$

Placing these values in eq 5, we finally have

$$u_p = \frac{a}{2}\int_{AB} \pm\frac{\sqrt{\rho^2+8Y\cos\alpha}\pm\rho\sin\alpha}{\sqrt{\rho^2+4Y\cos\alpha\pm\rho\sin\alpha\sqrt{\rho^2+8Y\cos\alpha}}}e^{-i\rho^2\pi/2}d\rho.$$

The two signs lead to two determinations of r as a function of ρ.

ρ becomes zero when M passes beyond the point Q' on the normal to the incident crests passing through P. It is logical to take ρ positive on one side of Q' and negative on the other, and one passes over the entire infinite line $X'X$ when ρ varies from $-\infty$ to $+\infty$.

When the point P, in relation to Ay (A being the first end of the breakwater reached by the swell), is on the side opposite to B (the second end of the breakwater reached by the swell) the parameters ρ_0 and ρ_1 relative to the ends of the breakwater A and B are negative; ρ_0 is negative and ρ_1 positive when P is found between Ay and By'; ρ_0 and ρ_1 are negative if P is on the side of By', which does not contain Ay. And one has

$$\rho_0 = \pm 2\sqrt{PA-PA_1}, \quad = -2\sqrt{2R_0}\sin\frac{\theta_0-\phi_0}{2}$$

$$\rho_1 = \pm 2\sqrt{PB-BB_1}, \quad = -2\sqrt{2R_1}\sin\frac{\theta_0-\phi_1}{2}$$

with $R_0 = PA$, $R_1 = PB$.

Figure 2 shows these conventions in the framed labels.

Restoring the factor $e^{i\sigma t}$ and retaining the real part, one sees that the superficial motion at P is

$$u_p e^{i\sigma t} = \frac{a}{2}\int_{\rho_0}^{\rho_1}\frac{\sqrt{\rho^2+BY\cos\alpha}-\rho\sin\alpha}{\sqrt{\rho^2+4Y\cos\alpha-\rho\sin\alpha\sqrt{\rho^2+8Y\cos\alpha}}}\cos\left(\sigma t-\frac{\pi}{2}\rho^2\right)d\rho$$

$$\equiv \frac{a}{2}\int_{\rho}^{\rho_1} P\cos\left(\sigma t-\frac{\pi}{2}\rho^2\right)d\rho. \tag{6}$$

The amplitude of the motion is given by the distance of the points of parameters ρ_0 and ρ_1 on the curve

$$\overset{X}{\alpha}=\frac{a}{2}\int_0^{\rho} P\cos\frac{\pi}{2}\rho^2 d\rho$$

and

$$\overset{Y}{\alpha}=\frac{a}{2}\int_0^{\rho} P\sin\frac{\pi}{2}\rho^2 d\rho.$$

Taking $a=1$, one obtains the relative amplitude. The curves (fig. 3) are analogous to the Cornu spirals, and to the spirals introduced with relation to normal incidence [5], and as long as $Y\geq 2$, they practically

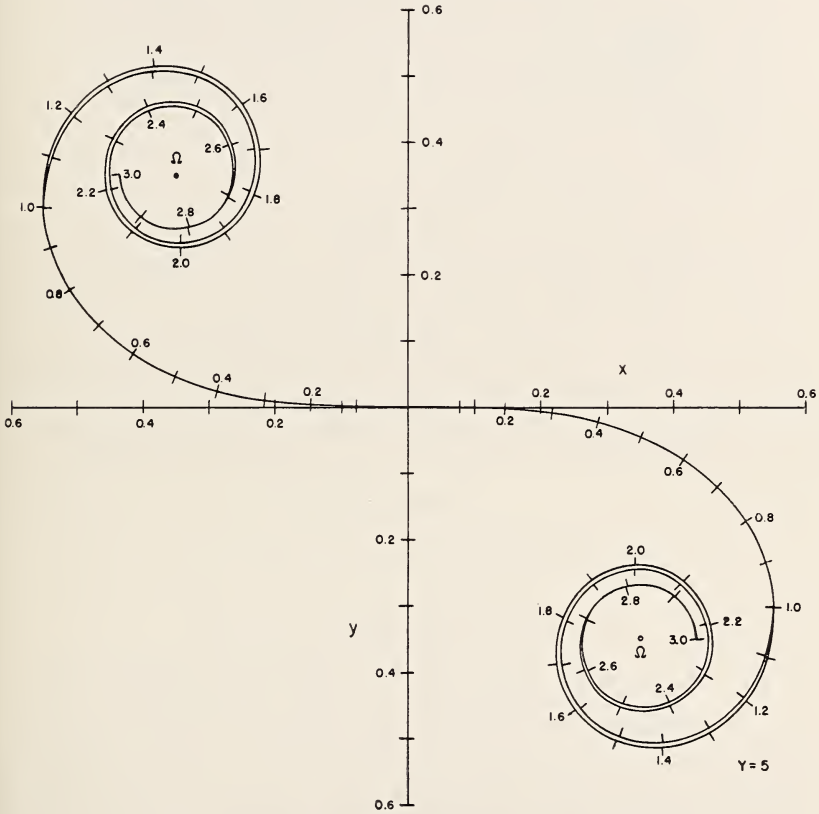

FIGURE 3. *Spirals of relative amplitudes.*

Take the interior spiral which is the Cornu spiral reduced in the ratio $1/\sqrt{2}$.

differ very little. The angle of contingence is $\pi\rho^2/2$; the radius of curvature at the point of the parameter ρ is $\Re=P/2\pi\rho$. The curves $\rho=$const. are parabolas which one can trace once and for all (fig. 4). The straight line $\rho=0$ corresponds to the parallel to the direction of propagation of the incident swell passing the end of the pass.

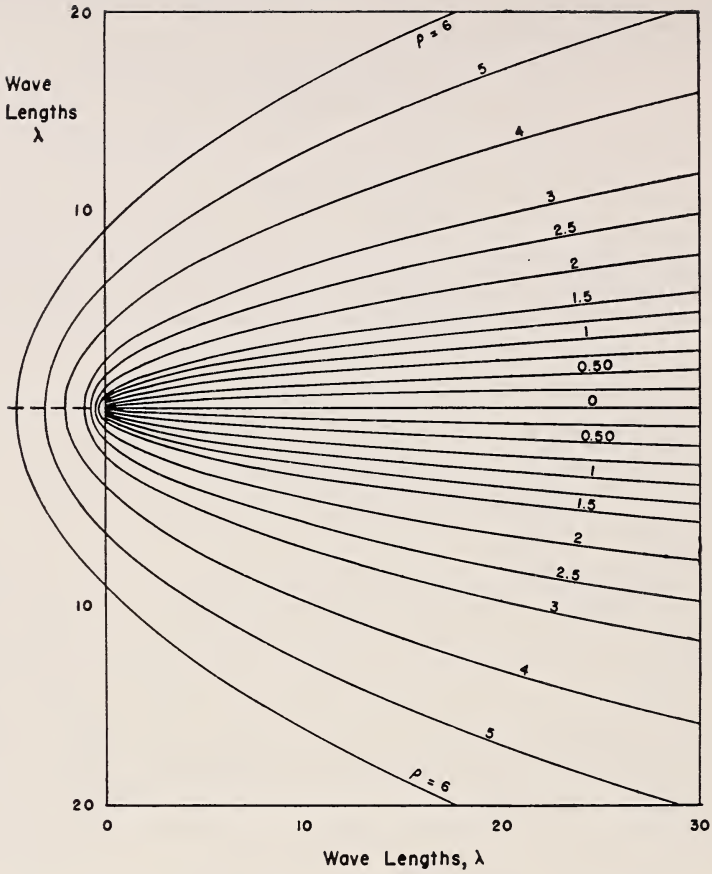

FIGURE 4. *Parabolas for $\rho = constant$.*

3. Some Practical Examples

3.1 Case of Very Large Passes. Semiinfinite Breakwaters

For Y greater than several units and $|\rho| \leq 2.5$ we have verified that the spirals were practically identical with the spirals of Cornu.[4] Thus on a straight line $y =$ constant, the motion is the same as for normal incidence because the parameter $\rho_0 = \pm 2\sqrt{R_a - y}$ has the same value as for normal incidence (fig. 5).

The curve obtained for $y = 4$ and $\alpha = 30°$ is, to the accuracy of the drawing, almost identical with the "simplified solution" proposed by J. A. Putnam and R. S. Arthur [6].

The curves of equal amplitude, for Y greater than a few units, are approximately parabolas having the end A of the pass as focus.

[4] Therefore symmetrical; it is thus not necessary to particularize the signs of ρ_0 and ρ_1 but it suffices to take the different branches of the spiral when $\rho_0\rho_1 < 0$.

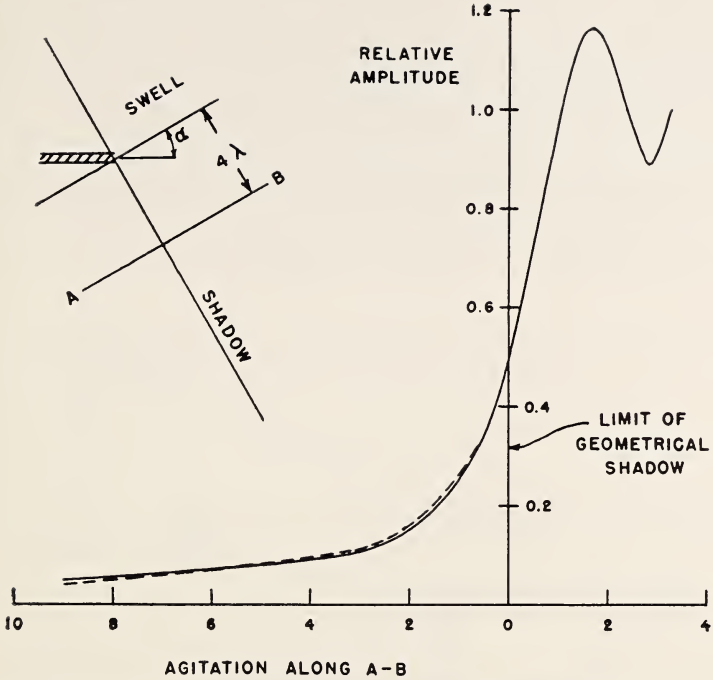

FIGURE 5. *Solution for $y=4$ and $\alpha=30°$ compared with simplified solution proposed by Putnam and Arthur.*

Dash line, proposed solution; full line, simplified solution by Putnam and Arthur

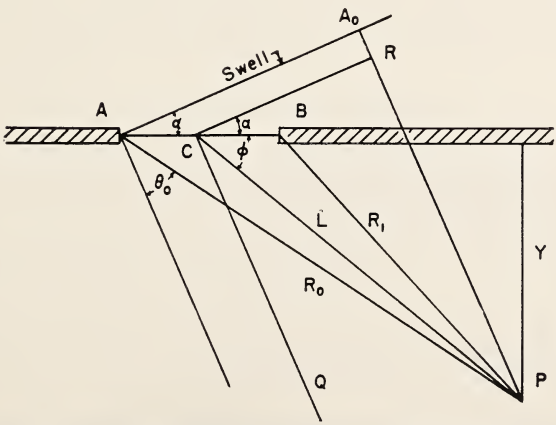

FIGURE 6. *Diagram of breakwater with narrow pass, showing notation.*

3.2 Case of Passes of Limited Dimensions

One effects the integration between the values ρ_0 and ρ_1 of the parameter corresponding to the ends A and B of the pass. The amplitude passes through minima, the parameters ρ_0 and ρ_1 being of the same sign, if the values of $\pi\rho_1^2/2-\pi\rho_0^2/2$ differ by a multiple of 2π; if they differ by an odd multiple of π, there is on the contrary a maximum.

If the *distance L from the center of the pass to the point under consideration is large in comparison to the dimension D of the pass* (D in wave lengths), the values of ρ are small and differ little in the neighborhood of the straight line passing through the center C of the pass and parallel to the direction of propagation (fig. 6). If far from this straight line, the values of ρ

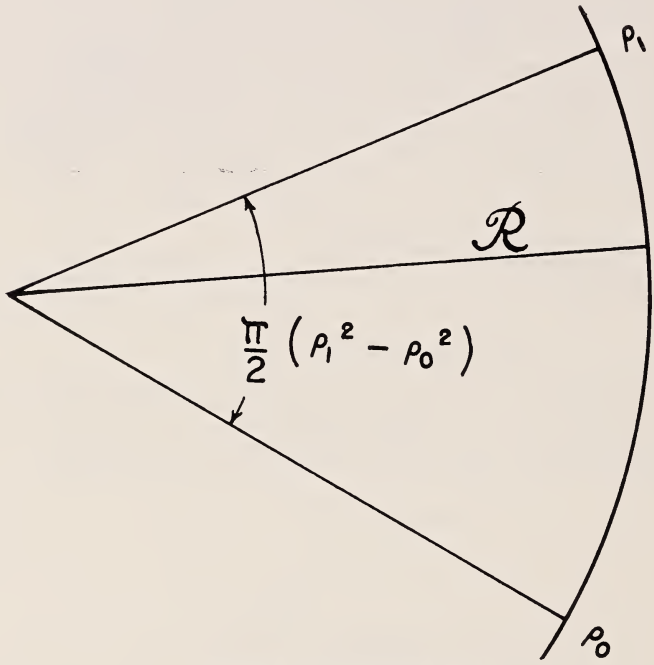

FIGURE 7. *Notation diagram.*

differ more but are large, and the spirals are thus almost circles. Thus the amplitude in all cases (fig. 7) becomes

$$2\mathfrak{R}\sin\frac{\pi}{4}(\rho_1^2-\rho_0^2), \tag{7}$$

$\mathfrak{R}$ being the radius of curvature pertaining to the value of ρ relative to the point C, namely,

$$\rho=-2\sqrt{2L}\sin\frac{\theta_0-\phi}{2}.$$

(See fig. 6 for significance of notation).

Under these conditions, one shows in a simple manner that the expression 7 becomes practically

$$\frac{D}{2\sqrt{L}}(\sin\theta_0+\sin\phi)\frac{\sin\pi D(\cos\phi-\cos\theta_0)}{\pi D(\cos\phi-\cos\theta_0)}, \tag{8}$$

where D and L are expressed in wave lengths.

For $\phi=\theta_0$, this expression takes a value equal to

$$\frac{D\sin\theta_0}{\sqrt{L}}=\frac{D\cos\alpha}{\sqrt{L}},$$

which gives the amplitude on the straight line passing through the center of the pass and parallel to the direction of propagation.

There are minima of very slight motion in the directions such that

$$\pi D\,(\cos\theta_0-\cos\phi)=n\pi,$$

whence $\cos\theta_0-\cos\phi=n/D$, n being a positive or negative integer.

The maxima of amplitude are found practically on the radius vectors such that

$$\cos\theta_0-\cos\phi=\frac{2p+1}{2D},$$

p being a positive or negative integer but not zero; there is a supplementary maximum found for ϕ a little larger than θ_0; the error with respect to θ_0 arises from the presence of the term $\sin\theta_0+\sin\phi$ and is so much the larger as ϕ varies more rapidly in the neighborhood of θ_0, that is to say that θ_0 is smaller. As a result there is a dissymmetry of the branches so much the greater as θ_0 is the smaller.

Whatever the case may be, one finds these diagrams of directivity at the "branches," [1, 5], the directivity being so much the greater as the pass is larger with respect to the wave length. These branches are, for normal incidence at least, visible on certain photographs obtained in the laboratory [7].

Figure 8 relates to an incidence of 60°; for a width of the pass of three wave lengths.

One deduces from formula 8, contrary to our assumptions, that the motion is not zero for $\phi=0$ and $\phi=\pi$, but small, on the interior face of the breakwater. The result obtained is thus only approximate and only model tests will make it possible to state that our assumptions will not lead to errors too large for practice.

4. References

[1] Morse and Rubenstein. The diffraction of waves by ribbons and slits. Phys. Rev. Vol. 54, Dec. 1938, pp. 895–8.

[2] Mathieu. Cours de physique mathematique. Gauthier-Villers. Paris, 1873, pp. 122–165.

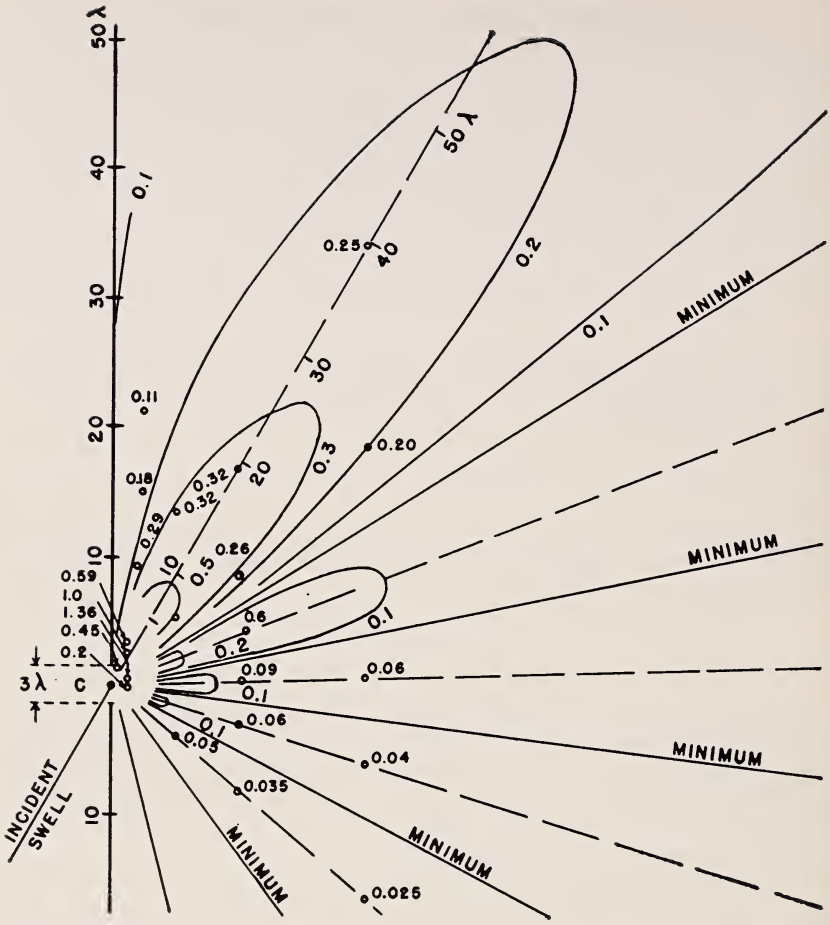

FIGURE 8. *Diagram of amplitudes for a pass width of three wave lengths, angle of incidence α equal to 60°.*

[3] L. de Broglie. Problèmes de propagations guidées des ondes electromagnétiques. pp. 91 et seg.
[4] Lamb. Hydrodynamics. 6th Edition, pp. 294–6.
[5] Lacombe. La diffraction de la houle en incidence normale. Annales Hydrographiques de 1949. Paris.
[6] Putnam and Arthur. Diffraction of water wave by breakwaters. Trans.-Amer. Geophys. Union. Vol. 29, No. 4, Aug. 1948.
[7] Blue and Johnson. Diffraction of water waves passing through a breakwater gap. Trans. Amer. Geophys. Union. Vol. 30, No. 5, Oct. 1949.

17. The Criterion for the Possibility of Roll-Wave Formation

By A. Craya [1]

The theoretical interpretation of roll waves, proceeding from the equations of Saint-Venant, can follow two primary lines of approach: the first considers the stability of flow in a channel, i.e., the damping or amplification of a perturbance of small initial amplitude; the second proceeds from a systematic analysis of the quasisteady regime introduced by H. A. Thomas.

The object of the study is to analyze, compare, and clarify these two points of view for a prismatic channel of arbitrary cross section and for resistance laws of general form. Both lead to the same criterion for the condition of roll-wave formation, which coincides for particular conditions with the formula obtained by Vedernikov from a somewhat different stability derivation.

1. Introduction

Within the vast family of gravity waves, "roll waves" do not occupy a place of major importance in engineering science; nevertheless, they are of a certain indirect interest, because they constitute a phenomenon at the border of the usual open-channel flow and thereby can serve to check the validity of the approximate equations by means of which we nowadays calculate these flows.

Since the time of Boussinesq, who initiated its study without being aware of it, many investigations have been devoted to this question by diverse methods and approximations; as a consequence, the theory has lost in unity while gaining in scope, and the logical relationship and the practical agreement of the various results do not always appear very clearly.

The object of this study is to give a simple and coordinated presentation of the theory without resorting to too complicated calculations; while still considering a very general case, i.e., channels of arbitrary cross section and arbitrary resistance laws. The line of approach of the investigation of quasi-steady regimes inaugurated by H. A. Thomas is first examined and its consequences are analyzed in a geometrical manner by introducing a convenient representative plane. Thereafter, the study of stability of a permanent regime is centered on the motion of an elementary wave, following a presentation which we have introduced in a previous publication.[2] We then finally emphasize the agreement of the results thus obtained and the complementary physical interpretations implied by each of the two lines of research.

---

[1] Iowa Institute of Hydraulic Research, Iowa City, Iowa. On leave from Etablissements Neyrpic and University of Grenoble, France.

[2] Craya, A., Calcul graphique des régimes variables dans les canaux, *La Houille Blanche*, No. 1, Nov. 1945, pp. 39–60.

2. Basic Equations

In the following treatment we shall use the well-known approximation of the equations of Saint-Venant. Letting x be the abscissa measured along the bottom, i the slope of the bottom (assumed to be constant but not necessarily small), U the mean velocity, Q the discharge, h the depth measured normal to the bottom, λ the coefficient of resistance, R the hydraulic radius, the dynamic equation and the equation of continuity are written

$$\left.\begin{aligned} &\frac{\partial}{\partial x}\left(h\cos i+\frac{U^2}{2g}\right)+\frac{1}{g}\frac{\partial U}{\partial t}=\sin i-\epsilon\lambda\frac{U^2}{gR}, \quad (\epsilon=\text{sign of } U) \\ &\frac{\partial Q}{\partial x}+\frac{\partial \omega}{\partial t}=0. \end{aligned}\right\} \tag{1}$$

These equations can be somewhat perfected by introducing, according to Boussinesq, a coefficient α of unequal velocity distribution; this factor certainly plays a role in the very turbulent flows which we are going to consider, but it is not at all certain that we can accept $\alpha=\text{const.}$, as is commonly done. We thus prefer to avoid this question and, in an attempt toward clarity, to follow the basic equations given previously.

3. Quasi-steady Regimes

The most simple solutions of eq 1 leading to important results in several domains are those corresponding to a mass propagation of a surge with a constant celerity; observed from reference axes moving with velocity c, the phenomenon is reduced to a steady flow condition, but with moving walls. The introduction of this very simple and very fruitful notion is due to H. A. Thomas.

Writing U and ω as functions of $x-ct$, the basic eq 1 are immediately translated into relative axes by

$$\frac{d}{dx}\left(h\cos i+\frac{U'^2}{2g}\right)=\sin i-\epsilon\lambda\frac{(c+U')^2}{gR}, \quad U'\omega'=Q'=\text{const.}, \tag{2}$$

where ϵ is the sign of $c+U'$, and U' and Q' are the relative velocity and the relative discharge, respectively. Evidently these equations define generalized backwater curves and reduce to the customary backwater curves of hydraulics when $c=0$. In what follows we shall, by convention, take the positive direction of x in the downstream sense. The term $\sin i$ is then positive, and the quantities U', Q', U, and Q are measured algebraically according to the positive direction chosen.

As in classical hydraulics the development of these new backwater curves is governed by the notions of critical depth and normal depth. The first one always corresponds to the minimum of the specific head E.

$$E=h\cos i+\frac{U'^2}{2g}.$$

The derivative E' of this quantity with respect to h is written

$$E' = \cos i - \frac{Q'^2}{g\omega^3} b,$$

where ω is the area of the cross section and b the width at the free surface. From this we obtain for the critical regime defined by $E' = 0$

$$Q' = \pm\sqrt{\frac{g\omega^3}{b} \cos i}. \tag{3}$$

In the following articles we shall make great use of a representative plane Q',ω which seems to us particularly well adapted to the results that we have in view; on such a plane (fig. 1) the curve of critical regime $E' = 0$

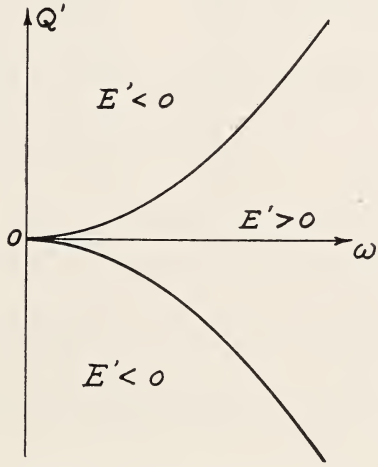

FIGURE 1. *Diagram of Q',ω plane.*

divides two regions corresponding, respectively, to so-called "shooting" flow ($E' < 0$ or $\omega < \omega_c$) and "tranquil" flow ($E' > 0$ or $\omega > \omega_c$). As to the notion of normal depth, we define it by the condition of uniform flow, that is, by the relation $F = 0$, where F is the right-hand member of the dynamic eq 2; this can also be written, designating by χ the wetted perimeter, in the form

$$F = \sin i - \epsilon\lambda \frac{(c\omega + Q')^2}{g\omega^3} \chi.$$

In order to represent these new uniform regimes on the plane Q',ω it is convenient to introduce the absolute velocity through the relation

$$Q = c\omega + Q',$$

and to find as a preliminary task the dotted curve of figure 2 representing

$$\sin i - \frac{\lambda Q^2}{g\omega^3} \chi = 0,$$

which is the law of ordinary uniform regimes $Q(\omega)$ for fixed sides; then, by laying off from the straight line Ot of slope $-c$, the ordinates mM equal to $m'M'$, we will obtain the desired curve of uniform regimes for moving side.

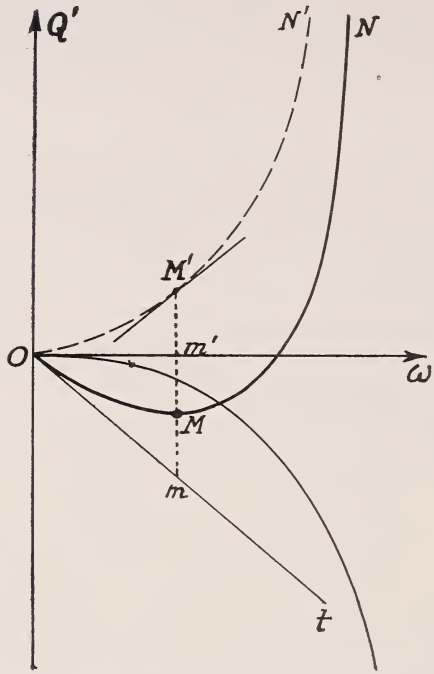

FIGURE 2. *Diagram for evaluating uniform regimes in plane Q',ω.*

With the introduction of the quantities E' and F the profile of the surge is written

$$dx=\frac{E'}{F}dh,$$

and the slope of the free surface with respect to the bottom depends on the depth of water with respect to the normal and critical depths. The over-all situation is clearly represented by the plane Q',ω, on which the curves of normal and critical regime are drawn (fig. 3); this plane is divided into regions in which the sign of E'/F remains constant; the cross-hatched regions correspond to positive values, i.e., to a depth of water increasing with distance downstream; each water-surface line is given by an intersection of the diagram by a straight line $Q'=$ Const.; during the passage across the critical regime the profile is (theoretically) normal to the bottom, and in the vicinity of the point of uniform flow we have an asymptote parallel to the bottom. A first essential point that we note at once and whose importance will become clear later is the possibility of two cases, depending on whether the minimum of the curves of uniform regime falls into the tranquil region (fig. 3a) or the rapid region (fig. 3b). Let us further note that fig. 3 corresponds to $c>0$, i.e., to surges moving downstream; we shall leave aside the case of the surges moving upstream,

which is in general less interesting for the subject with which we are concerned.

Figure 3 allows a systematic classification of surges of constant form to be made, and we note in passing that it shows a few supplementary

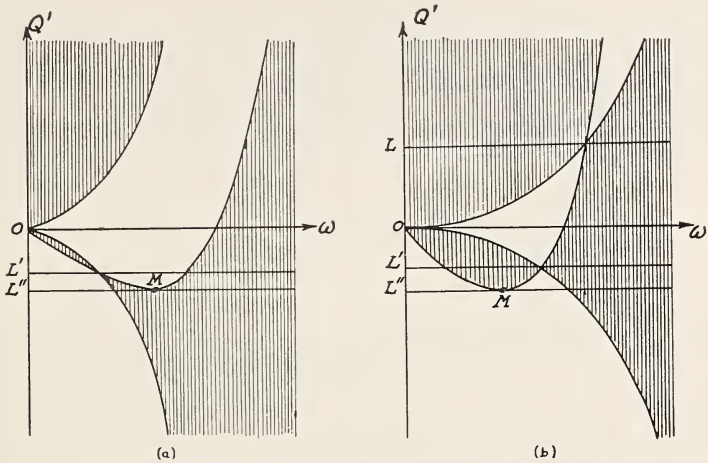

FIGURE 3. *Regions of normal and critical regime in plane Q',ω.*

(a) Minimum of uniform regime in tranquil region. (b) Minimum of uniform regime in rapid region.

cases in addition to those originally indicated by Thomas for a rectangular channel. But the second essential point which we would like to bring into light is Seddon's law for the celerity of surges. If we cut, for example, the graph in fig. 3a by a horizontal line comprised between the lines L' and L'', we obtain the surge of fig. 4, which corresponds to the passage of

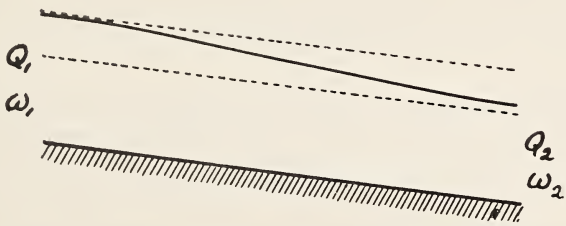

FIGURE 4. *Surge corresponding to passage from uniform regime $Q_1\omega_1$ to another uniform regime $Q_2\omega_2$.*

a uniform regime $Q_1\omega_1$ to another uniform regime $Q_2\omega_2$. By virtue of the relations

$$Q_1 = Q' + c\omega_1, \quad Q_2 = Q' + c\omega_2,$$

the celerity is then given as

$$c = \frac{\Delta Q}{\Delta \omega},$$

and if the perturbation is very small, i.e., if we consider an intersection by a line very close to L'', the celerity becomes the law of Seddon

$$c = \frac{dQ}{d\omega}.$$

We now come to the phenomenon of roll waves. As we have seen, surges of constant form do not allow periodic solutions; this is due to the approximation of the equations of Saint-Venant, and R. F. Dressler obtained solutions for such waves in this approximation by combining portions of the preceding surges with hydraulic jumps (fig. 5). Such a

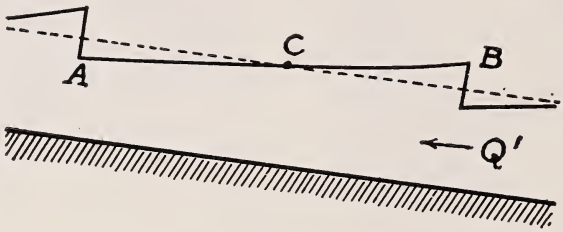

FIGURE 5. *Combination of surges with hydraulic jumps.*

section AB necessarily allows the crossing of the critical regime at C, and in this case it is a crossing without the usual circumstance of a water-surface line perpendicular to the bottom; in other words, in such a point C the denominator F of the backwater equation must be zero as well as E', which corresponds to the lines $L'L''$ of fig. 3a and L, L', L'' of fig. 3b. Furthermore, we must take into account the fact that, owing to well-known energy considerations, only the positive jump has a physical existence. With the sign of the discharge Q' indicated by fig. 3 and transferred on fig. 5, the backwater AB must necessarily increase in the downstream direction, which then excludes the case of fig. 3a; thus, if we assimilate roll waves into the scheme just described, they are only possible for the case of fig. 3b, i.e., for a minimum of the curve of normal regime in the rapid region.

Such is then the criterion to which one is led by following the water-surface line of quasi-steady regimes, and we are going to develop and translate this into equation form. If ω is the abscissa of the minimum M of fig. 3b, we note with reference to fig. 2 and to the manner in which the curve OMN relative to a certain celerity c is deduced from the ordinary law $OM'N'$ of uniform regimes, that this celerity c is the slope of the curve $OM'N'$ at the point M' of the same abscissa as the minimum M; we have, in fact, at the point M, $dQ'/d\omega = 0$, i.e., according to $Q' = Q - c\omega$,

$$c = \frac{dQ}{d\omega}.$$

Consequently, the ordinate Q' of the minimum M is known as soon as the abscissa is given; that is,

$$Q' = Q - \omega\frac{dQ}{d\omega}. \tag{4}$$

In other words, if we consider all the possible celerities c, the line connecting the corresponding minimums M is the curve defined by eq 4 where $Q(\omega)$ is the law of the uniform regimes. To clarify our criterion of the possibility of roll waves, we have then only to compare the different points of eq 4 with the curve of critical regimes given by eq 3, i.e., to write

$$Q-\omega\frac{dQ}{d\omega}<-\sqrt{\frac{g\omega^3}{b}\cos i}. \tag{5}$$

If a physical interpretation of the foregoing result is desired, we can, by grouping the terms differently and by dividing through by ω, rewrite the inequality 5 in the form

$$\frac{dQ}{d\omega}>U+\sqrt{\frac{g\omega}{b}\cos i}. \tag{5a}$$

As we have seen, $dQ/d\omega$ is the celerity of Seddon, i.e., the celerity of a small surge which has arrived at an invariable form and is governed essentially by the channel resistance. The right-hand side of the inequality, on the contrary, is the Lagrangian celerity for an elementary wave under the exclusive action of gravity and inertia. Roll waves are possible in the neighborhood of a uniform regime only when the first celerity is greater than the second. Later we shall see an additional interpretation of this fact starting from the idea of stability of a uniform regime.

For a detailed calculation of criterions, it is convenient to introduce systematically the mean velocity U instead of the discharge by means of the relation $Q=U\omega$; eq 5 then becomes

$$\omega\frac{dU}{d\omega}>\sqrt{\frac{g\omega}{b}\cos i},$$

or, again, by letting V be the relative celerity $\sqrt{(g\omega/b)\cos i}$,

$$\frac{V}{U}<\omega\frac{d}{d\omega}\log U. \tag{5b}$$

The ratio U/V is nothing but the Froude number of a uniform flow, and to make roll waves possible this factor must be greater than a certain limit. We shall take up this calculation later.

4. Stability of an Elementary Wave

Historically it is not from the previous viewpoint of quasi-steady regimes that the roll waves have first been analyzed, but rather from stability considerations. Starting from a uniform regime, for example, the evolution with time of a sinusoidal undulation of very small amplitude is studied and, depending upon the case, an exponential damping or amplification is found. This was first done by Harold Jeffreys for the case of Chezy resistance. In the same order of ideas a clearer physical picture of the phenomenon is obtained by substituting for the sinusoidal perturbation a steep wave front.

For the following discussion we shall define an elementary wave as a shock wave of very small amplitude (fig. 6). It is appropriate to note here that this is a schematic theoretical representation, since real wave fronts are in general complicated by secondary phenomena; still, this concept is extremely useful, and we have shown in a previous publication that it permits the theory of characteristics to be shown in a particularly

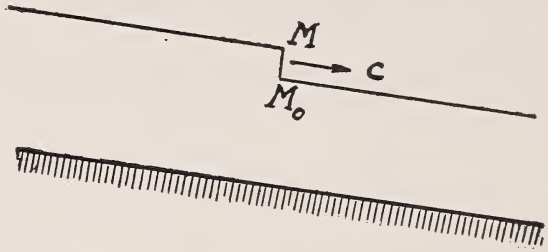

FIGURE 6. *Schematic shock wave of small amplitude.*

intuitive light. It is easily proved that within the conditions of fig. 6 the celerity of an elementary wave is

$$c = U + V, \quad \text{where} \quad V = \sqrt{\frac{g\omega}{b}\cos i},$$

and that the variation of the velocity ΔU and of the section $\Delta\omega$ across the wave are related in the form

$$\Delta U = \sqrt{\frac{g}{b\omega}\cos i}\,\Delta\omega,$$

which can then again be written $\Delta U = \Delta Z$ by introducing the new variable function of the depth of water

$$Z = \int_0^{\omega} \sqrt{\frac{g}{b\omega}\cos i}\,d\omega.$$

The theory of characteristics introduces systematically the viewpoint of an observer who would move along a channel of variable flow with the local celerity of an elementary wave; such an observer descending the current, for example, with a celerity $U+V$ notes on his way variations of velocity and height governed by the relation

$$d(U+Z) = M dt, \quad \text{where} \quad M = g\left(\sin i - \frac{\lambda U^2}{gR}\right).$$

We know that we have here an alternative expression of the equations of Saint-Venant, from which, indeed, it can be derived by a simple linear combination.

The foregoing properties, which we have recalled here briefly, permit calculation of the evolution of a wave front of very small amplitude, as we have indicated in our previous publication. In fact, let U and Z be the state of the wave front at the point M immediately upstream, and

U_0 and Z_0 the similar variables at M_0 on the downstream side (fig. 6). An observer accompanying the wave at M notes that

$$d(U+Z)=\frac{M}{U+V}dx.$$

On the other hand, an observer moving with M_0 notes that

$$d(U_0+Z_0)=\frac{M_0}{U_0+V_0}dx.$$

From these two relations we obtain by subtraction, and by noting that the variations ΔU and ΔZ remain constantly equal on the passage of the wave front, the expression

$$\frac{d}{dx}(\Delta Z)=\frac{1}{2}\Delta_f\left(\frac{M}{U+V}\right), \tag{6}$$

in which $\Delta_f M/(U+V)$ denotes the variation of $M/(U+V)$ across the elementary front wave and consequently for $\Delta U=\Delta Z$. As can readily be seen, this calculation assimilates the celerity of the elementary wave into that of the observer of characteristics at M, and this is the reason why it is applicable only to the limiting cases of an elementary wave; for a finite shock wave, a traveler accompanying the wave front is no longer an observer of characteristics at M and the independent calculation of the evolution of the wave front becomes impossible.

Equation 6 gives much more complete information than we shall content ourselves with supplying here; in fact, it does not suppose an initial uniform regime (it is, however, assumed steady); conveniently modified, it could apply to a channel of variable cross section; and finally, it gives the coefficient of exponential damping or amplification. If we limit ourselves to a uniform regime, this relation becomes, since M_0 is zero,

$$\frac{d}{dx}(\Delta Z)=\frac{1}{2}\frac{\Delta_f M}{U_0+M_0}, \tag{6a}$$

and the criterion of instability, i.e., of amplification, is thus $\Delta_f M>0$.

Let us consider a representative plane U,ω (fig. 7). The curve of uniform regime

$$M_0=g\left(\sin i-\frac{\lambda U^2}{gR}\right)=0,$$

divides this plane into two regions for which M is, respectively, positive and negative. The criterion consists of studying the sign of M in the vicinity of the point of uniform regime M and along the direction MF corresponding to $\Delta U=\Delta Z$, i.e.,

$$\Delta U=\sqrt{\frac{g}{b\omega}\cos i}\,\Delta\omega. \tag{7}$$

There will be amplification if the half-line MF directed toward the positive $\Delta\omega$ falls into the positive region of M, i.e., if the slope is greater than

that of the tangent to the curve of uniform regimes in M, hence if

$$\sqrt{\frac{g\cos i}{b\omega}}<\frac{dU}{d\omega}.$$

Upon multiplying by ω, we see that we obtain exactly the criterion given by the consideration of the quasi-steady regimes,

$$\sqrt{\frac{g\omega}{b}\cos i}<\omega\frac{dU}{d\omega}.$$

But our actual viewpoint yields an additional physical interpretation; we see on the diagram of fig. 7 that the representative point of the wave front is somewhere on the line MF, and that for this wave front the instability corresponds to an excess of the slope over the resistance.

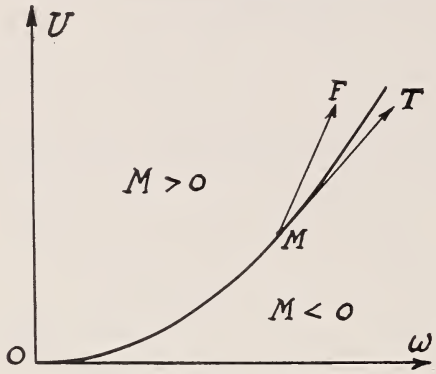

FIGURE 7. *Sign of M in U,ω plane.*

5. Criteria for the Possibility of Roll Waves

By two quite different ways the equations of Saint-Venant lead to the following criterion for the formation of roll waves: if U is the mean velocity of the uniform regime in a channel (known functions of the cross section ω), and if $V=\sqrt{g\omega/b\cos i}$ is the critical velocity relative to this section (or the relative velocity of an elementary wave front), there is instability and hence a possibility for the formation of roll waves when

$$\frac{V}{U}<\omega\frac{d}{d\omega}\log U. \tag{8}$$

If we want to specify this relation for the various types of resistance equations, we note first that in all cases where the notion of the hydraulic radius applies, i.e., for all cases where we can assume a rather uniform distribution of the frictional forces along the wetted perimeter, the mean velocity will be a function of the cross section ω through the single intermediary of the hydraulic radius R. Taking the derivative of the above equation first with respect to R and then with respect to ω, we obtain

$$\frac{V}{U}<\left(1-R\frac{d\chi}{d\omega}\right)R\frac{d}{dR}\log U. \tag{8a}$$

We can finally further elaborate and consider first the case where the coefficient of resistance λ depends on the Reynolds number in the approximate form of a monomial law $\lambda = K(UR)^{-\alpha}$ such that the law of the uniform regime is written

$$U = K' R^{\frac{1+\alpha}{2-\alpha}}.$$

Equation 8 becomes in this case

$$\frac{V}{U} < \left(1 - R\frac{dx}{d\omega}\right)\frac{1+\alpha}{2-\alpha}. \tag{8b}$$

If we are, however, in the domain of surface roughness with an approximate relation $\lambda = KR^{-\beta}$, i.e., with the law of uniform regimes

$$U = K'' R^{\frac{1+\beta}{2}},$$

the criterion of instability is written

$$\frac{V}{U} < \left(1 - R\frac{dx}{d\omega}\right)\frac{1+\beta}{2}. \tag{8c}$$

These last expressions have also been obtained by Vedernikov starting from a more complicated stability calculation.

For resistance laws which do not have the monomial form, we could utilize eq 8a, or more generally eq 8 for the cases of laminar regimes where the resistance law can be calculated independently of the notion of the hydraulic radius.

18. Waves and Seiche in Idealized Ports

By John S. McNown [1]

Both waves and significant mass oscillations, or seiches, can be caused within a port by the sea waves at the entrance. In certain cases for which the geometry is comparatively simple, analyses of this movement can be made which are useful both in the design of ports and in tests on scale models.

For the special case in which the horizontal velocity at the port entrance is zero, the possible movements are those occurring in a closed basin which were studied by Lord Rayleigh. The period of the internal movement corresponds to that of the external wave, and the amplitudes are related, somewhat less precisely, by the nearly complete formation of a clapotis at the entrance. For a given port geometry an infinite but discrete number of motions and corresponding periods are found; only those for comparatively long periods are treated in detail in this study.

For all other periods, the clapotis is incomplete and the horizontal velocity at the entrance is periodic and no longer equal to zero. For such motions, the corresponding mathematical conditions lead to infinite series of Bessel functions for a circular port, and to products of trigonometric and hyperbolic functions for a rectangular port.

From these analyses it is possible to demonstrate the significance of minor variations of the period, of the location of the entrance, and of the form of the port itself. In addition, correlations between results of theory and experiment provide a basis for extensive studies of the dissipation of energy within a port.

1. Introduction

Because of the extreme complexity of the formation by storm waves of surface disturbances and mass oscillations within a harbor, useful design criteria can probably best be obtained by first considering occurrences which take place within harbors of simplified geometry. In certain idealized cases, theoretical analyses can be completed and these can be compared with laboratory studies. In this way useful concepts can be provided for additional fundamental studies, for model investigations, and for certain phases of the design of ports.

For this study, harbor geometries were selected not as models representative of suitable designs, but on the contrary as forms in which certain undesirable phenomena could be isolated and studied. Once the nature and causes of these unwanted disturbances are better understood, determination of the necessary corrective measures should become much less difficult. Accordingly, forms were selected for which the walls are vertical and totally reflecting, the bottom is horizontal, and the plan of the harbor is simply definable in the geometrical case. An additional advantage in the study of such simplified forms is that available mathematical methods can be used as a guide to experimentation and in extending the results obtained.

External waves can stimulate two essentially different kinds of motion within a harbor, (1) resonant motions for which the possible modes are

[1] Etablissements Neyrpic and University of Grenoble, France. On leave from Iowa Institute of Hydraulic Research, Iowa City, Iowa.

identical to those occurring in completely closed basins, and for which there is no component of velocity normal to the plane of the entrance, and (2) the equally important although heretofore undiscussed nonresonant motions which are directly affected by a normal velocity component at the entrance other than zero. For a port of given dimensions an infinite but discrete series of periods exists for the various possible motions of the first type. These motions are resonant in the sense that once established, they continue with the addition of an amount of energy which is theoretically zero and actually negligibly small, in contrast to all the other, nonresonant, motions. These two types of motion can also be characterized by the essentially complete clapotis which forms immediately outside the entrance. Only for the resonant case does the crest line coincide with the entrance. Although there is evidently a gradual transition of nonresonant motions between successive pairs of resonant conditions, the distinction between the types of motion is important in the conduct of the corresponding analyses.

Resonant motions are closely analogous to the vibrations of a membrane, and it was this analogy that led Rayleigh to make a systematic analysis of surface oscillations occurring in a cylindrical container [1].[2] The only difference between the analyses of the two physical problems is that the amplitude is zero at the periphery of a taut membrane, whereas for the basin the amplitude is a maximum and the normal velocity is zero. Rayleigh and Bouasse [2] have presented discussions of a number of cases of resonant motions in circular and rectangular containers and have shown good correspondence between the results of calculations and of experiments conducted by Guthrie [3]. Lamb [4] also gives a brief resume of resonant motions and refers to much earlier but apparently incomplete studies by Poisson, Merian, and Ostrogradsky. However, neither the stimulation of these resonant motions by an external gravity wave nor the occurrence of nonresonant motions had been considered previously. Consequently, a basic study of idealized ports, described herein, was undertaken in order to determine the characteristic features of the motions within ports excited by wave motion at the entrance, both calculations and experiments being included.

The writer conducted this investigation at the Neyrpic Laboratory in Grenoble, France, while, as a Fulbright research scholar and exchange professor at the University of Grenoble, he was on leave from the Iowa Institute of Hydraulic Research. This report has been abstracted from a thesis submitted to the Faculty of the University of Grenoble in partial fulfillment of the requirements for the degree of Docteur es Sciences in the Department of Mathematics. Additional material as well as more complete detail is available in thesis form and will be published subsequently in La Houille Blanche. The subject of the investigation was suggested by P. Danel, director of the Neyrpic Laboratory. The method used in the calculation of the nonresonant motions was contributed by Professor J. Kravtchenko of the Faculty of Sciences at the University of Grenoble. Numerous members of the Neyrpic Staff, in particular Mr. Biesel and Mr. Chapus, advised or assisted the writer in various phases of the undertaking. Mr. Carvalho and Mr. Castanho, engineers from Portugal studying laboratory techniques at Neyrpic, assisted with the experiments and the preparation of the illustrative material.

[2] Figures in brackets indicate the literature references on p. 164.

2. Theoretical Investigations

Calculations based on the classical theory of wave motion formed an important part of this investigation. Once it was found by a comparison of calculated and observed results that certain restrictive assumptions did not result in significant discrepancies, results of the theory summarized in the following paragraphs were invaluable in the conduct of the experiments. The period and modes of the various resonant motions, the probability of resonant harmonics occurring, the effect of possible systematic errors, and other important characteristics could thus be calculated. Also, certain problems of stability and several phenomena which could not be studied easily in the Laboratory were also investigated by means of the theory obtained.

2.1 Derivation of Basic Equations

Analysis of the surface disturbance within a harbor consists of the determination of a periodic function satisfying the conditions: (1) that a particle on the surface has a zero velocity normal to the surface itself, (2) that the velocity normal to the solid boundary at the walls and bottom of the port is zero, and (3) that the horizontal component of velocity at the port entrance is a function of time and space determined from the fact that a clapotis forms outside the port entrance. The assumption that viscous effects are negligible makes possible the use of a velocity potential, and the boundary conditions are greatly simplified by the restrictions mentioned in the introduction that the bottom of the port is horizontal and the walls are vertical.

For irrotational motion, the velocity potential, which is evidently a function of both space and time, satisfies the Laplacian equation

$$\nabla^2\phi=0. \tag{1}$$

Also, if the amplitude of the motion is very small, the well known condition for the free surface can be expressed in equation form

$$\frac{\partial^2\phi}{\partial t^2}+g\frac{\partial\phi}{\partial z}=0, \quad (z=0), \tag{2}$$

in which z is taken as positive in the vertical upward direction with the origin in the free surface. If, in addition, the motion is supposed to be simply harmonic, ϕ can be written as a sum of elementary functions of the type

$$\phi_n=\frac{A_nV_0}{k}\cos\frac{2\pi t}{T}\frac{\cosh k(z+h)}{\cosh kh}F_n(x,y), \tag{3}$$

in which V_0 is an arbitrary velocity of reference occurring at the surface for the entire width of the entrance, k is an inverse length characterizing the horizontal dimensions, T is the period of the occurrence, and h is the depth of the water. The form of the function $F(x,y)$, through which the surface amplitudes are described, depends upon the geometry of the basin, and it has been defined only for closed basins of extremely simple description, such as rectangles and circles.

If the value of ϕ_n from eq 3 is substituted into eq 1, $F(x,y)$ is found to satisfy the criterion

$$\nabla^2 F + k^2 F = 0. \tag{4}$$

Also, if eq 2 is to be satisfied,

$$\left(\frac{2\pi}{T}\right)^2 = gk \tanh kh. \tag{5}$$

The two relationships, eq 4 and 5, are fundamental to this study, as well as to studies of other physical problems. More detailed presentations have been made by Lamb, Rayleigh, and others. The goal of the following analysis is the attainment of solutions that satisfy eq 4 and the assigned boundary conditions, eq 5 representing the relationship between the period of the occurrence, the depth of the water, and the parameter k.

2.2 Application to Circular Ports

If the wall of the port is a circle, the unknown function $F(x,y)$ is most readily describable in terms of Bessel, or cylindrical, functions. In fact, if eq 4 is expressed in polar coordinates the resulting differential equation is that characteristic of Bessel functions of the first kind, a typical solution being expressible in the form

$$F_n(r,\theta) = J_n(kr) \cos n\theta. \tag{6}$$

The general solution is an infinite series of such terms.

The boundary conditions at the walls and at the entrance can be fulfilled by means of the evaluation of the appropriate coefficients A_n in eq 3. It is first assumed that the motion induced at the entrance is that corresponding to the clapotis, formed at the entrance, the horizontal component of the velocity at the entrance being defined as follows:

$$V_r = V_0 \cos\frac{2\pi t}{T} \frac{\cosh k(z+h)}{\cosh kh}, \quad (-\beta \leq \theta \leq \beta). \tag{7}$$

The half angle β subtended by the entrance is considered to be sufficiently small that the arc and the chord at the entrance can be assumed to coincide. Along the remainder of the periphery, of course, the boundary condition is simply that V_r is zero if r is equal to R, the radius of the circular boundary. These two conditions can be imposed simultaneously through application of a Fourier expansion that defines a set of coefficients for an infinite series of cosine terms. An expression for V_R can also be obtained by differentiation of ϕ with respect to r in eq 3, and the resulting values can be equated term by term to those of the Fourier series. The resulting values of A_n are as follows:

$$A_0 = \frac{\beta}{\pi J_0'(kR)}, \quad A_n = \frac{2 \sin n\beta}{\pi n J_n'(kR)}. \tag{8}$$

Finally, the variation of the surface elevation can be determined by evaluating V_z and integrating with respect to time,

$$n = \int \frac{\partial \phi}{\partial t} dt = \frac{V_0 T}{2\pi} \tanh kh \sum_{n=0}^{\infty} A_n J_n(kr) \cos n\theta. \tag{9}$$

in which n represents the maximum (or minimum) value corresponding to $t=0$.

Once the arbitrary values k and h have been assigned, the period can be computed from eq 3 and, if R is known, n can be evaluated in terms of V_0 from eqs 8 and 9. It remains only to relate V_0 to the characteristics of the external wave. This can be done in accordance with the assumption that the amplitude and the surface velocity at the center of the entrance are the same for both the internal motion and the external clapotis. For the latter,

$$n_0^2+\left(\frac{V_0 T \tanh kh}{2\pi}\right)^2=a^2, \tag{10}$$

in which n_0 and V_0 are the maximum value of n and V_r at the entrance, and a is the amplitude of the clapotis (twice the amplitude of the incident wave if the clapotis is completely formed).

2.3 Resonant Motions

For certain combinations of values of k and n the denominator of the expression in eq 8 becomes zero, and, if the value of V_0 did not approach zero also, the corresponding value of A_n and of the amplitude would become infinite. For these resonant motions, n_0 is equal to a, and only a single term remains

$$n=a\frac{J_n(kr)}{J_n(kR)}\cos n\theta. \tag{11}$$

As indicated in a preceding section, these motions are identical to those occurring in a closed basin, except that they are considered to be excited at an opening in the wall by an external wave. Typical cases of elementary resonant movements are shown in figure 1. These motions are characterized by the number of nodal diameters, which is equal to n, and by the number of nodal circles, which is related to the value of k.

By the application of the preceding equations, it is possible to calculate the variation of the amplitudes and velocities of both resonant and nonresonant motions excited within a circular port by a periodic wave at the port entrance, and the same methods can be applied to other simply defined port geometries. It is noteworthy from the results already presented that amplitudes within the port can greatly exceed those of the incident wave. Also, these movements are dependent upon the width of the opening only insofar as the curved profile for the internal motion differs from the horizontal profile of the incident wave.

3. Laboratory Investigation

Experiments were conducted in a canal at the Neyrpic Laboratory which had been constructed with the canal bottom very carefully made horizontal for another study [5]. The canal is 4 m wide and 25 m long, with water depths possible up to 0.5 m. Waves of adjustable amplitude and period are produced at one end of the canal by a wave maker of the horizontal-displacement type. The circular port installed in it was made of 15 concrete blocks each 20 cm high and subtending an arc of $\pi/8$ radians. The entrance, of the same angle, was centrally placed on a diameter parallel

to the axis of the canal so that the approaching wave crests were parallel to the entrance chord. The diameter of the port was 3.20 m, and a constant water depth of 16 cm (or $R/10$) was utilized in all the experiments. A beach on either side of the entrance served to dissipate a large part of the energy of the oncoming wave. The use of a wave filter composed of wire mesh also provided damping of the unwanted reflections and harmonics [6].

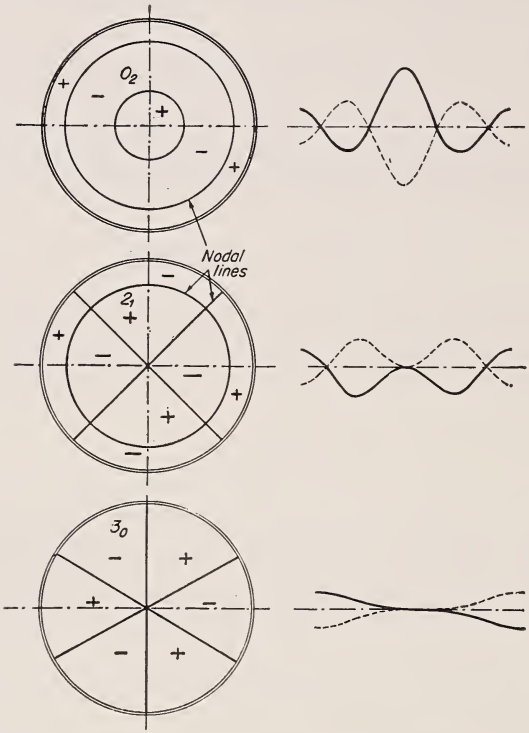

FIGURE 1. *Typical resonant movements in a circular port.*

The amplitudes of the motion of the oncoming wave and of that within the port were measured by means of a slightly modified point gage. A small horizontal arm was mounted near the point of the gage at the end of which a needle, sharpened on both ends, was affixed in the vertical position. Observations were then made for the points of minimum elevation with the upper end of the needle, and for the maximum elevation with the lower end. Observations were easily made, because the slight surface disturbances caused a marked change in the light pattern at the bottom of the canal. Traverses made by this method could be duplicated by two different observers within 0.2 mm. The periods of these motions were determined by measuring with a stop watch the elapsed time for 30 or 60 cycles.

Numerous motions of the resonant type have been observed, and for several of these detailed measurements have been made and compared with the corresponding Bessel functions. Measurements for two such motions are shown in figure 2, the upper for the case of no nodal diameter

(J_0) and two nodal circles, and the lower for the case of two nodal diameters (J_2) and one nodal circle. The double amplitudes at the entrance were assumed to be equal for both experiment and theory. The experimental points are reasonably close to the curves obtained theoretically indicating beyond question that the principal motion observed is the same as that predicated on theory. An effect of utilizing amplitudes which are by no means negligible is readily seen by comparing the two sets of points with crests and troughs interchanged, the crests being invariably more pointed than the troughs as for two-dimensional waves. Another disparity that was frequently found is illustrated by the points near the center for the J_2 movement. These disturbances were caused by harmonics of the fundamental wave, usually occurring with a frequency clearly defined as two, three, or four times that of the fundamental motion. For the J_2 motion shown in figure 2 the third harmonic was observed.

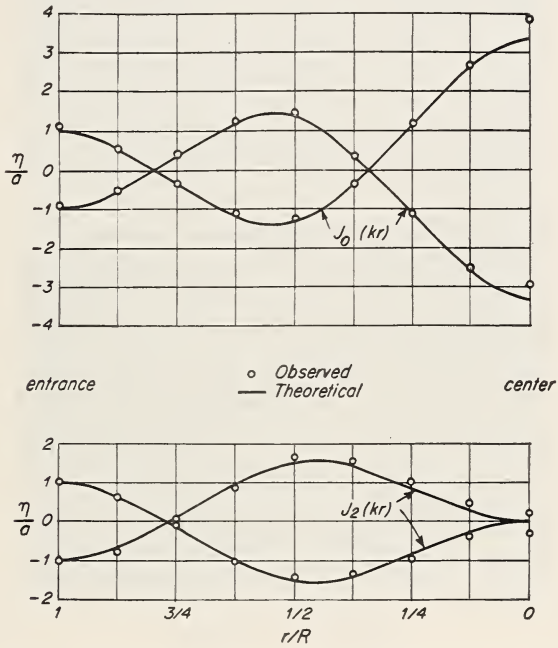

FIGURE 2. *Comparison of results of experiment and theory for resonant movements in a circular port.*

Photographs of these motions have also been taken, those for the J_0 case being presented in figure 3. The two separate photographs are for conditions of maximum amplitude out of phase by one-half period. The central hill, in the upper picture, and the ring in the lower one are strikingly apparent. Also apparent are the constancy of the elevation at the wall at any one time and the change of this elevation corresponding to the change from crest to trough at the entrance. In figure 4, similar photographs of the J_2 motion are somewhat more difficult to decipher. Because of the relative complexity of the surface configuration, a bar was placed across the basin so that an indication could be obtained from the distortion of the reflected image. The formation of the two crests,

on either side of the center in the upper photograph, and in front of and behind in the lower one, can be readily detected. Also it can be seen that the movement at the center is comparatively very small. For these photographs the exposure time was 1/100 second, and the lighting was nearly horizontal. The water was made relatively opaque by the addition of a large quantity of starch.

FIGURE 3. J_0 *movement.*

Calculated results and those obtained experimentally were also obtained for one movement classed as nonresonant. The value 6 was chosen for kR, as a typical value for which no one resonant condition would be dominant. The curves shown in figure 5 were then calculated point by point to obtain the variation of n along the axial diameter and around the wall. Sixteen terms were included in the summation, and in some cases an approximate integration was made for the remaining terms. Motions corresponding to J_4, J_5, and J_6 were found to be dominant, and the total contribution of terms after the sixteenth was found to vary between a negligible amount and slightly over 5 percent.

Results of experiments conducted for the same value of kR are also shown in figure 6, and once again the differences between the two results are found to be small. In this case the results were adjusted by an arbi-

trarily selected coefficient, so that it is the shape of the curves that is compared, not the absolute amplitudes. The largest difference is seen to occur at the entrance; this is a consequence of the fact that the computed amplitude varies considerably across the entrance, and, because the amplitude of the approaching wave is practically constant, some adjustment must take place. It is noteworthy that the assumed velocity discontinuity at each edge of the entrance was more or less substantiated in the laboratory by the intermittent occurrence of vortices at these points. It was also observed that the effects of harmonics were relatively more important for nonresonant than for resonant motion. That is, more dispersion was found in the results, and no true nodes were observed.

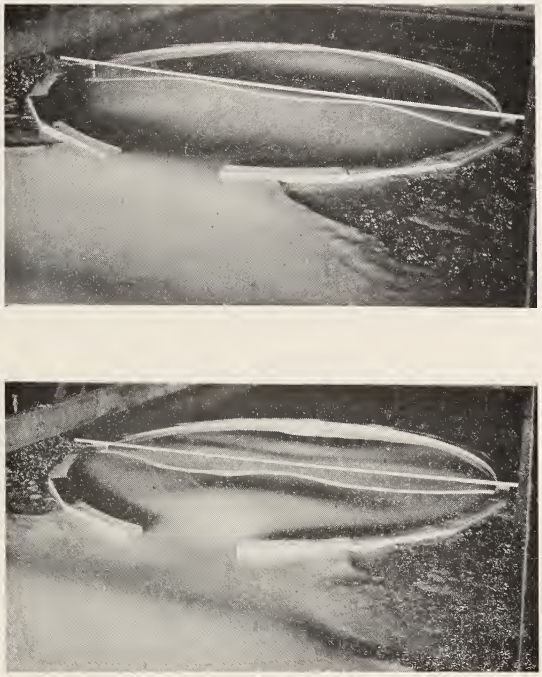

FIGURE 4. J_2 *movement.*

4. Interpretation of Results

Immediately evident from the comparisons of the theory of oscillations in the type of idealized port studied and the corresponding experiments is the fact that both qualitative and quantitative accord is found. Such simplifications in the theory as small amplitudes, linear superposition, irrotational motion, and the arbitrary inclusion of velocity discontinuities are found to be surprisingly close approximations. Thus additional calculations based on these same assumptions should be equally worth while. Other port shapes more nearly conforming to reality can also be computed, but because such calculations are still more difficult, verification of the underlying assumption in the study described herein was thought to be a necessary prelude to a more extensive investigation. It is

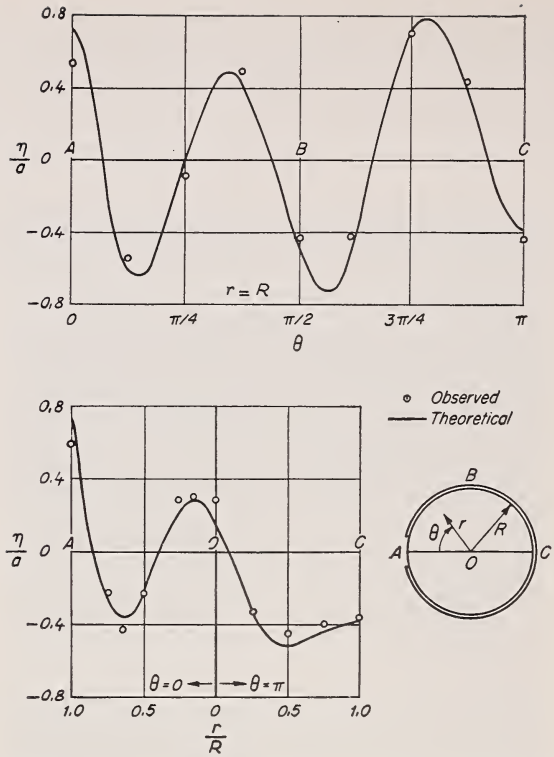

FIGURE 5. *Comparison of results of experiment and theory for nonresonant movement in a circular port.*

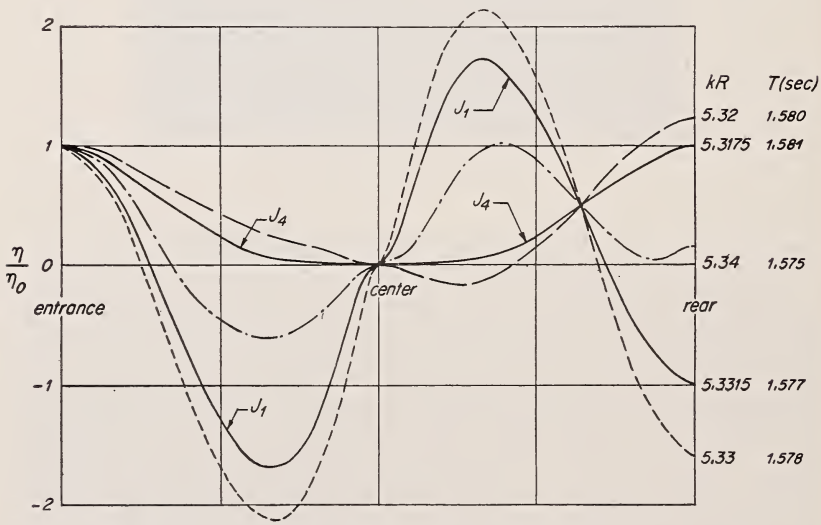

FIGURE 6. *Patterns of motion for periods in the vicinity of two nearly coincident resonances.*

nonetheless possible to derive certain conclusions from this study which are immediately useful.

One of the most troublesome features of nearly all model studies of the effect of waves on harbors is the instability of the phenomenon observed within the harbor. Because of the geometrical complexity of any natural port the isolation of factors causing this instability is practically impossible. However, with the idealized configurations discussed herein it is possible by means of either theory or experiment to consider a number of effects, only a few of which can be mentioned in this abbreviated treatment.

The effects of higher order harmonics, particularly those which may be resonant, have already been mentioned. Also, it is possible that slower movements may occur, these movements being characteristic of the model dimensions and not of the similar occurrence in nature. Another phenomenon of importance in model studies is the observed pumping effect of the wave at the entrance. From an analysis of the observed data, an increase of 1 to 3 mm in the water depth within the port was found to exist.

For certain conditions, it is possible that slight changes in the period of the artificially produced wave can produce disproportionate changes in the resulting movement. One such case has been analyzed for the circular port, and the results of the calculations are shown in figure 6. In this instance values of kR, or of the period, were selected in the immediate vicinity of two resonant conditions having nearly equal periods (J_1 with one nodal circle and J_4 with no nodal circle). The changes in the calculated movement with very small changes in the period are extremely marked, the total change in period for the entire range computed being only 0.006 sec, or 0.4 percent, of the period. With the several separate basins found in most harbor models such accidental synchronization is likely to occur frequently but in a degree perhaps less remarkable. From a practical viewpoint this indicates the utility of trying several different periods in an attempt to find one that is comparatively stable.

As it is the prevention rather than the production of large surface disturbances that is important in the design of harbors, the dissipation of the incoming energy is the most important phase of a broad investigation of ports. A comparison of the gradual dissipation of this energy without special devices, such as a beach or artificial disturbances, is shown in figure 7. In obtaining the results indicated by the two curves, the stimulations of the wave was stopped, in one case by simply stopping the wave machine, and in the other by inserting a barrier at the entrance coinciding with the circular interior. In each case, the motion (J_0 with two nodal circles) was found to be remarkably persistent. With the entrance open, for example, the surface outside the port became calm long before that inside, even though the dissipation was primarily caused in this case by the passage of waves from the port through the entrance.

It has been amply proved that the motion produced in a port can have an amplitude not only equal to but even a number of times greater than the amplitude of the wave that produces it. Furthermore, from theoretical considerations, this amplitude can occur equally well with an entrance width that is extremely small. This fact was qualitatively verified experimentally by reducing the angle of the opening from 22.5° to 7.5° by inserting two small blocks at either side of the entrance. The motions observed subsequently were found to be essentially the same as those presented herein, except for the fact that it was more difficult to obtain well-defined resonant motions. Although a relationship surely exists between the

energy entering the port and the structure necessary for dissipation, these rather elementary observations serve to emphasize the necessity for obtaining the dissipation of energy within a port in some other way than by narrowing the entrance.

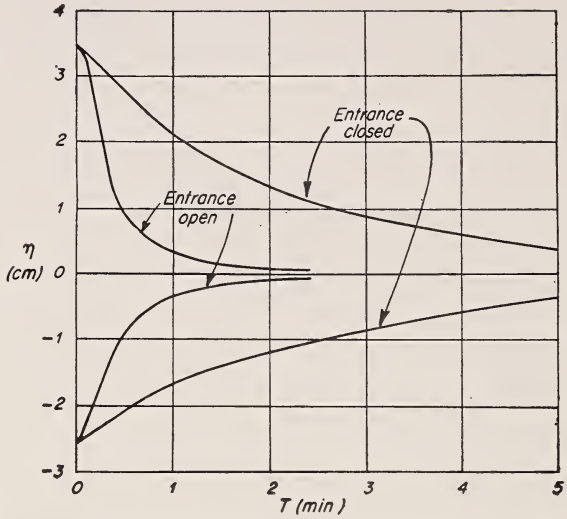

FIGURE 7. *Diminution of amplitude with time in the absence of stimulation by the external wave.*

5. Conclusion

From this preliminary study of surface disturbances and mass oscillations within idealized harbors, it is evident that analyses and experiments can be combined to furnish useful information for the design of ports. Approximate analyses give results that correspond well with measurement, thereby making possible the theoretical solution of problems not easily studied in the laboratory. Significant among the results observed are (1) the occurrence of disturbances within a port for which the amplitude is much larger than that outside, (2) the independence of this result on the width of the entrance opening, (3) the possibility of irregular motions in model studies resulting from chance synchronization of two or more resonant motions, and (4) the almost negligible rate of energy dissipation in the absence of special devices for the absorption of energy.

6. References

[1] Lord Rayleigh, On waves, Phil. Mag. [5], V.1, 1876, pp. 257–279.
[2] H. Bouasse, Houle, Rides, Seiche et Marées Librairie Delagrave Paris, 1924, pp. 92–145.
[3] F. Guthrie, On stationary liquid waves, Phil. Mag. [4] 50, 1875, pp. 290–302 and 377–388.
[4] H. Lamb, Hydrodynamics, Dover Publ., New York, 1945, pp. 282–290.
[5] G. F. Dixon, Thèses présentées à la Faculté des Sciences de l'Université de Grenoble, 1949.
[6] F. Biésel, Le filtre à houle, La Houille Blanche, No. spécial A, 1949, pp. 373–5.

19. The Propagation of Gravity Waves from Deep to Shallow Water

By Carl Eckart[1]

The Laplace equation, together with the appropriate boundary conditions at the free surface and the rigid bottom (of variable depth $h(x,y)$ beneath the undisturbed surface), is transformed into an integro-differential equation. This is shown to be approximated by the partial differential equation

$$\frac{1}{\mu}\left\{\frac{\partial}{\partial x}\left(\mu\frac{\partial p_0}{\partial x}\right)+\frac{\partial}{\partial y}\left(\mu\frac{\partial p_0}{\partial y}\right)\right\}+k^2p_0=0,$$

where $p_0/\rho g$ is the surface displacement and $\mu=1-\exp\ (-2\kappa h)$, $k^2=\kappa^2$ ctnh(κh), $\kappa=\omega^2/g$, $\omega=$frequency, radians per second, $g=$acceleration of gravity, $\rho=$density of the fluid.

It can be shown that the above expression for the wave-number k differs from the commonly accepted value, which is the root of the equation $\kappa=k\ \tanh(kh)$, by less than 4 percent for any value of kh; and, for both large and small values, by considerably less.

The integro-differential equation also leads to a series for the pressure at any depth in terms of p_0 and its derivatives. The excess pressure at the bottom, when calculated from the first two terms of this series, is

$$p(-h)=p_0\,[1-\exp(-\kappa h)]/\sinh(\kappa h).$$

If h is independent of x and y, the exact expression is known to be $p(-h)=p_0/\cosh(kh)$. The difference between these two expressions is again less than 5 percent for any value of kh, and approaches zero for both large and small values of kh.

When $h=sx$ (plane bottom of constant slope), the wave equation given above can be solved in terms of hypergeometric functions. This solution yields an analytic expression for the increase in height when the waves travel from very deep water into shallow water: a wave of unit amplitude in deep water, and of angle of incidence θ, increases to the height $H=(\frac{1}{2}\cos\theta)^{\frac{1}{2}}/(\kappa h)^{\frac{1}{4}}$ for small values of κh. The factor 1/2 is readily identified as being the ratio of the group and phase velocities in deep water.

1. Introduction

The propagation of gravity waves on the surface of an incompressible fluid involves a nonlinear boundary condition at the free surface. It is customary to simplify the problem by neglecting the nonlinear terms in this boundary equation, as well as in the Eulerian equations, and this will be done in the following also.

This linearized problem has been solved exactly only for the case of a plane bottom: these calculations for a horizontal plane are given by Lamb [1, Chap. IX][2] and an extensive treatment of the sloping plane (together with references to the relevant literature) has recently been given by Stoker. [2] More frequently, the problem is further simplified by supposing (1) that the water's depth is everywhere small compared to the wave length,[3] and (2) that the slope of the bottom, while not constant,

---

[1] Scripps Institution of Oceanography, University of California, La Jolla, Calif.

[2] Figures in brackets indicate the literature references on p. 173

[3] Strictly, small compared to the length that the waves would have if they were propagated on the surface of very deep water; for simplicity, this is called the "deep-water wave length."

is everywhere small. The basic equations of this "shallow-water theory," together with their solutions for a few special cases, are given by Lamb. [1, Chap. VII, p. 291]

It appears that it is possible to generalize the equations of the shallow-water theory so that it applies equally well to water of any depth. However, the assumption that the bottom slope is small enough to be negligible must be retained, and certain other terms must also be neglected. It has not been possible to formulate the necessary and sufficient conditions under which these approximations are justifiable, but various tests have been applied to the approximate equations, and these lead one to have reasonable confidence in them.

Since these approximate equations can be treated more readily (by the WKB and numerical methods if necessary) than can those of the exact linearized theory, they are useful in certain applications. Moreover, the methods employed in deriving them can also be used to obtain approximate solutions of other boundary-value problems.

2. Derivation of the Equations

Let the positive z-axis be vertically upward and the undisturbed free surface at $z=0$. Let the pressure be $-\rho gz+p(x,y,z,t)$, where ρ is the density of the fluid and g the acceleration of free fall. If the pressure over the fluid be zero, the linearized equation of the free surface will be

$$\rho gz=p(x,y,0,t)=p_0(x,y,t). \tag{1}$$

The free surface must also move with the fluid; to the same linearizing approximation, this results in the boundary condition

$$g\frac{\partial p}{\partial z}+\frac{\partial^2 p}{\partial t^2}=0, \quad \text{when} \quad z=0. \tag{2}$$

If the wave motion is simply harmonic, with period $2\pi/\omega$, eq 2 may be written

$$\frac{\partial p}{\partial z}=\omega^2 p/g=\kappa p, \quad \text{when} \quad z=0. \tag{2a}$$

where $2\pi/\kappa$ is the deep-water wave length.

If the equation of the bottom is

$$z=-h(x,y) \tag{3}$$

and it is impermeable, the remaining boundary condition is [4]

$$\frac{\partial p}{\partial x}\frac{\partial h}{\partial x}+\frac{\partial p}{\partial y}\frac{\partial h}{\partial y}+\frac{\partial p}{\partial z}=0, \quad \text{when} \quad z=-h. \tag{4}$$

[4] It is difficult to justify the inclusion of the terms in $\partial h/\partial x$, $\partial h/\partial y$ in eq 4 without also presenting arguments against the linearized eq 1 and 2. However, the omission of these terms from eq 4 yields results that are demonstrably false. The inclusion of the analogous terms in eq 1 and 2 yield nonlinear equations that cannot easily be solved. These matters will not be discussed further, but are mentioned here because they present problems that need clarification.

Finally, the function p must satisfy Laplace's equation

$$\frac{\partial^2 p}{\partial x^2}+\frac{\partial^2 p}{\partial y^2}+\frac{\partial^2 p}{\partial z^2}=0. \tag{5}$$

The present problem is the approximate solution of these equations.

It will be necessary to consider the values of p at two different levels, z and ζ, and to introduce the auxiliary function

$$g(\zeta,z)=(1/\kappa)\sinh \kappa(\zeta-z), \tag{6}$$

which satisfies the differential equation

$$\frac{\partial^2 g}{\partial \zeta^2}=\kappa^2 g. \tag{7}$$

Equation 5 may be rewritten

$$\frac{\partial^2 p}{\partial \zeta^2}=-\Delta p, \tag{5a}$$

where

$$\Delta=(\partial/\partial x)^2+(\partial/\partial y)^2.$$

Multiplying eq 7 by $p(\zeta)$, eq 5a by g and subtracting, one obtains

$$\frac{\partial}{\partial \zeta}\left[p(\zeta)\frac{\partial g}{\partial \zeta}-g\frac{\partial p(\zeta)}{\partial \zeta}\right]=g\left[\Delta p(\zeta)+\kappa^2 p(\zeta)\right].$$

On integrating this from $\zeta=0$ to z, the result is

$$p(z)-p(0)\cosh \kappa z-\frac{1}{\kappa}\left(\frac{\partial p}{\partial \zeta}\right)_{\zeta=0}\sinh \kappa z=\int_{\zeta=0}^{z} g(\zeta,z)[\Delta+\kappa^2]p(\zeta)d\zeta. \tag{8}$$

Using eq 2a, this becomes

$$p(z)=p_0\exp(\kappa z)+\frac{1}{\kappa}\int_{\zeta=0}^{z}\sinh \kappa(\zeta-z)[\Delta+\kappa^2]p(\zeta)d\zeta, \tag{9}$$

which is an integro-differential equation that is in all respects equivalent to the two equations, eq 5 and eq 2a. If the function $p_0(x,y)$ is known, eq 9 determines the function $p(x,y,z)$ uniquely. It therefore remains to determine p_0 so that eq 4 is satisfied.

Before proceeding to this, we note that

$$\kappa \sinh \kappa(\zeta-z)d\zeta=d[\cosh \kappa(\zeta-z)-1],$$

so that eq 9 may be transformed by partial integration into

$$p(z)=p_0\exp(\kappa z)+(1/\kappa^2)[1-\cosh \kappa z][\Delta p_0+\kappa^2 p_0]$$
$$+\frac{1}{\kappa^2}\int_0^z[1-\cosh \kappa(\zeta-z)][\Delta+\kappa^2]\frac{\partial p(\zeta)}{\partial \zeta}d\zeta. \tag{9a}$$

Under some circumstances, the value of the integral will be small compared to the values of the other two terms in eq 9a; then an approximate

solution is obtained by simply ignoring the integral. Without examining the justification for this approximation, it will be adopted throughout the following.

If this approximate value of p is substituted into eq 4, the result is

$$0=\exp(-\kappa h)\left\{\frac{\partial p_0}{\partial x}\frac{\partial h}{\partial x}+\frac{\partial p_0}{\partial y}\frac{\partial h}{\partial y}+\kappa p_0\right\}+(1/\kappa)\sinh \kappa h\left\{\Delta p_0+\kappa^2 p_0\right\}+\ldots, \tag{10}$$

where the dots indicate terms involving third derivatives of h, etc.; these will be neglected.[5]

The approximate eq 10 determines $p_0(x,y)$, and hence completes the determination of $p(x,y,z)$. It may be written more systematically as the wave equation

$$\frac{1}{\mu}\left\{\frac{\partial}{\partial x}\left(\mu\frac{\partial p_0}{\partial x}\right)+\frac{\partial}{\partial y}\left(\mu\frac{\partial p_0}{\partial y}\right)\right\}+k^2 p_0=0, \tag{11}$$

where

$$\mu=1-\exp\,(-2\kappa h), \tag{12}$$

$$k^2=\kappa^2 \operatorname{ctnh}\,(\kappa h). \tag{13}$$

3. Some Tests of the Validity of the Approximation

As a first test of the validity of these results, one may recover the usual equation for very shallow water. If $\kappa h \ll 1$,

$$\mu \to 2\kappa h, \quad k^2 \to \omega^2/gh,$$

and eq 11 becomes

$$\frac{\partial}{\partial x}\left(h\frac{\partial p_0}{\partial x}\right)+\frac{\partial}{\partial y}\left(h\frac{\partial p_0}{\partial y}\right)+\omega^2 p_0/g=0,$$

which has long been accepted as correct in this limiting case. [1, Chap. VII, p. 291]

As a second test, let h be constant; a rigorous solution is known [1, p. 364] to be

$$p_0=A\cos\,(kx-\omega t), \tag{14}$$

where A is a constant of integration, and k is the root of the transcendental equation

$$\kappa=k\tanh\,(kh). \tag{15}$$

Since μ is constant in this case, eq 11 also has a solution of this form, but k is determined by eq 13 and not by eq 15. The great formal difference between the two is misleading, as is shown in figure 1; the solid line of this figure is the graph of eq 15, while the circles represent values of k calculated from eq 13. The agreement between the two is very satisfactory, even when $kh \sim 1$, and is extremely close for both larger and smaller values.

[5] An alternative derivation can be given by substituting the rigorous eq 9 into eq 4, then integrating by parts and neglecting the integral. The terms indicated by dots in eq 10 are then absorbed in the integral and disappear with it. While this is more systematic, it is also more elaborate, and no easier to justify than is the derivation here given.

One may also use the simplified eq 9a to calculate the pressure on the bottom, and compare the result with that deduced from the known rigorous solutions. Equation 9a yields

$$p(-h)=p_0[1-\exp(-\kappa h)]/\sinh \kappa h, \tag{16}$$

while the rigorous value of this ratio is

$$p(-h)=p_0/\cosh kh. \tag{17}$$

These two equations are compared numerically in figure 2, and again, the comparison is satisfactory.

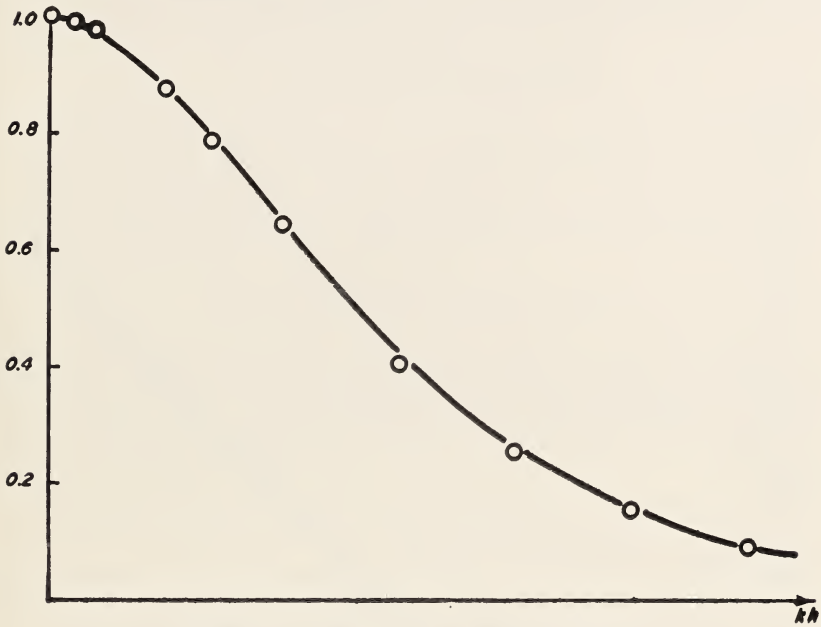

FIGURE 1. *Comparison of equations 13 and 15.*

—, $p(-h)/p_0=1/\cosh kh$
○, $p(-h)/p_0=(1-e^{-kh})/\sinh kh$

4. Solution of the Equation for a Bottom of Constant Slope

If the bottom has a constant slope, eq 11 can be solved in terms of the hypergeometric function. In this case

$$h=sx \tag{18}$$

s being the slope of the plane bottom. The introduction of a new independent variable

$$\xi=\exp(-2\kappa h) \tag{19}$$

results in

$$\mu=1-\xi, \quad k^2=\kappa^2(1+\xi)/(1-\xi). \tag{20}$$

The eq 11 is separable in this case, so that there are solutions of the form

$$p_0(x,y)=q(\xi)\exp(iby), \tag{21}$$

where $b=\kappa \sin\theta$ is a constant, and θ is the angle of incidence of the waves before refraction in the shoaling water. The function q satisfies the hypergeometric equation

$$\xi\frac{d}{d\xi}\left[\xi(1-\xi)\frac{dq}{d\xi}\right]+\left[(\kappa^2-b^2)-(\kappa^2+b^2)\xi\right]q/4\kappa^2s^2=0. \tag{22}$$

The abbreviations

$$\left.\begin{aligned}\alpha^2&=(b^2-\kappa^2)/4\kappa^2s^2=-\cos^2\theta/4s^2\\ \beta^2&=[b^2+\kappa^2(1+s^2)]/4\kappa^2s^2\end{aligned}\right\} \tag{23}$$

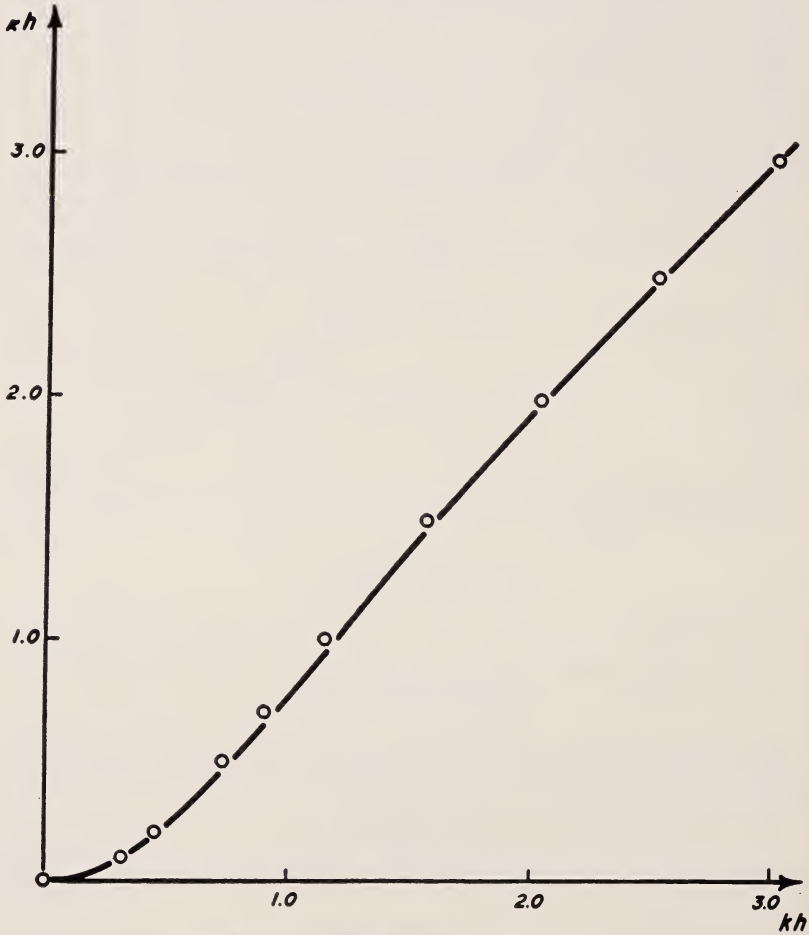

FIGURE 2. *Comparison of equations 16 and 17.*

—, $kh=kh \tanh kh$

○, $k^2h^2/\tanh kh=k^2h^2$

are convenient, and it is readily found that two solutions of eq 22 are

$$q_{\pm}=\xi^{\pm\alpha}F(\pm\alpha+\beta+\frac{1}{2},\ \pm\alpha-\beta+\frac{1}{2},\ 2\alpha+1,\xi), \tag{24}$$

where F is the hypergeometric series [3] [4, Chap. VI] [5, Chap. IV, No. 7, Chap. XVII] [6, Chap. II.].

$$F(l,m,n,x)=1+\frac{lm}{1\cdot n}x+\frac{l(l+1)m(m+1)}{1\cdot 2\cdot n(n+1)}x^2+\ldots.$$

It is to be noted that, for large positive values of x (deep water), ξ is very small, and the approximation

$$q_{\pm}=\xi^{\pm\alpha}=\exp(\pm i\kappa x\cos\theta) \tag{25}$$

is valid, so that $p_0=\exp i\kappa(\pm x\cos\theta+y\sin\theta)$. These two solutions therefore reduce approximately to the known solution for deep-water waves in this region.

For the shallow-water region, x is small, and $\xi\sim 1$, so that the series in eq 24 converge very slowly. There are other solutions, however, that converge more rapidly. One of these is

$$q_1=\xi^{\alpha}F(\alpha+\beta+\tfrac{1}{2},\ \alpha-\beta+\tfrac{1}{2},\ 1,\ 1-\xi). \tag{26}$$

In general, there is a second solution, obtainable from q_1 by changing the sign of α. However, because the third argument of F in eq 25 is an integer, this solution becomes identical with q_1 and it is necessary to find a more complicated expression, which involves a logarithmic singularity at $\xi=1$. This is q_0, where

$$\pi q_0=\{\psi(l)+\psi(m)+\log[\gamma^2(\xi-1)]\}q_1+F_1(l,m,1,1-\xi)$$
$$+F_1(m,l,1,1-\xi)+2F_3(l,m,1,1-\xi), \tag{27}$$

and

$$l=\alpha+\beta+\frac{1}{2};\quad m=\alpha-\beta+\frac{1}{2};\quad \psi(l)=\frac{d}{dl}\log\Gamma(l);\quad \gamma=1.7811\ldots;$$

$$F_1(l,m,n,x)=\frac{\partial}{\partial l}F(l,m,n,x);\quad F_3(l,m,n,x)=\frac{\partial}{\partial n}F(l,m,n,x).$$

The expressions for q_0 and q_1 are too elaborate to be readily calculated numerically. However, just as it was possible to obtain approximations to $q_{\pm}$ for small values of ξ, so it is possible to obtain approximations to q_0 and q_1, that are valid when $1-\xi$ is small, and both $|\alpha|$ and β are large. (This latter condition is fulfilled when the slope of the bottom is small and the waves are incident from a direction that is not too nearly parallel to the beach.)

The approximation is

$$\left.\begin{aligned} q_0&=N_0[2(\kappa x/s)^{\frac{1}{2}}],\\ q_1&=J_0[2(\kappa x/s)^{\frac{1}{2}}],\end{aligned}\right\} \tag{28}$$

where N_0 and J_0 are the Neumann and Bessel functions, respectively.

This is again very satisfactory, for these are the solutions obtained by Stoker and others from the shallow-water theory [2].

The eq 25 thus gives simple expressions for q_+ and q_- in deep water, and eq 28, simple expressions for q_0 and q_1 in shallow water. It remains to find the relations between the four solutions. These are the known formulas for the analytic extensions of the hypergeometric function and may be written

$$\left.\begin{aligned} q_1 &= A(-\alpha,\beta)q_+ + A(\alpha,\beta)q_-, \\ q_0 + iq_1 &= B(\alpha,\beta)A(-\alpha,\beta)q_+, \end{aligned}\right\} \tag{29}$$

where

$$\left.\begin{aligned} A(\alpha,\beta) &= \Gamma(2\alpha)/\Gamma\left(\alpha+\beta+\frac{1}{2}\right)\Gamma\left(\alpha-\beta+\frac{1}{2}\right); \\ B(\alpha,\beta) &= \sin(2\pi\alpha)/\cos[\pi(\alpha+\beta)]\cos[\pi(\alpha-\beta)]. \end{aligned}\right\} \tag{30}$$

The function $A(\alpha,\beta)$ can be transformed, by using known properties [6, p. 1] of the gamma function, into

$$A(\alpha,\beta) = [-2\pi\alpha|B(\alpha,\beta)|]^{-\frac{1}{2}}\exp[i\Theta(\alpha,\beta)], \tag{31}$$

where the function $\Theta(\alpha,\beta) = -\Theta(-\alpha,\beta)$ is difficult to evaluate. Physically, this function represents the total change in phase of the waves as they move from deep to shallow water, and is of little interest. Of greater interest is the change in amplitude of the waves, and this is independent of the function Θ.

Using the known asymptotic expansions of the Bessel functions

$$\left.\begin{aligned} N_0(\sigma) &= \sin(\sigma-\pi/4)/(\pi\sigma/2)^{\frac{1}{2}}, \\ J_0(\sigma) &= \cos(\sigma-\pi/4)/(\pi\sigma/2)^{\frac{1}{2}}, \end{aligned}\right\} \tag{32}$$

it is seen that for the shallow-water region,

$$q_0 + iq_1 = \pi^{-\frac{1}{2}}(s/\kappa x)^{\frac{1}{4}}\exp i\left[\frac{3\pi}{4} - 2\left(\frac{\kappa x}{s}\right)^{\frac{1}{2}}\right]. \tag{33}$$

For the deep water region,

$$q_+ = \exp(-i\kappa x\cos\theta). \tag{34}$$

Hence, the second of eq 30 shows that a wave of unit height in deep water will have the height

$$H = [2\alpha/|B(\alpha,\beta)|]^{\frac{1}{2}}(s/\kappa x)^{\frac{1}{4}} \tag{35}$$

in shallow water. For small values of s, this simplifies further, to

$$H = (\tfrac{1}{2}\cos\theta)^{\frac{1}{2}}/(\kappa h)^{\frac{1}{4}}. \tag{36}$$

The dependence of H on the water depth is well known from the usual shallow-water theory [1, Chap. VII, p. 291] and the factor $(\cos\theta)^{\frac{1}{2}}$ can easily be derived from considerations of the laws of refraction and the assumption that the energy is propagated in the direction of the rays. The factor $(\frac{1}{2})^{\frac{1}{2}}$ results from the fact that, in deep water, the group velocity is half the phase velocity, whereas in shallow water the two are equal.

5. Summary

An approximate wave equation has been derived, for the propagation of gravity waves on water of any depth.

Although the precise conditions for the validity of the approximations have not been established, they appear to be justifiable in a wide variety of cases.

A byproduct of this investigation is an approximate solution of the usual equation connecting the deep-water wave number, κ, to the wave number k at depth h. The supposedly exact equation is eq 15, and its approximate solution is given by eq 13, in a closed form suitable for use in analytic applications.

Certain applications of the results here obtained will be reported elsewhere.

6. References

[1] H. Lamb, Hydrodynamics. Sixth edition, Cambridge University Press, 1932.

[2] J. H. Stoker, Surface waves in water of variable depth. Quarterly of Applied Mathematics, vol. 5, pp. 1–54, 1947.

[3] F. Klein, Die hypergeometrische Reihe. Leipzig, 1894.

[4] A. R. Forsyth, Treatise on differential equations. Sixth edition, MacMillan, 1948.

[5] T. M. MacRobert, Spherical harmonics. Dover Publications, New York, 1947.

[6] W. Magnus and F. Oberhettinger, Formulas and theorems for the special functions of mathematical physics. Chelsea, New York, 1949.

20. On the Propagation of Waves from a Model Fetch at Sea[1]

By Willard J. Pierson, Jr.[2]

The previously known solutions; vis, the simple sine wave, the Cauchy-Poisson problem, and the Gaussian Wave Packet, to gravity wave propagation in infinitely deep water are shown to be inadequate in practical wave forecasting problems. The new exact solutions are presented; one for a finite wave group, and the other for a finite wave train.

The finite wave group is given by, $\eta_{\mathrm{I}}(0,0,t) = Ae\sigma^{-\sigma^2 t^2} \sin 2\pi t/T$ at $x=0$, $y = 0$. If most spectral components travel in the positive x direction, the solution, $\eta_{\mathrm{I}}(x,t)$, is given. The group is called a finite wave group because its parameters can be chosen so that it passes $x=0$ in about 1 minute. The modification of the group as it travels is discussed.

The finite wave train is given by the formula,

$$\eta_{\mathrm{II}}(0,0,t) = A \sin 2\pi t/T, \text{ if } -nT < t < nT,$$

and by zero otherwise. The solution for n of the order of 10^3 is given, and it is shown that the train advances with the group velocity determined by T, and that the ends are modulated by Fresnel Integrals.

The problem of waves propagating into calm air and still water from the edge of an area of generation is then considered. Three or four hundred finite wave groups of the form given above are propagated at time intervals, (τ), of the order of 2 minutes into the area of decay. The case considered can be given by the equation

$$\eta_{\mathrm{III}}(0,0,t) = \sum_{n=-p}^{n=+p} A_n e^{-\sigma^2(t-n\tau+\delta_n)^2} \sin\left(\frac{2\pi}{T}(t-n\tau+\delta_n)+\theta_n\right).$$

It is shown that forerunners of swell can be obtained from the equation, that the transformation from sea into swell can be demonstrated, and that it is not necessary to assume selective attenuation of the lower periods in order to explain the period increase of ocean swell.

It is concluded that a sound wave forecasting theory must be based upon the properties of the spectrum of the waves at the source region, and until some quantitative information about this spectrum is obtained the forecasting of ocean waves will be inaccurate.

1. Introduction

The sea surface at the forward edge of a stationary storm at sea is very complex. Waves of varying amplitude are propagated out of the storm into an area of relatively still water. They are in reality short crested waves, and they appear to occur frequently in groups of high waves separated by times at which the waves are relatively low.

---

[1] The results of this paper have been obtained under the sponsorship and generous assistance of the Beach Erosion Board, Corps of Engineers, United States Army as part of the results of a contract administered by the Research Division of New York University.

[2] New York University, New York, N. Y.

2. Previous Models

Various models of such a storm at sea have been considered. They approximate reality as described above quite crudely when one attempts to apply them to practical wave-forecasting problems. One such model is the simple sine wave for infinitely deep water, where $L=gT^2/2\pi$ (see Lamb [6] [3]) and where the sea surface is given by eq 1.

$$\eta(x,t)=A\sin\left(\frac{4\pi^2x}{gT^2}-\frac{2\pi t}{T}\right). \tag{1}$$

If used as a model of a storm at sea, the above equation is most unrealistic because the storm never started and will never stop.

Another model is the Cauchy-Poisson wave train (Lamb [6] for example) given by eq 2 for the case of an infinitely high, infinitesimally wide, infinitely long column of water that starts to fall into the sea surface at $x=0$ at the time $t=0$

$$\eta(x,t)=\sqrt{\frac{g}{\pi x}}\cdot\frac{t}{2x}\cos\left(\frac{gt^2}{4x}-\frac{\pi}{4}\right). \tag{2}$$

The Cauchy-Poisson problem has been used frequently to derive certain wave-forecasting properties. Some of these results are inaccurate because the spectrum of the disturbance at the source is a white-noise spectrum; i.e., all spectral frequencies have the same amplitude. Since the sea surface does not have a white-noise spectrum as evidenced by the fact that a "significant" period can be defined in the source region, periods are frequently forecasted to be present in the decay area that were never present in the original disturbance. As an extreme example, if the spectrum of the disturbance were constant from $\mu=2\pi/10$ to $\mu=2\pi/5$ and zero everywhere else, it would be physically impossible to observe periods greater than 10 seconds and less than 5 seconds in the decay area.

The Gaussian Wave Packet as discussed by Coulson [2] is another model. The solution that is given is an approximation, and comparison of the Gaussian Wave Packet to the results to be presented here will show that the approximation makes the results useless for application to the problem at hand.

3. A Model Wave Group

Consider a disturbance at the point $x=0$ on the sea surface as a function of time. Let it be given by eq 4.

$$\eta_{\mathrm{I}}\ (0,t)=Ae^{-\sigma^2t^2}\sin\frac{2\pi t}{T}. \tag{4}$$

If $T=10$ seconds, $\sigma=1/20$ seconds^{-1}, and A = 10m, for example, the amplitude of the disturbance is very very small after only 2 minutes have elapsed. If the most of the disturbance is traveling in the positive x direction, and if the crests are infinitely long in the y direction, it would be of interest to find out what the disturbance is like at a great distance x from $x=0$ and at a time, t, several hours after $t=0$.

[3] Figures in brackets indicate the literature reference on p. 186

The problem can be solved by the application of Fourier Integral Theory, and the spectrum of the disturbance is given by eq 5. (See Sommerfeld [8] for the definition of the symbols employed.)

$$b(\mu)=\frac{A}{\pi}\int_{-\infty}^{+\infty} e^{-\sigma^2 t^2}\sin\frac{2\pi t}{T}\sin\mu t dt$$

$$=\frac{A}{2\sqrt{\pi}\sigma}\left[-e^{-\left(\mu+\frac{2\pi}{T}\right)^2/4\sigma^2}+e^{-\left(\mu-\frac{2\pi}{T}\right)^2/4\sigma^2}\right]. \tag{5}$$

Then, if a correct spectral wavelength is assigned to each spectral frequency, $\eta_I(x,t)$ is given by eq 6.

$$\eta_I(x,t)=\frac{-A}{2\sqrt{\pi}\sigma}\int_{-\infty}^{+\infty} e^{-\left(\mu-\frac{2\pi}{T}\right)^2/4\sigma^2}\sin\left(\frac{\mu^2 x}{g}-\mu t\right)d\mu. \tag{6}$$

The solution is then given in the form of eq 7 by integration of eq 6, where D is given by $D=1+(16\sigma^4x^2/g^2)$. Note that when $x=0$, eq 7 reduces to eq 4.

$$\eta_I(x,t)=\frac{-A}{D^{\frac{1}{4}}}e^{-\frac{16\pi^2\sigma^2}{gT^2D}\left(x-\frac{gT}{4\pi}t\right)^2}\cdot\sin\left(\frac{4\pi^2x}{DgT^2}-\frac{2\pi t}{DT}-\frac{4\sigma^4t^2x}{Dg}+\frac{1}{2}\tan^{-1}\frac{4\sigma^2x}{g}\right). \tag{7}$$

Equation 7 is a product of two terms. The first term is a slowly varying function of time and space. It represents the envelope of the wave train. The second term is the pseudo-sinusoidal term that varies rapidly as a function of time and space and represents the waves under the envelope.

The term that represents the envelope is a maximum for a fixed value of x, say x_1, when $t=4\pi x_1/gT$. Thus the maximum travels with the group velocity of waves with the period T, and at the point x_1 the maximum amplitude is $A/D^{\frac{1}{4}}$.

Now let $t=4\pi x_1/gT+t'=t_0+t'$ so that the behavior of the group can be studied near the time, $t'=0$, when the maximum amplitude passes the point x_1. Then the envelope has the value $AD^{-\frac{1}{4}}\exp(-(\sigma t')^2/D)$. For large x_1, which means a large D, t' must vary through a large range of values before the amplitude becomes small. The envelope of the finite wave group therefore travels with the group velocity of waves with a period, T; it dies down in amplitude and spreads out over the sea surface.

Now consider the argument of the sinusoidal term in eq 7. After the substitution of $t=4\pi x_1/gT+t'$, the argument of the sine becomes eq 8, where the terms involving x_1 alone are lumped into $\theta(x_1)$ because interest is to be confined to variations with t'.

$$\text{Arg } s(\eta)=-\frac{2\pi t'}{T}-\frac{4\sigma^4x_1(t')^2}{DgT}+\theta(x_1). \tag{8}$$

T^* can be defined to be the apparent local period, by the condition that the argument of the sine decreases by 2π when t' increases by T. Equation 9 is the result.

$$\frac{d(\text{Arg } s(\eta))}{dt'}\cong\frac{\Delta(\text{Arg } s(\eta))}{\Delta t'}=-\frac{2\pi}{T^*}=-\frac{2\pi}{T}-\frac{8\sigma^4x_1t'}{DgT}. \tag{9}$$

Therefore, the apparent local period is given by eq 10. When t' equals zero,

$$\frac{1}{T^*}=\frac{1}{T}+\frac{8\sigma^4 x_1 t'}{2\pi D g T}, \tag{10}$$

the apparent local period is equal to the apparent period at $x_1=0$. For x_1 not zero, and for t' less than zero, T^* is greater than T; and for t' greater than zero, T^* is less than T. Thus high period waves arrive first at x_1, followed by waves at maximum amplitude of period, T, and finally by shorter period waves. It can be shown that the waves in the group travel along through the group increasing in period and amplitude as

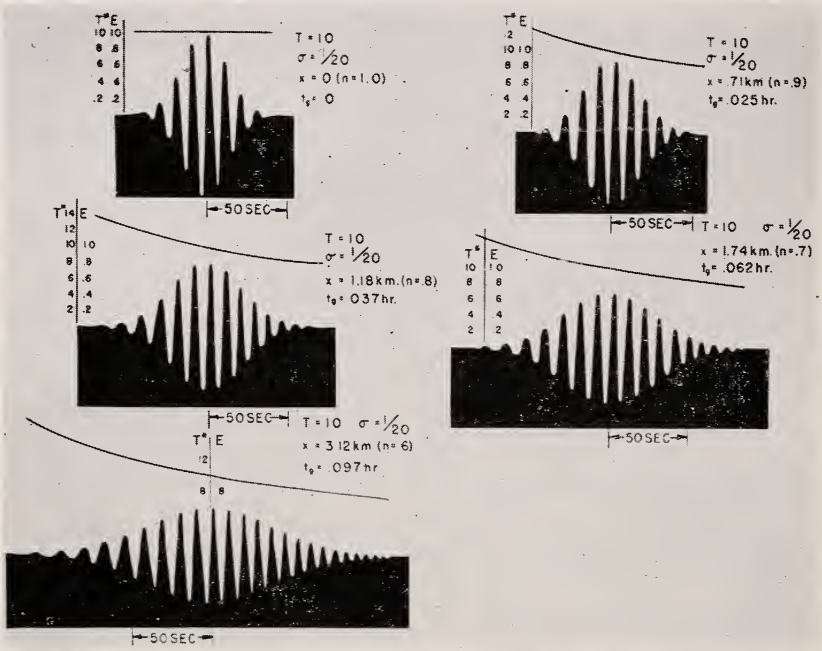

FIGURE 1. *Form of the finite wave group as a function of time when it passes various points.*

they travel and then pass through the group still increasing in period but decreasing gradually in amplitude to zero. Figure 1 shows the appearance of the wave record as a function of time at various fixed x_1.

4. A Model Wave Train

Consider a disturbance at the point $x=0$ on the sea surface as a function of time. Let it be given by eq 11.

$$\eta_{\mathrm{II}}(0,t)=\begin{cases} A\sin\dfrac{2\pi t}{T}, & -nT\leq t\leq nT, \\ 0, & \text{otherwise.} \end{cases} \tag{11}$$

If T equals 10 seconds and n equals 1,800, the wave amplitude would be zero up to 5 hours before t equals zero. Then a full-amplitude sinusoidal wave would be observed until 5 hours after t equals zero, and then the sea surface would become and remain flat again.

For other x, the problem can again be solved by the application of Fourier Integral Theory, and the spectrum of the disturbance is given by eq 12.

$$b(\mu)=\frac{A}{\pi}\left[-\frac{\sin nT\mu}{\frac{2\pi}{T}+\mu}-\frac{\sin nT\mu}{\frac{2\pi}{T}-\mu}\right]. \tag{12}$$

Under the assumption that most of the waves are traveling in the positive x direction, and if correct spectral wavelengths are assigned to the spectral periods, the sea surface as a function of x and t is given by eq. 13.

$$\eta_{\mathrm{II}}(x,t)=\frac{A}{\pi}\int_{-\infty}^{+\infty}\frac{\sin n\,T\mu}{\left(\frac{2\pi}{T}-\mu\right)}\cdot\sin\left(\frac{\mu^2x}{g}-\mu t\right)d\mu. \tag{13}$$

Integration of eq 13 then yields eq 14, where G and H are given by eqs 15 and 16.

$$\eta_{\mathrm{II}}(x,t)=\sqrt{G^2+H^2}\cdot\sin\left(\frac{4\pi^2x}{gT^2}-\frac{2\pi t}{T}+\tan^{-1}\frac{H}{G}\right). \tag{14}$$

$$G=\frac{A}{2}\left[-\int_0^{\sqrt{\frac{g}{4\pi x}}\left(\frac{4\pi x}{gT}-t+nT\right)}\left(\cos\frac{\pi}{2}\delta^2+\sin\frac{\pi}{2}\delta^2\right)d\delta\right.$$
$$\left.+\int_0^{\sqrt{\frac{g}{4\pi x}}\left(\frac{4\pi x}{gT}-t-nT\right)}\left(\cos\frac{\pi}{2}\delta^2+\sin\frac{\pi}{2}\delta^2\right)d\delta\right]. \tag{15}$$

$$H=\frac{A}{2}\left[\int_0^{\sqrt{\frac{g}{4\pi x}}\left(\frac{4\pi x}{gT}-t-nT\right)}\left(\cos\frac{\pi}{2}\delta^2-\sin\frac{\pi}{2}\delta^2\right)d\delta\right.$$
$$\left.-\int_0^{\sqrt{\frac{g}{4\pi x}}\left(\frac{4\pi x}{gT}-t+nT\right)}\left(\cos\frac{\pi}{2}\delta^2-\sin\frac{\pi}{2}\delta^2\right)d\delta\right]. \tag{16}$$

G and H are combinations of Fresnel integrals as tabulated, for example, by Janke and Emde [5]. When the upper limit of integration is greater than 8.5, the integral from zero to 8.5 of $\sin(\pi/2)\delta^2d\delta$ and $\cos(\pi/2)\delta^2d\delta$ is essentially one-half. For a fixed x_1, the solution shows that the sharp rise in amplitude of the wave height arrives at the point x_1, at a time determined by the group velocity of waves with a period, T; that the wave train is essentially constant in amplitude and takes essentially $2nT$ seconds to pass x_1; and that the wave-train amplitude dies out again rapidly after the $2nT$ seconds. The amplitude of the forward edge of the wave train is given as a function of t' at various x_1 in figure 2. t' here is defined by $t=(4\pi x_1/gT)-nT+t'$. When t' equals zero or $2nT$, the amplitude of the waves is one-half of A. A number of low waves arrive

before t' equals zero, and a few are still present after t' equals $2nT$. A rise to full amplitude occurs 20 to 30 minutes after t' equals zero for typical values of x_1. The waves under the envelope have the period T due to the fact that the spectrum, eq. 12, is concentrated very sharply at $\mu = (2\pi/T)$ for $\mu > 0$ when n is large.

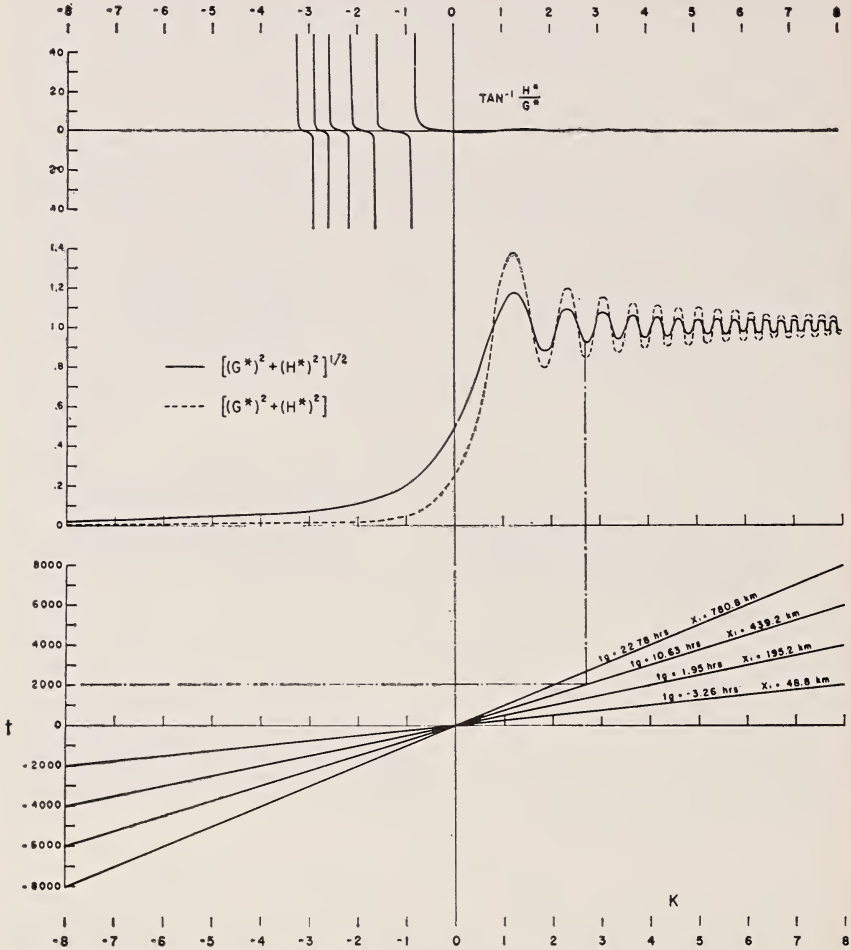

FIGURE 2. *Variation of the envelope, the average potential energy, and the phase of the crests for relatively large values of X_1 as a function of t'.*

5. Waves From a Model Fetch at Sea

The model wave group studied above lasts for only a short time. One wave group does not make a storm. The model wave train lasts long enough, but it is far too regular at the source to be very realistic. However, if wave groups such as those studied in eq 3 are sent out one after the other from the storm area at time intervals of the order of τ equal to

100 seconds, and if the wave groups vary in amplitude and phase, then a fairly realistic storm at sea can be manufactured mathematically.

Consider, then, eq 17 given below, where the A_n are arbitrary. θ_n ranges randomly from $-\pi$ to π, τ is of the order of 100 seconds, and δ_n is randomly distributed with a range of, say, 10 seconds.

$$\eta_{\mathrm{III}}(0,t)=\sum_{n=-p}^{n=+p} A_n e^{-\sigma^2(t-n\tau+\delta_n)^2} \sin\left(\frac{2\pi}{T}(t-n\tau+\delta_n)+\theta_n\right). \tag{17}$$

$\eta_{\mathrm{III}}(x,t)$ can be found immediately with the use of eq 7 by substitution of $t-n\tau+\delta_n$ for t in eq 7, by the addition of θ_n to the argument of the sine and by setting A equal to A_n. Each wave group then travels as described in section 3. However, as the wave groups travel they overlap, and very complicated sums would have to be evaluated in order to find out what occurs.

A simpler case can be studied by setting the A_n equal, and δ_n and θ_n equal to zero. η^*_{III} can then be given by eq 18 at x equal to zero.

$$\eta^*_{\mathrm{III}}(0,t)=\sum_{n=-p}^{n=+p} A e^{-\sigma^2(t-n\tau)^2} \sin\left(\frac{2\pi}{T}(t-n\tau)\right). \tag{18}$$

The spectrum of η^*_{III} can then be given by eq 19, and the free surface as a function of x and t is then found to have the form of eq 20.

$$b(\mu)=\frac{A}{2\sqrt{\pi}\,\sigma}\sum_{n=-p}^{n=+p}\cos n\tau\mu\left[-e^{-\left(\mu+\frac{2\pi}{T}\right)^2/4\sigma^2}+e^{-\left(\mu+\frac{2\pi}{T}\right)^2/4\sigma^2}\right]. \tag{19}$$

$$\eta^*_{\mathrm{III}}(x,t)=-\frac{A}{2\sqrt{\pi}\,\sigma}\int_{-\infty}^{+\infty}\sum_{n=-p}^{n=+p}\cos n\tau\mu e^{-\left(\mu-\frac{2\pi}{T}\right)^2/4\sigma^2}\sin\left(\frac{\mu^2 x}{g}-\mu t\right)d\mu. \tag{20}$$

The expression, which involves the sum over n of $\cos n\tau\mu$, can be expressed as a finite harmonic series, and the use of eq 21, plus some rearrangement of terms, yields eq 22.

$$\sum_{n=0}^{p} e^{in\tau\mu}=\frac{1-e^{i(p+1)\tau\mu}}{1-e^{i\tau\mu}}. \tag{21}$$

$$\sum_{n=-p}^{n=+p}\cos n\tau\mu=\sum_{n=0}^{p} e^{in\tau\mu}+\sum_{n=0}^{p} e^{-in\tau\mu}-1=\frac{\sin(p\tau+\tau/2)\mu}{\sin\tau\mu/2}. \tag{22}$$

The term $1/\sin(\tau/2)\mu$ is plus or minus infinity, depending upon how μ approaches $2\pi m/\tau$, and it can be expressed in series form by eq 23.

$$\frac{1}{\sin\frac{\tau}{2}\mu}=\frac{2}{\tau}\sum_{m=-\infty}^{m=+\infty}\left(\frac{(-1)^{m+1}}{\frac{2\pi m}{\tau}-\mu}\right). \tag{23}$$

Equations 22 and 23 substituted into eq 20 then yield eq 24.

$$\eta^*_{\mathrm{III}}(x,t)=\frac{-A}{\sqrt{\pi}\sigma\tau}\int_{-\infty}^{+\infty}\sum_{m=-\infty}^{m=+\infty}(-1)^{m+1}\frac{\sin(p\tau+\tau/2)\mu}{\left(\frac{2\pi m}{\tau}-\mu\right)}$$

$$e^{-\left(\mu-\frac{2\pi}{T}\right)^2/4\sigma^2}\sin\left(\frac{\mu^2x}{g}-\mu t\right)d\mu\cdot \tag{24}$$

The factor $\exp[-\left(\mu-\frac{2\pi}{T}\right)^2/4\sigma^2]$ is small for μ less than or equal to zero for appropriate values of σ and T. For a fixed m, the term $(\sin\,(p\tau+\tau/2)\mu)/\left(\frac{2\pi m}{T}-\mu\right)$ is a spike at $\mu=2\pi m/\tau$, and therefore the integral can be adequately approximated by the substitution of $\mu=2\pi m/\tau$, in the exponential factor and by the omission of the terms involving m less than or equal to zero.[4] Equation 25 is then a valid approximate result.

$$\eta^*_{\mathrm{III}}(x,t)\cong\frac{A\sqrt{\pi}}{\sigma\tau}\sum_{m=1}^{\infty}e^{-\left(\frac{2\pi m}{\tau}-\frac{2\pi}{T}\right)^2/4\sigma^2}$$

$$\frac{(-1)^m}{\pi}\int_{-\infty}^{+\infty}\frac{\sin(p\tau+\tau/2)\mu}{\frac{2\pi m}{\tau}-\mu}\sin\left(\frac{\mu^2x}{g}-\mu t\right)d\mu \tag{25}$$

The term to be integrated in eq 25 is very similar to eq 13, where τ/m replaces the T in eq 13. If $(p\tau+\tau/2)$ were equal to an integer, say k, times τ/m, then eq 11 would be satisfied. This implies that eq 26 holds.

$$p\tau+\tau/2=K\tau/m, \tag{26}$$

or

$$mp+m/2=K. \tag{27}$$

K is an integer if m is even, and the results of section 4 apply directly. If m is odd, a problem similar to eq 11 can be solved with the sinusoidal term of full amplitude from $-(n+\frac{1}{2})T\leq t\leq(n+\frac{1}{2})T$ instead of as given in eq 11. The solution does not differ from eq 14 in any important aspects.

Therefore, the free surface given by $\eta^*_{\mathrm{III}}(x,t)$ consists of a number of wave trains which take $(2p+1)\tau$ seconds to pass the point $x=0$. The first train has a period of τ seconds and an amplitude of

$$(\sqrt{\pi}A/\sigma\tau)\exp(-\left(\frac{2\pi}{\tau}-\frac{2\pi}{T}\right)^2/4\sigma^2)\cdot$$

The second train has a period of $\tau/2$ seconds and an amplitude of

$$(\sqrt{\pi}A/\sigma\tau)\exp(-\left(\frac{2\pi 2}{\tau}-\frac{2\pi}{T}\right)^2/4\sigma^2)$$

[4] These very low components travel in the negative x direction, and do not affect the results in principle. The assumption, however, does permit the easy integration of eq 6.

seconds, and so forth. The periods of the waves that would propagate into the area of decay, for $\tau=100$ seconds, would be 100 seconds, 50 seconds, 33.3 seconds, 25 seconds, 20 seconds, 16.7 seconds, 14.3 seconds, 12.5 seconds, 11.1 seconds, 10 seconds, and so forth through 4 seconds for $m=25$, 2 seconds for $m=50$, and 1 second for $m=100$. If T were 10 seconds, the train with a 10-second period would have a maximum amplitude, and for typical values of σ the trains with 1- and 100-second periods would be very low.

For the values of σ, T, and A of section 3, and for $\tau=100$ seconds, the amplitude of the 100-second component would be less than 10^{-12} m, and the amplitude of the 10-second component would be 3.55 m.

If p were equal to 180, the wave system represented by eq 18 would require 10 hours and 2 minutes (36,100 seconds) to pass the point $x=0$. From eqs 4, 15, 16, and 25, this wave system can be broken down into a number of wave trains of different spectral periods, and each wave train would advance with its own group velocity into the area of decay. Each wave train would take essentially 10 hours to pass a point in the area of decay, but they would pass at different times.

For the chosen values of parameters of eq 18, only periods ranging from 17 to 7 seconds are important. All others are associated with wave trains less than $\frac{1}{2}$ cm in height. The spectral periods, the wave-train amplitude, and the 1,000-km travel times are shown in table 1.

TABLE 1. *Component periods, amplitudes, and 1,000-km travel times for the important wave trains in eq 25*

m	Period	Amplitude	Travel time of forward edge to a point 1,000 km away
	Seconds	*Meters*	*Hours*
1	100	$<10^{-12}$	....
6	16.7	0.006	21.4
7	14.3	.094	25.0
8	12.5	.755	28.5
9	11.1	2.39	32.0
10	10.0	3.53	35.6
11	9.09	2.39	39.2
12	8.33	0.755	42.7
13	7.69	.094	46.3
14	7.14	.006	49.8

The sum of the amplitudes in table 1 is 10 m within the accuracy of the computations, so that the amplitude at phase reinforcement equals the maximum amplitude of the wave groups in eq 18.

Figure 3 shows the effect of dispersion on the original wave system. The waves that would be observed at a point 1,000 km away are shown on a time-period coordinate system. A sinusoidal wave train with an amplitude of 0.6 cm would arrive 21.4 hours after the wave system started at x equal to zero, as shown on the first bar in the upper left of the figure. It would pass completely in 10 hours, and 31.4 hours after the start of the wave system at x equal to zero the component would no longer be present. Similar remarks can be made about each bar in the diagram. When the various bars of the diagram overlap the sea surface is the sum of the various sinusoidal terms indicated. Sine waves of different periods will sometimes add to a maximum and sometimes cancel to a minimum. In fact, there will be a point of phase reinforcement every 100 seconds in this model. The maximum amplitudes present are therefore just the sums

of the amplitudes of the components. The peak amplitudes are shown above the dispersion diagram as a function of time along with the periods that go to make up the peak amplitudes.

The forerunners of swell discussed in the literature are clearly shown in this model. This swell will be more regular than the original model waves. What is of more interest is the trailing end of short-period waves, which is not discussed or emphasized as much in the literature. The waves that arrive after 42 hours will have periods less than the apparent period in the original storm, and the question as to why they are not observed more often arises.

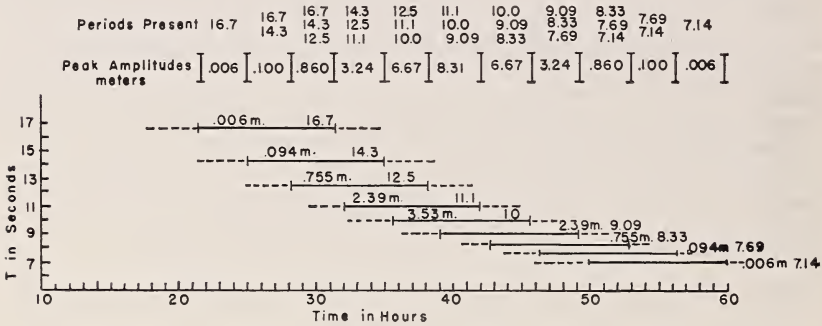

FIGURE 3. *Dispersion curve for model wave system.*

|— □ —| Half-amplitude points.

- - - - - -, Leakage.

The decrease in wave period of waves arriving from a distant storm has been observed. The work of Deacon [3] is the paramount example that this model agrees crudely with what occurs in nature. The spectrum of waves from a distant hurricane given by Donn [4] is a second example. The wave records from a distant hurricane given by Pierson [7] are another example. The current wave-forecasting methods of Sverdrup and Munk [9] extended in part by Arthur [1] provide no means to forecast this trailing end of the waves from the storm.

Now consider eq 17. It differs from eq 18 in that it is more random in a somewhat artificial way. Figure 4 shows the appearance of segments of eq 17 and 18 where the irregular wave record applies to eq 17. Equation 17 cannot be treated by the techniques of eq 19 through 27. However, other techniques that will be discussed in detail in a forthcoming paper permit a study of eq 17.

It can be shown that after the waves travel a short distance from x equal to zero, they become much more regular in appearance; that a sorting of the spectral components, such as shown by figure 3, occurs; and that the analysis given in figure 3 is a very good approximation to the waves that arrive at a distant point, except that the growth to half amplitude and to full amplitude is slower because there is more leakage. Only one condition needs to be imposed in order to obtain all of the above conclusions. The condition is that the A_n in eq 17 must be randomly distributed (not necessarily with a normal distribution) and that the A of eq 18 be chosen to be equal to the square root of the average of the

squares of the A_n. That is, eq 28 should hold within a small error for N of the order of 20 or 30.

$$A^2=\frac{1}{N}\sum_{n=q}^{n=q+N} A_n^2, \tag{28}$$

where

$$-p\leq q<q+N\leq p.$$

Equation 28 imposes the condition that there is no trend in the wave-group amplitudes and that the disturbance is in a steady state.

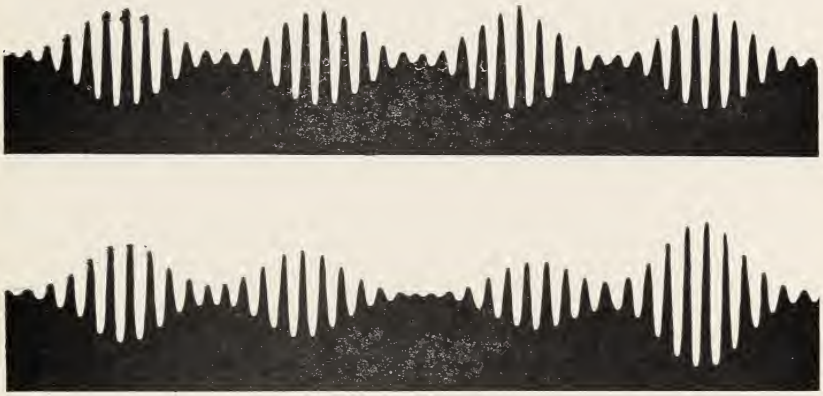

FIGURE 4. *Random and nonrandom storm waves.*

6. Summary and Conclusions

The model fetch discussed in this paper sent out model wave groups at successive time increments. The model fetch is infinitely wide, and all spectral components are assumed to be traveling in the positive x direction. The crests of the model waves are infinitely long in the y direction. Models have been constructed for fetches of finite width which send out irregular short crested waves with spectral components that travel in many directions. These models will also be discussed in the forthcoming paper referred to above. The models are very realistic in that they are not restricted to any particular spectrum.

Although the model waves discussed in this paper are not too realistic, they do serve to emphasize one extremely important point. The waves propagated into the area of decay were described quantitatively in terms of parameters determined at the source. These parameters, were A, τ, and discrete values of the continuous spectrum given by eq 5. If the spectrum had been different, the results would have been different. Very little is known quantitatively about these parameters in nature. Until these parameters (or better yet, those that follow from the model fetch of finite width which sends out short crested waves) are measured accurately in the storm area, wave-forecasting methods will always be inaccurate.

7. References

[1] Arthur, R. S., 1948: Revised wave forecasting graphs and procedure. Wave Report No. 73. Scripps Institution of Oceanography, University of California.

[2] Coulson, C. A., 1943: Waves. Interscience Publishers, Inc.

[3] Deacon, G. E. R., 1949: Recent studies of waves and swell, ocean surface waves. Annals of the New York Academy of Sciences, vol. 51, art. 3, pp. 475–482.

[4] Donn, W. L., 1949: Studies of waves and swell in the western North Atlantic. Trans. American Geophysical Union, vol. 30, No. 4, pp. 507–516.

[5] Janke, E., and Emde, F., 1945: Tables of functions with formulae and curves (Functionentafeln mit Formeln und Kurven). Fourth Edition, Dover Publications, New York.

[6] Lamb, Sir Horace, 1932: Hydrodynamics. Sixth Edition, Dover Publications, or Cambridge University Press.

[7] Pierson, W. J., Jr., 1951: The accuracy of present wave forecasting methods with reference to problems in beach erosion on the New Jersey and Long Island coasts. Beach Erosion Board Technical Memorandum No. 24.

[8] Sommerfeld, A., 1949: Partial differential equations in physics. Academic Press, Inc., pp. 17–21.

[9] Sverdrup, H. U. and Munk, W. H., 1947: Wind, sea, and swell; theory of relations for forecasting. U. S. Navy Hydrographic Office. H. O. Pub. No. 601.

21. On the Theory of Short-Crested Oscillatory Waves

By Robert A. Fuchs [1]

The irrotational motion of an infinite periodic wave train which is not of the cylindrical or long-crested type is investigated to a second approximation for water of an arbitrary finite depth. The surface profile is doubly periodic or short-crested and sinusoidal to a first approximation, as Jeffreys first pointed out. In a manner similar to the long-crested theory of Stokes, the elevations are no longer similar to the depressions, as was the case for the linear theory, but the depressions are broader and the elevations narrower. The surface profiles of short-crested waves are compared with the profiles of long-crested waves having the same steepness ratios in deep water. The assumptions of conservation of power and constancy of both the wave period and the ratio of the wave lengths involved leads to approximate expressions for the changes in wave lengths and amplitudes of short-crested waves moving shoreward. The long-crested wave appears from this analysis to be the most prominent in shallow water.

The linearized irrotational theory is applied to the treatment of a finite wave group generated by an initial elevation doubly periodic over a square region on the still water level and zero elsewhere. The motion of the emitted wave groups is discussed by the method of stationary phase applied to the appropriate double Fourier integral. Particular attention is paid to the two dimensional frequency spectrum.

1. Introduction

In 1924 Jeffreys [4][2] investigated wave systems that are periodic in both the direction of propagation and in the crest direction. The term short-crested was introduced in order to characterize such wave systems in which the two associated wave lengths were of the same order of magnitude. Waves whose crest wave lengths were much larger than the wave length in the direction of propagation were called long-crested waves. These include as special cases the cylindrical waves of Stokes. In figure 1, we show a typical system of short-crested waves near breaking. Notice the typical diamond-shaped pattern with flat troughs and steep crests. Jeffreys made use of the shallow-water theory in discussing the transformation of a mixture of short- and long-crested waves moving shoreward. The dependence of the motion on the wave height was investigated by determining the second-order terms in the equation for the wave profile for shallow water of constant depth. This method was open to objection, however, because it yields waves of nonpermanent form in the shallow-water theory.

The theory of such waves is placed on a more satisfactory foundation by extending Stokes' [9] theory for irrotational cylindrical waves in water of finite depth to the general case of short-crested waves. All systems of

[1] University of California, Berkeley, Calif.

[2] Figures in brackets indicate literature references on p. 200.

periodic rectilinear waves are readily obtained by choosing the involved parameters appropriately; in particular cylindrical waves are included by choosing the wave number in the crest direction equal to zero or equivalently by choosing the wave length in this direction to be infinite. The calculations are carried out to the second order of approximation, neglecting terms of the order of the cube of the wave height. The transformation of short-crested waves on a sloping beach is approximately determined by assuming that the power transmitted with the waves is conserved. A typical interference pattern of a simple short-crested wave group is obtained by superimposing two short-crested waves having nearly the same periods and wavelengths and the same amplitude. Finally, we discuss the case, of perhaps most practical interest, namely, the motion of waves generated by an initially localized displacement.

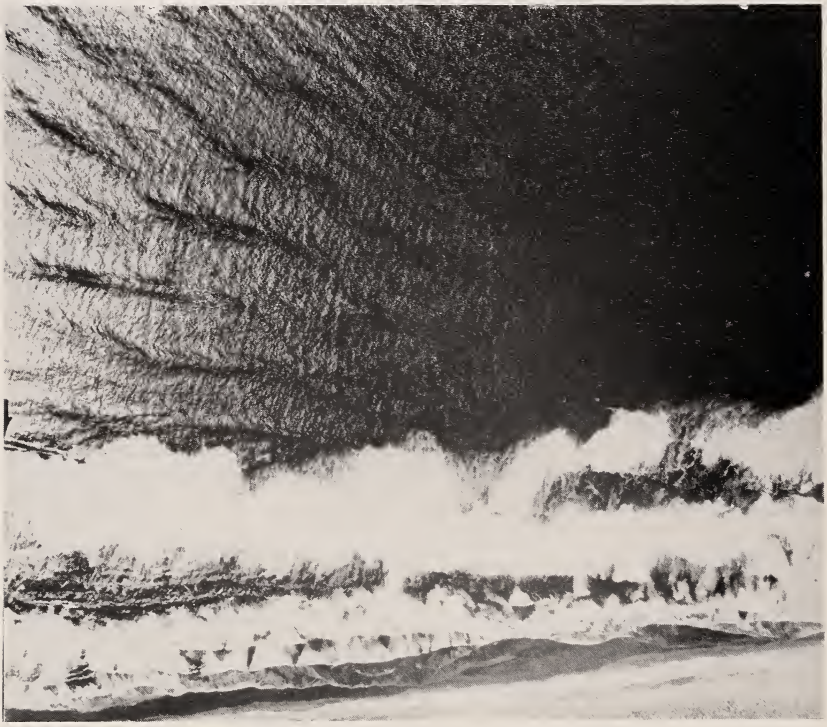

FIGURE 1. *Aerial photograph of short-crested waves.*

The importance of short-crested wave systems has been indicated by Jeffreys [5] when he showed that the weakest wind capable of raising waves generates long-crested waves but stronger winds generate short-crested waves. According to Jeffreys, this is due to the turbulence of the wind being random not only in the direction of propagation but also at right angles to this direction. This helps to explain the absence of long-crested waves in deep water, as reported by many different observers, including recently Side and Panton [8] and Williams [10].

2. Basic Equations of Hydrodynamics

The basic equations describing irrotational motion in three dimensions for water of finite depth d bounded by a free surface of zero pressure are in the usual notation (Lamb 1932).

$$\begin{aligned} &\Delta\phi=\phi_{xx}+\phi_{yy}+\phi_{zz}=0,\\ &\frac{p}{\rho}=gy-\phi_t-\tfrac{1}{2}(\phi_x^2+\phi_y^2+\phi_z^2)+\text{const}, \qquad (1)\\ &\phi y=0 \text{ on the horizontal bottom},\\ &p \ =\text{const on the free surface}. \end{aligned}$$

For convenience, we choose the positive y-axis directed downward and the x-axis in the direction of wave propagation. For a constant velocity of propagation c in the x-direction the motion can be reduced to a steady state by replacing $x-ct$ by x. Then

$$\frac{p}{\rho}=g(y+k)+c\phi_x-\tfrac{1}{2}(\phi_x^2+\phi_y^2+\phi_z^2), \qquad (2)$$

$$(\phi_x-c)p_x+\phi_y p_y+\phi_z p_z=0, \quad \text{when } p=0. \qquad (3)$$

These equations we proceed to solve by successive approximations subject to the indicated boundary conditions. Expanding ϕ about the plane $y=0$ and with the understanding that from now on all derivatives will be evaluated at $y=0$, we find the surface elevation is

$$\eta=-k-\frac{c}{g}\phi_x+\frac{c^2}{g^2}\phi_x\phi_{xy}+\frac{1}{2g}(\phi_x^2+\phi_y^2+\phi_z^2), \qquad (4)$$

where

$$g\phi y-c^2\phi_{xx}=c\phi_x\phi_{yy}-\frac{c^3}{g}\phi_x\phi_{xxy}-2c(\phi_x\phi_{xx}+\phi_y\phi_{xy}+\phi_z\phi_{xz}), \qquad (5)$$

and terms of order higher than the second are neglected.

3. Linear Theory

Separating variables in Laplace's equation we find the typical solution $\phi=A\cosh r(d-y)\cos mx\cos nz$, where $r^2=m^2+n^2$. By eq 5, neglecting terms of the second order, the velocity of propagation is given by

$$c^2=\frac{gr}{m^2}\tanh rd\geq\frac{g}{m}\tanh md, \qquad (6)$$

or

$$c^2=\frac{gL}{2\pi}\sqrt{1+\left(\frac{L}{L'}\right)^2}\tanh\frac{2\pi d}{L}\sqrt{1+\left(\frac{L}{L'}\right)^2}\geq\frac{gL}{2\pi}\tanh\frac{2\pi d}{L},$$

where L, L' are wavelengths in the x and z directions, respectively. One sees in particular that the cylindrical wave propagates most slowly for

a given wave length L and depth d. In terms of the wave amplitude, a the characteristics of the wave motion are

$$\left.\begin{aligned}
\eta &= a \sin mx \cos nz, \\
\phi &= \frac{ga}{cm} \frac{\cosh r(d-y)}{\cosh rd} \cos mx \cos nz, \\
\frac{p}{\rho g} &= y - a \frac{\cosh r(d-y)}{\cosh rd} \sin mx \cos nz, \\
u = -\phi_x &= \frac{ga}{c} \frac{\cosh r(d-y)}{\cosh rd} \sin mx \cos nz, \\
v = -\phi_y &= \frac{gar}{cm} \frac{\sinh r(d-y)}{\cosh rd} \cos mx \cos nz, \\
w = -\phi_z &= \frac{gan}{cm} \frac{\cosh r(d-y)}{\cosh rd} \cos mx \sin nz.
\end{aligned}\right\} \tag{7}$$

The total energy per unit surface area $= \frac{1}{2}$ kinetic energy $= \frac{1}{4} g\rho a^2$. The corresponding total energy of cylindrical waves per unit surface area is $\frac{1}{2} g\rho a^2$.

The paths of the water particles are obtained by integrating the equations for the particle velocity components u, v, w after replacing x by $x-ct$. The orbital paths are ellipses with one axis in the direction of wave propagation, and making with a vertical plane an angle β given by

$$\tan \beta = \frac{n}{r} \tan nz \coth r(d-y). \tag{8}$$

The ellipses have their greatest inclination to the vertical at the still water level and become entirely horizontal at the bottom. The length of the semi x-axis of the ellipse is

$$A = \frac{am}{r} \frac{\cosh r(d-y)}{\sinh rd} \cos nz, \tag{9}$$

and the semilength of the inclined axis is

$$B = \frac{a \sinh r(d-y)}{\sinh rd} \cos nz \sec \beta. \tag{10}$$

These expressions reduce to the classical ones for cylindrical waves if one sets $n=0$. Representative ellipses are given in figure 2.

4. Second Approximation

When the first approximation for ϕ is substituted into the right hand side of eq 5 one finds, after some calculation,

$$g\phi_y - c^2\phi_{xx} = \frac{cA^2 m \sin 2mx}{2} \left(2n^2 \cosh^2 rd - \frac{3r^2}{2} - \frac{3r^2}{2} \cos 2nz \right). \tag{11}$$

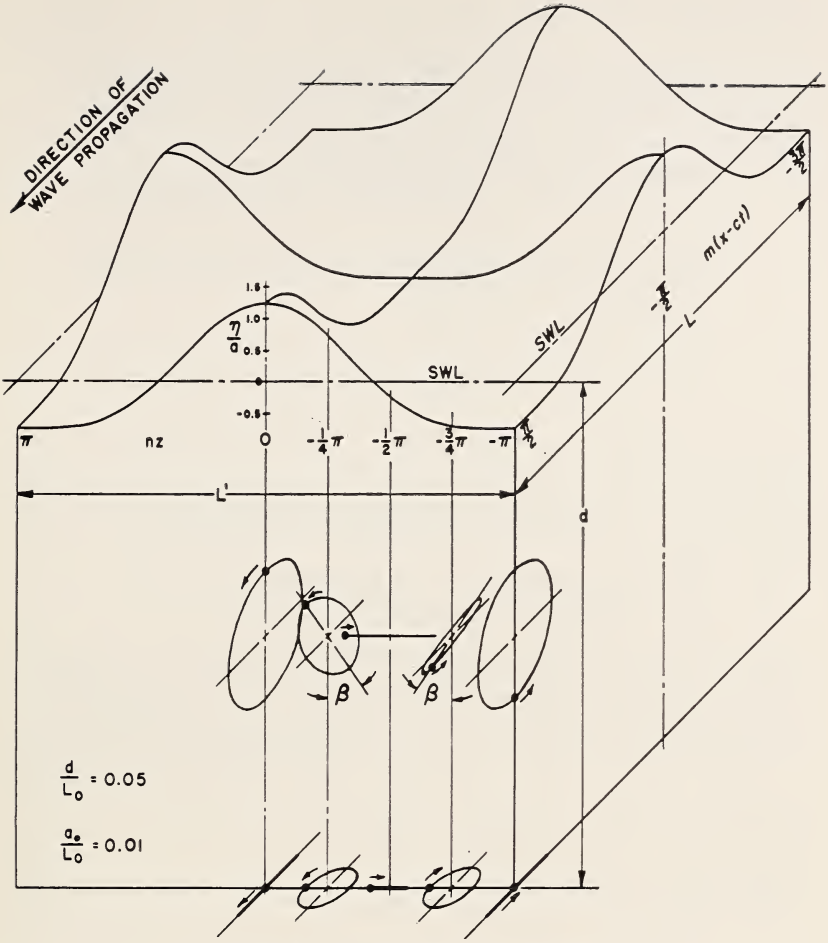

FIGURE 2. *Second-order surface profiles.*
First-order elliptical particle orbits.

The most general form for ϕ of the type indicated by separation of variables and satisfying this equation with the given first-order expression is

$$\phi = A \cosh r(d-y) \cos mx \cos nz + B \cosh 2r(d-y) \sin 2mx$$
$$\cos 2nz + D \cosh 2m(d-y) \sin 2mx. \tag{12}$$

Substituting and collecting terms we find

$$D = \frac{A^2}{8mc} \frac{4n^2 \cosh^2 rd - 3r^2}{2 \cosh 2md - \dfrac{m \sinh 2md}{r \tanh rd}}; \quad B = \frac{-3}{16} \frac{A^2 r^2}{cm \sinh^2 rd}. \tag{13}$$

The equation of the wave profile then is

$$\eta = a \sin mx \cos nz + \frac{a^2 r}{4 \sinh 2rd}\left(2 \sinh^2 rd - 1 + \frac{3 \cosh 2rd}{\sinh^2 rd}\right)$$

$$\cos 2mx \cos 2nz + \frac{a^2(m^2 - n^2 \cosh 2rd)}{4r \sinh 2rd} \cos 2nz + \frac{a^2}{4r \sinh 2rd}$$

$$\left(\frac{(3r^2 - 4n^2 \cosh^2 rd) \cosh 2md}{\cosh 2md - \dfrac{m \sinh 2md}{2r \tanh rd}} - m^2 \cosh^2 rd + 3r^2 \sinh^2 rd\right.$$

$$\left. + n^2 \cosh^2 rd\right) \cos 2mx. \tag{14}$$

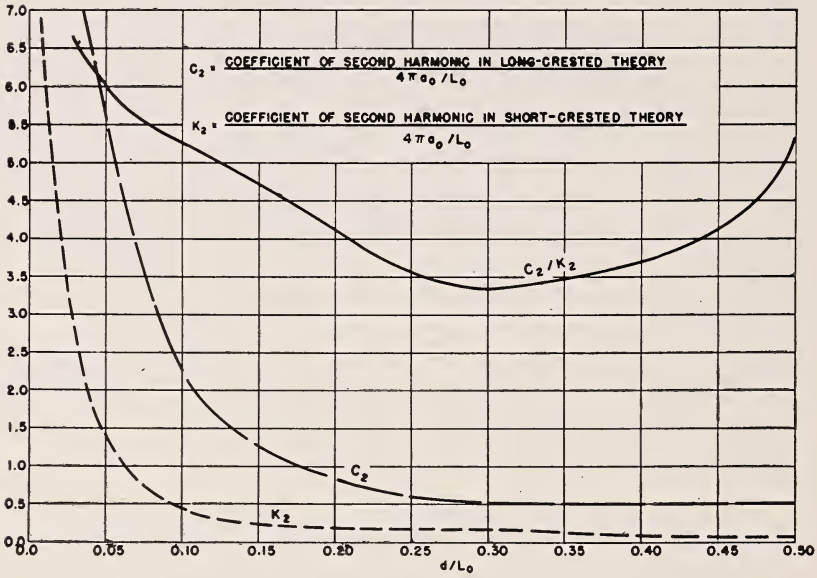

FIGURE 3. *Coefficients of second harmonics in equations for wave profiles.*

A comparison is given in figure 3 between the coefficients of the second harmonic terms in the surface profile of long- and short-crested waves in terms of the same initial steepness in deep water, the transformation being given in section 4. This figure shows that for a mixture of long- and short-crested waves having the same steepness in deep water the long-crested wave will be predominant in shallow water. The predominant second harmonic term for short-crested waves is proportional to $\cos 2mx \cos 2nz$.

This expression 14 reduces essentially to Stokes' classical second-order formula for the surface elevation when $n=0$. It is of course not possible to express this surface elevation by a simple superposition of two cylindrical waves of second order meeting at an angle, even though this was

possible to the first order. A pictorial sketch of the free surface is given in figure 2 for conditions made clearer in section 5.

The particle motion can be determined by expanding the particle coordinates about an equilibrium position, neglecting third-order terms and integrating the resulting formulas for particle velocity components. The resulting motion is quite complicated. One finds that in addition to the oscillatory motion the particles are propagated in the direction of the wave motion with a constant velocity.

$$U=\frac{a^2\,\mathrm{cm}^2\coth^2 rd}{4r^2}\left[r^2\,(\tanh^2 rd+1)+\cos 2nz(r^2\tanh^2 rd+m^2-n^2)\right]. \quad (15)$$

Thus U is a maximum for lines in the direction of propagation passing through crests and troughs and a minimum for lines midway between these. These maximum mass transport velocities coupled with the large translational velocities of the short-crested waves breaking on these lanes give rise to eddy cells in the near-shore circulation. One would expect then that the separation between lanes of maximum current would vary with the crest wave length being large for long-crested waves and small for short-crested waves. This behavior has been noted by Shepard and Inman [7] in their studies of rip currents.

5. Energy Flux; Refraction

Approximate expressions for the transformation of waves on gently sloping beaches can be determined by applying Rayleigh's method of assuming that the average power transmitted per unit surface area in a regular wave train is conserved. One finds that this average power transmitted per unit area (Lamb 1932) is

$$p=1/8\rho g a^2\frac{m^2}{r^2}c\left(1+\frac{2rd}{\sinh 2rd}\right). \quad (16)$$

Equating values of p between neighboring orthogonals a distance Δl apart, we find

$$\frac{a}{a_0}=\sqrt{\frac{c_0\left(\frac{m_0}{r_0}\right)^2\bar{n}_0}{c\left(\frac{m}{r}\right)^2\bar{n}}}\sqrt{\frac{\Delta l_0}{\Delta l}}, \qquad n_0\rightarrow\bar{n}_0, \quad (17)$$

where

$$\bar{n}=\tfrac{1}{2}\left(1+\frac{2rd}{\sinh 2rd}\right), \quad n\rightarrow\bar{n},$$

and the subscript 0 refers to "deep waters." Assuming that m is always equal to n this expression can be written on the form

$$\frac{a}{a_0}=\overline{\left(\frac{a}{a_0}\right)}K_D=\frac{H}{H_0}K_D, \quad (18)$$

K_D indicates the extent to which the height of the wave is modified by refraction. The first factor $\overline{a/a_0}=H/H_0$ is the ratio of wave heights for

waves approaching at right angles to the depth contours. This ratio, together with the ratio of velocities for constant period, is presented in figure 4, as a function of d/L_0. If one assumes in addition that the period is constant, one can compute the refraction of waves for parallel contours according to Snell's law, following the procedure given in Breakers and Surf [2] for long-crested waves. This is included in figure 5.

Using this information, together with the equations for the surface profiles of the long- and short-crested waves, we can trace approximately the relative behavior of these waves as they move shoreward, assuming they have the same height and wave lengths in deep water. The short-crested wave, which was doubly sinusoidal in deep water, transforms as it moves into shallower water, becoming higher and steeper in the crests and broader and shallower in the troughs. The effect is to tend to produce a doubly periodic system of isolated mounds separated by relatively flat valleys. In this respect it suggests the behavior of long-crested waves in approaching the solitary wave form. This behavior is illustrated in figure 2. One sees that the long-crested wave peaks up much more rapidly than the short-crested wave in shallow water. Actually, our approximations are rather poor, however, for one would expect flow transverse to the direction of propagation, tending to transform short-crested waves into a long-crested form. This flow would be expected to be large for high waves in shallow water, and hence it would increase rapidly as the waves approach breaking.

6. Simple Group

The simple group is generated by superimposing two sinusoidal wave trains of neighboring wave lengths and frequencies and of the same amplitude. Thus we have

$$\eta = a\cos(m_1x-\sigma_1t)\cos n_1z + a\cos(m_2x-\sigma_2t)\cos n_2z,$$

which can be written in the form

$$\begin{aligned}\frac{\eta}{a} &= 2\cos(\alpha x-\beta t)\cos(mx-\sigma t)\cos\gamma z\cos nz \\ &\quad +2\sin(\alpha x-\beta t)\sin(mx-\sigma t)\sin\gamma z\sin nz,\end{aligned} \tag{19}$$

where $m_1=m-\alpha$, $m_2=m+\alpha$, $\sigma_1=\sigma-\beta$, $\sigma_2=\sigma+\beta$, $n_1=n-\gamma$, $n_2=n+\gamma$.

The amplitude factors $2a\cos(\alpha x-\beta t)\cos\gamma z$ and $2a\sin(\alpha x-\beta t)\sin\gamma z$ are slowly varying functions of x and z giving rise to a two-dimensional beat pattern. As an example, take $m=n, \alpha=\gamma$, $\sigma^2=\sqrt{2}gm$, $\alpha=m/10$. Figure 6 illustrates a typical set of cross sections of the free surface.

7. Initial Localized Disturbance

Jeffreys [6] has remarked that a short-crested wave may be considered as the resultant of two long-crested waves moving in different directions. Waves in a storm area will consist largely of short-crested waves, and as these waves leave the storm area they will tend to separate into long-crested components. As we have seen, this is true to a first approxima-

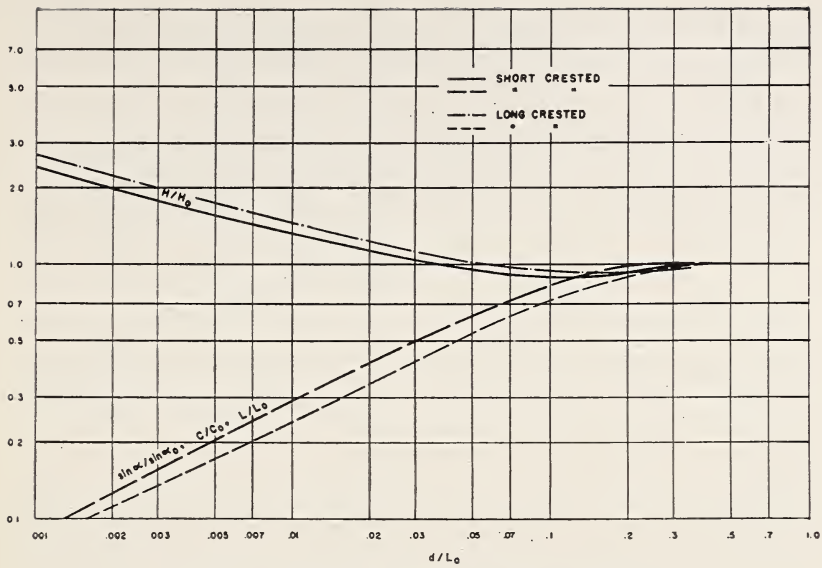

FIGURE 4. *Transformation of waves in shallow water.*

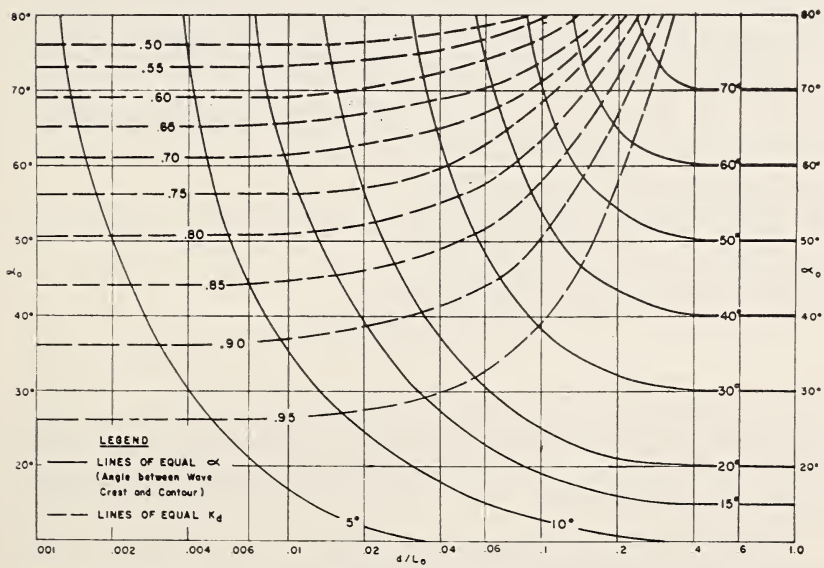

FIGURE 5. *Change in wave direction and height due to refraction on beaches with straight, parallel depth contours, for short-crested waves* ($L = L'$).

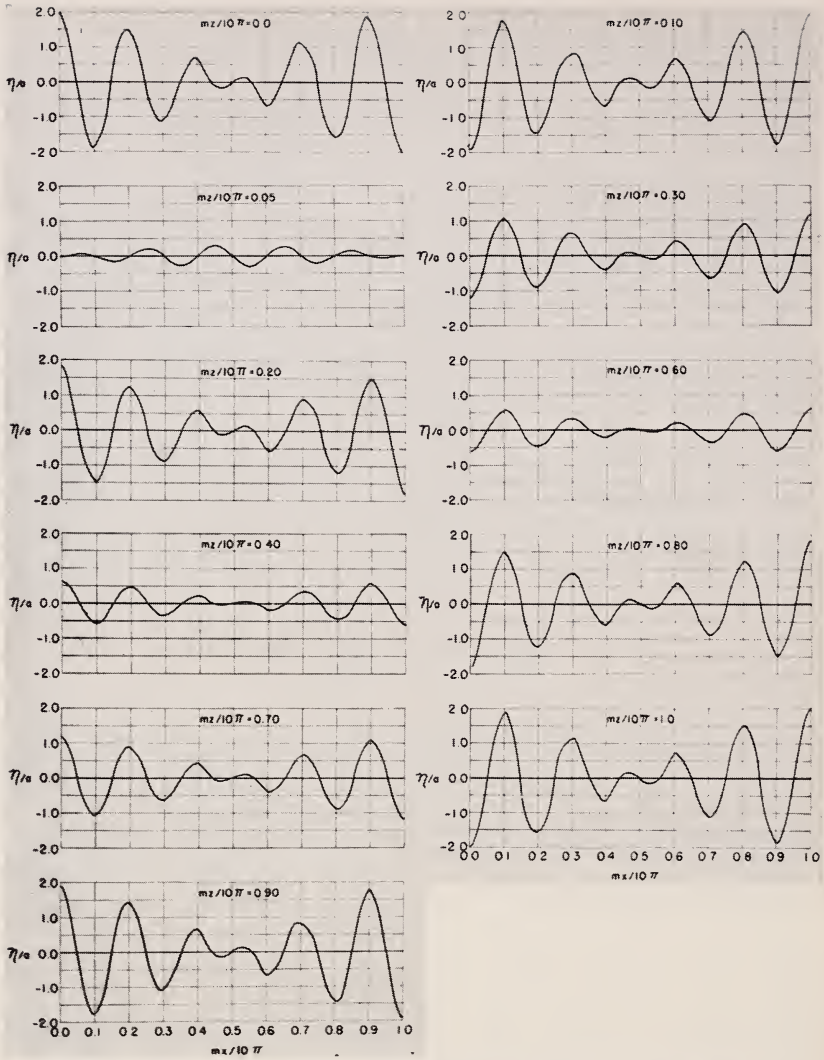

FIGURE 6. *Surface profiles of a simple short-crested group of waves in deep water.*

tion for infinite wave trains, since a product of the form $\cos mx \cos ny$ can always be written in the form of a sum of simple cosines. A fundamental question then is to what extent does this separation take place for localized disturbances. This is by no means answered by the simple remark above.

In order to attempt to answer this question, we shall solve the initial value problem for which the surface displacement has the form

$$\zeta(x,y,0)=f(x,y), \quad \frac{\partial\zeta(x,y,0)}{\partial t}=g(x,y), \tag{20}$$

by superposition of plane waves, using Fourier's integral theorem. One finds that

$$\left.\begin{aligned}
\zeta &= \int\int_{-\infty}^{\infty} e^{i(kx+ly)}\left(N\cos\sigma t+\frac{M}{\sigma}\sin\sigma t\right)dkdl \\
N &= \frac{1}{(2\pi)^2}\int\int_{-\infty}^{\infty} f(x,y)e^{-i(kx+ly)}dxdy \\
M &= \frac{1}{(2\pi)^2}\int\int_{-\infty}^{\infty} g(x,y)e^{-i(kx+ly)}dxdy.
\end{aligned}\right\} \tag{21}$$

We consider for convenience the case $g(x,y)=0$, and we suppose the water is infinitely deep, so that

$$\sigma^2=g\sqrt{k^2+l^2}.$$

Thus ζ can be represented as a variety of plane waves moving in opposite directions.

$$\zeta=\tfrac{1}{2}\int\int_{-\infty}^{\infty} N(k,l)e^{i(kx+ly-\sigma t)}\,dkdl \quad +\tfrac{1}{2}\int\int_{-\infty}^{\infty} N(k,l)e^{i(kx+ly+\sigma t)}dkdl. \tag{22}$$

Now ζ can be evaluated approximately by applying the method of stationary phase to each integral separately. Introducing polar coordinates r, θ, one finds that stationary values of the phases occur for

$$k_0=\frac{gt^2}{4r^2}\cos\theta, \quad l_0=\frac{gt^2}{4r^2}\sin\theta. \tag{23}$$

Expanding the phase about these stationary points, one finds on making the usual approximations that

$$\zeta=\frac{N(k_0,l_0)}{t\sqrt{B^2-AC}}\cos\left(\frac{gt^2}{4r}\right), \tag{24}$$

where A, B, C are the derivatives σ_{kk}, σ_{kl}, σ_{ll} evaluated at k_0, l_0. As a particularly important case, consider that of an initial elevation of the form $\cos ax \cos ay$ for a square region of length $2n+\frac{1}{2}$ wave lengths about the origin and zero outside. This generalizes Havelock's [3] model for cylindrical waves. Then

$$N(k,l)=\frac{1}{\pi^2a^2}\frac{\cos\left\{(2n+\frac{1}{2})\frac{\pi k}{a}\right\}\cos\left\{(2n+\frac{1}{2})\frac{\pi l}{a}\right\}}{\left(1-\frac{k^2}{a^2}\right)\left(1-\frac{l^2}{a^2}\right)}. \tag{25}$$

Substituting, one finds

$$\zeta=\frac{gt^2}{2\sqrt{2\pi a^2r^3}}\phi(\tau^2\cos\theta)\phi(\tau^2\sin\theta)\cos\left(\frac{gt^2}{4r}\right),$$

$$\zeta=\frac{4\sqrt{2}}{\pi ar}\tau^2\phi(\tau^2\cos\theta)\phi(\tau^2\sin\theta)\cos\left(\frac{gt^2}{4r}\right), \tag{26}$$

where

$$\phi(\tau^2)=\frac{\cos\{(2n+\frac{1}{2})\pi\tau^2\}}{1-\tau^4}, \tag{27}$$

and

$$\tau^2=\frac{gt^2}{4r^2a}.$$

These are waves moving radially outward from the origin with a variable amplitude factor $A(\tau,\theta)=\tau^2\phi(\tau^2\cos\theta)\phi(\tau^2\sin\theta)$ for fixed r. Since τ is proportional to t, $A(\tau,\theta)$ gives essentially the time history of the motion.

The wave length and period are

$$\left.\begin{aligned}\lambda&=-2\pi\Big/\frac{d\alpha}{dr}=\frac{8\pi r^2}{gt^2},\\ T&=2\pi\Big/\frac{d\alpha}{dt}=\frac{4\pi r}{gt},\\ \alpha&=\text{phase angle}=\frac{gt^2}{4r}.\end{aligned}\right\} \tag{28}$$

Hence

$$\text{group velocity}=\tfrac{1}{2}\text{ wave velocity}=\frac{gT}{4\pi}=\frac{1}{2}\sqrt{\frac{g\lambda}{2\pi}}. \tag{29}$$

In general one finds that the group velocity for any depth is

$$d=\tfrac{1}{2}(\text{wave velocity})\left(1+\frac{2rd}{\sinh 2rd}\right). \tag{30}$$

The wave length at the point of maximum amplitude is easily determined for $\theta=0,\pm\pi/4,\pm\pi/2,\ldots$. For $\theta=0$, $A(\tau,\theta)$ is a maximum for $gt^2/4r^2=a$ or $\lambda=2\pi/a$. The maximum of the disturbance for $\theta=0$ propagates with a group velocity associated with the original wave length $2\pi/a$. For $\theta=\pi/4$ the maximum amplitude occurs when $\tau^2=\sqrt{2}$, which implies $\lambda\pi/4=\lambda_0/\sqrt{2}$. This is the wave length of a long-crested component of an infinite train of the short-crested waves given initially. After a fixed time the distances traveled by the maximum disturbance will be in the ratio of the corresponding group velocities, which implies that the distance along $\theta=0$ is $\sqrt[4]{2}$ times the distance along $\theta=\pi/4$. The maximum disturbance occurs along $\pi/4$, and one finds for fixed r

$$\frac{\text{maximum amplitude at }\theta=\pi/4}{\text{maximum amplitude at }\theta=0}=\sqrt{2}(2n+\tfrac{1}{2})\frac{\pi}{2}, \tag{31}$$

which is quite large for a large number of initial waves.

The amplitude factors $A(\tau,\theta)$ for $\theta=0$, $\pi/4$ are plotted in figure 7 for $4\frac{1}{2}$ complete wave lengths of the initial disturbance about the origin. The principal effect occurs in the group moving with the group velocities corresponding to the initial wave lengths. In advance of these oscillations, however, are several other groups of appreciable amplitude with wave lengths of $\frac{9}{2}\lambda_0$, $\frac{9}{4}\lambda_0$, $\frac{9}{6}\lambda_0$, for $\theta=0$, $\pi/2, \ldots$, where λ_0 is the initial wave length $2\pi/a$. These groups moving with their corresponding group

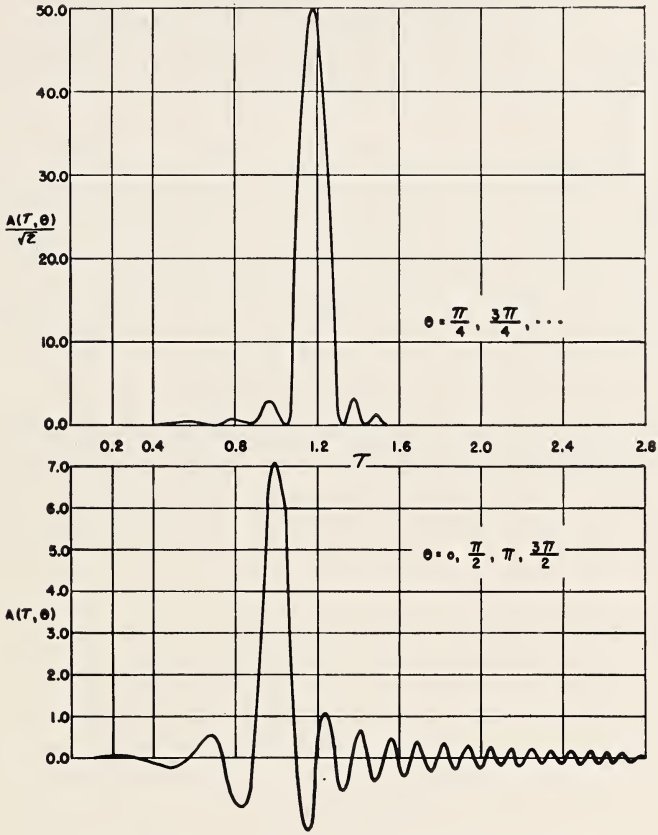

FIGURE 7. *Amplitude factor $A(\tau,\theta)$ for localized displacement 4.5 wave lengths long.*

velocities will arrive first at a given place. After the arrival of the maximum disturbance, one will find smaller disturbances having wave lengths of $\frac{9}{12}\lambda_0$, $\frac{9}{14}\lambda_0$, $\frac{9}{16}\lambda_0, \ldots$ for $\theta=0$, $\pi/2, \ldots$. In any particular group the period decreases with time at a given position like $1/t$. This leads to a broadening of the frequency spectrum toward shorter wave lengths, as observed by Barber and Ursell [1].

The behavior of the amplitude factor should be regarded only as indicating the trend of the amplitude as a function of time. Inherent in the use of the group approximation is the condition that at large distances the waves appear to be due to a concentrated point displacement of infinite amplitude. In order to secure amplitudes that are of the same order of

magnitude as the assumed initial amplitude, one must go to distances large compared with the dimensions of the initial disturbance. This may be neither convenient nor possible in actual situations. The solution of these difficulties requires a more refined asymptotic treatment of integrals such as eq 21.

8. References

[1] Barber, N. F. and Ursell, F. 1948. The generation and propagation of ocean waves and swell. I. Wave periods and velocities. Phil. Trans. Roy. Soc., London (A) **1,** 527.

[2] Breakers and Surf, Principles in Forecasting. 1944. Hydrographic Office Publ. No. 234.

[3] Havelock, T. H. 1914. The propagation of disturbances in dispersive media. Cambridge Univ. Press, p. 37.

[4] Jeffreys, H. 1924. On water waves near the shore. Phil. Mag. (Ser. 6) **48,** 44.

[5] Jeffreys, H. 1925. On the formation of water waves by wind. Proc. Roy. Soc. London (A) **107,** 189.

[6] Jeffreys, H. 1934. Additional notes to a book by V. Cornish—Ocean waves and kindred geophysical phenomena. Cambridge Univ. Press.

[7] Shepard, F. P. and Inman, D. L. 1950. Nearshore water circulation related to bottom topography and wave refraction. Trans. Amer. Geophysical Union **31,** 196.

[8] Side, E. A. and Panton, R. H. 1946. The modification of wave patterns in shallow water. Ministry of Supply, Wave report No. 15.

[9] Stokes, G. G. 1847. On the theory of oscillatory waves. Trans. Camb. Phil. Soc. **8,** 441.

[10] Williams, W. W. 1948. The determination of gradients on enemy held beaches. The Geophysical Journal, p. 196.

22. The Present Status of the Resonance Theory of Atmospheric Tides

By C. L. Pekeris[1]

A review is given of the resonance theory of atmospheric tides with a view of clarifying the apparent difficulties arising from the requirement of fine tuning, and from the fact that the upper stratosphere has a controlling influence on the free period, although its mass is only a fraction of 1 percent of the total mass in an atmospheric column. It is shown that in treating problems of atmospheric tides, which depend on the thermal structure of the atmosphere above about 100 km, one must include the quadratic terms in the equations of motion, since these become greater than the linear terms retained, at heights above about 130 km. The emergence of the quadratic terms in the differential equations is illustrated in figures 4 and 5.

Some other outstanding problems in atmospheric tides are then briefly discussed.

It is not generally recognized that our atmosphere, like the ocean, undergoes tidal oscillations. The tide in the atmosphere is manifested by a semidiurnal oscillation of the barometer. This phenomenon is most marked in the tropics, where, on the one hand, the amplitude of the atmospheric tide is at a maximum, and, on the other hand, the weather disturbances are generally weaker than in northern latitudes. Figure 1

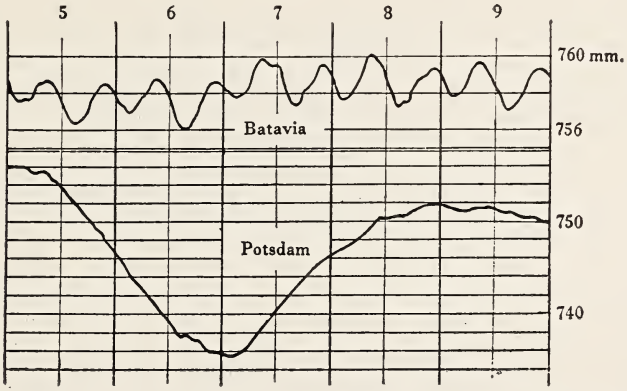

FIGURE 1. *Barographs taken at Batavia and Potsdam during November 5 to 9, 1919.*

shows a barograph for the period of November 5 to 9, 1919, taken at Batavia, latitude 6° S, exhibiting clearly the semidiurnal oscillation. On the barograph at Potsdam the tide, which is of smaller amplitude there, is completely masked by the passage of a "low." The atmospheric tide is a world-wide phenomenon, and shows greater regularity than the

[1] The Weizmann Institute of Science, Rehovoth, Israel.

oceanic tide. In contrast to the latter, it follows the sun and not the moon. Table 1 shows the times of maxima of the tide for a number of equatorial stations, and it is seen that, with one exception, they occur between 9:30 and 10 local time.

TABLE 1. *Time of maxima of atmospheric tide at some equatorial stations of different longitude*

Simpson, Quart. J. Roy. Met. Soc. **44**, 1, 1918.

Station	Latitude	Longitude	Time of maximum local time (a.m. and p.m.)
San Jose	9°56′ N.	84°4′ W.	9.6
Quito	0°14′ S.	78°32′ W.	10.0
Para	1°27′ S.	48°29′ W.	10.0
Quixeramdbin	5°16′ S.	39°56′ W.	10.3
Ascension	7°55′ S.	14°25′ W.	9.8
Gabun	0°25′ N.	9°35′ E.	9.9
Cameroons	4°3′ N.	9°40′ E.	9.7
St. Paul de Loanda	8°49′ S.	13°7′ E.	9.8
Kwai	4°45′ S.	38°18′ E.	10.0
Zanzibar	6°10′ S.	39°10′ E.	9.9
Dar-es-Salaam	6°49′ S.	39°19′ E.	9.6
Trivandrum	8°31′ N.	76°59′ E.	9.5
Singapore	1°15′ N.	103°51′ E.	9.8
Batavia	6°11′ S.	106°50′ E.	9.7
Finschhafen	6°34′ S.	147°50′ E.	9.5
Nauru	0°26′ S.	166°56′ E.	9.7
Jaluit	5°55′ S.	169°40′ E.	9.5

There is also a weak lunar tide in the atmosphere, but its amplitude is only $\frac{1}{16}$ of the solar tide. Because the tidal potential of the moon is greater than the tidal potential of the sun by a factor of 2.2, the preponderance of the lunar tide in the ocean is quite understandable. The reversed situation in relative magnitudes of the atmospheric tides has puzzled mathematicians for over 150 years. Laplace [1][2] was led to the conclusion that the tide in the atmosphere is excited thermally and not gravitationally. It was pointed out, however, by Sir William Thompson [2] that on the thermal hypothesis one would expect an even larger diurnal atmospheric tide of global regularity, which is not observed. Kelvin then proposed the resonance theory, according to which the atmosphere possesses a free period of oscillation very close to 12 solar hours, so that the gravitational semidiurnal solar tide is magnified by resonance. The tuning required to produce the observed magnification of about 100 has to be to within about 4 minutes [3] of 12 solar hours.

An obvious objection to the resonance theory is the unlikelihood that the atmosphere invariably retains that particular vertical temperature distribution which is required for the sharp tuning. Actually, it turns out that within a specified general pattern, the vertical temperature distribution may vary within appreciable limits before detuning sets in. Thus the temperature distributions shown in figure 2 [4] are, with the exception of cases *F* and *I*, consistent with a period of free oscillation close to 12 solar hours.

The general pattern of the resonating atmospheres shown in figure 2, is a rise of temperature between the levels of about 35 to 55 km, followed by a drop to about 75 km. At the time when this type of thermal structure of the atmosphere was proposed [4], there was strong evidence for only the rising portion of the temperature curve as derived from anomalous

[2] Figures in brackets indicate the literature references on p. 208.

sound propagation [5] but for the falling portion there was only the indication from the existence of noctilucent clouds [6]. Tidal theory shows [4] that *unless the drop of temperature between 55 to 75 km exists, the atmosphere will not possess a free period of 12 hours.* The existence of this region of falling temperature has since been verified by direct soundings with V-2 rockets, as shown in figure 3.

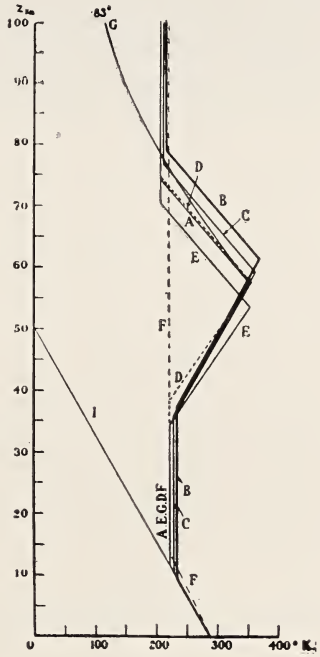

FIGURE 2. *The atmospheres with the vertical temperature distributions shown above (except F and I) have a period of free oscillation close to 12 solar hours.*

Nevertheless, one may ask how can the thermal structure of the upper stratosphere have such a deciding influence on the period of free oscillation when its mass is only a small fraction of the total mass in an atmospheric column? Thus, how is one to explain the result of tidal theory that atmosphere F in figure 2 is nonresonating, whereas atmospheres A, B, C, D, E, and G are, when the fractions of the total mass in an atmospheric column lying above the levels of 30, 40, 50, and 60 km are 1.1, 0.27, 0.091, and 0.033%, respectively? The answer is that the difficulty posed by the above query would be valid only if the amplitude of the tidal velocities were of the same order of magnitude throughout the atmospheric column, for only then would the dynamic effect of the upper stratosphere be directly related to its mass. Actually, theory shows that the amplitudes of the tidal velocities u increase with height, almost, but not quite, as rapidly as $\rho_0^{-\frac{1}{2}}$, where $\rho_0(z)$ denotes the mean density at height z. As a result, the energy density of wave motion E, which is proportional to $\rho_0 u^2$, remains of the same order of magnitude throughout the first 80 km for the 12-hourly free oscillation. This is illustrated by the curve E in figure 4, where it is seen that the value of E at 60 km is the same as at the

ground, and that the area under the E-curve above 30 km is more than twice as large as the area of the E-curve in the atmospheric column below 30 km. Because the total energy of wave motion in the upper stratosphere is more than twice as large as the energy in the lower regions, it is not surprising that the period of free oscillation for this mode depends markedly on the thermal structure of the upper stratosphere. It would also follow that in considering the problem of the maintenance of a tuned state for the semidiurnal oscillation, we should take into account not the striking atmospheric variability in the troposphere and lower stratosphere due to weather, topography, latitude, and seasons, but the probable considerably smaller variability of the structure of the whole atmospheric column extending from the ground up to about 80 km.

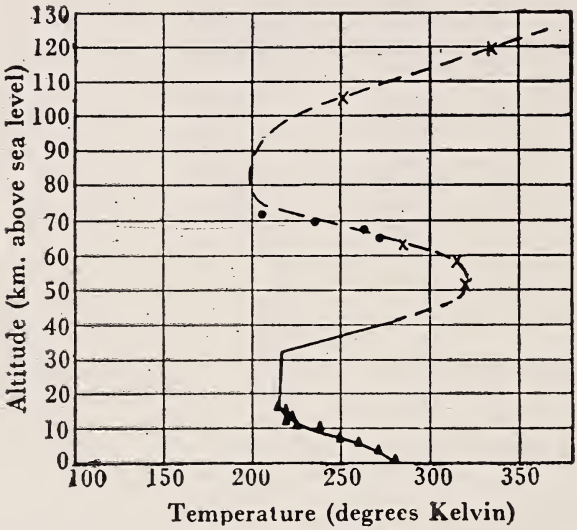

FIGURE 3. *Vertical temperature distribution determined by a V-2 rocket sounding at White Sands, New Mexico, on March 7, 1947 (N. Best, R. Havens, and H. La Gow, Phys. Rev.* **71**, *915, 1947).*

The above considerations apply only to the 12-hourly oscillation. The atmosphere possesses another free mode of oscillation with a period of about $10\frac{1}{2}$ hours. This is the mode by which the pressure wave caused by the Krakatau eruption of 1883 was carried three times around the world [7]. Tidal theory shows that the energy of this wave is concentrated in the troposphere and lower stratosphere. As a result, all of the atmospheres shown in figure 2 have nearly the same period of oscillation for this mode, with atmosphere I differing from the others by about 10 minutes only.

There remain some unsolved problems in the resonance theory of atmospheric tides that are associated mainly with the thermal structure of the atmosphere above 80 km. One is the discovery made by Appleton and Weekes [8] of the existence of a lunar tide in the E-layer of the ionosphere, which is situated at about 110 km. The amplitude of this oscillation in height of the E-layer is about 1 km, and its phase agrees with that of the lunar pressure oscillation at the ground. According to the commonly

accepted theory of the mechanism of ionization in the E-layer, the height of the E-layer should be in phase with the pressure oscillation there, from which it would follow that the lunar pressure variation at 110 km is in phase with the pressure oscillation at the ground. On the other hand, the resonance theory of atmospheric oscillations, when applied to atmospheres having the structural pattern shown in figure 2, predicts [4] that the pressure oscillation above 30 km is 180° out of phase with the pressure oscillation at the ground. Weekes and Wilkes [9] have shown that there is no difficulty in reconciling the above experimental results with theory if one assumes that, in addition to the temperature maximum at 60 km, there exists another temperature maximum at 110 km. This suggestion meets, however, with the difficulty which will be treated in detail presently, that above about 100 km, the quadratic terms in the tidal equations which were considered negligibly small, become comparable to the linear terms which were retained.

The difficulty with the emergence of the quadratic terms in the tidal equations above 100 km also besets any attempt at the solution of the second outstanding problem in the resonance theory, which is to determine whether a given temperature distribution in the ionosphere, such as, for example, the one shown in figure 3, can be reconciled with the existence of a free period of 12 solar hours. According to the usual linearized tidal theory the amplitude of the tidal velocities u increases with height, reaching values in the ionosphere which are about a thousand times greater than at the ground. Now at the ground the particle velocity u near the equator is about 35 cm/sec for the solar semidiurnal tide. With a magnification of 1,000, the particle velocity becomes comparable to the velocity of sound, when it is no longer permissible to neglect the quadratic terms in the tidal equations. Thus in the equation

$$\rho\frac{Du}{Dt}=\rho\left(\frac{\partial u}{\partial t}+u\frac{\partial u}{\partial x}+w\frac{\partial u}{\partial z}\right)=-\frac{\partial p}{\partial x}-\rho\frac{\partial \Omega}{\partial x}, \tag{1}$$

where Ω denotes the tidal potential, it is customary to substitute $\partial u/\partial t$ for Du/Dt. We may evaluate the error thus committed by determining the ratio of the neglected term $u(\partial u/\partial x)$ to $\partial u/\partial t$. Now in a wave progressing in the x direction

$$\frac{\partial u}{\partial x}=-\frac{1}{V}\frac{\partial u}{\partial t}, \tag{2}$$

where V denotes the phase velocity. Hence

$$\frac{\partial u}{\partial t}+u\frac{\partial u}{\partial x}=\frac{\partial u}{\partial t}\left[1-(u/V)\right]. \tag{3}$$

It follows that the neglect of the quadratic terms in the tidal equations is justified only when the particle velocity u is negligibly small in comparison with the phase velocity V. This phase velocity is of the order of the mean sound velocity in that portion of the atmospheric column in which the bulk of the wave energy is concentrated. Since the sound velocity varies only as $T^{\frac{1}{2}}$, V is in the neighborhood of 320 m/sec.

It follows from linearized eq 1 that

$$p_1\equiv p-p_0=\rho_0 uV, \tag{4}$$

where p_1 denotes the pressure oscillations. Hence

$$\frac{u}{V}=\frac{p_1}{\rho_0 V^2}=\frac{p_1(z)RT_0(z)}{\rho_0(z)V^2}=\frac{p_1(z)H_0(z)}{p_0(z)H}, \tag{5}$$

with

$$H_0(z)=(R/g)T_0(z), \quad V^2\equiv gH. \tag{6}$$

The factor $H_0(z)/H$ varies relatively little with height, so that *the ratio of the quadratic terms to the linear term is of the order of the ratio of the pressure of oscillation to the undisturbed pressure at the level considered.* Obviously, the linearized equations cease to be valid when (p_1/p_0) approaches unity.

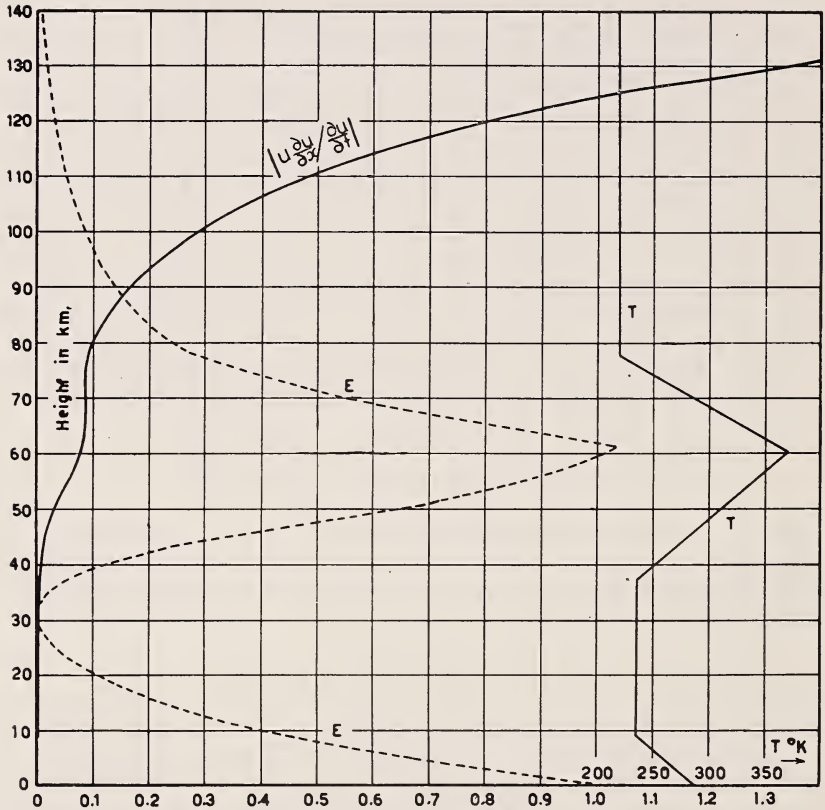

FIGURE 4. *Ratio of the neglected term $u(\partial u/\partial x)$ to the term $(\partial u/\partial t)$, which is retained in the equations of atmospheric oscillations.*

Curve T is the assumed temperature distribution, E the wave energy density.

The regions of validity of the linearized equations is illustrated in figures 4 and 5. The atmosphere in figure 4 is the one designated by B in figure 2. It is seen that whereas in the first 80 km the quadratic term is less than 0.1 of the linear term, the two terms become equal at 125 km. Above that height, the retained linear term becomes even smaller than the quadratic terms that are neglected in the linearized tidal equations.

The linearized equations, therefore, become inadequate for the determination of the tidal motion above that level. One may, however, venture to suppose that for this atmosphere the period of free oscillation will not differ materially from that given by the linearized theory, because the energy under the E-curve above 100 km is only a small fraction of the wave energy in the whole atmospheric column.

Figure 5 gives similar results for an atmosphere treated by Weekes and Wilkes [9]. Here, again, the quadratic terms exceed the linear terms above 130 km.

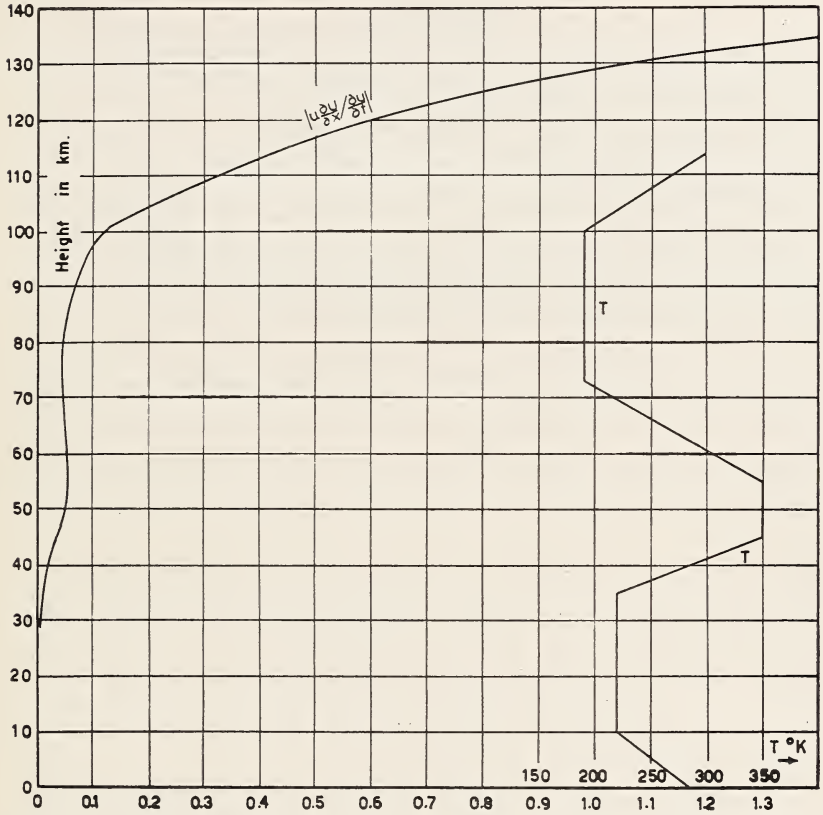

FIGURE 5. *Ratio of the neglected term $u(\partial u/\partial x)$ to the term $(\partial u/\partial t)$, which is retained in the theory of atmospheric oscillations.*

Curve T shows the assumed temperature distribution.

It follows from the above considerations that those features of atmospheric oscillations which depend on the thermal structure in the ionospheric levels cannot be treated adequately by the linearized tidal theory. Any conclusion derived from the linearized tidal theory that is conditioned on the assumption of a particular temperature distribution in the ionosphere is therefore open to question.

There are other outstanding problems in the theory of atmospheric tides that await solution. One of these is an explanation of the fact that

the maximum of the solar semidiurnal pressure wave occurs at 10 o'clock rather than at 12. This problem has been dealt with by Chapman [10], but it would be worth returning to it in the light of the considerations on the observed variation with height of the phase, which have recently been made by Bjerknes [11].

Another problem that still requires elucidation is the origin of the stationary component of the solar semidiurnal tide. This pressure oscillation has an amplitude of about 0.1 mm, and is at a maximum at high latitudes. There is also an appreciable 8-hourly oscillation.

References

[1] Laplace, Mechanique celeste **5,** 149, Paris (1823).
[2] W. Thompson, Proc. Roy. Soc. Edin. **11,** p. 396 (1882).
[3] S. Chapman, Quart. J. Roy. Met. Soc. **50,** 166 (1924).
[4] C. L. Pekeris, Proc. Roy. Soc. **158,** [A] 654 (1937).
[5] F. J. W. Whipple, Quart. J. Roy. Met. Soc. **60,** 510 (1934).
[6] Humphreys, Mon. Weather Rev. **61,** 228 (1933).
[7] G. I. Taylor, Proc. Roy. Soc. [A] **156,** 378 (1936); C. L. Pekeris, Proc. Roy. Soc. [A] **171,** 434 (1939).
[8] E. V. Appleton and K. Weekes, Proc. Roy. Soc. [A] **171,** 171 (1939).
[9] K. Weekes and M. V. Wilkes, Proc. Roy. Soc. [A] **192,** 80 (1947).
[10] S. Chapman, Quart. J. Roy. Met. Soc. **50,** 166 (1924).
[11] J. Bjerknes, J., Marine Research **7,** 154 (1948).

23. Analysis of Sea Waves

By G. E. R. Deacon[1]

The understandable reluctance of statisticians to use the periodogram technique to search for periodicities in short graphs of economic events has been used to dissuade oceanographers from employing it to analyze wave-pressure records, which look like mixtures of sine waves and approximate in length to the infinite duration required for full definition of the spectrum. The method of autocorrelation may have some advantage in the search for a single periodicity, because its cross multiplication will accentuate the principal periodic variation, but application of both methods to the same record indicates that there is little to choose between them in this respect. For the analysis of records which have been shown to approximate to mixtures of sine waves autocorrelation seems to be an unnecessary intermediate step: the resulting correlogram must itself be submitted to Fourier Analysis to obtain the desired information.

Experimental justification of the usefulness of the periodogram technique is available. By taking proper account of the response of a resonant filter to a gliding tone (Barber and Ursell, 1948), the first ocean-wave analyzer gave the amplitudes of Fourier components of artificial records correct to within 5 percent up to the sixtieth harmonic (Barber, Ursell, Tucker, and Darbyshire, 1946). The significance of prominent frequency bands that persist through analyses of consecutive records is demonstrated by success in confirming applications of hydrodynamical theory to wave propagation (Barber and Ursell, 1948, and Ursell, 1950). Confirmation of the theory that microseisms are produced in a region of wave interference between similar wave trains traveling in opposite directions (Longuet-Higgins, 1950) by analysis of simultaneous records of waves and microseisms (Darbyshire, 1950) might also be mentioned.

The first outcome of the improved methods of wave recording used during the past 6 or 7 years has been the accumulation of a large number of complex records from which the essential information can only be disentangled with some difficulty. There have been two methods of approach: on the one hand, the complexity of the records and scarcity of information about the basic processes in the generation area has been used as sufficient justification for a direct statistical approach, and on the other, an attempt has been made to select incidents of sufficiently simple nature and obvious interpretation to find simple rules or reasonable assumptions that might be confirmed by statistical methods when, for practical reasons, only crude observations can be made. As in other branches of science the methods are complementary, serving different purposes, and an attempt to assess their capabilities is not out of place at the present time. Barber and Ursell (1948) have set up a fairly precise physical model. Using the classical theory of Cauchy, Poisson, and others, they conclude that the waves should behave roughly as though they originated in an instantaneous point disturbance or a number of such disturbances distributed over the generating area. The result would be a continuous spectrum of waves, and a wave pattern that at any time would be the sum of a large number of component wave trains. After they leave the storm areas, the component waves, if not too steep, should travel independently with the group velocities appropriate to their

[1] National Institute of Oceanography, London, England.

periods, and if the generating area is well defined and far enough from the recording station, it should be possible to distinguish the component wave trains one after another at the recording station and to trace them back to the generating area by the group-velocity method. This conclusion was confirmed by taking wave-pressure records of 20 to 30 minutes duration every 2 hours at a point on the west coast of Cornwall, and analyzing the records on a specially constructed Fourier Analyzer (Barber, Ursell, Tucker, and Darbyshire, 1946).

It was soon found that most of the wave-frequency bands that appeared in the analyses could be attributed without uncertainty to particular storms shown on the meteorological charts, and by selecting well-defined storms at various distances from the recording station, the travel times could be measured with some accuracy. As expected, it was found that the waves leaving the storm area behaved as a continuous spectrum, each element of which traveled independently toward the distant coast with the classical group velocity appropriate to its period. It was also found that there was an upper limit of wave period that depended on the greatest wind strength. It has since been found that there may be some deviations from the classical behavior when the waves travel through an area in which they are acted on by a strong wind, but these are not large enough to upset the conclusions.

Seiwell and Wadsworth (1949), have set up an alternative model. They believe that the new research method of autocorrelation analysis should provide more information than the method of Fourier analysis, and after working on 30 records taken more or less at random from the North Atlantic Ocean, Mediterranean Sea, and Eastern American coast (Seiwell, 1949, p. 527), they conclude that the sea-surface pattern consists of a single cyclical component, or in rare cases two, on which is superposed a random variation "due to random motions of the water and local intermittent wind action." For the propagation of waves from the storm area it was assumed that "the ocean acts as a filter, so that after a certain distance from the generating area, swell of a single period is all that remains of the wave pattern" (Seiwell, 1950 pp. 245–46). The demonstration by Barber and Ursell that the upper and lower limits of wave period at a distant station changed from hour to hour according to simple expectation from hydrodynamical theory was dismissed as being "based on misleading indication of periods from periodogram analyses of finite amounts of data." No theoretical justification was given for the new model, but it was claimed to be a more realistic and more simplified picture of the physical characteristics of the sea surface.

In the interests of future progress in wave research it is necessary to decide whether the method of autocorrelation does give more information when applied to sea waves, whether the idea of a single wave plus random variations is more realistic than that of a wave pattern composed of trains of waves of different period, and whether it is better to begin by analyzing continuous series of records from simple well-defined incidents rather than records taken from here and there without reference to the prevailing meteorological conditions.

Mathematically, there is nothing to choose between the methods of autocorrelation and Fourier analysis. Ursell (1950 p. 455) points out that they both give perfect resolution of the available information. Only difference in the ease with which one or the other form of resolution can be used will make one method preferable to the other. Lee, Cheatham, and Wiesner (1950) emphasize that the correlation method can make no theoretical claim to be superior to the other, but they can make better

use of it because, from an engineering aspect, it makes many equivalent operations more practicable and feasible. The argument of the wave researchers who use the Fourier analyzer is that they prefer it because it makes the interpretation of wave records more practicable and feasible. In the interpretation of wave records both analyses are examined visually, the correlogram to see if it looks like a sine wave or mixture of sine waves, and the periodogram to see if one or more parts of the envelope of the

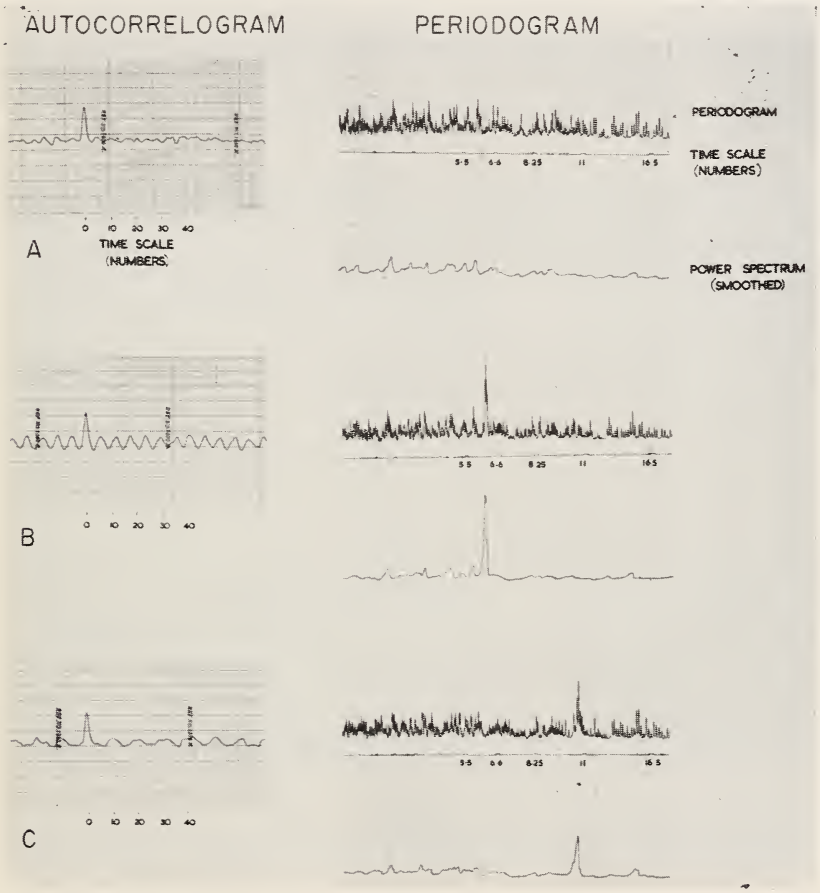

FIGURE 1. *Autocorrelograms and periodograms of artificial and real wave records.*
A, 560 random numbers 0 to 70; *B*, 560 random numbers plus 93 "waves" +10 to −10; *C*, 560 random numbers plus 56 "waves" +12 to −12.

Fourier ordinates in the spectrum stand well above the rest. To give some indication of what it involves the autocorrelograms and periodograms of four artificial records and one wave record are shown side by side in figure 1. They were obtained with a photoelectric correlation meter made in the Admiralty Research Laboratory, Teddington, by the staff of the newly formed Institute of Oceanography, and with the Fourier analyzer described by Barber, Ursell, Tucker, and Darbyshire in 1946.

The performance of each machine has been checked by analyzing standard records.

When random numbers are analyzed (first pair of records in fig. 1) the correlogram shows no obvious periodicity, and no part of the envelope of the Fourier ordinates in the periodogram stands well above the rest. When a periodic variation, repeating every six numbers, is superposed on the random numbers (second pair of records), the correlogram looks like a sine wave with a period of six numbers, and the periodogram has a very distinct peak at six numbers. A longer periodicity repeating every 10 numbers added to the same random numbers (third pair of records) is also apparent in both analyses, although, for some reason, the sine wave on the correlogram and the peak in the periodogram are not quite so well-developed as those obtained from the somewhat smaller, shorter, superposed variation used for the second pair.[2]

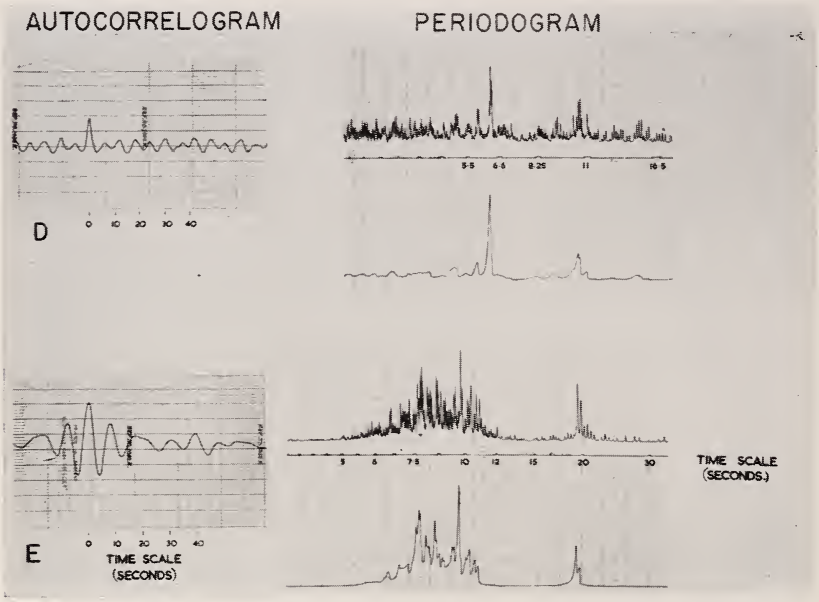

FIGURE 1 (continued). *Autocorrelograms and periodograms of artificial and real wave records.*

D, 560 random numbers plus both "wave" trains; *E*, wave pressure record 30 minutes, 40 ft. Perranporth 1900 hr, September 4, 1948.

The fourth pair of records represents corresponding analyses of the random numbers with both periodic variations superposed on them. The periodogram shows two peaks at 6 and 10 numbers like those in the second and third periodograms, but interpretation of the correlogram is not so easy. It looks like the sum of two or more sine waves and might be the sum of those in the second and third correlograms, but the periods could not be determined with any certainty except by submitting the correlogram to Fourier analysis. The resulting power spectra for the

[2] The spreading of the longer period into adjacent harmonics, and slight differences in the appearance of the background, are possibly due to small variations in speed of the recording camera.

correlograms in figure 1 would be very similar to the power spectra shown below each periodogram in the figure, which were obtained by incorporating in the Fourier analyzer a circuit that squares and slightly smoothes the output of the filter.

The fifth pair of records in figure 1 shows the autocorrelogram and periodogram of a 30-minute wave record. The correlogram suggests the presence of a number of periods, the periodogram gives a clear indication that there is a wide band of wave periods from 5 to 12 seconds and a narrow band of swell of 19 to 20 seconds. The record from which the analysis is made is part of a continuous series, and examination of the spectra of preceding and succeeding lengths of record and the relevant meteorological charts leaves no doubt that the narrow band of swell was part of the swell from a tropical storm that developed off the coast of Florida and moved northward along the eastern American coast. Comparison with the other analyses in figure 1 shows that the background is very small, and this is an almost universal feature of wave-pressure records. Seiwell's papers give the impression that what he really objected to was the apparently arbitrary way in which the exponents of the periodogram technique had to decide whether a particular peak was significant or not But he overrated the difficulty, since they have the great advantage of looking for a pattern. Spurious indications might appear in individual analyses, but they would not appear in every spectrum of a long series with upper and lower limits in precisely the places where simple hydrodynamical theory says the upper and lower limits of the swell from a storm that has already appeared on the chart should arrive.

The fact that Bartels, Wilson, Yule, Kendall, and others cast doubts on the suitability of the periodogram technique for detecting periodicities in short series of such unaccountable events as are dealt with in Ayres' Index of American Business Activity, or the Marriage Rate in England and Wales, need not worry us in the least: in contrast to such economic series our wave-pressure records contain at least 60 of the waves we wish to detect; they look like mixtures of sine waves, and it is reasonable (Barber and Ursell, 1946, p. 552) to treat them as such.

For certain problems, such as the scatter of individual wave heights about the mean height over a short interval, and attempts to predict wave motion two or three waves ahead from a record of the previous motion, statistical methods are more appropriate; but the main problem in wave research is still to show how the general character of the wave pattern changes in relation to wind and with distance from the generating area under all sorts of conditions. This requires detailed analysis of continuous observations, and Fourier analysis has proved itself the most useful method up to the present.

One of the outstanding examples of its usefulness in providing accurate information about wave periods is that which led to the theory that microseisms are produced in a region of interference between similar wave trains traveling in opposite directions (Longuet-Higgins, 1950) and to confirmation of the theory by analysis of simultaneous records of waves and microseisms (Darbyshire, 1950). A demonstration of how measurements of wave spectra from local and distant storms are leading to a closer understanding of the changes in general character of the wave pattern from hour to hour and day to day in relation to weather conditions would be the most useful argument I could produce at this Symposium. I think a good case could be made, but feel that it should be left until my colleagues who are working on these lines can bring it forward with all the detail that is necessary.

We, in Britain, would like to take this opportunity of acknowledging the help that we have received from the late Dr. Seiwell in wave research and other aspects of oceanography, and to express our deep regret at his untimely death.

Barber, N. F. and Ursell, F. 1946. The generation and propagation of ocean waves and swell. Phil. Trans. Roy. Soc. [A] **240**, 527.

Darbyshire, J. 1950. Identification of microseismic activity with sea waves. Proc. Roy. Soc. [A] **202**, 439.

Lee, Y. W., Cheatham, T. P. and Wiesner, J. B. 1950. Application of correlation analysis to the detection of periodic signals in noise. Proc. I. R. E. **38**, 1165.

Longuet-Higgins, M. S. 1950. A theory of the generation of Microseisms. Phil. Trans. Roy. Soc. [A] **243**, 1.

Seiwell, H. R. 1949. The principles of time series analyses applied to ocean wave data. Proc. N. A. S. **35**, 518.

Seiwell, H. R. and Wadsworth, G. P. 1949. A new development in ocean wave research. Science **109**, 271.

Seiwell, H. R. 1950. Problems in statistical analyses of geophysical time series. Science **112**, 243.

Ursell, F. 1950. On the application of harmonic analysis to ocean wave research. Science **111**, 445.

24. Some Observations of Breaking Waves

By Martin A. Mason[1]

Progressive oscillatory waves produced in a laboratory tank were made to break on a sloping, impermeable beach. The geometry and character of the breaking wave were observed by motion-picture photography at speeds up to about 800 frames a second. Two beach slopes, 1 to 5 and 1 to 15, were used, and the range of wave steepness varied from 0.005 to about 0.038. The experiments were largely exploratory in character, for the purpose of defining the probable significant parameters controlling the geometry and dynamics of breaking waves.

1. Observations

The experiments to be discussed were made for the purpose of observing the general features of a breaking progressive oscillatory wave and exploring the significance of various parameters as indicators of the geometry and dynamics of these waves. It was recognized at the outset that the internal motions of the water in the breaking wave probably offer the most significant and sensitive measure of the dynamics of the breaking wave. However, in view of the extreme difficulty presently of determining these motions in nature observations of internal movements in the breaking wave were not made. This exclusion does not imply in any way a belief on the part of the author that such observation would not be productive; it was felt rather that the possibilities of simpler methods of definition should be explored first.

The principal objective of the experiments was to define the phenomenon of breaking waves, it being the author's belief that definition of what happens when a wave breaks is a necessary preamble to the development of a theory, rather than the converse. The information to be presented is therefore primarily descriptive and its principal value lies in whatever use it may be to those who will attempt development of a theory of breaking waves.

The breaking wave was studied in its simplest aspect, that of an essentially uniform wave breaking on a uniform, impermeable slope, with no material transportation involved. The waves were generated in a tank 96 feet long, 1.5 feet wide, and in water 1.33 feet deep by a simple pusher-type wave generator. In order to reduce the complicating feature of reflected waves only the first few waves generated were observed. The waves were observed visually and photographically, the latter by means of 16 mm motion pictures taken at speeds of 64 and 800 exposures a second. Considerable difficulty was experienced in obtaining satisfactory photography with sufficient definition of detail of the breaking wave. The problem appears to be one of lighting the breaking wave in such fashion as to emphasize the features it is desired to observe and obscure

[1] Beach Erosion Board, Washington, D.C.

the less significant features, primarily the broken water and foam that are the most apparent features of a breaking wave.

Breaking waves were produced on slopes of 1 to 5 and 1 to 15 for a range of values of initial steepness in deep water from 0.009 to 0.044. The breakers obtained included the "spilling" and "plunging" types described previously by investigators at the University of California.

The process of breaking as observed can be described in the following manner. As the wave approaches the area of breaking, it begins to deform rapidly by a reduction in the speed of advance of the forward face and consequent overtaking of the forward face by the seaward face of the crest. The deceleration of the forward face appears to be related to the speed and depth of the backwash from the preceding broken wave. In fact, there seems to be an area of limited extent around the intersection of the advancing forward face and the backwash within which the backwash flow is halted and the water surface rises rapidly, suggesting a conversion of the kinetic energy of the backwash to potential energy in the form of a rise in water-surface elevation. This area of energy conversion progressed shoreward in the cases observed over a distance approximating perhaps one-half wave length before initial breaking of the wave and at a speed considerably less than the speed of travel of the advancing wave crest. During this interval the advancing forward face of the wave steepened rapidly until the initial break occurred. If the breaker was of the spilling type, no further steepening was observed, the water at the crest tumbling down the slope of the forward face, with that slope remaining apparently at about the same inclination for a short time, then flattening as the break was completed. If the breaker was of the plunging type, the steepness of the forward face continued to increase, reversed slope so that the crest of the wave overhung the point of initial break, and finally the crest appeared to project forward as a jet curving

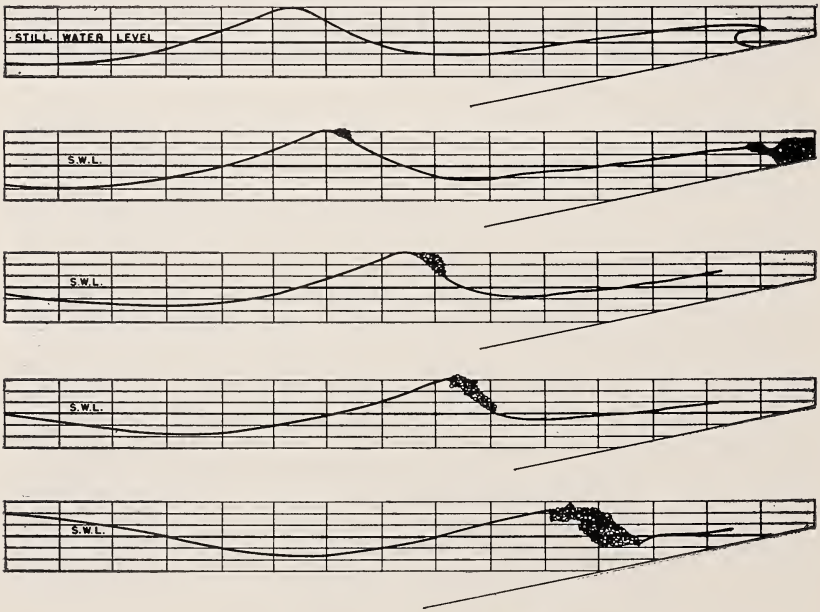

FIGURE 1. *Spilling breaker.*

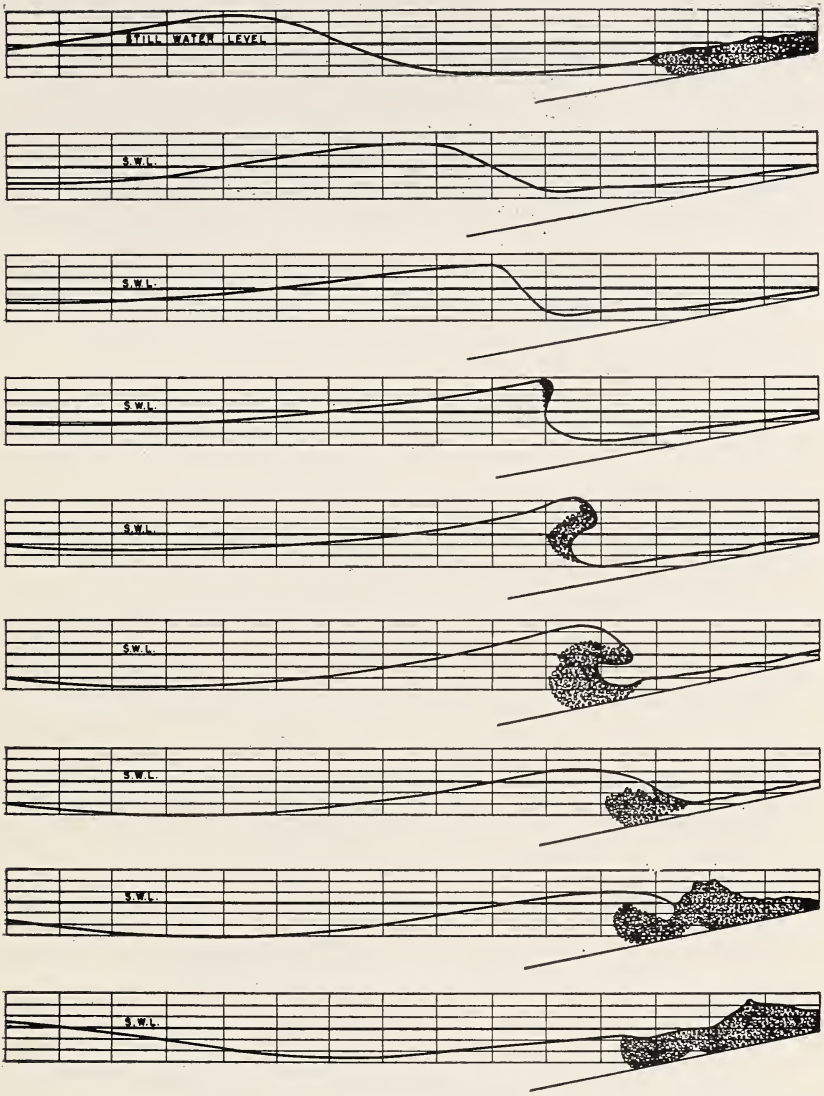

FIGURE 2. *Plunging breaker.*

out and down to meet the backwash just in advance shoreward of the broken water associated with the initial break.

The geometry of the breaks described is shown on figures 1, 2, and 3.

It was observed that breaking waves were not of either the spilling or plunging type exclusively, waves were observed to break clearly as one or the other type and also in all intermediate fashions. It seems clear that the spilling and plunging characteristics probably represent extreme limits and that breakers may occur in any fashion between these limits.

It was noted that breaking is always initially signaled by the appearance of broken water at the highest point on the forward face of the wave.

In every case examined this point was the point of most abrupt change of slope of the wave surface. High-speed photography showed the broken water to be small masses or slugs or water probably mixed with entrapped air giving them a characteristic foamy appearance, that detach from the advancing face but are not projected or do not travel far from the face. In fact, they appear simply to be detached and roll over the advancing face. In a spilling breaker the separation of these masses appears to spread like a grass fire, over the advancing forward face without penetrating into the wave but rather forming a bulbous protuberance of the

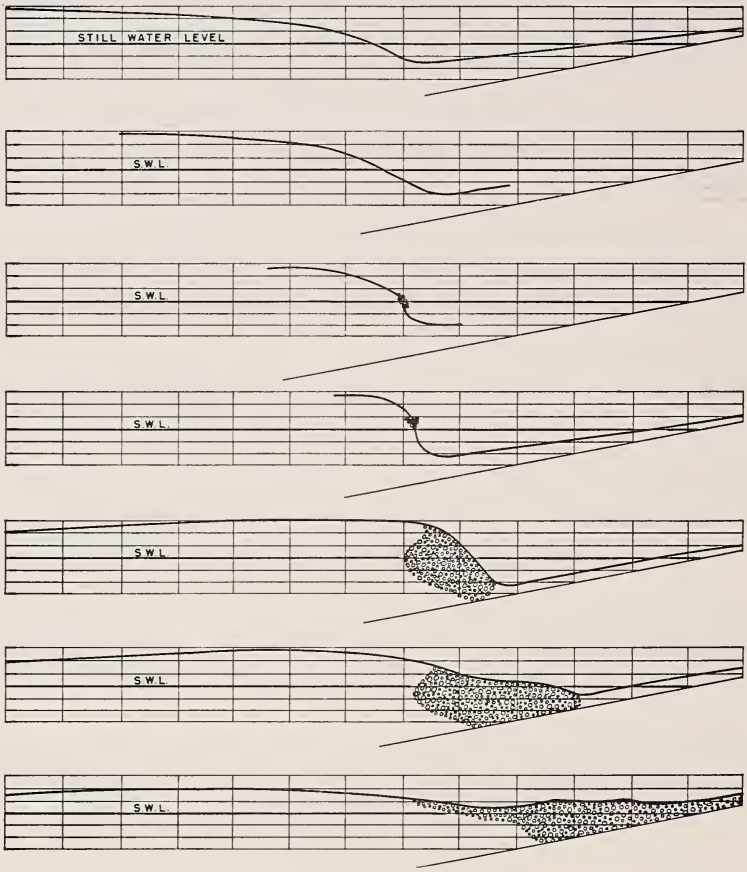

FIGURE 3. *Intermediate breaker.*

advancing face. In a plunging breaker the initial separation is of very short duration, being succeeded by the forward and downward projection of a tongue or jet of water from the crest of the forward face, the jet curling down much in the form of a free-discharge jet to entrap the initial broken water and plunge into the backwash of the preceding wave.

In connection with the initiation of breaking it was noted that at the moment the break starts the highest elevation of the water surface usually is seaward of the point of initial break. It appears, in fact, that the

point of initial break is not necessarily the point of highest elevation of the wave surface; however, in the tests made it always was located at the point of most abrupt change in slope of the wave surface.

The horizontal-axis eddy frequently described as an important feature of breaking waves was totally absent in the case of spilling-type breakers, was observed most prominently when the breaker was of an intermediate type, and was present for very short durations in the case of plunging breakers. When the eddy motion was observed by high-speed photography, it seemed to be of very short duration, the rotational motion then being supplanted by random motion. The impression obtained is that of a short-duration eddy motion modified rapidly to a random motion characteristic of large-scale, high-intensity turbulence. The turbulence did not appear to be isotropic, however such a determination made on the basis of visual observation probably has little validity. In this connection, I should cite some unpublished observations of high speed photography of material transportation in breaking waves that I made some time ago that confirm the short duration of rotational eddy motion in the breaker and the presence of turbulence as indicated by thorough mixing of the transported material.

All of the breaking action of the wave appears to occur shoreward of the point of initial break, indicating that the forward travel of the wave is always sufficient to overcome and reverse the backwash of the preceding wave. This obvious observation appears to be of some significance in the evaluation of the energy dissipated in breaking. Certainly the portion of the energy of the advancing wave dissipated in overcoming the backwash of the preceding wave cannot be considered as available to transport material or to contribute to the uprush of the wave. Both these matters are of importance when determining the effects of breaking waves on beaches and structures.

Nonmiscible drops injected into the breaking wave about one-eighth wave length seaward of the point of break did not show motion characteristic of the breaker region; in fact, their motion did not appear to be greatly different, if different at all, from the normal orbital motion of the wave. Unfortunately, the quality of the photography was not sufficiently good to permit measurement of the actual orbital paths and velocities.

An attempt was made to measure the included angle between the forward and seaward faces of the wave at breaking. Two difficulties prevented obtaining valid results. One was the obscuring of the water surface on the forward face at the time of initial break by the detaching masses of water previously mentioned. The other lay in the determination of the inclination of the water surface. By reference to the figures it will be noted that the surface of the about-to-break wave is a curve of continuously changing radius of curvature, with one point of abrupt and large change in curvature, this being the point at which breaking starts. In this region of rapidly varying curvature the measurement of included angle presents some difficulty, particularly if one attempts to measure the angle by the use of tangents.

Measurements made by tangents to the curve fell within a wide range, included angles at the point of break, ranging from a minimum of 88° to a maximum of 145°. Other investigators have noted a similar lack of agreement with the theoretical value of 120°. However, in those instances, as in the results reported here, there is some question as to the angle measured. Certain investigators are known to have employed the angle included between a line from the intersection of the shoreward face of the breaker with the still-water line and tangent to the forward part of

the crest, and a line tangent to the seaward side of the breaker. My observations lead me to the belief that the angle so measured is not a criterion for breaking.

There is a good possibility that the initial break occurs whenever and wherever the slope of the forward face of the wave becomes vertical, or essentially so. Close observation of the photography obtained in the tests reported herein showed that whenever an initial break occurred there was an associated portion, however small, of the forward face that was vertical or very nearly so. This condition appeared to hold for spilling as well as for plunging breakers, although in this case there is room for some uncertainty due to the limitations of the available photography.

2. Further Experimentation

As a result of the observations described the following ideas are proposed for further investigation.

There appears to be some reason to believe that breaking of a wave is chiefly due to deformation of the wave shape, for whatever cause, beyond a limiting shape. The limiting shape apparently may be of varying form, since the widely different forms represented by spilling and plunging breakers are both associated with breaking. The shape criterion for breaking apparently involves as its chief element the occurrence of a vertical, or nearly vertical, slope on some portion of the forward face of the wave.

The occurrence of vertical slopes on the forward face of the wave may be occasioned by the retardation of advance of the forward face and consequent overtaking of the forward face by the remainder of the wave. It will be noted that this behavior is not contradictory for the cases of breakers in nonshoaling depths and in opposing currents.

Wave breaking is believed to be initially a local phenomenon, involving limited areas of the forward face of the wave. Depending upon the stability of form of the wave, i.e., continuance or not of occurrence of slopes approximating the vertical, the initial break may propagate to a complete break or fail to propagate with resultant recovery of stability. In the study of this phenomenon investigation should be made of breaking in both shoaling and nonshoaling situations.

The turbulence phenomenon in the breaking wave should be given attention. There appears to be considerable reason to doubt that the horizontal-axis eddy, or roller, sometimes considered an important element in the dissipation of energy in a breaking wave, is, in fact, of any major significance in the energy-dissipation process. The observations reported here lead the author to suspect that the loss of energy in the breaking process is relatively small and due chiefly to turbulence losses. Study of the turbulence mechanism in a breaker should be rewarding, although of great difficulty.

Study of the nature and rates of deformation of the wave shape immediately prior to breaking should offer a fruitful field of investigation. In such study particular attention should be paid to the distribution of potential and kinetic energies in the wave as it approaches breaking.

In conclusion, attention is called to the probable advantages attaching to the study of breakers in nonshoaling situations, such as in an opposing current of known characteristics, or under an opposing wind, where the complicating effects of backwash from previous waves are not present, and to the obvious usefulness of high-speed motion pictures to enable adequate observation of details of the phenomena.

25. Fourier Analysis of Wave Trains

By Garrett Birkhoff[1] and Jack Kotik[2]

Various difficulties in defining a satisfactory general class of one-dimensional trains of gravity waves are pointed out. Formal Fourier transform theory is used to suggest plausible existence and uniqueness theorems. In particular, the following three conditions on a wave train are shown to be formally equivalent: the spectra of the components traveling in opposite directions are nonoverlapping; the total kinetic energy in space is independent of time; the total kinetic energy (density) observed at a point, totalled over time, is independent of the location of the point in space.

Finally, a Fourier analysis is made of the relation between elevation and pressure.

1. Introduction

It is well known [1, 2][3] that ocean waves in an actual "seaway" are usually complex superpositions of waves of many frequencies with various origins. It is also generally agreed that Fourier analysis affords the proper mathematical approach to the phenomenon. There is, however, little agreement as to the statistical nature of this superposition, beyond the idea that it consists of an underlying, nearly periodic "swell" due to distant storms, disguised by an irregular, shorter period heaving and tossing due to local causes.

We suggest below (sections 4 to 6) a new statistics for describing pressure and elevation variations. Its characteristic features are that the mean density of wave energy per unit area is not zero, and that the phases of Fourier components are random. We believe that these features are characteristic of an actual seaway. As "Fourier's Integral Theorem" has only been established (by Plancherel; see [6, Ch. I]) for systems that have finite total energy; we believe the reliance usually placed in it [3, pp. 364, 384, 400] is unjustified. Therefore, we use it below only as a heuristic tool.

We shall assume the usual Airy theory of infinitesimal gravity waves, partly because it seems sufficiently accurate in deep water [1, appendix 1], and partly because we know of no effective way to analyze nonlinear wave trains into periodic constituents. We shall thus assume any wave train to be characterized by a scalar *velocity potential* ϕ, whose gradient $\nabla\phi = u$ is the instantaneous particle velocity and which satisfies,

$$\nabla^2\phi = 0, \tag{1}$$

and suitable regularity conditions at infinity. We shall ignore atmospheric-pressure variations (wind effects), and suppose the pressure, p, given by

$$p - p_{atm} = \rho(gy - \phi_t), \tag{2}$$

[1] Harvard University, Cambridge, Mass.
[2] Massachusetts Institute of Technology, Cambridge, Mass.
[3] Figures in brackets indicate the literature references on p. 234.

where y is depth below surface level. The *elevation function* $\eta(x,z;t)$ is related to ϕ by the kinematic condition

$$\eta_t = -\phi_y, \quad \text{on } y=0; \tag{3}$$

moreover, neglecting capillary forces, it is directly determined from ϕ by the free surface condition

$$g\eta = -\phi_t, \quad \text{on } y=0. \tag{4}$$

Conversely, using potential theory, one can prove rigorously that η determines ϕ up to an additive function $\phi(x,z)$ without physical significance—that is, essentially uniquely—by eq 3. Hence wave trains can be defined by their elevation functions.

Fourier's Integral "Theorem" asserts that the elevation function of a plane wave train can be written in the form

$$\eta(x;t) = \int_0^\infty \left\{A(k)\cos(kx-\sigma t) + B(k)\sin(kx-\sigma t)\right\}dk$$
$$+ \int_0^\infty \left\{A_1(k)\cos(kx+\sigma t) + B_1(k)\sin(kx-\sigma t)\right\}dk. \tag{5}$$

and that analogous formulas hold for $\phi(x,y;t)$ and in the three-dimensional case [3, pp. 364, 384, 400]. Here $\sigma^2 = gk$ for ocean waves; $\sigma^2 = gk \tanh kh$ in water of constant depth, h; $\sigma^2 = Tk^3/\rho$ for capillary waves, etc.

Many consequences follow readily from eq 5. For instance, in an ocean of infinite depth,

$$\phi_{tt} = g\phi_y, \quad \text{for all } y>0, \tag{6}$$

if capillarity is neglected [4]; not neglecting capillarity

$$\phi_{tt} = g\phi_y + (T/\rho)\phi_{yyy}. \tag{6'}$$

Second, the initial-elevation function $\eta(x,z;0)$ and rate of rise $\eta_t(x,z;0)$ completely determine a wave train. Third, for motions that are parallel to the (x,y)-plane, wave trains are determined by the elevation $\eta(0,t)$ and slope $\eta_x(a,t)$ at any point $x=a$, as functions of time. Fourth, the expression 5 decomposes any plane wave into oncoming and outgoing components, traveling in opposite directions.

Fifth, and last, the following three conditions are mathematically equivalent: (i) $\int_{-\infty}^{\infty} \eta^2(a,t)dt$ is independent of a, (ii) $\int_{-\infty}^{\infty} \eta^2(x,t)dx$ is independent of t, (iii) the spectra of the oncoming and outgoing components are nonoverlapping. Similar results hold for pressure (at any fixed depth, y_0, in an ocean with a horizontal bottom), etc.

Conditions (i) to (iii) may be regarded as characterizing the absence of "clapotis"; unless they hold, the storm intensity observed by a pressure or wave height recorded will depend on its horizontal location, as well as its depth.

2. Existence and Uniqueness Theorems

Although by Plancherel's Theorem, the preceding results are rigorously established for an interesting class of wave trains, it would be preferable to prove them in more complete generality. We have had some success in this.

Thus we have proved eq 6 and 6′ in an ocean of infinite depth. From eq 6 we have proved that, if surface tension is neglected, ϕ is an *analytic* function of all variables, in $y>0$. This permits one to use derivatives and power series freely, in this case.

If we are given bounded analytic initial values $\eta(x,0)$, $\eta_t(x,0)$ of the elevation and velocity, then we can construct a motion having these initial values, and this motion is essentially unique, as discussed after eq. 4. If we are given bounded, analytic values $\eta(0,t)$, $\eta_x(0,t)$ of the elevation and slope at a point for all time, then there is at most one motion with the assigned values, but the existence has not been demonstrated. In the case of constant finite depth, we can also prove that there is at most one motion with assigned initial elevation and velocity; the existence is an open question. The three-dimensional analogue of the first result is also correct; the various remaining cases are being worked out.

Our only other result is negative: *in an ocean of constant finite depth h, there is no linear homogeneous partial differential equation $L[\phi]=0$, not a consequence of eq 1, satisfied even by all simply periodic waves traveling in one direction.*

We sketch the proof, using the operational calculus. By [3, p. 364], the simply periodic waves are given by

$$\phi_{k1}=\cosh k(y+h)\sin(kx-\sigma t). \tag{7}$$

Let us write $D_x\phi_{k1}=k\phi_{k2}$, $D_y\phi_{k1}=k\phi_{k3}$, $D_xD_y\phi_{k1}=k^2\phi_{k4}$, so that ϕ_{k2}, ϕ_{k3}, ϕ_{k4} are obtained from ϕ_{k1} by substituting sinh for cosh and/or cos for sin. Again, since $D_{yy}=(\nabla^2-D_{xx})$, any $L[\phi]$ can be written as $L[\phi]=L_1[\phi]-M[\nabla^2\phi]$, where $L_1[\phi]$ involves no powers of D_y above the first. Since $M[\nabla^2\phi]=0$ follows trivially from eq 1, it will suffice to prove that $L_1=0$ if every $L_1[\phi_{k1}]=0$.

To prove this, we expand $L_1[\phi_{k1}]$ as a polynomial

$$0=L_1[\phi_{k1}]=\sum_{i,m,n}(-)^{m+n}k^{2m}\sigma^{2n}f_{m,n,i}(x,y;t)c_{ki}\phi_{ki}, \tag{8}$$

which follows from $D_{xx}=-k^2$ and $D_{tt}=-\sigma^2$, writing

$$L_1=\sum_{m,n}(D_x)^{2m}(D_t)^{2n}\sum_i f_{m,n,i}(x,y,t)D_i,$$

where the eight D_i are I, D_x, D_y, D_{xy}, D_t, D_{xt}, D_{yt}, D_{xyt}, and the c_i are 1, k, k^2, σ, σk, σk, σk^2. Since $\sigma^2=gk\tan hk$ is a transcendental (i.e., nonalgebraic) function of k, the coefficients of each monomial $k^r\sigma^s$ must vanish in eq 8, identically in x,y,t. This will give us, for each m,n four identities of the form

$$f_{m,n,1}\phi_{k1}+f_{m-1,n-4}\phi_{k4}=0 \text{ from } r=2m,\ s=2n,$$

$$f_{m,n,2}\phi_{k2}+f_{m,n,3}\phi_{k3}=0 \text{ from } r=2m+1,\ s=2n,$$

$$f_{m,n,5}\phi_{k5}+f_{m-1,5,8}\phi_{k8}=0 \text{ from } r=2m,\ s=2n+1,$$

$$f_{m,n,6}\phi_{k6}+f_{m,n,7}\phi_{k7}=0 \text{ from } r=2m+1,\ s=2n+1.$$

In order that these equations be literally correct, we define f's with negative indices to be zero. Write the typical equation as $f_1\phi_1+f_2\phi_2=0$. The essential point is that the f's are independent of k, while the ϕ's are not. If one of the f's (say f_2) were ever different from zero, we could divide by it, and get (say)

$$\frac{f_1}{f_2}=-\frac{\phi_2}{\phi_1}$$

a contradiction. Hence all the f's are zero, and $L_1=0$.

3. Energy Spectrum and Autocorrelation Function

Assuming Fourier's Integral "Theorem," it is logical to define a wave train moving in one direction by (cf. [3, p. 369]),

$$\phi(x,y;t)=\int_0^\infty C(k)\cosh k(y+h)\cos(kx-\sigma t-\epsilon(k))dk. \tag{9}$$

Here $C(k)>0$ is called the amplitude spectrum of ϕ, and $\epsilon(k)$ is called its phase spectrum.

If $C(k)$ is quadratically integrable, then $\phi(x,y_0;t_0)$ is also, and $C^2(k)dk$ is related to the total energy $I(k)dk$ in an infinitesimal band at wave number k, by [3, p. 370]

$$2gI(k)=\rho C^2(k)\sigma^2\cosh^2 kh. \tag{10}$$

Following Wiener [6, p. 163], one might even call $C^2(k)$ the "energy spectrum" in eq 9 directly. Since the elevation $\eta=-\phi_t$ at $y=0$, one can infer $C(k)$ from the amplitude spectrum $\sqrt{A^2(k)+B^2(k)}$ of the elevation function $\eta(x,t)=\int_0^\infty [A(k)\cos\alpha(k)\cos t+B(k)\sin\alpha(k)\sin t]dk$ at any point x; specifically, $C(k)=\sigma^{-1}\sqrt{A^2(k)+B^2(k)}$. One can also infer $C(k)$ from the amplitude spectrum of the difference

$$\Delta p=p-gy=\int_0^\infty P(k)\cos(\sigma t-\beta(k))dk \tag{11}$$

between the pressure at any point (x,y), and the hydrostatic pressure there, by the formula

$$C(k)=\frac{P(k)\sin\beta(k)}{\sigma\cosh k(h+y)\sin(\beta(k)-kx)}. \tag{11'}$$

For mixtures of wave trains from different directions, with overlapping spectra, the transformation from $P(k)$ to $E(k)$ depends on x as well as y, by the remark at the end of section 1.

Wiener [5, 6] has defined the "energy spectrum" of a wide class of functions $f(t)$ with $\overline{f}=0$ and $\overline{f^2}>0$, not quadratically integrable, as the Fourier cosine transform $\mathfrak{C}F$ of the (unnormalized) *autocorrelation function*, $F(h)$, itself defined by

$$F(h)=\lim_{T\to\infty}\frac{1}{2T}\int_{-T}^{T}f(t)f(t+h)dt=\overline{f(t)f(t+h)}. \tag{12}$$

From $\mathfrak{C}F$ the physical *energy* and *power* spectra of a simple wave train can be inferred, by transformation formulas like eq 10 and 11′, whether $f(t)$ is a wave height *or* a pressure record.

Since the utility of $F(h)$ has been debated, we might express our opinion. $F(h)$ has the advantage of depending smoothly on $f(t)$, unlike the Fourier transform $g(k)$ of $f(t)$ (cf. [1]; also section 6); hence it can be accurately *measured*. If $f(t)$ is almost periodic (i.e., if it has a *line* spectrum), one gets $F(h)$ from $f(t)$ by bringing all components into phase. If $f(t)$ has a *continuous* spectrum one gets $F(h)$ from $f(t)$ by bringing all components into phase and squaring their amplitudes. In general, $F(h)=F(-h)$, while $F(0)$ represents $\overline{f^2}$, $-F''(0)$ represents $\overline{f_t^2}$, $F^{\text{IV}}(0)$ represents $\overline{f_{tt}^2}$, etc.

In ocean swell from distant storms, $F(h)$ does not tend rapidly to zero, but *persists for scores of wave lengths*. This follows from the Cauchy-Poisson Theory [3, p. 387, (23)]; it would be interesting to prove that, conversely, $F(h)\to 0$ slowly implies that energy is concentrated in narrow bands.

The slowness with which $F(h)\to 0$ makes it difficult to compute its cosine transform; moreover, since $F(h)$ involves squared amplitudes, $F(h)$ will not bring out the low amplitude "forerunners" of an approaching heavy swell, except perhaps when $F(h)$ is only considered for large h. For this purpose of storm *forecasting*, periodogram analysis of $f(t)$ may be more practical than Fourier-transforming the autocorrelation function $F(h)$.

On the other hand, $F(h)$ may yield good estimates of the total energy in broad bands $-K\leqq k<K'$, using the formula

$$E_{k,k'}(f)=\int_0^\infty h^{-1}(\sin K'h-\sin Kh)F(h)dh. \tag{13}$$

Hence it may be useful in analyzing storm *records*.

In the same spirit, following Seiwell [2, p. 483], one might try to "filter" the long-period ocean swell "signal" from local "noise," by expanding $f(t)$ in Fourier series on the (normalized) interval $\{-\pi,\pi\}$ and subtracting the component

$$f_{k,k'}(t)=\frac{1}{\pi}\int_{-\pi}^{\pi} f(t)\frac{\sin(K'+\frac{1}{2})(t-\tau)-\sin(K-\frac{1}{2})(t-\tau)d\tau}{2\sin\frac{1}{2}(t-\tau)} \tag{14}$$

due to a narrow band indicated by a study of $F(h)$ for large h, or by periodogram analysis. This seems to us more logical than trying to fit $f(t)-A\cos(kt-\epsilon)$ for suitable A, k, and ϵ, by an "autoregressive sequence" (solution of a stochastic difference equation), as Seiwell did in a paper to be published soon.

4. The Principle of Random Phase

A quantity computed from a sample of a stationary phenomenon will be called physically significant if it does not depend on the sample. For example, let the function

$$f(t)=A\cos t+B\cos 2t \tag{15}$$

be observed over an interval $\alpha-T\leqq t\leqq\alpha+T$, where T is known but α is random. What is observed is a function of $\tau-t-\alpha$,

$$g(\tau)=A_1\cos\tau+A_2\sin\tau+B_1\cos\tau+B_2\sin\tau,$$

where $A_1=A\cos\alpha$, $A_2=-A\sin\alpha$, $B_1=B\cos 2\alpha$, and $B_2=-B\sin 2\alpha$. Clearly, the squared amplitudes $A_1^2+A_2^2$ and $B_1^2+B_2^2$ of the observed Fourier components are physically significant; so is their relative phase

$$2\tan^{-1}(A_2/A_1)-\tan^{-1}(B_2/B_1),\quad \bmod \pi.$$

But neither A_1 alone, nor the phase of either periodic component alone, is physically significant.

We shall generalize this result, by stating without proof a new general principle.

Principle of Random Phase: Let Ω be any statistical ensemble [4] of physical systems ω, each described by one or more functions $f_\omega(t)$ of time. If the statistics of Ω are time independent, then the phases $\epsilon_\omega(k)$, if definable, are random, and the phases of components having incommensurable frequencies are statistically independent.

That is, we suppose the $f_\omega(t)$ to be Fourier-analyzed in some manner by the formula

$$f_\omega(t)=\int_0^\infty A_\omega(k)\cos(kt-\epsilon(k))dk[A_\omega(k)>0],$$

unspecified except for the phase transformation formula

$$f_\omega(t+c)=\int_0^\infty A_\omega(k)\cos(kt-\epsilon_1(k))dk,\quad [\epsilon_1(k)=\epsilon(k)-kc].$$

Then for any fixed k, $\epsilon_\omega(k)$ is an evenly distributed random variable. Further, if k_1 and k_2 are incommensurable, then $\epsilon_\omega(k_1)$ and $\epsilon_\omega(k_2)$ have independent distributions.[5]

If the $f_\omega(t)$ have continuous spectra—as seems to be the case for waves in a seaway—then almost all pairs of frequencies are incommensurable. This fact, combined with the Principle of Random Phase, suggests that phase statistics, in the ordinary sense, have no physical significance.

In our opinion, the point is simply that the ordinary concept of phase and Fourier's Integral "Theorem" is inapplicable, even formally, to functions with $\overline{f^2}>0$ and a continuous spectrum. Thus, although phase in the ordinary sense has no physical significance, the amplitude spectrum gives only a partial description of random functions with $\overline{f^2}>0$. This idea will be developed in section 7.

5. A New Statistical Model

We shall first describe briefly a new statistical model for ocean swell, which is suggested by the Principle of Random Phase, and the fact that the decay of ocean swell is gradual. We believe the model applicable to the analysis of $\Delta p(t)$ or $\eta(t)$ at a fixed point.

---

[4] See [7] for precise mathematical definitions of this and other concepts involved in the Principle of Random Phase. A corresponding result holds for functions of n variables. A rigorous proof will be published elsewhere.

[5] If $k_1, k_2, k_3, \ldots$ are incommensurable, then the $\epsilon_i=\epsilon(k_i)$ are distributed according to Daniell measure on the infinite-dimensional torus.

We prescribe a function $I(k)=dE/dk$, which corresponds to the energy spectrum of the swell. For each index m we select an (almost periodic) function

$$f_m(t)=\frac{E(\infty)^{\frac{1}{2}}}{m}\sum_1^m \cos(k_i t-\epsilon_i),$$

where the k_i are selected at random with probability density $I(k)$, and the ϵ_i by the Principle of Random Phase. The components of $f_m(t)$ all have the same amplitude, but there tend to be more of them in bands where $I(k)$ is large; now let $m\to\infty$. This procedure defines, in a natural way, distributions for the Fourier coefficients of functions defined on an interval $-T<t<T$, as follows. The quantities k and ϵ have distributions, and these determine distributions for the Fourier coefficients of $(E/m)^{\frac{1}{2}}\cos(kt-\epsilon)$, and hence, by convolution, of the Fourier coefficients of $F_m(t)=(E/m)^{\frac{1}{2}}\sum_1^m \cos(k_i t-\epsilon_i)$. By the Central Limit Theorem,[6] the statistical distribution of the nth (sin or cos) Fourier coefficient of $f_m(t)$ approaches a normal distribution as $m\to\infty$, which is completely determined by its variance.

More precisely, if we choose units so that $T=\pi$, and write

$$f(t)=\sum_1^\infty A_n\cos nt+B_n\sin nt,$$

we have, for the second moments,

$$\overline{A_n^2}=\frac{2}{\pi^2}\int k^2\sin^2[(k-n)\pi]\cdot[k^2-n^2]^{-2}I(k)dk, \tag{16a}$$

$$\overline{B_n^2}=\frac{2}{\pi^2}\int n^2\sin^2[(k-n)\pi]\cdot[k^2-n^2]^{-2}I(k)dk, \tag{16b}$$

$$\overline{A_mA_n}=\frac{2}{\pi^2}\int(-)^{m+n}\cdot k^2\frac{1-\cos 2\pi k}{(k^2-n^2)(k^2-m^2)}I(k)dk, \tag{16c}$$

$$\overline{B_mB_n}=\frac{2}{\pi^2}\int(-)^{m+n}\cdot mn\frac{1-\cos 2\pi k}{(k^2-n^2)(k^2-m^2)}I(k)dk, \tag{16d}$$

$$\overline{A_mB_n}=0. \tag{16e}$$

A simple but instructive special case occurs when $I(k)=\delta(k-n)$, δ the delta function. Then $f(t)$ idealizes the sound from a large orchestra of perfectly tuned violins playing one note in unison. The output is simply harmonic; the amplitudes A_n,B_n are normally distributed. Hence the sound intensity $E=a(A_n^2+B_n^2)$ should be distributed statistically (at any fixed distance from the orchestra) like the area under the curve $y=(E/C)\exp(-E^2/2C^2)$, where $\sqrt{\pi}C/4$ is the expected energy.

The preceding example is due to Rayleigh.[7] For any $I(k)$ our model

[6] In a vector space of infinitely many dimensions, for the finite-dimensional case, see H. Cramer, *Random variables and probability distributions*, Cambridge, 1937, p. 113.

[7] Phil. Mag. [5] **10**, No. 60 (1880) p. 73. For an abstract definition of Gaussian processes, see H. Cramer, Annals of Math. **41** (1940) 215–230, especially S9; also J. L. Doob, Annals of Math. Stat. **15** (1944) 229.

describes what is usually called a *Gaussian process*; this means that the multivariate distribution of $f(t_1), \ldots, f(t_n)$ is normal or Gaussian, for any $t_1 < \ldots < t_n$. The main novelty of our approach, apart from its intuitive motivation, consists in its relevance to solutions of partial differential equations with constant coefficients. Thus, for any statistical distribution of energy, as a function of wave-length and direction of propagation, the Principle of Random Phase determines a unique Gaussian process, as a limit of superpositions of simply harmonic Airy waves. To analyze such directional energy distributions, simultaneous observations from two or more wave recorders would have to be correlated.

But before considering such elaborate situations, it seems wise to make some simple remarks. Thus, we note that a *statistical* approach resolves the difficulty suggested at the end of section 1. Statistical data in an unlimited ocean of constant depth will be independent of the horizontal location (x and z coordinates) of a recorder. Near shore, the "clapotis" of reflected waves may, however, change this.

6. Application

The preceding model seems to us to shed light on a vexing problem. It is obvious that the spectrum of even a simply harmonic "swell," whose period is incommensurable with the interval (say 20 minutes) during which a pressure record is taken, will be split up into many lines, if an ordinary periodic analysis of the record is made. Specifically,

$$\cos kt = \sum_1^\infty \frac{1}{\pi} \cdot \frac{2k}{k^2-n^2} \sin(k-n)\pi \cdot \cos nt + \frac{1}{\pi} \cdot \frac{k}{k^2-n^2} \cdot \sin k\pi, \tag{17a}$$

$$\sin kt = \sum_1^\infty \frac{1}{\pi} \cdot \frac{2n}{k^2-n^2} \sin(k-n)\pi \cdot \sin nt + 0. \tag{17b}$$

It is easy to construct artificial examples in which the correlation between the "real" spectrum of a function and its "apparent" spectrum is far worse. Thus let

$$f(t) = \frac{\pi}{17} \cos \frac{17}{2} t + \frac{\pi}{21} \cos \frac{21}{2} t + \frac{\pi}{25} \cos \frac{25}{2} t + \frac{\pi}{29} \cos \frac{29}{2} t.$$

A graph contrasting the "real" with the "apparent" spectrum of $f(t)$ over $(-\pi, \pi)$ is shown as figure 1.

It would be interesting to know *statistically* what is the expected spectrum-spreading error introduced by periodic analysis of pressure records, in this way. Although we cannot give a complete answer, we can give the expected spectrum from waves whose energy is "really" uniformly distributed in the interval $N \leqq k \leqq N+1$, where N is an integer. This is presumably typical, as regards the incommensurability of k with T/π. We can substitute in eq 16d and 16e, where $I(k)$ is a step function.

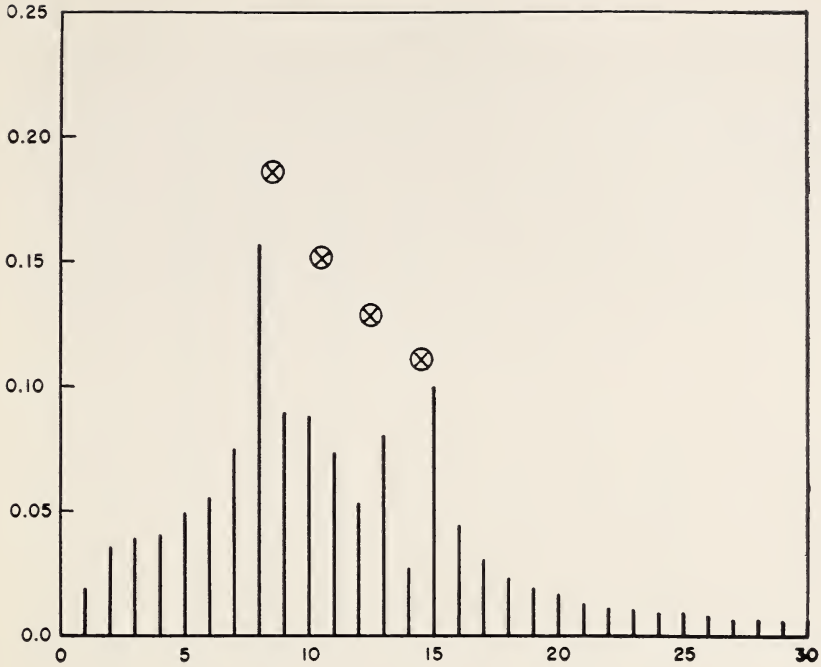

FIGURE 1. *Absolute values of Fourier coefficients of*

$$f(x)=\frac{\pi}{17}\cos\frac{17}{2}x+\frac{\pi}{21}\cos\frac{21}{2}x+\frac{\pi}{25}\cos\frac{25}{2}x+\frac{\pi}{29}\cos\frac{29}{2}x.$$

The a_{2n} are actually negative.

In closed form, the integrals are

$$\overline{A_n^2}=\left\{\frac{1}{4\pi^2 n}\log\left|\frac{k-n}{k+n}\right|+\frac{1}{2\pi}(SI(2\pi(k-n))+SI(2\pi(k+n)))+\right.$$
$$\left.\frac{1}{4\pi^2 n}(CI(2\pi(k+n))-CI(2\pi(k-n)))\right\}_{k=N}^{k=N+1} \tag{18a}$$

$$\overline{B_n^2}=\left\{\frac{-1}{4\pi^2 n}\log\left|\frac{k-n}{k+n}\right|+\frac{1}{2\pi}(SI(2\pi(k-n))+SI(2\pi(k+n)))+\right.$$
$$\left.\frac{1}{4\pi^2 n}(CI(2\pi(k-n))-CI(2\pi(k+n)))\right\}_{N}^{N+1}. \tag{18b}$$

We have tabulated in table 1 the numerical amplitude expectations obtained in this way for $N=1, \ldots, 20$, and $N-7\leq n\leq N+7$.

Table 1

	$N=1$	$N=2$	$N=3$	$N=4$	$N=5$	$N=6$	$N=7$	$N=8$	$N=9$	$N=10$
A_{N-7}	.....	.....	.....	.....	.....	.....	.....	.0015	.0012	.0011
B_{N-7}	.....	.....	.....	.....	.....	.....	.....	.0001	.0000	.0001
A_{N-6}	.....	.....	.....	.....	.....	.....	.0019	.0017	.0013	.0018
B_{N-6}	.....	.....	.....	.....	.....	.....	.0001	.0001	.0001	.0002
A_{N-5}	.....	.....	.....	.....	.....	.0025	.0021	.0019	.0017	.0015
B_{N-5}	.....	.....	.....	.....	.....	.0001	.0001	.0003	.0003	.0003
A_{N-4}	.....	.....	.....	.....	.0036	.0029	.0025	.0023	.0022	.0020
B_{N-4}	.....	.....	.....	.....	.0000	.0003	.0003	.0005	.0006	.0006
A_{N-3}	.....	.....	.....	.0056	.0035	.0039	.0035	.0033	.0032	.0030
B_{N-3}	.....	.....	.....	.0004	.0005	.0009	.0010	.0011	.0012	.0014
A_{N-2}	.....	.....	.0098	.0088	.0069	.0063	.0059	.0056	.0055	.0053
B_{N-2}	.....	.....	.0012	.0016	.0021	.0024	.0027	.0028	.0029	.0031
A_{N-1}	.....	.0238	.0121	.0167	.0157	.0150	.0144	.0140	.0139	.0135
B_{N-1}	.....	.0040	.0133	.0077	.0183	.0088	.0094	.0098	.0099	.0101
A_N	.2667	.2545	.2407	.2371	.2349	.2333	.2323	.2316	.2310	.2304
B_N	.1929	.1993	.2119	.2153	.2171	.2185	.2193	.2200	.2206	.2212
A_{N+1}	.2006	.2094	.2136	.2160	.2178	.2189	.2196	.2203	.2209	.2214
B_{N+1}	.2550	.2438	.2384	.2358	.2340	.2329	.2320	.2313	.2305	.2302
A_{N+2}	.0055	.0071	.0082	.0088	.0092	.0095	.0099	.0101	.0103	.0104
B_{N+2}	.0205	.0179	.0164	.0152	.0146	.0143	.0139	.0137	.0135	.0132
A_{N+3}	.0013	.0017	.0022	.0026	.0027	.0029	.0030	.0030	.0033	.0034
B_{N+3}	.0087	.0073	.0066	.0060	.0057	.0055	.0054	.0052	.0051	.0050
A_{N+4}	.0005	.0007	.0009	.0011	.0012	.0014	.0015	.0015	.0014	.0015
B_{N+4}	.0049	.0041	.0037	.0035	.0032	.0030	.0029	.0029	.0028	.0027
A_{N+5}	.0003	.0004	.0004	.0006	.0005	.0006	.0007	.0008	.0008	.0008
B_{N+5}	.0033	.0028	.0024	.0022	.0021	.0020	.0021	.0018	.0018	.0018
A_{N+6}	.0001	.0002	.0002	.0004	.0005	.0004	.0006	.0005	.0005	.0005
B_{N+6}	.0023	.0020	.0018	.0016	.0015	.0014	.0014	.0013	.0011	.0013
A_{N+7}	.0001	.0002	.0001	.0002	.0003	.0002	.0004	.0003	.0003	.0003
B_{N+7}	.0017	.0014	.0013	.0012	.0011	.0010	.0010	.0011	0009	.0009

Table 1 indicates that $\overline{A^2_{N+h}}$, $\overline{B^2_{N+h}}$ have limiting values as $N\to\infty$. We give an asymptotic expression that confirms this and shows that as soon as the third term is negligible we have $A_N=B_{N+1}$, $B_N=A_{N+1}$, $A_{N-1}=B_{N+2}$, etc., as indicated by the table. Starting with eq 18a and 18b, and using the asymptotic expansions of $SI(x)$ and $CI(x)$ given in [9], we get

$$\left.\begin{matrix}\overline{A^2_{N-h}}\\ \\ B^2_{N-h}\end{matrix}\right\}=\begin{matrix}+\dfrac{1}{+2\pi}[SI[2\pi(h+1)]-SI[2\pi(h)]+\dfrac{1}{4\pi^2(N-h)}[-CI[2\pi(h+1)]\\ +\log 2\pi|h+1|+CI[2\pi(h)]-\log 2\pi|h|]\end{matrix}\begin{matrix}-\\ +\end{matrix}\frac{1}{4\pi^2(N-h)(2N-h)}+0(N^{-3}),$$

with the natural convention $\log 0-CI(0)=0$. The accuracy of this approximation depends on the magnitude of $N-h$: using the first two terms in all cases, we have, for $N=10$, $h=-4$, .0016, .0026 instead of the tabulated .0015, .0027; for $N=10$, $h=4$, we have .0022, .0003 instead of .0020, .0006; for $N=10$, $h=0$, we have .2304, .2210 instead of .2304, .2212; for $N=20$, $h=20$, we have .2281, .2234 instead of .2281, .2233; for $N=20$, $h=-4$, we have 0018, .0024 in both cases for $N=20$, $h=4$, we have .0016, .0009 instead of .0016, .0010.

Table 1 (*Continued*)

	$N=11$	$N=12$	$N=13$	$N=14$	$N=15$	$N=16$	$N=17$	$N=18$	$N=19$	$N=20$
A_{N-}	.0010	.0009	.0009	.0008	.0008	.0008	.0008	.0008	.0006	.0007
B_{N-7}	.0002	.0001	.0001	.0002	.0002	.0002	.0002	.0002	.0002	.0003
A_{N-6}	.0012	.0011	.0010	.0011	.0010	.0009	.0008	.0010	.0009	.0009
B_{N-6}	.0002	.0003	.0004	.0003	.0004	.0003	.0004	.0004	.0003	.0005
A_{N-5}	.0015	.0014	.0013	.0013	.0012	.0013	.0011	.0012	.0011	.0012
B_{N-5}	.0005	.0004	.0005	.0005	.0006	.0005	.0005	.0006	.0005	.0006
A_{N-4}	.0019	.0019	.0018	.0018	.0017	.0017	.0016	.0016	.0016	.0016
B_{N-4}	.0007	.0007	.0008	.0008	.0009	.0009	.0010	.0010	.0010	.0010
A_{N-3}	.0028	.0027	.0027	.0027	.0026	.0026	.0026	.0026	.0025	.0025
B_{N-3}	.0014	.0015	.0015	.0015	.0016	.0016	.0016	.0016	.0017	.0017
A_{N-2}	.0052	.0051	.0050	.0050	.0048	.0049	.0047	.0048	.0046	.0046
B_{N-2}	.0032	.0033	.0034	.0034	.0034	.0035	.0035	.0036	.0036	.0036
A_{N-1}	.0133	.0132	.0132	.0131	.0130	.0129	.0129	.0128	.0128	.0127
B_{N-1}	.0103	.0104	.0104	.0105	.0106	.0107	.0107	.0108	.0108	.0109
A_N	.2299	.2295	.2292	.2289	.2288	.2286	.2284	.2282	.2281	.2281
B_N	.2215	.2221	.2224	.2225	.2226	.2228	.2230	.2232	.2235	.2233
A_{N+1}	.2216	.2221	.2224	.2226	.2227	.2230	.2231	.2233	.2234	.2235
B_{N+1}	.2298	.2293	.2292	.2290	.2287	.2286	.2283	.2281	.2282	.2279
A_{N+2}	.0104	.0105	.0106	.0106	.0108	.0108	.0109	.0108	.0109	.0109
B_{N+2}	.0132	.0131	.0130	.0130	.0128	.0128	.0127	.0128	.0127	.0127
A_{N+3}	.0033	.0033	.0035	.0034	.0036	.0035	.0036	.0036	.0036	.0037
B_{N+3}	.0049	.0049	.0049	.0058	.0048	.0047	.0046	.0046	.0046	.0046
A_{N+4}	.0017	.0016	.0016	.0016	.0017	.0017	.0017	.0017	.0018	.0018
B_{N+4}	.0027	.0026	.0016	.0026	.0025	.0025	.0025	.0024	.0024	.0024
A_{N+5}	.0009	.0009	.0010	.0010	.0009	.0010	.0010	.0010	.0010	.0010
B_{N+5}	.0017	.0017	.0016	.0016	.0017	.0016	.0016	.0016	.0015	.0015
A_{N+6}	.0006	.0005	.0006	.0006	.0006	.0006	.0006	.0006	.0007	.0007
B_{N+6}	.0012	.0011	.0012	.0010	.0011	.0011	.0011	.0011	.0011	.0011
A_{N+7}	.0004	.0003	.0004	.0004	.0004	.0004	.0004	.0004	.0004	.0005
B_{N+7}	.0010	.0009	.0010	.0009	.0008	.0008	.0008	.0008	.0008	.0008

7. The Sojourn Function

For a given wave or pressure record $f(t)$, let $P(y)$ denote the proportion of time during which $f(t)<y$. Let $D(y)=P'(y)$ be called the "sojourn function" for $f(t)$; for a differentiable $f(t)$, $D(y)$ is the frequency of occurrence of solutions of $f(t)=y$, times the mean of the reciprocal of $f'(t)$ when $f(t)=y$. It can be estimated by sampling $f(t_i)=y_i$, and plotting the distribution of the y_i.

If $f(t)=A\cos(\sigma t-\epsilon)$ is simply harmonic, then $D(y)=0$ if $|y|>|A|$, while $D(y)=\pi(A^2-y^2)^{-\frac{1}{2}}$ if $|y|<A$. For superpositions $f(t)=A\cos(\sigma_1 t+\epsilon_1)+A\cos(\sigma_2+\epsilon_2)$ of two simply harmonic amplitudes, $D(-y)=D(y)$, and

$$D(y)=\frac{1}{\pi^2}\int_{y-A}^{y+A}\frac{d\xi}{\sqrt{(A^2-\xi^2)(A^2-(y-\xi)^2)}}, \tag{19}$$

which can be expressed in terms of elliptic integrals.

The random linear superposition of infinitely many small disturbances having independent origins (or incommensurable phases) will yield a *normal* distribution. Thus, all models of the type of section 5 with

continuous energy spectrum $I(k)$ will have as sojourn function

$$D(y)=\frac{1}{\sqrt{2\pi E}}e^{-y^2/2E}, \tag{20}$$

when normalized so that $\overline{f}=0$.

We have plotted in figure 2 four graphs of $D(y)$ from three independent sources.[8] We tested the data for skewness and peakedness by computing $\overline{f^3}$ and $\overline{f^4}$. We then tested for normality by the χ^2-test with six subdivisions, corresponding to equal portions of a normal distribution with the observed $\overline{f^2}$.

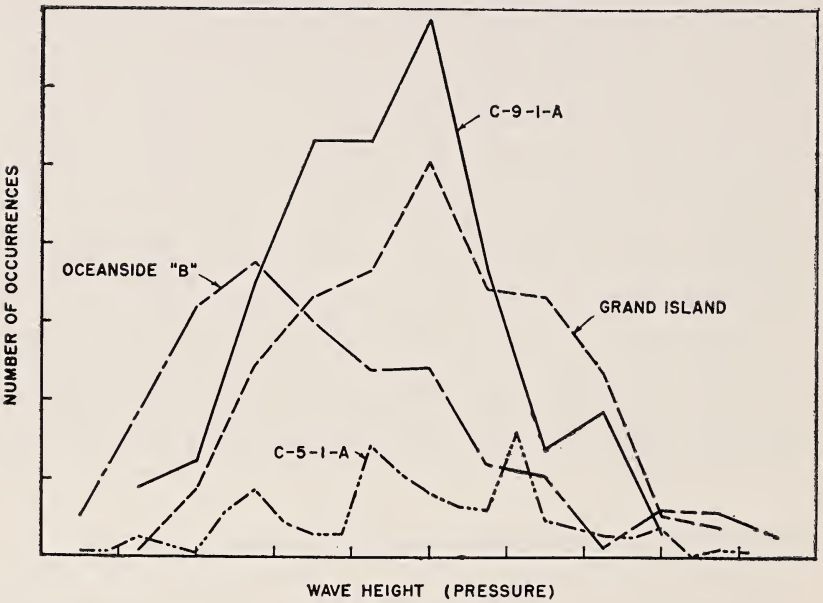

FIGURE 2. *The horizontal axis measures wave height except for the Oceanside curve, where it measures pressure.*

The vertical axis measures the number of occurrences of the corresponding height (or pressure) in a set of equally spaced observations. These curves are cruder than the set of numbers used in preparing them. Points on the curves are obtained by lumping together two, and in the case of C–5–1–A, four observations. The χ^2-test was based on the observations. The scale is different for each curve. The number of observations is 375 for C–9–1–A, 423 for Grand Island, 354 for Oceanside, and 368 for C–5–1–A.

A wave-height record from Grand Island, Louisiana supplied by M. Mason gave a normal $D(y)$; so did one of two wave-height records (C–9–1A, 1–375) taken by Seiwell at Bermuda. A second wave-height record (C–5–1A, 1–368) taken by Seiwell at Bermuda was not normal; neither was pressure record B from Oceanside, California, as given in [8]. The latter record was peculiar, for other reasons stated in section 8.

By eq 20 $D(y)$ is the same for all models of the type of section 5 having a continuous spectrum and the same $\overline{f^2}$. But it is easy to construct

[8] $D(y)$ is not the same as the frequency distribution in wave height, previously studied by Admiralty Mining Establishment Informal Report 1483/50, by W. R. Swann and N. F. Barber, or Univ. of California Tech. Rep. HE116–318, by R. R. Putz.

random time series with $\overline{f^2}>0$ and nonnormal $D(y)$. This shows that $D(y)$ is not determined by $I(k)$, and suggests that the two are largely independent. If so, $D(y)$ supplements the amplitude spectrum of functions with $\overline{f^2}>0$, in somewhat the same way that the phase spectrum $\epsilon(k)$ does in ordinary Fourier analysis.

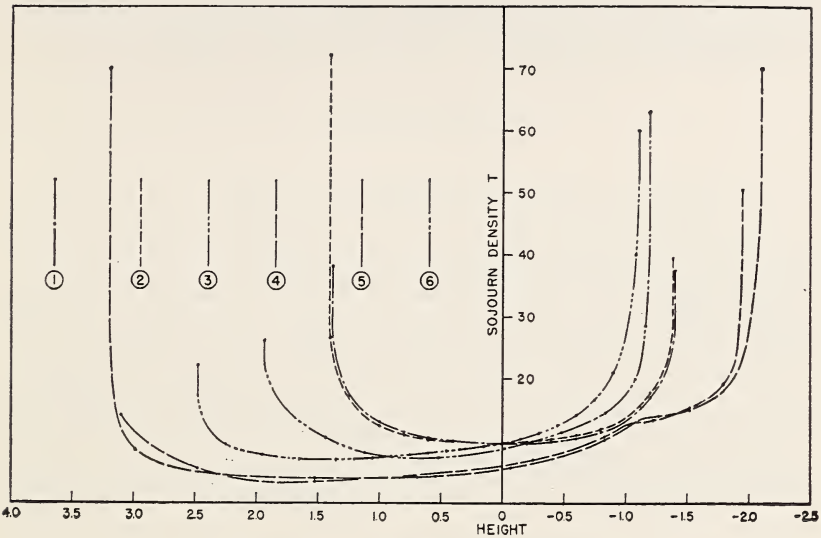

FIGURE 3. *Frequency distributions.*

1. Frequency distribution of cosine curve:
$$T=\cos^{-1}\left(\frac{y}{1.5}\right)\frac{910.56}{2\pi}.$$
2. Frequency distribution of approximate trochoid:
$$y=\frac{1}{k}\cos^{-1}\left(\frac{y}{\beta e^{ky}}\right),\quad k=0.0069,\quad \beta=1.5,\quad ka=0.01035.$$
3. Frequency distribution of approximate trochoid:
$$y=\frac{1}{k}\cos^{-1}\left(\frac{y}{\beta e^{ky}}\right),\quad k=.0628,\quad \beta=5,\quad ka=0.3484.$$
4. Frequency distribution of $y=a(\cos k+\frac{1}{2}ka\ \cos 2kx+\frac{3}{8}k^2a^2\ \cos 3kx)$, $a=7.9618$, $k=0.0628$, $ka=0.5$.
5. Frequency distribution of $y=a(\cos kx+\frac{1}{2}ka\ \cos 2kx+\frac{3}{8}k^2a^2\ \cos 3kx)$, $a=0.5$, $k=1$, $ka=0.5$.
6. Frequency distribution of $y=a(\cos kx+\frac{1}{2}ka\ \cos 2kx+\frac{3}{8}k^2a^2\ \cos 3kx)$, $a=5.5484$, $k=0.0628$, $ka=0.3484$.

Graphs 3, 4, and 6 have had their scales multiplied by constants to get them on the figure.

8. Principle of Random Sign

The marked skewness of the record from Oceanside is very disturbing, because it is incompatible with linear wave theories. This is a special case of the following general mathematical principle, whose proof involves group theory, like the Principle of Random Phase—but applied to the dependent instead of the independent variables.

Principle of Random Sign. Let Ω and the $f_\omega(t)$ be as in the Principle of Random Phase. If all information about the f_ω can be expressed by linear homogeneous, or other *odd* order differential equations, then the statistics are unchanged if each f_ω is replaced by $-f_\omega$.

Thus if such data can be taken at face value, linear theories of ocean waves must be considered as inapplicable to the instruments or physical

behavior of waves. Assuming the instruments to be working properly, it is very hard to explain what they record, especially as the "steepness" h/λ of the waves recorded was only about $.42'/448' = .00094$. We have graphed in figure 3 the sojourn function $D(y)$ for trochoidal, long-crested periodic waves; it is clear that the asymmetry is much too small to explain the Oceanside B records.

Explanations based on the idea that "wind-driven waves are peaked," and on a tendency to break in the shallow water involved, are also unconvincing, for such small h/λ.

9. References

[1] N. F. Barber and F. Ursell, The generation and propagation of ocean waves and swell, Phil. Trans. Roy. Soc., vol. 240 (1948), pp. 527–560.

[2] H. R. Seiwell, Ocean surface waves, Ann. New York Acad. Sci., vol. 51 (1949), Art. 3.

[3] H. Lamb, Hydrodynamics, 6th edition, Cambridge, 1932.

[4] Henri Vergne, Ondes liquides de gravite, Actualities Scientifiques et Industrielles, Paris, 1928.

[5] N. Wiener, Generalized harmonic analysis, Acta Math., vol. 55 (1930), pp. 117–258.

[6] N. Wiener, The Fourier integral, Cambridge, 1933.

[7] J. Kampé de Fériet, Sur l'analyse spectral d'une function stationnaire en moyenne, Actes du Colloque Inst. de Mecanique, Poitiers, vol. 3 (1950).

[8] R. R. Putz, Idealized reconstructions of ocean surface waves as inferred from measurements on twenty-five subsurface pressure records, Univ. of California, Eng. Res. Projects, Series 3, Report 317, 1950.

[9] Tables of sine, cosine, and exponential integrals, vol. 1, Federal Works Agency, Work Projects Administration for the City of New York.

26. Water Waves Over Sloping Beaches

By A. S. Peters[1]

Abstract

The study of water waves over sloping beaches leads to the problem of solving the wave equation $\Delta^2\phi - k^2\phi = 0$ subject to mixed boundary conditions on the sides of a sector of arbitrary angle. The equation arises when we wish to study progressing waves whose lines of constant phase at great distances from the shore make an arbitrary angle with the shore line.

This paper presents a method for solving the problem. The method depends upon the use of the Laplace transform of ϕ taken along the radius vector ρ. The transform is used to change the problem into a potential problem for a strip with more complex boundary conditions than those which go with the wave equation. The potential problem, in turn, is reduced to the solution of a certain q-difference equation, and this is solved by function theory methods.

The two solutions which are derived are out of phase in the surface at infinity by $\pi/2$ radians. One solution is regular at the shore; the other has a logarithmic singularity there. The integral forms in which these solutions are finally presented are valid both for $k \neq 0$ and $k = 0$.

---

[1] Institute for Mathematics and Mechanics, New York University, New York, N. Y.

27. Stability of Uniform Flow and Roll-Wave Formation

By Robert F. Dressler[1]

A uniform open channel flow down an inclined aqueduct sometimes changes into a complicated periodic motion with a progressing-wave profile, the profile moving downstream faster than the water particles. This phenomenon called "roll-waves" is investigated by three completely different methods:

(1) The construction of actual roll-wave solutions is effected by joining certain special continuous solutions together by means of moving discontinuities or bores. Of the three shock conditions of mass, momentum, and energy, the energy condition requires the use of a resistance term whose magnitude varies inversely with the hydraulic radius, as well as directly with the square of the velocity; otherwise, the equations are not sufficiently non-linear to produce roll-wave solutions. These waves cannot exist if resistance is absent, or if it exceeds a certain critical value. A two-parameter family of solutions is obtained; in all cases, the flow is subcritical at the peaks and supercritical in the valleys.

(2) By a perturbation procedure using maximum curvature of the profile as expansion parameter, continuous periodic progressing waves are found in terms of elliptic functions. These waves possess greater profile curvature than the discontinuous solutions of the non-linear shallow water theory. The perturbation also yields a two-parameter family of waves; these also are supercritical at peaks and subcritical in the valleys.

(3) Using a stability analysis which observes the location of roots in the right or left half-plane, the same critical condition on resistance causing instability is obtained as in Section 2. This method likewise shows that a resistance term varying only with velocity will produce uniform flows which are always stable, hence no roll-waves. A more general analysis indicates that instability may occur whenever resistance varies directly with any power of velocity, and inversely with any nonzero power of the hydraulic radius.

1. Introduction

A uniform open channel flow down an inclined aqueduct sometimes changes into a complicated progressing wave, periodic in distance, the profile moving downstream faster than the water. These roll-waves develop after the uniform flow becomes unstable. Some analyses have been made of certain aspects of the final roll-wave motion by Thomas [4][2] and the author [2]. Results giving necessary criteria for the existence of the waves were obtained by considering the correct slope of the wave profile, or by satisfying the energy inequality at the moving shock discontinuities (bores). The present purpose is to investigate the instability of the original uniform flow, and to compare and correlate results with previous conclusions arrived at from the different standpoints of shock conditions and perturbation procedures [2].

Both the uniform and roll-wave flows are turbulent, hence any completely satisfactory explanation would require a foundation in turbulence

[1] Institute for Mathematics and Mechanics, New York University, New York, N. Y.

[2] Figures in brackets indicate the literature references on p. 241.

theory, emphasizing the resistive effect on the main flow due to the turbulent components. The status of turbulence theory and mathematical techniques seems to offer little hope of success at present in this direction. Instead, hydraulicians resort to some more or less accurate empirical resistance function, used in conjunction with the nonlinear shallow-water equations.

Our present purpose is to discover what particular aspect of the complicated resistance mechanism is responsible for instability and subsequent roll-wave formation. Within the limits of using an empirical function, we would like to explain what causes roll-waves and to isolate the mathematical terms directly responsible for this phenomenon. Cornish [1], with appendix by Harold Jeffreys, has presented some interesting qualitative discussions on the formation of the waves with respect to the resistive action of the stream bed.

A stability analysis of the uniform flow was presented by Jeffreys [3] based upon the nonlinear shallow water equations plus the conventional Chezy resistance formula. This discussion will extend the results of Jeffreys to a general resistance function. It is known empirically that the turbulence creates a resistive force roughly dependent upon some power of the velocity u, and indirectly upon some power of the hydraulic radius (in this case the depth y), with a proportionality constant depending upon the stream bed. Let r^2 be the constant, and θ the inclination of the channel. The Chezy formula takes resistance as $-r^2u^2/y$. Using this, Jeffreys obtained a criterion for instability of uniform flow as

$$\tan\theta > 4r^2. \tag{1}$$

This same criterion was found to be a necessary condition for the existence of roll-waves in [2 and 4].

Using the shock energy inequality to construct discontinuous roll-wave solutions, the author noted that solutions could never be constructed if the variation of resistance with depth was ignored. That is, if the resistance depended only upon the square of the velocity, the energy shock condition for the bores of the waves was always violated. Such a simplifying assumption is often made, however, particularly when the depth is considered to be approximately constant. We wish now to determine whether the agreement between the energy and stability analyses extends also to this case and to see more generally how instability depends upon the form of the resistance function.

2. Stability Analysis for General Resistance

For a two-dimensional flow, let u be the velocity component parallel to the inclined stream bed, and let y be the depth. The resistance function will be taken quite generally as $-r^2u^n/y^m$, with $m,n>0$ but otherwise arbitrary. The nonlinear shallow water equations are then

$$u_t+uu_x+g\cos\theta y_x=g\sin\theta-\frac{r^2u^n}{y^m},\quad yu_x+uy_x+y_t=0. \tag{2}$$

The possible uniform flow is then $u=U$, $y=Y$ where

$$U=\left(\frac{gY^m\sin\theta}{r^2}\right)^{\frac{1}{n}}. \tag{3}$$

Considering small deviations given by $u=U+\bar{u}(x,t)$, $y=Y+\bar{y}(x,t)$, and linearizing in the usual manner yield two equations for $\bar{u}$ and $\bar{y}$,

$$\bar{u}_t+U\bar{u}_x+g\cos\theta\bar{y}_x=\frac{gm\sin\theta}{Y}\bar{y}-r^2\frac{nU^{n-1}}{Y^m}\bar{u},\quad U\bar{y}_x+Y\bar{u}_x+\bar{y}_t=0. \tag{4}$$

After eliminating $\bar{y}$, we get the second-order linear equation for $\bar{u}(x,t)$

$$\bar{u}_{tt}+2U\bar{u}_{xt}+(U^2-gY\cos\theta)\bar{u}_{xx}+\frac{r^2nU^{n-1}}{Y^m}\bar{u}_t+\left(mg\sin\theta+\frac{r^2nU^n}{Y^m}\right)\bar{u}_x=0. \tag{5}$$

We now study the growth or decay of the large class of progressing wave solutions of type

$$u=Ae^{rt}\begin{pmatrix}\cos\\ \sin\end{pmatrix}\left(\beta\left[x+\frac{s}{\beta}t\right]\right)$$

with wave speed s/β and wave length proportional to $1/\beta$. Letting $r+is=\gamma$, insertion of solutions $Ae^{\gamma t+i\beta x}$ into eq 5 implies the relation between γ and β

$$\gamma=-\frac{r^2nU^{n-1}}{2Y^m}-iU\beta\pm\left(\frac{r^4n^2U^{2n-2}}{4Y^{2m}}-\beta^2gY\cos\theta-i\beta gm\sin\theta\right)^{\frac{1}{2}}.$$

For stability, we require both roots to be in the left half of the complex γ plane. If parameters are adjusted so that the first square root in eq 5 will have real part equal to $r^2nU^{n-1}/2Y^m$, then the corresponding γ value will be on the imaginary axis, and the other value in the left half-plane. We therefore equate this square root to $(r^2nU^{n-1}/2Y^m)+i\delta$, equate reals and imaginaries, eliminate δ, and use relation 3. The condition for the right root to be on the s axis is then

$$m^{2n}g^{2-n}Y^{2m-n}\sin^2\theta=n^{2n}r^4\cos^n\theta. \tag{6}$$

When the expression on the left is greater or smaller, it can be shown that the root moves to the left or to the right, respectively. Furthermore, considering the expressions in eq 6 as functions of θ, we see that eq 6 will always have a solution for one critical value of θ between 0 and $\pi/2$. Hence we have the stability criterion for our general resistance,

$$m^{2n}g^{2-n}Y^{2m-n}\sin^2\theta\lesseqgtr n^{2n}r^4\cos^n\theta, \tag{7}$$

implying stability for the two top signs, and instability for the bottom sign.

For the special case of the Chezy formula, $m=1$, $n=2$, eq 7 reduces to the relation (1) $\tan\theta\lesseqgtr 4r^2$. Likewise, $m=\frac{4}{3}$, $n=2$ yields the criterion for the Manning formula.

To see what is the essential nonlinearity in eq 2 causing instability and roll-waves, we now consider two special limit cases of eq 7.

Case 1: $m\to 0$, $n>0$.

In this limit case, eq 7 reduces to only one possibility $0<n^{2n}r^4\cos^n\theta$, hence we conclude that any flow governed by a resistance varying with any power of the velocity, but independent of depth, must always remain stable.

Case 2: $n \to 0$, $m > 0$.

Now, by virtue of the relation for the constant flow

$$Y = \left(\frac{r^2}{g \sin \theta} \right)^{\frac{1}{m}},$$

the only possibility for eq 7 is the equality $g^2 Y^{2m} \sin^2 \theta = r^4$. One can see that both γ roots move to the s axis, still a region of stability. Although this case, representing a kind of hydraulic Coulomb friction, may not correspond accurately to any actual flows, the analysis nevertheless indicates that *both* effects of depth and velocity are needed to create instability.

We thus arrive at the following conclusions:

(1) *When turbulent resistance effects behave directly with any power of the velocity and inversely with any power of the depth, there will always exist an angle of declination beyond which the uniform flow becomes unstable.*

(2) *This critical angle where instability occurs is the same angle which is obtained as a condition for the existence of roll-waves by satisfying the shock energy inequality.*

(3) *Instability cannot occur if resistance depends only upon velocity variation, or only upon depth variation; the simultaneous action of both effects is required. This can be concluded either from the stability analysis, or the shock energy approach.*

For this reason, since one-dimensional compressible gas flow is governed by the same equations as above, with resistance depending only upon velocity, one would not expect any instability to develop in such flows.

3. Roll-Wave Solutions With Discontinuities

The material in this and the following section has been published in [2]. It is desired here to correlate all results on roll-waves from the three different points of view. By considering all possible progressing wave solutions with velocity c to the eq 2 with the Chezy formula, the profile equation is

$$\frac{dY}{d\zeta} = -\frac{Y(gm - \{r^2(cY-K)|cY-K|/Y^3\})}{(K^2/Y^2) - gY}, \tag{8}$$

where $\zeta = x - ct$, $Y(\zeta)$ is depth, $U(\zeta)$ is velocity, $K = (c-U)Y$, and $m = \tan \theta$. There are no continuous periodic solutions to this, but discontinuous solutions can be pieced together, using the only solution to eq 8 which is partly subcritical and partly supercritical, relative to the moving wave.

This solution is given inversely by

$$\zeta = C + \frac{1}{m} Y + \frac{Y_A^2 + Y_A Y_0 + Y_0^2}{m(Y_A - Y_B)} \ln(Y - Y_A) - \frac{Y_B^2 + Y_B Y_0 + Y_0^2}{m(Y_A - Y_B)} \ln(Y - Y_B), \tag{9}$$

where Y_A, Y_B, and Y_0 are known constants. Parameters C and K can always be chosen to satisfy the shock conditions of mass and momentum; but satisfying the energy inequality, namely that particles must enter a shock at supercritical speed and leave at subcritical speed, leads to the

necessary condition $\tan\theta > 4r^2$, the relation (1). The resulting roll-waves are subcritical at peaks and supercritical in the valleys. This method leads to a two-parameter family of solutions. Furthermore, if the Chezy formula is simplified by assuming that resistance does not depend upon *both* velocity and depth, then it can be shown that the energy condition will never be satisfied.

4. Continuous Roll-Waves With Larger Curvature

By a perturbation on the exact Eulerian equations, with expansion parameter $\sigma = \omega^2 h^2$ taken with ω as maximum surface curvature and h as depth, the nonlinear shallow water equations are obtained as lowest approximations. Using the Chezy formula here, and neglecting resistance in the next approximation, continuous periodic progressing waves are obtained only by perturbing about the critical uniform flow. Their profile can be expressed by

$$Y = -y_2 + (y_1 + y_2)\,\mathrm{cn}^2\left(\frac{\omega}{\Delta}\zeta, k\right),$$

where *cn* is the Jacobi elliptic function, and y_1, y_2, Δ, and k are known constants. We obtain a two-parameter family, also having the property that the flow is subcritical at peaks and supercritical in the valleys.

Summarizing results from the approaches 1, 2, and 3, we have: 1 and 2 yield same conditions on slope; 1 and 2 show that a simplified resistance will produce only a uniform flow; 2 and 3 both produce a two-parameter family of roll-waves, and both types exhibit the same subcritical and supercritical pattern.

5. References

[1] Cornish, V., Ocean waves and kindred geophysical phenomena. Cambridge University Press, London (1934).

[2] Dressler, R. F., Roll-waves in inclined open channels. Communications on Pure and Applied Mathematics **II**, No. 2/3 (June 1949).

[3] Jeffreys, H., Flow of water in an inclined channel of rectangular section. Philosophical Magazine **XLIX** (1925).

[4] Thomas, H. A., Propagation of stable wave configurations in steep channels. Carnegie Institute of Technology, Pittsburgh, Pa.

28. Study of Wave Propagation in Water of Gradually Varying Depth

By F. Biesel[1]

The present paper is a theoretical study of periodic waves progressing in water of variable depth. Although the theory can be extended to three-dimensional motion, we shall only consider the two-dimensional case which can be briefly described as that of waves advancing in a straight channel with rectangular cross section and variable depth. This problem has already been studied by various authors, but the solutions obtained have always been restricted to flat sea bottoms of constant slope and can be worked out in practice only for a limited number of singular values of the bottom slope (cf. the works of Miche, Stoker, Loewy, etc.) or for small bottom slopes and very small relative depth (Lowell, Miche). The solution obtained by the present theory is subject to the restriction that the slope of the bottom is so small that its square is negligible. Bottom curvature and higher derivatives of depth with respect to distance along the wave course are also neglected. Provided these assumptions are satisfied, the bottom may have any shape whatsoever.

In the first part of this paper, investigations are limited to first-order theories, that is, the squares of the velocities due to the presence of waves are neglected (this is the case for all previous theories of waves on sloping bottoms). In the second part, a second-order correction is introduced, and it is shown by numerical examples that this correction may be important in some respects.

1. Outline of Fundamental Formulas

Rectangular coordinate axes OX and OZ will be used, OX being located at mean sea level, with positive x in the direction of wave propagation, OZ being directed vertically upward. The calculations always refer to a section of unit thickness. The notation adopted is as follows:

x,z = coordinates referred to the OX, OZ axes,
u,w = OX and OZ velocity components,
p = pressure,
X,Z = displacements of particles from their mean positions,
T = period,
$k=(2\pi/T)$ = angular frequency,
L = wave length measured from crest to crest,
$m=2\pi/L$,
λa = wave amplitude,
T_0,K_0,L_0,m_0,a_0 = values of above quantities in an infinite depth,
h = depth,
$\alpha=-(\partial h/\partial x)$ = slope of bed,
ϕ = velocity potential.

[1] Etablissements Neyrpic, Grenoble, France.

Since the equations that will be derived are of the first order in respect to amplitude, use may be made either of the Lagrange or of the Euler system of coordinates.

The latter system has been used to establish the basic equations, since it is more usual. However, the results obtained will be finally expressed in terms of Lagrange variables, since first-order equations of waves in constant depth give a far better picture of reality in the Lagrange system than in the Euler system. It seems reasonable to suppose that this will also be the case for waves in slowly varying depths.

In order to obtain the equations of the irrotational motion of an incompressible fluid, it suffices to find a velocity potential $\phi(x,z,t)$, from which the velocity components are deduced by

$$u=\frac{\partial\phi}{\partial x},\quad w=\frac{\partial\phi}{\partial z}. \tag{1}$$

This function should be harmonic with respect to x and z, i.e., that

$$\nabla^2\phi=\frac{\partial^2\phi}{\partial x^2}+\frac{\partial^2\phi}{\partial z^2}=0, \tag{2}$$

and should, moreover, satisfy both the boundary condition at the bed which can be written, without taking account of second-order quantities,

$$\frac{\partial\phi}{\partial z}-\alpha\frac{\partial\phi}{\partial x}=0,\quad \text{for } z=-h, \tag{3}$$

and the constant surface pressure condition

$$\frac{1}{g}\frac{\partial^2\phi}{\partial t^2}+\frac{\partial\phi}{\partial z}=0,\quad \text{for } z=0, \tag{4}$$

ignoring second-order quantities.

These four conditions are satisfied, to within terms of the order of α^2, by the function:

$$\begin{aligned}\phi(x,z,t)=-a\frac{k}{m}\frac{1}{\sinh mh}\Bigg[&\cosh m(z+h)\sin\left(kt-\int mdx\right)\\ &+\alpha\left\{\frac{1}{D^2\tanh mh}m(z+h)\sinh m(z+h)-m(z+h)\cosh m(z+h)\right.\\ &\left.+\frac{m^2(z+h)^2}{D\sinh mh\cosh mh}\cosh m(z+h)\right\}\cos\left(kt-\int mdx\right)\Bigg].\end{aligned} \tag{5}$$

In this equation

$$D=1+\frac{mh}{\sinh mh\cosh mh}, \tag{6}$$

m, k, and h are related by

$$gm\tanh mh=k^2, \tag{7}$$

and

$$a=\frac{a_0}{(D\tanh mh)^{\frac{1}{2}}}, \tag{8}$$

a_0 being constant. Moreover, the integration limits of $\int m dx$ are not defined; thus the phase of the motion remains undetermined, but this causes no difficulty in the present study.

It can easily be seen that if one considers only the first term of the square bracket of formula 5, together with 7 and 8, one finds precisely the same result as that given by the energy method. In effect, formula 7 shows that the relation between wave length, frequency, and depth is the same as for a constant depth wave, and formula 8 shows that at each point the amplitude is such as to make the energy flux constant. This confirms the validity of the energy method as a first approximation.

But if we reduced this function to this first term its Laplacian ∇^2 would not be zero. It would, in fact, be of the order of magnitude of α, and not be negligible to the order of approximation required. The introduction of the other terms reduces $\nabla^2\phi$ to a negligible quantity of the order of magnitude of α^2. This can be shown by computing $\nabla^2\phi$ with due regard to formulas 6, 7, and 8. This calculation is rather long, as m, a, and h are functions of x, and of no special interest; it was therefore thought unnecessary to reproduce it in this paper.

It is easier to make sure tha conditions 3 and 4 are fulfilled to within the desired approximation.

We have

$$u=\frac{\partial\phi}{\partial x}=\frac{ak}{\sinh mh}\Bigg[\cosh m(z+h)\cos\left(kt-\int m dx\right)$$
$$-\alpha\Bigg\{\frac{1}{D^2\tanh mh}\Big[\cosh m(z+h)+m(z+h)\sinh m(z+h)\Big]$$
$$+\frac{1}{D\sinh mh\cosh mh}\Big[m(z+h)\sinh m(z+h)+\frac{m^2(z+h)^2}{2}\cosh m(z+h)\Big]$$
$$-\Big[\sinh m(z+h)+m(z+h)\cosh m(z+h)\Big]\Bigg\}\sin\left(kt-\int m dx\right)\Bigg], \qquad (9)$$

$$W=\frac{\partial\phi}{\partial z}=-\frac{ak}{\sinh mh}\Bigg[\sinh m(z+h)\sin\left(kt-\int m dx\right)$$
$$+\alpha\Bigg\{\frac{1}{D^2\tanh mh}\Big[\sinh m(z+h)+m(z+h)\cosh m(z+h)\Big]$$
$$+\frac{1}{D\sinh mh\cosh mh}\Big[m(z+h)\cosh m(z+h)+\frac{m^2(z+h)^2}{2}\sinh m(z+h)\Big]$$
$$-\Big[\cosh m(z+h)+m(z+h)\sinh m(z+h)\Big]\Bigg\}\cos\left(kt-\int m dx\right)\Bigg]. \qquad (10)$$

If we put $z=-h$ in these equations, we obtain the velocity values on the bed

$$U_{z=-h}=\frac{ak}{\sinh mh}\left[\cos\left(kt-\int m dx\right)-\frac{\alpha}{D^2\tanh mh}\sin\left(kt-\int m dx\right)\right], \qquad (11)$$

$$W_{z=-h}=\alpha\frac{ak}{\sinh mh}\cos\left(kt-\int m dx\right). \qquad (12)$$

From this it can be seen that condition 3 is fulfilled to within the desired approximation. Taking into account relationship 7 and the particular way in which ϕ depends on the time, eq 4 may be written

$$\phi m \tanh mh = \frac{\partial \phi}{\partial z}, \quad \text{for } z=0. \tag{13}$$

The expressions of ϕ and of $\partial\phi/\partial z$ for $z=0$ are

$$\phi_{z=0} = -\frac{ak}{m \sinh mh}\left[\cosh mh \sin\left(kt - \int m dx\right) + \alpha\left\{\frac{1}{D^2 \tanh mh}\left(mh \sinh mh - mh \cosh mh\right) + \frac{1}{D \sinh mh \cosh mh}\frac{m^2h^2}{2}\cosh mh\right\}\cos\left(kt - \int m dx\right)\right], \tag{14}$$

$$\left(\frac{\partial \phi}{\partial z}\right)_{z=0} = -\frac{ak}{\sinh mh}\left[\sinh mh \sin\left(kt - \int m dx\right) + \alpha\left\{\frac{1}{D^2 \tanh mh}\left(mh \cosh mh + \sinh mh\right) + \frac{1}{D \sinh mh \cosh mh}\left(mh \cosh mh + \frac{m^2h^2}{2}\sinh mh\right) - (\cosh mh + mh \sinh mh)\right\}\cos\left(kt - \int m dx\right)\right]. \tag{15}$$

When the necessary calculations are carried out, it is easily seen that these two expressions satisfy condition 13.

2. Study of Wave Motion

We already remarked that with a constant depth it is very advantageous to utilize the Lagrange system of coordinates to express the results of the first-order theories; a wave motion that is very similar to reality is thereby obtained. For instance, a trochoidal free surface is obtained from the start and the existence of a limiting value of wave camber is immediately evident. On the contrary the linear theory expressed in Euler coordinates gives a sine profile with no limiting camber.

It is thought reasonable to expect, that the Lagrange coordinates will retain their advantages for waves in slightly varying depths.

The equations are therefore transformed into Lagrange coordinates, and the X and Z components of the displacement of the particle, having the initial coordinates x and z, are

$$X = \frac{a \sin\left(kt - \int m dx\right)}{\tanh mh} + \alpha a\left\{\frac{1}{D^2(\tanh mh)^2}[1 + mh \tanh mh] + \frac{1}{D \sinh mh \cosh mh}\left[mh + \frac{m^2h^2}{2 \tanh mh}\right] - \left[1 + \frac{mh}{\tanh mh}\right]\right\}\cos\left(kt - \int m dx\right), \tag{16}$$

$$Z=a\cos(kt-\int mdx)-\alpha a\left\{\frac{1}{D^2}\left[\frac{1}{\tanh mh}+\frac{mh}{(\tanh mh)^2}\right]+\right.$$

$$\left.\frac{1}{D\sinh mh\cosh mh}\left[\frac{mh}{\tanh mh}+\frac{(mh)^2}{2}\right]-\left[\frac{1}{\tanh mh}+mh\right]\right\}\sin(kt-\int mdx). \quad (17)$$

These formulas can be written more simply

$$X=a_0A\sin(kt-\int mdx)+a_0\alpha A_1\cos(kt-\int mdx), \quad (18)$$

$$Z=a_0B\cos(kt-\int mdx)+a_0\alpha B_1\sin(kt-\int mdx), \quad (19)$$

A, A_1, B, and B_1 being convenient functions of mh.

The free-surface equations are then expressed parametrically by

$$\xi=x+a_0A\sin(kt-\int mdx)+\alpha a_0A_1\cos(kt-\int mdx), \quad (20)$$

$$\zeta=a_0B\cos(kt-\int mdx)+\alpha a_0B_1\sin(kt-\int mdx), \quad (21)$$

ξ and ζ being the coordinates of a point of the free surface.

The trajectory of a particle of mean position x, y is first studied. The time factor, which is the only variable, becomes the parameter of eq 20 and 21. It is then apparent that the trajectory is an ellipse, of which the axes are generally inclined (fig. 1). Their slope i is easily calculated from formulas 18, 19, 20, and 21.

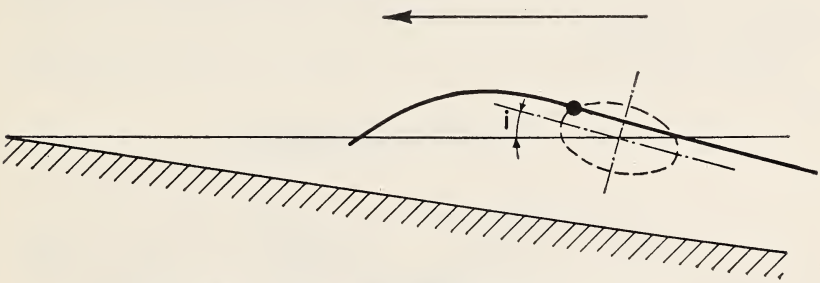

FIGURE 1. *Slope of axis of trajectory of surface particle.*
First-order theory.

Neglecting terms of the order of α^2, we have

$$i=\alpha\frac{BA_1+B_1A}{A^2-B^2}, \quad (22)$$

$$i=\alpha\frac{(\cosh mh)^2-D(\sinh mh)^2}{D^2}. \quad (23)$$

Replacing D by its value 6, eq 23 becomes

$$i=\alpha\frac{1-mh\tanh mh}{\left(1+\dfrac{mh}{\sinh mh\cosh mh}\right)^2}. \tag{24}$$

For sufficiently small values of the relative depth, it can be seen that the orbit inclination for particles resting on the surface is only a fourth of that of the bed (and has the same sign). We thus find a result which has already been given by Miche. Formula 24 shows that the orbit inclination is reduced to zero for a relative depth such that

$$1-mh\tanh mh=0. \tag{25}$$

This remarkable value of the relative depth corresponds to the minimum amplitude point indicated by Havelock and Miche.

With greater depths, the sign of the inclination of the major axis of the orbits *becomes the opposite to that of the bed slope, and the orbit-inclination/bed-slope ratio becomes greater as the depth increases.*

This latter result may seem surprising and may even lead to doubts on the validity of the theory. Indeed, the effect of the bed slope should vanish as the depth increases, and, consequently, it appears inadmissible that the orbit inclination should increase with the depth.

The above reasoning is perfectly correct, but, in point of fact, there is no contradiction.

Indeed, when the relative depth is great, the orbits of the surface particles become almost perfect circles and an extremely small deformation is sufficient to change the direction of the axes.

In short, this increase of axis inclination is therefore a mathematical phenomenon of no physical importance; this is, moreover, fortunate, since the formulas given suppose that i is small. They become useless when i becomes too large, as is the case for great depths, but since this angle then no longer has any appreciable physical significance, no further analysis is necessary.

Reference is once again made to eq 18 and 21 for the study of the form of the free surface.

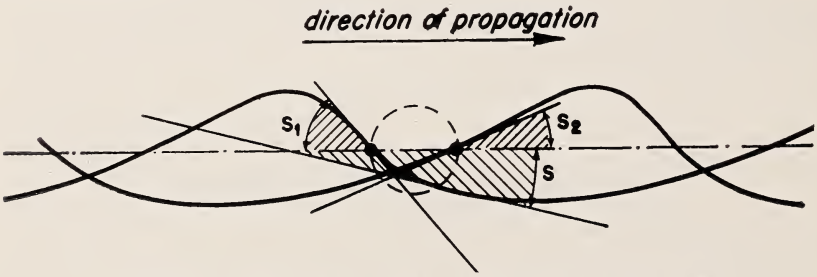

FIGURE 2. *Slopes of wave profile at level of initial water surface.*
Second-order theory.

We shall first investigate the lack of symmetry of the wave shape. In order to do this, we shall fix our attention on a given surface particle and shall compare the surface slope of the wave when this particle crosses the plane $z=0$ on the front face of the wave (position M, fig. 2) and when it recrosses the same plane on the back face (position M').

The free surface slope is given at each point by:

$$s=\frac{\frac{\partial\zeta}{\partial x}}{\frac{\partial\xi}{\partial x}}=\frac{ma_0B\sin(kt-\int mdx)+(-m\alpha a_0B_1+a_0B')\cos(kt-\int mdx)}{1-ma_0A\cos(kt-\int mdx)+(m\alpha a_0A_1+a_0A')\sin(kt-\int mdx)}. \quad (26)$$

The aim is to compute the slope in the neighborhood of the particle, with the initial coordinates $(x,0)$ at the instant when it crosses the plane $z=0$.

We then have $z=0$, or

$$B\cos(kt-\int mdx)+\alpha B_1\sin(kt-\int mdx)=0,$$

whence two sets of possible values for cos $(kt\text{-}mdx)$ and sin $(kt\text{-}mdx)$,

$$\cos(kt-\int mdx)=\alpha\frac{B_1}{B},\quad \sin(kt-\int mdx)=-1, \quad (27)$$

$$\cos(kt-\int mdx)=-\alpha\frac{B_1}{B},\quad \sin(kt-\int mdx)=1. \quad (28)$$

The above values, in which, of course, terms of the order of α^2 are neglected, correspond, respectively, to the passage of the front face $(\sin(kt-\int mdx)=-1)$ and to the passage of the back face $(\sin(kt-\int mdx)=1)$.

Combining eq 27 and 28 with 26, the slopes are obtained always to the same degree of approximation.

$$s_1=-ma_0B-m^2a_0^2\alpha(AB_1+A_1B)-ma_0^2A'B, \quad (29)$$

for the front of the wave, and

$$s_2=ma_0B-m^2a^2\alpha(AB_1+A_1B)-ma_0^2A'B, \quad (30)$$

for the back of the wave.

The mean slope $s=(s_1+s_2)/2$ may be taken as characteristic of the lack of symmetry in the wave profile; the geometrical significance of this is clearly shown in figure 2.

In particular, a negative mean slope would show that, at a given point, the wave fronts are steeper than the rear slopes.

From formulas 29 and 30, the equation

$$s=-m^2a_0^2\alpha(AB_1+A_1B)-mA'B \quad (31)$$

is immediately deduced.

When A, B, A_1, and B_1 are replaced by their values, we have

$$s=m^2a_0^2\alpha\frac{3+\frac{mh}{\tanh mh}-3mh\tanh mh}{D^2(\sinh mh)^2\tanh mh}. \quad (32)$$

The preceding calculation thus shows that the lack of symmetry or dissymmetry is a second-order quantity.

Consequently, eq 32 is logically speaking questionable, since the whole theory is based on a first-order approximation only.

However, as mentioned in the Introduction, it is thought reasonable to assume that the information thus obtained gives a correct approximation of reality, thanks to the use of Lagrangian coordinates.

Formula 32 shows clearly that the real dissymmetry tends to infinity when the depth tends to zero. Of course, if one wished to study the dissymmetry for very great values of s, it would be necessary to modify the calculation in which s was supposed small. Nevertheless, the result that has just been given shows that the dissymmetry has a marked tendency to increase rapidly when the relative depth becomes small.

On the contrary, when the depth increases, the dissymmetry decreases, is reduced to zero, and changes sign for $mh=1.7$ approximately. For higher values of mh, which correspond to fairly deep water, dissymmetry is usually very small and continues to tend rapidly toward zero as the depth increases.

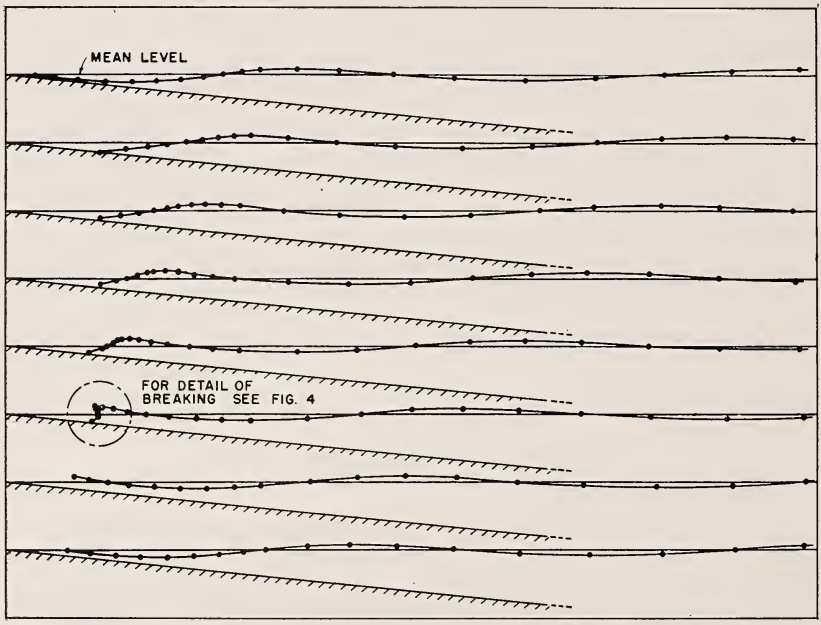

FIGURE 3. *Progression and breaking of a wave on a beach of 1 in 10 slope.*

First-order theory.

Eight successive phases at intervals of $T/8$. Steepness approximately 1/80.

This first discussion on the formulas that have just been obtained concludes with a numerical example. Figure 3 shows eight successive phases of the motion of a wave, with a steepness equal to approximately 1/80 ($0.04/\pi$ exactly), on a 1-in-10 slope beach. Each phase differs by one-eighth period from the preceding one; the eight phases thus give a complete cycle.

The steepening of the front face of the wave is very apparent, and finally gives the wave an overhang that is characteristic of the plunging, breaking movement. Successive phases at the breaking point are reproduced in greater detail and on a larger scale in figure 4 where the time interval separating successive profiles is $T/48$, the vertical segment on the left side of this figure representing the amplitude in infinite depth.

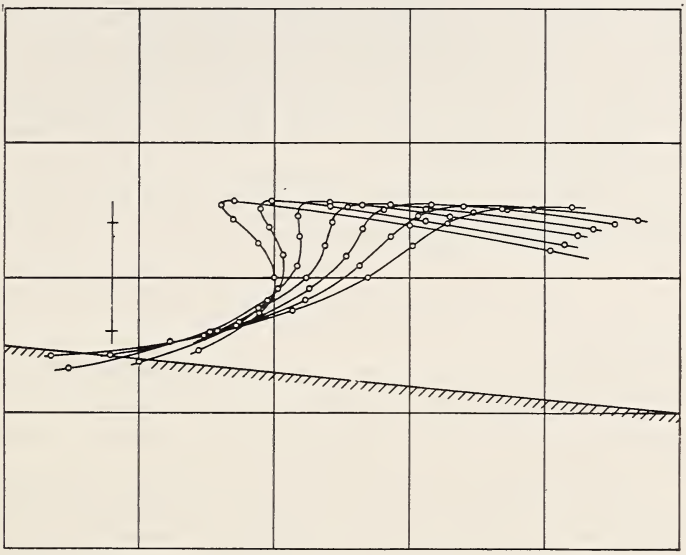

FIGURE 4. *Details of breaking of wave shown in figure 3.*
First-order theory.

The great rapidity with which the waves change near the breaking point can be seen in this figure. On a scale model, where the waves have, for example, a 1-second period (approximately 5 feet long in infinite depth), the time interval between two successive positions shown in figure 4 would be only one fiftieth second. It is evident that the analysis of such a rapidly changing phenomenon cannot be made by direct observation.

With full-scale waves, the evolution would, of course, be much slower.

There is, thus, a surprisingly good qualitative agreement between the shapes of real waves and the profiles given by the theory. It must be pointed out that, although the results obtained are satisfactory in appearance, the theory is only a first approximation and as yet unfit for the study of the actual breaking as, at this point, our assumptions are no longer valid for two reasons:

1. The wave steepness is far from being infinitely small, and the theories of the first order in the amplitude are therefore of uncertain accuracy.

2. The relative depth is small; this lessens the validity of the approximations for two reasons. It is known, first of all, that the terms of higher order than the first become more important as the depth decreases; the same is also true for terms in α of greater order than the first. The

approximations made herein thus rapidly lose their validity and become incorrect when the depth decreases. The results concerning waves on the point of breaking are therefore more of a qualitative nature than of a quantitative one.

The preceding theory may be improved by taking into account terms of the order of a^2. Keeping to the same order of approximation in α as before, this may lead to the introduction of terms of the order of αa^2. Such terms could probably be computed in much the same way as for those of the order of αa, but this calculation, if not particularly difficult, would be very long. It is, however, possible to introduce terms of the order of a^2, neglecting terms of the order of αa^2, without any further theoretical analysis, because the former terms are identical with the corresponding ones for constant-depth waves.

This procedure can be justified theoretically by assuming that a and α are small quantities of the same order, and that calculations are effected only to the second order of approximation.

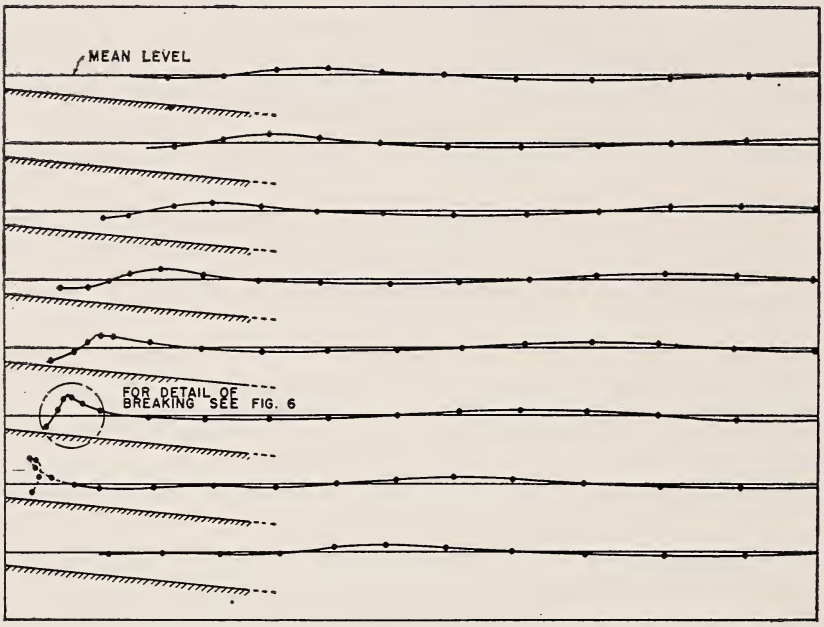

FIGURE 5. *Progression and breaking of a wave on a beach of 1 in 10 slope.*
Second-order theory.
Eight successive phases at intervals of T/8. Steepness approximately 1/80.

The introduction of the "classical" second-order terms in the calculation gives rise to important changes in the final results.

By way of comparison the motion of the same wave as given in figures 3 and 4 has been drawn in figures 5 and 6, using the second-order equations just spoken of. The second-order profiles differ from the first-order profiles in the following ways:

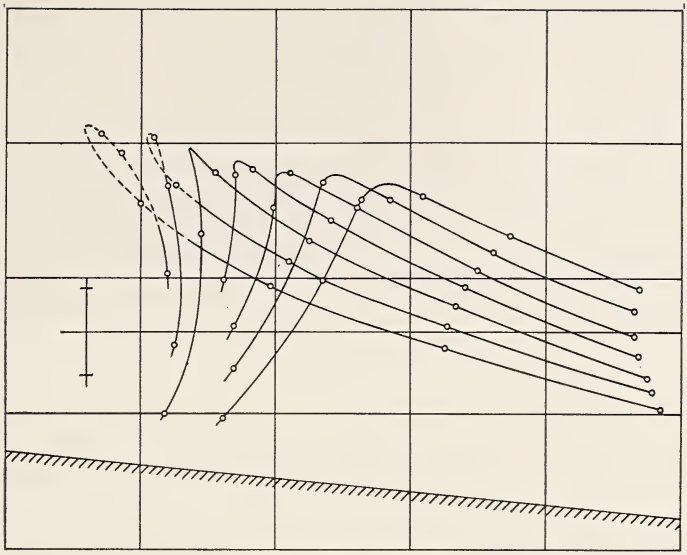

FIGURE 6. *Details of breaking of wave shown in figure 5.*
Second-order theory.

1. Breaking seems to take place earlier in (a greater depth).
2. The height of the wave at breaking point is much greater.
3. The tendency of the theoretical profile to plunge into the sea bed, after the breaking point is greatly reduced.

A systematic comparison of the first- and second-order theories with experiment remains to be made, but preliminary checks show that, in many cases, agreement seems to be good even near the breaking point.

29. Methods Used at the National Hydraulic Laboratory of Chatou (France) for Measuring and Recording Gravity Waves in Models

By J. Valembois[1]

In the study of gravity waves at the Laboratory, for the experimental verifications of theoretical results as well as for the study of particular problems, it is necessary to have available means for measuring and recording waves under the best possible conditions.

After having tried various procedures, the National Hydraulique Laboratory of Chatou has settled on two methods that complement each other, and which, in most cases, permit the carrying out of the measurements with all the precision required.

1. The "Starred-Sky" Method

1.1 Principle

This method, due to Mr. Barrillon, Ingénieur Général du Génie Maritime, makes it possible in studies of harbor installations to obtain with much less delay a single photograph giving a general scheme of the movement in the model. It is susceptible of giving good precision, but experience has shown us that its interest lies chiefly in the possibility of comparing the effects of various constructions very rapidly, and therefore of trying a large number of tests at small cost.

The principle is very simple. Above the model is placed a grid of luminous points, the image of which is photographed in the mirror formed by the surface of the water. If this is motionless, the image of each point is a fixed point. If the surface of the water is disturbed by a periodic motion (wave, seiche), it is periodically deformed and the images of the luminous points during the passage of each wave describe closed curves the form and amplitude of which give immediate information on the movement of the water.

For a simple progressive wave, each point describes a segment of a straight line in the direction of propagation of the wave, its length being proportional to the amplitude.[2]

Figure 1b corresponds to a pure clapotis, figure 1c to a composite swell, for which the trajectories are circles or ellipses.

One can obtain an analogous result by sprinkling the surface with small

[1] Laboratoire Nationale d'Hydraulique de Chatou, France.
[2] The perspective view requires corrections, which are explained later.

floats or confetti, but in this case the general currents, which are added to the periodic movement, confuse the images obtained. Again, the floats have a tendency to clump together and their inertia cannot be negligible.

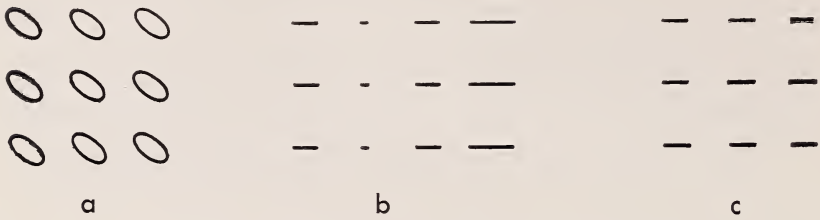

FIGURE 1. *Images of illuminated points for simple waves.*

1.2 Formula Permitting the Determination of the Inclination of the Water Surface From the Displacements of the Luminous Points

Consider a liquid surface, a luminous point L at the height z, a camera P at the height Z. I is the image of L viewed from P when the water surface is undisturbed, D the distance of p (the projection of P on the water surface) from I.

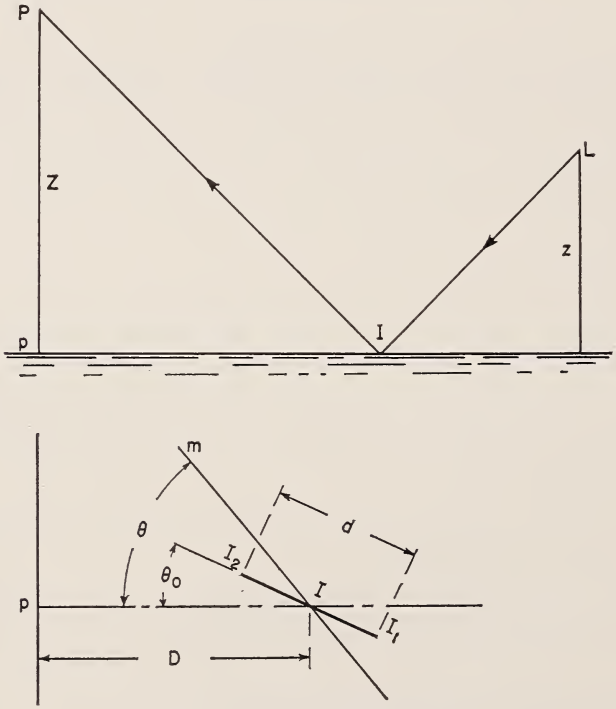

FIGURE 2. *Diagram of light reflection.*

Suppose that the slope of the tangent plane at I to the liquid surface varies from $+\alpha$ to $-\alpha$, the line of slope Im of the plane making the angle θ (in projection on the plane of the water) with pI. If we are dealing with a swell, Im is its direction of propagation.

The image of the luminous point, viewed from P, will go, at the level of the plane of the water, from I_1 to I_2 in passing through I. On the photograph, one measures $I_1I_2=d$ and the angle θ_0 between pI and I_1I_2. A simple calculation[3] shows that one can deduce θ and α from θ_0 and d by means of the following formulas

$$\left.\begin{aligned} \theta &= f(\theta_0, D/Z), \\ \alpha &= \left(1+\frac{Z}{z}\right)\frac{d}{4Z}xk(\theta_0, D/Z). \end{aligned}\right\} \tag{1}$$

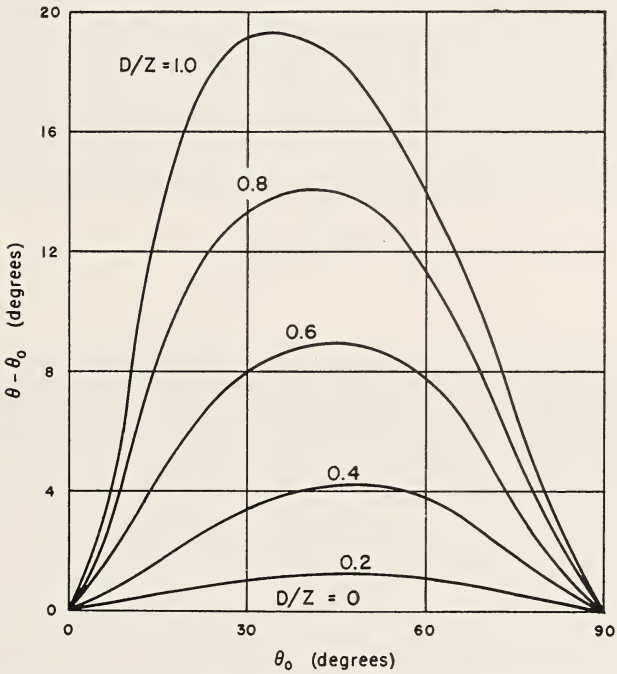

FIGURE 3. *The angle $\theta-\theta_0$ as a function of the angle θ_0 and the ratio D/Z.*

The graphs in figures 3 and 4 give $\theta-\theta_0$ and k as functions of θ_0 and D/Z. According as one deals with a swell or with a clapotis, the figures present some slight difference with which we will not concern ourselves, because

[3] For

$$\theta=0, \theta_0=0, \text{ and } \alpha=\left(1+\frac{Z}{z}\right)\frac{d}{4Z}\left(1+\frac{D^2}{Z^2}\right)$$

$$\theta=\pi/2, \theta_0=\pi/2 \text{ and } \alpha=\left(1+\frac{Z}{z}\right)\frac{d}{4Z}.$$

For intermediate values of θ, the composition of two displacements along rectangular axes parallel to $\theta=0$ and $\theta=\pi/2$ permits the calculation of the values of θ_0 and α.

a long use of this method has shown us that it is of special interest when a detailed analysis of the movement of the water at each point is less important than the overall determination of the movement in the model.

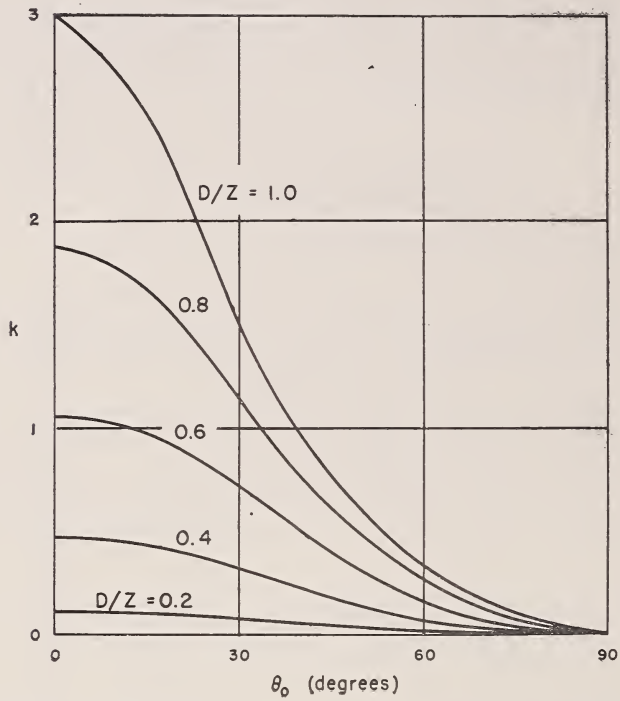

FIGURE 4. *The factor k as a function of the angle θ_0 and the ratio D/Z.*

1.3 Practical Realization

At Chatou, the "starred sky" is constructed of square elements that can be placed together. Electric lights can be placed in each element to form the pattern of luminous points desired. Current for the lamps is obtained from a grid of metallic bars supported on two parallel frames electrically insulated.

One should, naturally, determine the heights of the "starred sky" and of the camera above the water as a function of the waves that one wishes to detect, in such a fashion that, for the greatest curvatures of the liquid surface, each luminous point will correspond to only one single reflected point.

Examples. Figures 5, 6, 7, and 8 relate to the study of the protection of the port of Quiberon against swells. One sees the difference in the motion in the harbor according as the channel is closed or not, and the slight advantage gained by the additional breakwaters in figure 6. (Actual periods 8 and 9 seconds).

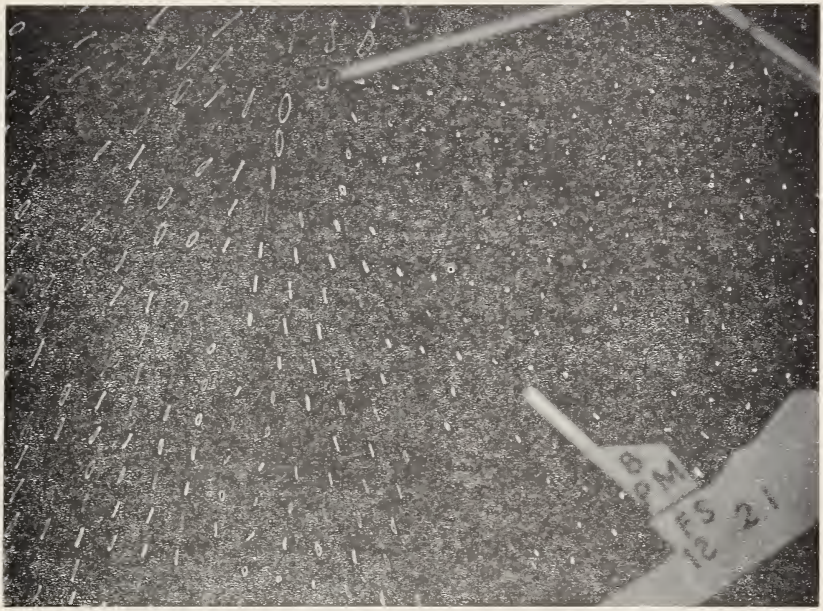

FIGURE 5. *Observations in model of the port of Quiberon.*
Channel closed.

FIGURE 6. *Observations in model of the port of Quiberon.*
Channel open.

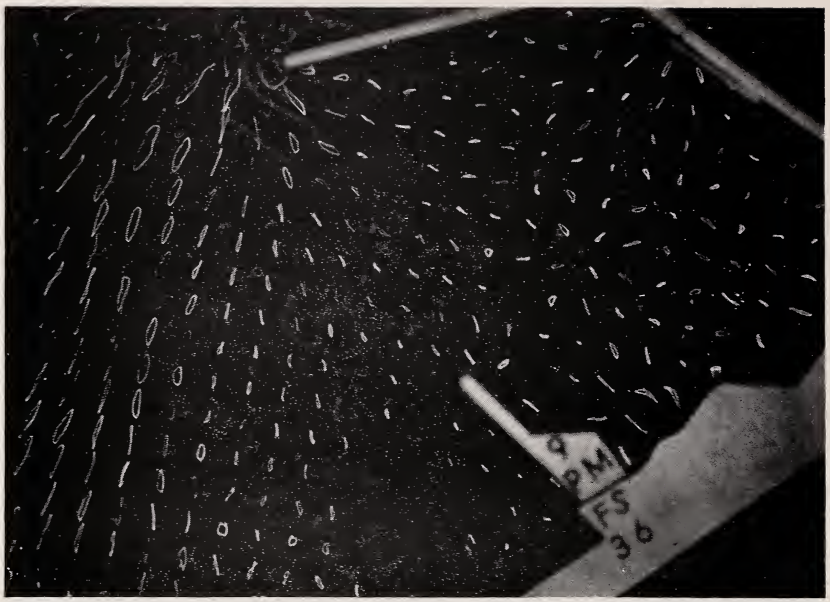

FIGURE 7. *Observations in model of the port of Quiberon, with additional breakwaters.*
Channel closed.

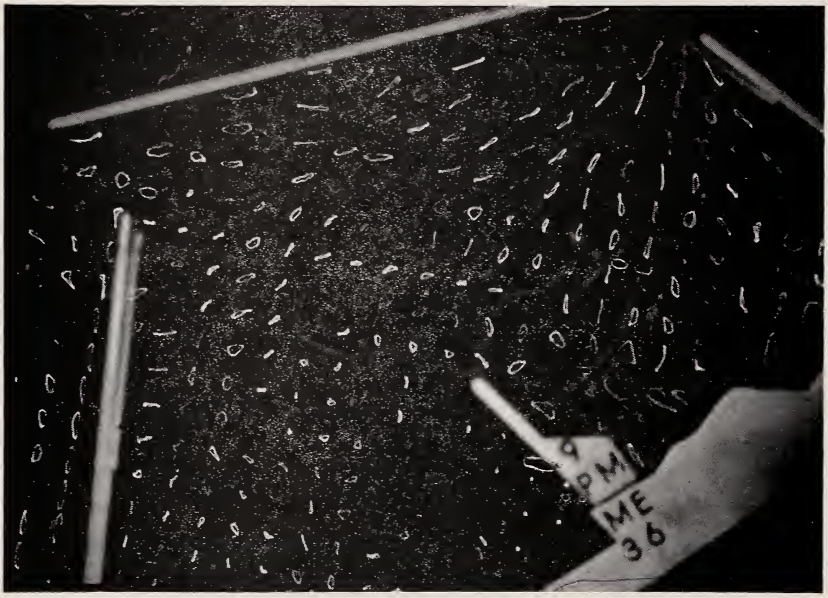

FIGURE 8. *Observations in model of the port of Quiberon, with additional breakwaters.*
Channel open.

2. Limnigraph With Vibrating Point

2.1 Principle of the Level Detector

This apparatus is one application of the detection of level by a vibrating point, conceived and recently placed in operation at Chatou.[4] It permits the recording of very rapid variations in level with great precision.

A fine platinum needle is made to vibrate vertically. If the water surface whose level, one wishes to measure or record is between the two limits of oscillation of the needle's point, this level is characterized by the fraction of the period of oscillation during which the needle is in contact with the water.

To avoid the effects of surface tension and the entrainment of small drops of water by the needle, one must make it vibrate with sufficient rapidity. Experience has shown that the electric-current frequency (50 cycles a second in Europe) is perfectly suitable. To vibrate the needle we use a loud-speaker motor driven by 50-cycle current and provided with an auxiliary device for centering.

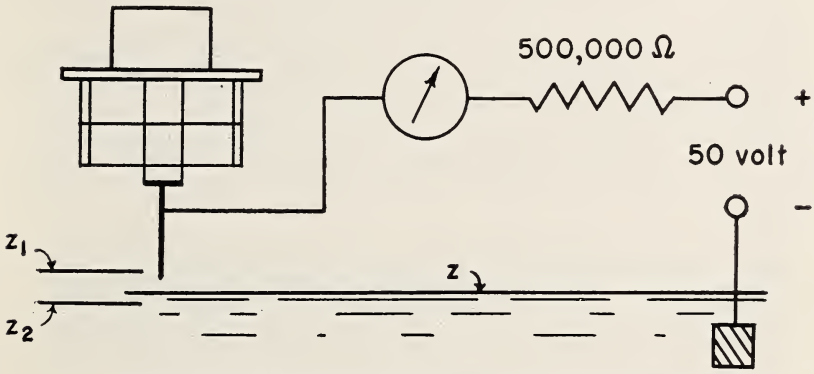

FIGURE 9. *Sketch of electric circuit for limnigraph with vibrating point.*

The following example shows a simple method of using the procedure for measuring a static water level (fig. 9). The interrupter formed by the needle and the water is inserted in a direct-current electric circuit. In the example chosen, the current is $100\mu A$ in the circuit during the time, t, when the point is in contact with the water at each period T. The average current that passes through the microammeter and that this integrates is then $100\mu A\ t/T$. The curve in figure 10 gives the value of the current as a function of the level of the water; z_0 and z, being the limits of the sinusoidal oscillation of the lower extremity of the point. One sees that there exists a practically linear relation between the measured current and the level as long as it stays within the zone indicated by cross-hatching, which corresponds practically to two-thirds of the amplitude of vibration.

[4] Brevet français no. 578.615 P.V. U. S. patent applied for. See "La Houille Blanche," no. spécial B 1950, H. Gridel: "La mesure précise et l'enregistrement des niveaux stables ou fluctuants au moyen de pointes limnimétriques à vibrations entretenues."

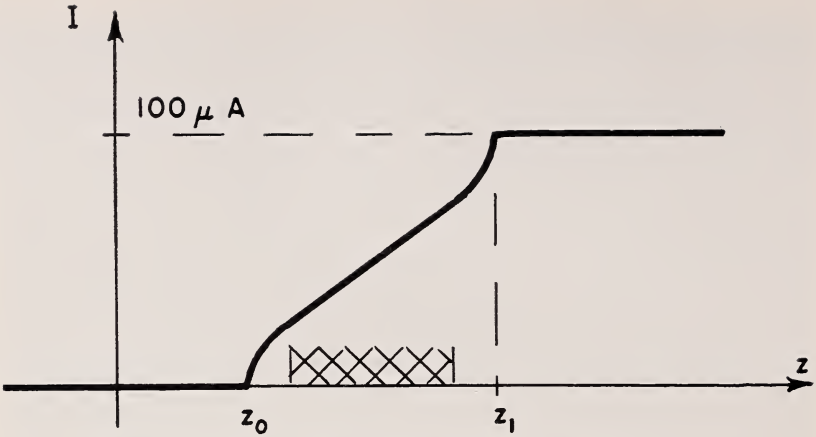

FIGURE 10. *Current in limnigraph circuit as function of the water level:*

2.2 Limnigraph With Vibrating Point

The above arrangement does not give sufficient power for operating a graphical recorder directly, so an amplifying relay specially designed for good response is used. With this procedure, liquid waves can be recorded with frequencies up to 10 a second. This frequency can be increased for recording capillary waves by making the needle vibrate more rapidly and by using a graphical recorder with greater rapidity of response.

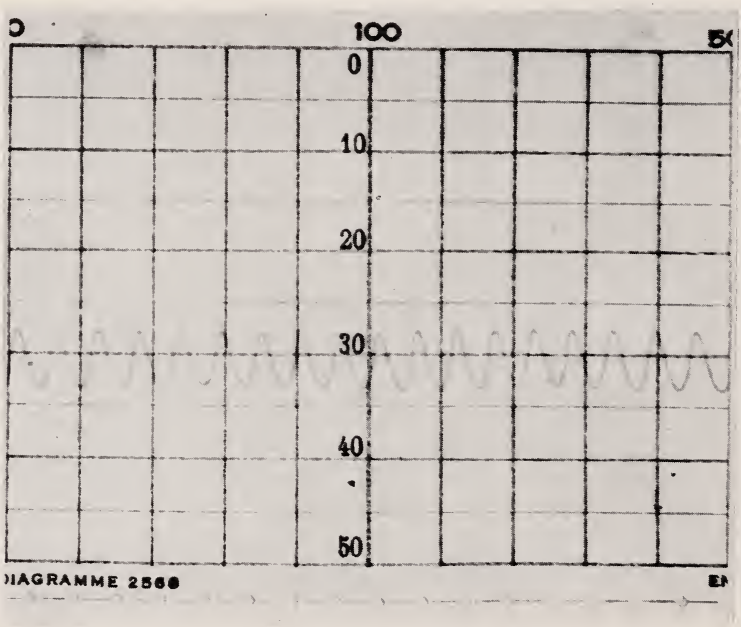

FIGURE 11. *Record of simple wave in model of the port of Quiberon.*

Actually, one is limited, in the maximum amplitude of waves to be recorded, to about 5 mm. An arrangement is under study with a view to permitting the recording of larger waves (several centimeters).

The sensitivity is regulated by the amplitude given to the vibration. At maximum sensitivity of the apparatus constructed at Chatou, 1/100 mm is represented on the diagram by 2 to 3 mm. The stability of the measurement is assured at least to 1/100 mm.

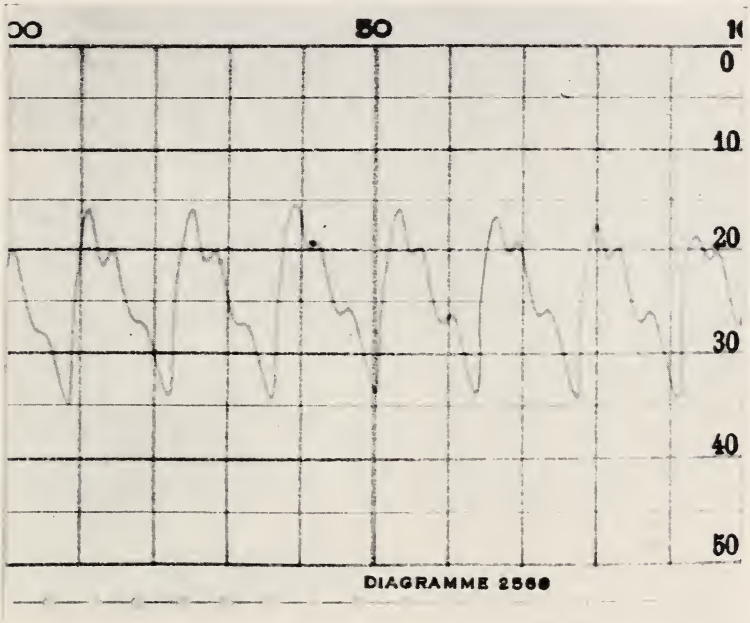

FIGURE 12. *Record of complex wave in model of the port of Quiberon*

2.3 Example of Records of Swells at the Laboratory

The records presented in figures 11 and 12 have been obtained in the model of the port of Quiberon.

30. The Slope of Lake Surfaces Under Variable Wind Stresses

By Bernhard Haurwitz [1]

Abstract

It has been observed that the inclination of a lake surface caused by a wind stress shows a distinct time lag in adjusting itself to changing winds. To analyze this phenomenon, use is made of the hydrodynamic equations that are simplified by integrating over the whole depth of the lake so that the total horizontal water transport in each water column, rather than the velocity at each depth separately, is considered. The resulting equation governing the motion of the water is closely related to the equation for seiches, the essential difference being an additional term representing the effect of the wind stress acting on the water surface.

It is found that the time required by the lake to respond to changing wind stresses depends on the lengths of the seiche periods, which, in their turn, depend on the vertical and horizontal dimensions of the lake. Such a dependence of the rapidity with which the lake level adjusts itself to the variable wind can be expected a priori.

Particular attention is given to the case of a wind which changes its direction. Such a wind shift took place during the passage of the hurricane of 26–27 August 1949, over Lake Okeechobee, Fla. During this time very detailed observations were obtained by the Corps of Engineers, U. S. Army, Jacksonville Florida District, in cooperation with the U. S. Weather Bureau. These observations comprise, among others, wind speed and direction and water-surface contours during intervals of half an hour while the hurricane center moved over the northeastern part of the lake. In conjunction with the passage of the hurricane center the wind turned rapidly counterclockwise through about 180° during a time of roughly 3 hours. This turning of the wind was accompanied by a turning of the isohypses of the lake surface, but the latter rotated more slowly than the wind direction, so that for some time the wind blew parallel rather than perpendicular to the isohypses It is shown that the theory explains this behavior of the lake surface.

[1] New York University, New York, N. Y.

31. The Tide in an Enclosed Basin

By W. B. Zerbe [1]

The surface of the water in an enclosed basin tends to remain perpendicular to the plumb line. But the direction of the plumb line does not remain fixed with respect to the rigid Earth. It is affected by the attraction of the Sun and Moon, that is, by the tide-producing forces. Since the tilt of this surface is determined by the tide-producing forces, its motion conforms to tidal periods and can be computed. The tangent of the angle of deflection of the plumb line, and hence that of the tilt of the water surface, is equal to the ratio of the horizontal component of the tide-producing force to the acceleration g of gravity.

The formula involving the horizontal component of the tide-producing force is developed, providing the means of computing for any time the angle of tilt in a vertical plane in any desired azimuth. The maximum value of this angle (semirange of surface oscillation) is about 0.022″ due to the Moon and 0.009″ for the Sun. Observations made in 1947 of the tide in the David Taylor Model Basin are discussed and show that the observed oscillation is less than that computed by the formula. The ratio of observed to computed tilt is about 0.75, which is in agreement with results obtained by other observers using other methods. The failure of the observed tilt to equal that computed for a rigid Earth is accounted for by the fact that the observed tilt is measured with respect to the Earth's surface, which also tilts, for the Earth itself yields to the tidal forces and is affected by the varying load of tidal water on the nearby coast.

This discussion pertains only to relatively small basins enclosed by rigid boundaries as opposed to oceanic basins, which are usually large and bounded at least in part by other water areas.

The surface of the water in such an enclosed basin—whether it be a lake or a teacup—tends to remain level; that is, it tends to adjust itself everywhere perpendicular to the plumb line. But the direction of the plumb line does not remain fixed with respect to the rigid Earth. It is affected by the attraction of the Sun and Moon—that is, by the tide-producing forces. A surface that remains normal to the forces acting upon it is an equilibrium surface.

Over a large area, this terrestrial surface of equilibrium will be a curved surface, but for a basin even as large as one of the Great Lakes, it can be treated as a plane surface for our purpose without introducing material error, which simplifies matters considerably.

Since the tilt of this plane is determined by the tide-producing forces, its motion conforms to tidal periods. Whether the water surface in a particular basin can thus continually adjust itself parallel to the equilibrium surface depends upon whether the basin is deep enough for a long wave to travel from one end to the other within the tidal period. The formula for the velocity of a long wave is

$$v=\sqrt{gd}, \tag{1}$$

where g is the acceleration of gravity, and d is the average depth of the basin.

[1] U. S. Coast and Geodetic Survey, Washington, D. C.

Figure 1 depicts in a rather simplified way what happens to the surface of the water in a basin under the influence of the lunar tide-producing force. In this figure, we are looking down from above the North Pole. The basin is located on the Equator and the Moon is over the Equator. The Earth is depicted as a circle undisturbed by the tide-producing forces (though we will later see that it also yields somewhat). We will not be concerned with the more or less permanent deformation of the Earth due to the centrifugal force of the Earth's rotation, since we may assume that the disturbance of this spheroidal surface by the tidal forces will not differ materially from the disturbance of a true spherical surface due to the same forces.

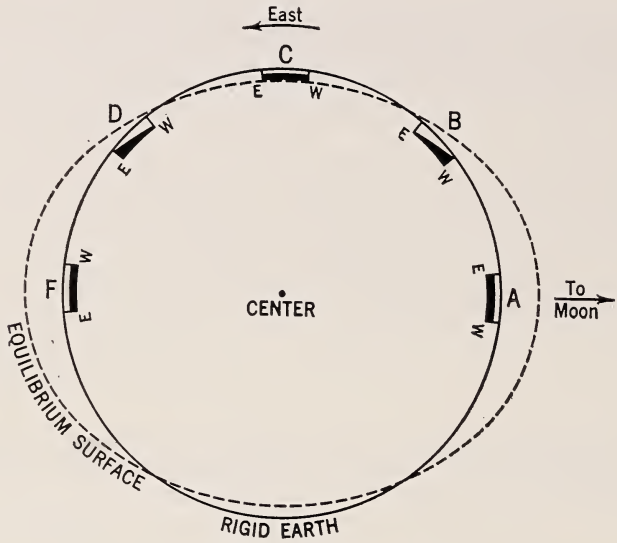

FIGURE 1. *Equatorial cross section.*

As the Earth rotates, the water in a basin oscillates with respect to the Earth while remaining parallel to the equilibrium surface.

The surface of equilibrium is ellipsoidal. If the surface of the water in the basin remains normal to the plumb line, it will be parallel to this surface, and as the Earth rotates, it will oscillate as shown. At position A it will be parallel to the Earth's surface (or parallel to the top edge of the basin); at position B it will be high in the west end; at C it will again be parallel to the top of the basin; and at D it will be low in the west end. At F it will again be parallel to the top of the basin, and during the next half day the oscillation will be repeated. The picture will be varied in some degree by the declination of the Moon and by having the basin in other latitudes, as well as by introducing the Sun.

Now the plumb line remains perpendicular to the surface of the water in the basin, and it will be seen that at position A it is also perpendicular to the surface of the Earth and therefore points to the center of the Earth. This is also true at C. At intermediate points, such as at B, the plumb line is deflected.

It is through the horizontal component of the tide-producing force that we can account for the deflection of the vertical. The angle of

deflection of the vertical is also the angle of tilt of the surface of the water in the basin. We will call this angle θ.

It is common in tidal work to speak of the tide-producing acceleration as a force, which is satisfactory if we consider the acceleration as acting on unit mass. This force is directed toward the attracting body at all points on the Earth's hemisphere nearest that body. At all points on the other hemisphere, it is directed toward an opposite point. Point C is on the dividing line, and at this point there is no horizontal component of the tide-producing force. At A the total force is vertical, so that there is no horizontal component there either. At all points on the Earth's surface between A and C, the force will be oblique to the surface, and it will have a horizontal component.

The tangent of the angle of deflection of the plumb line is equal to the ratio of the horizontal component of the tide-producing force to the acceleration of gravity. Though g minus the vertical component of the tide-producing force is a more accurate value for actual acceleration of gravity than g alone, this refinement will change the value of the tangent by less than 1×10^{-14}, so that the use of g alone is adequate considering the size of the quantities involved.

Let us now develop a formula for the horizontal component of the tide-producing force, and this will give us immediately the tangent of the angle θ. So far as practicable, we will use the notation and method used by Schureman in his "Manual of the Harmonic Analysis and Prediction of Tides."

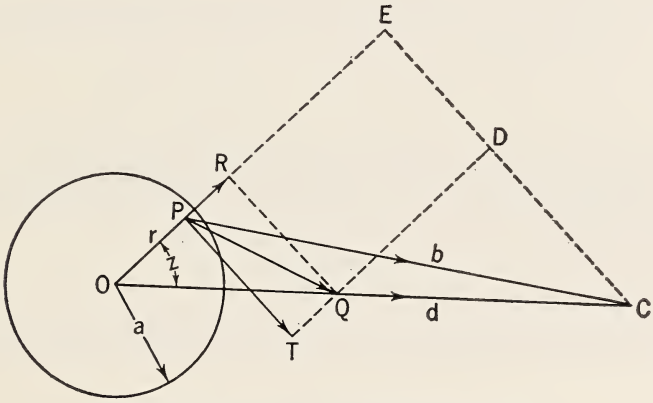

FIGURE 2. *Diagram of tide-producing forces.*

The tide-producing force is represented graphically in figure 2, where

O is the center of the Earth,
C is the center of the Moon,
P is any point within or on the surface of the Earth,
$b=PC=$distance of point P from center of Moon,
$d=OC=$distance of center of Earth to center of Moon,
$r=OP=$distance of point P from center of Earth,
$a=$mean radius of Earth, and
$z=<COP$, the zenith distance of the Moon.

OC and PC will represent the direction of the attraction of the Moon at points O and P. If in the same figure we take PC as representing the magnitude of the attraction at P, we can represent the magnitude of the attraction at O by a line QC taken of such length that

$$\frac{QC}{PC}=\frac{\overline{PC}^2}{\overline{OC}^2}, \tag{2}$$

since attraction varies inversely as the square of the distance.

The tide producing force at any point is the difference in attraction that tends to change the position of a particle at that point with respect to the Earth as a whole. The Earth can be considered as concentrated at its center O. According to figure 2, the point O is acted upon by attraction QC, and the point P is acted upon by attraction PC, which can be resolved into components PQ plus QC. Because QC is an identical attraction acting upon O and P, it will not change the position of one with respect to the other. That leaves PQ as the difference in attraction that tends to alter the position of P with respect to O and is the tide-producing force of the Moon at P. The force PQ may be resolved into the vertical and horizontal components PR and PT, respectively.

Now let

θM = mass of Moon,

E = mass of Earth,

μ = Constant of gravitation, or attraction between unit masses at unit distance,

g = Mean acceleration of gravity at Earth's surface.

Because gravitational attraction varies directly as the masses of the attracting bodies and inversely as the square of the distance between them, the magnitude of the attraction of the Moon for unit mass at point O in the direction OC is

$$QC=\frac{\mu M}{d^2}, \tag{3}$$

and the attraction of the Moon for unit mass at point P in direction PC is

$$PC=\frac{\mu M}{b^2}. \tag{4}$$

We can resolve these attractions into vertical and horizontal components, but here we are concerned only with the horizontal. The horizontal components will be taken perpendicular to the line OP in the plane OPC with the positive direction being in the azimuth of the Moon. Then, from eq 3 and 4 and figure 2,

$$\text{Horizontal component of attraction at } O=DC=\frac{\mu M}{d^2}\sin z. \tag{5}$$

$$\text{Horizontal component of attraction at } P=EC=\frac{\mu M}{b^2}\sin CPR. \tag{6}$$

The horizontal component PT (which we will call F) of the tide-producing force PQ is equal to ED, which is the difference between eq 5 and 6. Then

$$F=PT=ED=\mu M\left(\frac{\sin CPR}{b^2}-\frac{\sin z}{d^2}\right). \tag{7}$$

From the plane triangle COP, we can obtain the relation

$$b^2=r^2+d^2-2rd\cos z=d^2\left[1-2\frac{r}{d}\cos z+\left(\frac{r}{d}\right)^2\right], \tag{8}$$

and

$$\sin CPR=\sin CPO=\frac{d\sin z}{b}=\frac{\sin z}{\left[1-2\frac{r}{d}\cos z+\left(\frac{r}{d}\right)^2\right]^{\frac{1}{2}}}. \tag{9}$$

Substituting in eq 7 values of b and $\sin CPR$ from eq 8 and 9, we obtain

$$F=\frac{\mu M}{d^2}\left\{\frac{\sin z}{[1-2(r/d)\cos z+(r/d)^2]^{\frac{3}{2}}-\sin z}\right\}. \tag{10}$$

Since

$$g=\frac{\mu E}{a^2},\quad \text{then } \mu=\frac{ga^2}{E}. \tag{11}$$

Substitute eq 11 in eq 10 and transpose g, because it was seen that the tangent of the angle of tilt, θ, of the water in a basin equals F/g. We have then

$$\tan\theta=\frac{F}{g}=\frac{M}{E}\left(\frac{a}{d}\right)^2\left\{\frac{\sin z}{[1-2(r/d)\cos z+(r/d)^2]^{\frac{3}{2}}-\sin z}\right\}. \tag{12}$$

Formula 12 represents completely the horizontal component of the lunar tide-producing force at any point in the Earth. If the point is on the Earth, then r will equal a, leaving only two variables, the Moon's zenith distance z and the sine of its horizontal parallax a/d. It is still a rather complicated formula, however, and it can be simplified by expanding the quantity with the fractional exponent as a binomial into a series of terms arranged according to ascending powers of r/d. Thus

$$\begin{aligned}\frac{1}{[1-2(r/d)\cos z+(r/d)^2]^{\frac{3}{2}}}=1&+3\cos z(r/d)\\&+3/2(5\cos^2 z-1)(r/d)^2\\&+5/2(7\cos^3 z-3\cos z)(r/d)^3\\&+\ldots\end{aligned} \tag{13}$$

The ratio r/d has, for the Moon, a maximum value of 0.018. Neglecting the cube and higher powers of r/d, we substitute eq 13 in eq 12. Then if we limit the discussion to points on the Earth's surface, r becomes the mean radius a, and we obtain the formula shown in eq. 14.

$$\begin{aligned}\tan\theta=F/g=&(3/2)(M/E)(a/d)^3\sin 2z+\\&(3/2)(M/E)(a/d)^4\sin z(5\cos^2 z-1).\end{aligned} \tag{14}$$

This represents the lunar portion of the tide-producing force. The solar portion will be obtained by substituting solar for lunar values in eq. 14. The first term, which involves the cube of the parallax, represents about 98 percent of the lunar force and an even higher percentage of the solar force. The second term, which involves the fourth power of the parallax is of little practical importance. It is interesting to note that, of the many harmonic constituents commonly used in tide prediction, only the relatively unimportant and seldom used M_3 is derived from the second term of eq 14, all others being derived from the first term. At this point then we will drop the second term of eq 14 and continue the development of the first term only.

The positive direction is in the azimuth of the Moon, and this first term has its maximum positive value when $z=45°$ and an equal maximum negative value when $z=135°$. It is zero when $z=0°$, 90°, or 180°. Extreme values of F/g, obtained when the Moon and Sun are nearest the Earth and $z=45°$, are

$$1.05\times10^{-7} \text{ for the lunar portion,} \tag{15}$$

and

$$0.41\times10^{-7} \text{ for the solar portion.} \tag{16}$$

The corresponding maximum value of angle θ is then about 0.022″ due to the Moon and 0.009″ due to the Sun. The angle θ is the tilt of the surface of the water from its mean position, hence the semirange.

A difficulty in the use of formula 14 arises from the fact that the force is in the azimuth of the Moon (or Sun), and therefore the angle θ is in the vertical plane that is also in the azimuth of the attracting body,—and this azimuth is continually changing. Moreover, the azimuths of the Sun and Moon at any instant are seldom the same. The values in eq 14 are usually wanted for some fixed azimuth, such as that of a basin. In adapting the formula to this purpose we will complicate the formula somewhat, while greatly improving its usefulness.

We will first resolve the force represented by the first term in eq 14 into south and west components and from them derive a formula for force in any desired azimuth. Letting subscripts s and w designate south and west components, respectively, and A designate the azimuth of the Moon, then

$$F_s/g=(3/2)(M/E)(a/d)^3 \sin 2z \cos A, \tag{17}$$

$$F_w/g=(3/2)(M/E)(a/d)^3 \sin 2z \sin A. \tag{18}$$

Although we will not go into the detail of their derivation, the following formulas are readily derived from a consideration of the celestial sphere, in which Y=latitude of the observation point, D=declination of the Moon, t=hour angle of the Moon.

$$\cos z=\sin Y \sin D+\cos Y \cos D \cos t. \tag{19}$$

$$\sin z \cos A=-\cos Y \sin D+\sin Y \cos D \cos t. \tag{20}$$

$$\sin z \sin A= \cos D \sin t. \tag{21}$$

Multiplying eq 20 and eq 21 by the value of $2 \cos z$ from eq 19, we obtain

$$\sin 2z \cos A = (3/4) \sin 2Y[(2/3) - 2 \sin^2 D] - \cos 2Y \sin 2D \cos t \tfrac{1}{2} \sin 2Y \cos^2 D \cos 2t \tag{22}$$

$$\sin 2z \sin A = \sin Y \sin 2D \sin t + \cos Y \cos^2 D \sin 2t. \tag{23}$$

Substituting these values in eq 17 and eq 18, we have

$$\begin{aligned}\tan \theta_s = F_s/g = {} & (9/8)(M/E)(a/d)^3 \sin 2Y[(2/3) - 2 \sin^2 D] \\ & - (3/2)(M/E)(a/d)^3 \cos 2Y \sin 2D \cos t \\ & + (3/4)(M/E)(a/d)^3 \sin 2Y \cos^2 D \cos 2t\end{aligned} \tag{24}$$

$$\begin{aligned}\tan \theta_w = F_w/g = {} & (3/2)(M/E)(a/d)^3 \sin Y \sin 2D \sin t \\ & + (3/2)(M/E)(a/d)^3 \cos Y \cos^2 D \sin 2t\end{aligned} \tag{25}$$

If we let α designate any desired azimuth, then

$$\tan \theta_\alpha = F_\alpha/g = F_s/g \cos \alpha + F_w/g \sin \alpha. \tag{26}$$

Formula 26 shows that the horizontal force in the desired azimuth, or the tangent of the angle θ in the vertical plane in the desired azimuth, will be obtained by multiplying the terms of eq 24 by $\cos \alpha$ and those of eq 25 by $\sin \alpha$ and then combining them. This now permits the calculation of the angle of tilt along the axis of any basin for each hour or for any time desired. The second term of eq 24 can be made positive if desired by substituting $(t+180°)$ for t.

Formula 26 can be developed into a series of cosine terms representing the harmonic tidal constituents. We will omit the development but will show the final formula so that amplitudes and epochs of the harmonic constituents can be computed for use in predicting or for comparison with the harmonic constants obtained by analysis of observations. The formula is

$$\begin{aligned}\tan \theta_\alpha = F_\alpha/g = {} & (9/8)(M/E)(a/c)^3 P_0 \sum fC \cos E \\ & + (3/2)(M/E)(a/c)^3 P_1 \sum fC \cos (E - \kappa_1) \\ & + (3/2)(M/E)(a/c)^3 P_2 \sum fC \cos (E - \kappa_2).\end{aligned} \tag{27}$$

in which a/c is the mean parallax, and the value of $(M/E)(a/c)^3$ is 0.5582×10^{-7}. The equivalent expression for the Sun equals 0.2569×10^{-7}; f is the factor by which the mean amplitude of a lunar constituent is multiplied to obtain the amplitude for a particular year; the 18.6-year lunar variation, due to the variation in the obliquity of the Moon's orbit, is taken care of in this way. For solar constituents the value of f is unity; C is the mean coefficient of the constituent; E is the constituent argument, often given as $V+u$;

$$P_0 = \sin 2Y \cos \alpha; \tag{28}$$

$$P_1 = (\cos^2 2Y \cos^2 \alpha + \sin^2 Y \sin^2 \alpha)^{\frac{1}{2}}; \tag{29}$$

$$P_2 = \cos Y (\sin^2 Y \cos^2 \alpha + \sin^2 \alpha)^{\frac{1}{2}}; \tag{30}$$

$$\text{Epoch } \kappa_1 = \tan^{-1}\left(\frac{\sin Y \sin \alpha}{-\cos 2Y \cos \alpha}\right); \tag{31}$$

$$\text{Epoch } \kappa_2 = \tan^{-1}\left(\frac{\sin \alpha}{\sin Y \cos \alpha}\right). \tag{32}$$

The formulas for epoch assume an absence of lag due to friction or inertia. The values of f, C, and E for each constituent are readily obtained from tables in any manual on tide prediction.

The last term of eq 27 represents the semidiurnal constituents and is derived from the last terms of eq 24 and 25, which are functions of $2t$. The second term of eq 27 is derived from the terms of eq 24 and 25, which are functions of t and represents the diurnal constituents. The first term of eq 27 is derived only from the first term of eq 24 and represents the long-period constituents that have periods of a fortnight or more. They do not depend upon the Earth's rotation but vary only with parallax and declination. There is no west component of the long-period variation.

Observations in the David Taylor Model Basin

Observations of the tidal oscillation in the David Taylor Model Basin were made in 1947 and were reported upon in the Transactions of the American Geophysical Union. Observations of water level were made every half-hour in both the east and west ends of the basin during the 7-day period from September 8 to 15, 1947. The gages were near the ends of the basin and 2668 feet apart. The basin was 52 feet wide and 22 feet deep. The long dimension of the basin was oriented in a W16°N to E16°S direction. The basin is near Washington, D. C., in latitude 38°58′30″N. and longitude 70°11′30″W.

A plotting of the observations made at each gage is shown in figure 3. The original setting of the gages was arbitrary so that the distance between the two sets of readings on the graph has no significance. There is a general downward drift due to several possible causes that are not tidal. The semidiurnal tidal oscillation with a diurnal inequality is clear. When the water rose in one end of the basin, it fell in the other. The range of the oscillation increased during the period as the Moon progressed from quadrature to a new Moon in perigree. The observational period was not long enough to bring out the long-period variations.

To compare the observed tide to the tide as computed by formula, the observations were reduced to a horizontal datum by scaling the readings from the sloping mean level line and replotting them using a horizontal line as mean level. The original mean level was found by averaging 50 consecutive half-hourly observations, which cover about a tidal day, plotting the mean at the midpoint of the group, and then moving along hour by hour, repeating the process.

Because the tide at the east end should be just the reverse of that at the west end, we concentrated on the tide at the west end and removed some of the irregularities from the observations by inverting the curve for the east end and averaging it with the one for the west end. The curve for the west end for the 2 days September 12 and 13, processed in this way, is shown in figure 4. The computed curve is shown in the same figure for comparison.

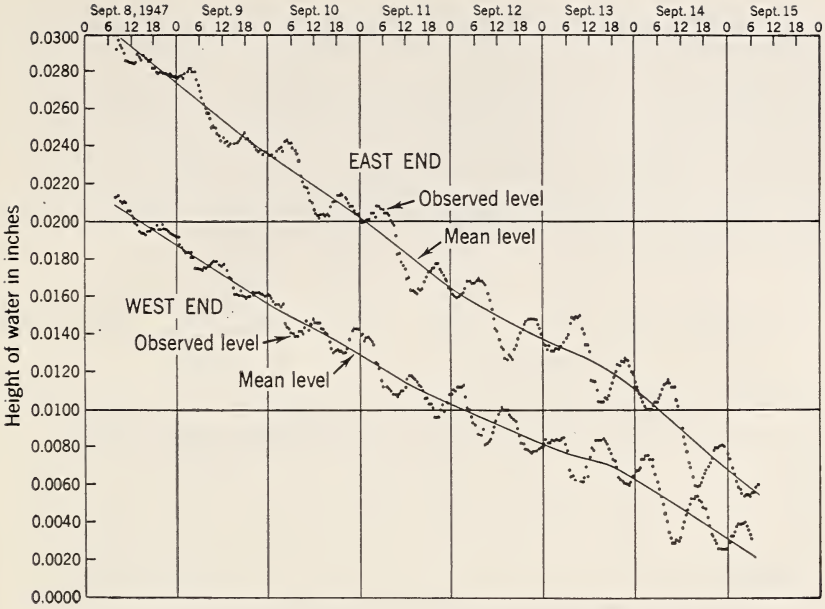

FIGURE 3. *Half-hourly observations of water levels in the east and west ends of the Taylor Basin.*

While computations by formulas 26 or 27 give the tangent of the angle of tilt rather than the height of the water, it is evident that the height of the oscillation at the gage equals tan θ multiplied by the distance of the gage from the center of the basin or, in this case, by half the distance between the gages.

Means of 14 highs and 13 lows for the 7 days give ranges of 0.00181 inch and 0.00241 inch for the observed and computed tides, respectively. Corresponding values for angle θ (semirange) are 0.024″ and 0.031″.

The computed curve shows the tide in the basin relative to a rigid Earth. The observed curve shows the tidal motion relative to the actual Earth. The difference between the two, as shown in figure 5, suggests that the Earth's surface also moves with a tidal period.

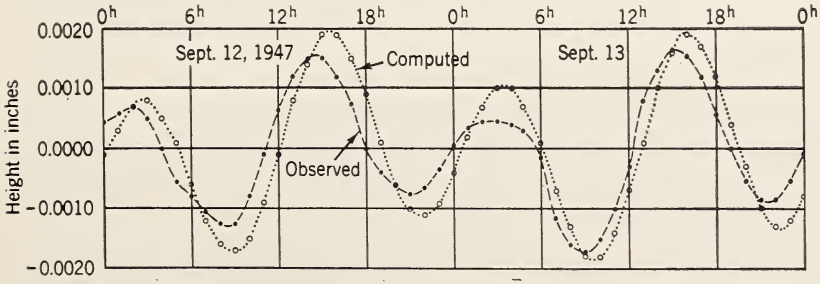

FIGURE 4. *The tide in the west end of the Taylor Basin.*

It has been established by many observers that there is a tidal motion in the Earth's crust. It is due to several causes. There is the direct response to the tide-producing forces, which is considered to be nearly instantaneous, as well as local deformations due to the variations in the load of tidal water on the nearby coast. The latter variation will vary with the locality, and both will be affected by the geology of the area. Moreover, the tidal motion of the water in the basin will be affected by the change in attraction brought about by this periodic shifting of part of the Earth's mass.

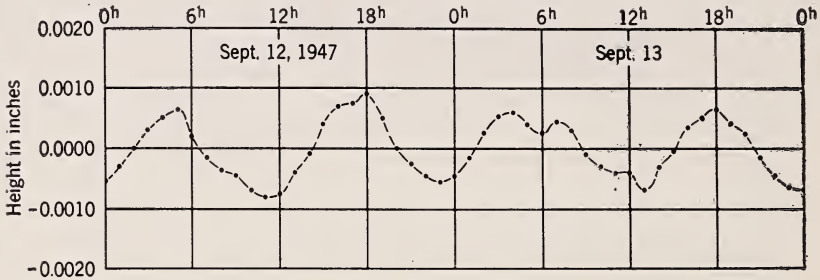

FIGURE 5. *Earth movement determined from Taylor Basin observations.*

It is interesting to know that from these observations it was computed that the yielding of the Earth to the tidal forces has a range about half that of the equilibrium surface and averages about 6 inches in the latitude of Washington. But for purposes of this discussion it is more important to know how much the actual or computed tide in the basin will appear to be reduced when measured relative to the Earth, which itself yields to the tide-producing forces.

One of the most satisfactory methods of determining such a relationship is through the harmonic constants. The 7-day series was analyzed for the harmonic constants of the eight most important tidal constituents. The amplitudes and epochs of the same eight constituents were computed by means of formula 27. The results are shown in table 1. The difference in phase was found to be due largely to the loading effect of the ocean tide. The ratio of the observed to computed amplitude was determined for each constituent, and a mean was obtained by weighting these ratios according to the size of the theoretical or computed amplitude. The ratio so obtained is 0.75.

A mean factor based upon many observations would be desirable. Upon investigation, we find that factors based upon long periods of observations made by various methods vary from 0.69 obtained by Michelson and Gale, and also by Nishimura, to 0.84 by Schweydar. It appears that the factor obtained from the Taylor Basin observations will serve as a satisfactory mean.

In order then to compute the size of the tide oscillation that would most likely be observed in a basin, the hourly values from formula 26 or the amplitudes from formula 27 should be multiplied by the ratio 0.75.

TABLE 1. *Harmonic Constants*

Constituent	Computed by formula		From observations		Amplitude ratio	Phase difference
	H_c	κ_c	H_0	κ_0	H_0/H_c	$\kappa_0-\kappa_c$
	Inch	*Degrees*	*Inch*	*Degrees*		
M_2	0.000922	100.2	0.000720	73.5	0.781	−26.7
S_2	.000429	100.2	.000300	78.1	.700	−22.1
N_2	.000178	100.2	.000149	73.8	.837	−26.4
K_2	.000117	100.2	.000082	78.1	.701	−22.1
K_1	.000430	84.6	.000318	105.6	.739	21.0
O_1	.000306	84.6	.000228	76.0	.747	−8.6
P_1	.000142	84.6	.000105	105.6	.739	21.0
Q_1	.000059	84.6	.000039	65.1	.654	−19.5
				† Weighted mean —	0.752	.....

† Mean of amplitude ratios weighted according to size of amplitude of equilibrium constituent.

Michelson, A. A., and Gale, H. G., The rigidity of the Earth, Astrophysical J. **L**, No. 5, pp. 330–345, 1919.

Nishimura, Eiichi, On Earth tides, American Geophysical Union, Transactions, **31**, pp. 357–376, 1950.

Schureman, Paul, Manual of harmonic analysis and prediction of tides, U. S. Coast and Geodetic Survey Special Publication No. 98, revised (1940) edition, Washington, 1941.

Schweydar, W., Totschwankung und Deformation der Erde durch Flutkräfte. Zentralbureau der International Erdmessung, No. 30, Berlin, 1921.

Zerbe, W. B., The tide in the David Taylor Model Basin, American Geophysical Union, Transactions, **30**, pp. 357–368, 1949.

32. The Characteristics of Internal Solitary Waves

By Garbis H. Keulegan [1]

Abstract

An application of the method of approximations initiated by Boussinesq, to the disturbances of the interface points to the existence of waves of permanent form; the internal solitary wave. The system considered is a layer of liquid resting on another layer of greater density, the liquids of the layers being initially at rest and of constant total depth.

The analysis is carried out assuming irrotational motions throughout and utilizing the kinematic and dynamic boundary conditions in forms appropriate to the upper free surface, the interface, and the horizontal rigid bottom. The effect of viscosity in the region at the interface is ignored.

Analysis reveals that the forms of permanent waves are symmetrical with indefinite wave lengths. When the depth of the lower layer is smaller than the depth of the upper layer, the wave is one of elevation, that is with a single crest above the level of the undisturbed interface. When the depth of the lower layer is greater than that of upper, the wave is one of depression, that is, the trough is below the level of the undisturbed interface. When the depths of the layers are equal, no solitary wave of the symmetrical form is possible.

Our experimental work has been confined to solitary waves of the positive type. Results of observations appear to verify theoretical deductions as regards the dependence of wave velocity on wave height, on density differences, and on layer thicknesses. Confirmation has been obtained also as regards the form of wave and particle displacements.

The study was undertaken as part of a project relating to model laws of density currents, a project initiated and supported by the Corps of Engineers of the Department of the Army.

---

[1] National Bureau of Standards, Washington, D. C.

33. Growth of Wind-Generated Waves and Energy Transfer

By J. Th. Thijsse [1]

Observations in the wind flume of the hydraulics laboratory at Delft, Holland, and on Dutch lakes have been used to check the graph given by Sverdrup and Munk for the growth of waves by wind. There is some difference, but in general the agreement is fair.

Many observations were made on waves which cannot be considered as "short" ones. An extension of the graph for limited depth of the water was made on the strength of these observations.

Combined observations in the same wind flume and on a water current flowing over a fixed (paraffin) model of a wind-generated wave have lead to a rough evaluation of the terms in the energy equation for growing waves. It appears that by far the greater part of the energy in the waves is transmitted by the work of the normal pressure on the surface. This work is positive because the wave itself and the normal pressure both are asymmetric in respect of the crest. A trochoidal wave would hardly grow under the influence of the wind.

The "sheltering coefficient" introduced by Sverdrup and Munk may be calculated starting from these observations.

Nikuradse's "roughness length" was also determined. It turned out to be about half the height of the wave.

1. Growth of Wind—Generated Waves

In many hydraulic experiments done in our laboratory waves of various kinds have to be considered. Although not much basic research upon waves has been done, a considerable quantity of data has been assembled, belonging to most of the topics mentioned in the program of the symposium on gravity waves, viz., generation of waves; impact of waves on beaches, shores, and structures; application of optical theory; internal waves, and tides.

A few remarks on generation of waves will be made in the following.

2. Generation of Waves

In the wind flume of the laboratory, constructed in 1936 and enlarged in 1941, many observations have been made on the growth of waves by wind. In most cases the depth of the water was about 1 foot. The width of the flume is 4.0 m (13 ft 1½ in.), its effective length about 50 m (165 ft). A wind with a velocity up to 17 m/sec (35 mph) may be applied. The roof of the wind channel is slightly more than 2 feet over the water level. In the lower foot the distribution of the wind velocity follows the logarithmic law. This means that the influence of the roof on the phenomena near the water surface must be small.

---

[1] Waterloopkundig Laboratorium, Delft, Netherlands.

The dimensions of the waves have been compared with the graph given by Sverdrup and Munk [1][2]. A difficulty proved to be the definition on wind velocity. Sverdrup does not mention the level at which his wind velocity has been measured. If we assume an anemometer is generally installed 20 or 25 feet above sea level (z) and the velocity W of the wind is in many cases 35 to 40 miles, then it appears that

$$z = (W^2/g)/5.$$

In our wind flume we calculate by extrapolating on the logarithmic diagram the velocity of the air at a level equal to one-fifth of Sverdrup's "velocity-length" W^2/g. This velocity is used in plotting the points in the diagram.

Waves have been raised with a height, H, of 1 inch to 4 inches, a length λ, of 1 foot to 15 feet. The "dimensionless" fetch is 1 to 15.

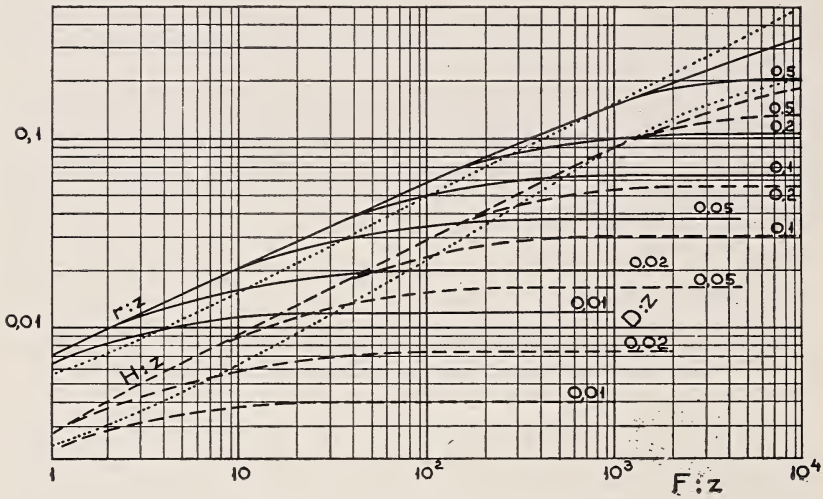

FIGURE 1. *Growth of waves by wind.*

r = radius of generating circle (= wave length/2π); H = height of the significant wave; F = fetch; D = depth below mean level; Z = double velocity head of wind = W^2/g Curves of Sverdrup and Munk shown by dotted lines.

Two lines have been drawn in the diagram (fig. 1): one for the wave height, H, another for $r = \lambda/2\pi$, both made dimensionless by dividing by the "velocity-length."

Both lines are decidedly higher than Sverdrup's, which are shown as dotted lines.

It is not certain that the difference may be attributed to the above-mentioned definition of W.

The steepness of the waves agrees well with the value given by Sverdrup.

Besides the observations in the wind flume, which may be considered as very accurate—as accuracy goes in observation of waves—a number of observations have been collected on lakes in Holland. In these cases the dimensionless fetch is high, and here the same values for height and length of waves have been found as Sverdrup's. At the greatest fetch there is even an indication that the waves are somewhat smaller than Sverdrup's.

[2] Figures in brackets indicate the literature references on p. 287.

This is confirmed by waves raised by the trade wind, measured near Curacao by photographing the broadside of a tanker that is hove to.

The impression is that for a very long fetch waves are not quite as high as Sverdrup's graph would indicate, and that also the length is somewhat less. Here the difference is more than in the case of the height; this means that the steepness of these waves is greater than Sverdrup's.

There are few observations at moderate fetches, so it is not possible to confirm the maximum of steepness that should occur at a relative fetch of about 1,000. There is no reason, however, to contradict the existence of this maximum.

The lines discussed up to now are valid for "short" waves in very deep water, when the wave length is not more than twice the depth. The longest waves generated in the wind flume are longer than this, so the friction along the bottom must have an appreciable influence. It takes energy from the waves and in consequence limits the process of growing. It is important to know the state of equilibrium, in which the work done by the friction along the bottom combined with the internal friction counterbalances the energy transmitted from the air current to the wave system.

A tentative effort has been made to complete Sverdrup's graph for waves other than short ones. The limited length of the wave flume was overcome by reproducing the wave generated at the lower end of the flume by wind at the upper end by a moving blade—a wave generator of the usual type. At the lower end this wave—increased by the wind—was measured. By repeating this process several times, a state of equilibrium was eventually reached. It is evident that this method is not exact, but the inaccuracy cannot be very great.

The result is shown in figure 1. The depth has been made dimensionless by dividing it by the "velocity-length." There is a bundle of lines now, each line starting from the one for unlimited depth and curving until it is horizontal; the wave does not grow any more when the fetch increases.

Figure 1 must be considered as a first tria'. Many observations have still to be collected in order to get an improved set of lines.

Meanwhile the graph is used in the Netherlands, e.g., for predicting the consequences of deepening a shallow lake (this often happens when the bottom consists of sand, as there is a shortage of sand in this country). Many of these lakes have a depth of about 1.5 m (s'). Suppose they will be dredged to a depth of 7.5 m. We want to know what happens when the velocity of the wind, measured at a height of 6 m, is just over 17 m/sec, thus $z=17^2/g=30$ m. The relative depth is $1.5/30=0.05$, which will be increased to $7.5/30=0.25$.

Take a small lake, 150 m long ($=F$), a medium one of 600-m length, and a greater one of 7,500 m. The results are given in Table 1.

TABLE 1. *Results of deepening shallow lakes*

Shallow; $D/z=0.05$				Dredged; $D/z=0.25$		
150	600	7500	F	150	600	7500
5	20	250	F/z	5	20	250
0.0065	0.011	0.016	H/z	0.0065	0.013	0.047
0.20	0.33	0.48	H (m)	0.20	0.39	1.41
0.015	0.025	0.038	r/z	0.015	0.029	0.87
0.45	0.75	1.14	r (m)	0.45	0.87	2.61
2.8	4.7	7.3	(m)	2.8	5.5	16.4
1.3	1.7	2.3	T (sec)	1.3	1.9	3.2

In the small lake the bottom has no influence on the growth of the waves; dredging does not affect them.

Before dredging the waves in the medium-sized lake are influenced by the bottom in the later part of their way. They are still growing, but slowly. After dredging the bottom is not felt any more. At the lee shore the height of the waves has been increased from 0.33 to 0.39 m, the period from 1.7 to 1.9 sec.

After a fetch of 7,500 m the effect of dredging is very great; increase in height from 0.48 to 1.41 m and in period from 2.3 to 3.2 sec. Protecting the lee shore against erosion by waves is quite another problem after dredging than it was before.

Observations of the speed of the waves in the wind flume have shown values equal to or slightly more than the theoretical ones $c=\sqrt{grth(d/r)}$. The excess, ascribed to the direct influence of the wind, is less than 10 percent.

3. Transfer of Energy From Wind to Waves

Recently a study on the transfer of energy from the wind into the wave system has been started.

None of the terms of the equation: energy transmitted from wind by normal pressure + energy transmitted from wind by tangential stress = work done by internal friction + work done by friction along the bottom + increase of energy.

$$R_N+R_T=W_1+W_B+\Delta E$$

is sufficiently well known.

A start was made with R_N. In another paper of Sverdrup and Munk [2] this term has been discussed at length. The trouble is the "sheltering coefficient," which has to be deduced from field data.

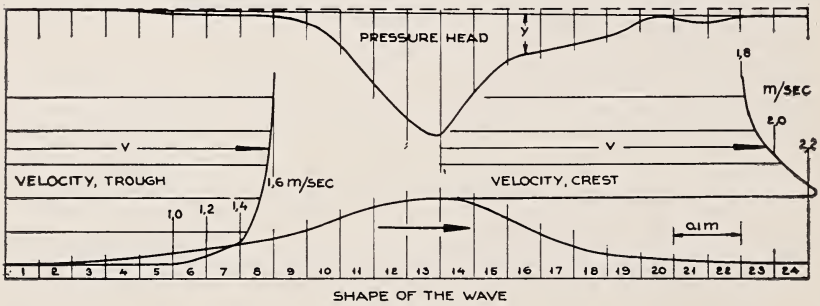

FIGURE 2. *Measurements on paraffin model of wind-generated wave.*

In the Delft laboratory R_N was measured in the following way. A wave was generated by blowing air in the wind flume. Its shape was photographed through the glass wall. The height, H, was 0.10 m, the length 1.2 m ($r=0.19m=\lambda/2\pi$). The crest was slightly asymmetrical, the lee side steeper than the weather slope. On the whole the crest was steeper than the trochoid, the trough flatter (fig. 2). A paraffin model (natural scale) of this wave was placed in one of the flumes of the laboratory, 0.25 m wide. A current of water was made to flow over the wave. The

roof over this current was curved according to the shape of the paraffin wave but much flatter. The mean height of the water current was 0.38 m. The pressure was measured along the surface of the wave. The velocity of the water was observed with a Pitot tube in a vertical over the crest of the wave and in one over the trough.

In the wave flume the velocity of the wind was measured while the waves were passing under the Pitot tube. Pressure drop of the air and slope of the water level were also measured.

The pressure on the surface of the wave is not symmetrical; on the lee side of the crest the graph shows a "shoulder" where the pressure is nearly constant. The current follows the surface; no eddy has been observed. There may be one near the shoulder if the wave is steeper still.

Over the next trough the pressure does not rise again to the original value; the deficit corresponds with the loss of head caused by the presence of the wave and the friction along the walls and the roof of the flume.

The pressure difference between crest and trough agrees perfectly with the difference of velocity head in the current near the surface.

In the wind flume the velocity of propagation of the wave was 1.33 m/sec. This value was subtracted from the observed velocities of the wind in order to find the relative speed.

These data are sufficient for calculating R_N. The wave is divided in 24 short sections Δx. For each the vertical component of the displacement of the surface is multiplied with the pressure head y (corrected for the loss of head).

The result is shown in table 2.

TABLE 2. *Data for calculation of R_N*

Section	Slope, $\Delta z/\Delta x$	y	† $(y\Delta z/\Delta x)10^3$
		m	
1	0.03	0	0
2	.05	−.001	−.05
3	.06	−.001	−.06
4	.08	−.001	−.08
5	.11	−.002	−.22
6	.12	−.004	−.48
7	.17	−.005	−.85
8	.20	−.007	−1.40
9	.24	−.009	−2.16
10	.36	−.025	−9.00
11	.29	−.075	−21.8
12	.21	−.129	−27.1
13	.06	−.170	−10.2
14	−.20	−.152	+30 4
15	−.38	−.087	+33.1
16	−.48	−.062	+29.8
17	−.38	−.054	+20.6
18	−.20	−.050	+10.0
19	−.12	−.029	+3.48
20	−.08	−.005	+0.40
21	−.06	−.009	+.54
22	−.04	−.006	+.24
23	−.03	−.002	+.06
24	−.01	0	0

† The sum of $y\Delta z/\Delta x$ is +0.0552m.

The work done by the current over the wave is positive. This is caused by the fact that on the side of the wave where the surface is rising the mean value of the pressure is smaller than on the other half.

The work is found by multiplying the sum by $c\rho g\Delta x$ (c = velocity, ρ density of the medium passing over the wave, g acceleration of gravity). $R_N = c\rho g\Delta \times \sigma y dz/dx = 1.33 \times 1000 \times 9.8 \times 0.05 \times 0.0552 = 36$ W/m. This must be divided by the proportion of the products ρv^2 of water (over the paraffin wave) and air (relative speed in respect of the wave). This proportion cannot be calculated accurately, but it will not be very far from 25.

Extrapolating the wind velocity in the wind flume, it appears that at a height of 6 m the velocity is 17 m/sec.

So the result is as follows: A wind of 17 m/sec at a level of 6 m over the surface of the sea raises after a fetch of 50 m a wave with a length of 1.2 m and a height of 0.10 m, traveling with 1.33 m/sec. The energy transferred to the water by normal pressure is $36/25 = 1.44$w on a surface with the length of the wave and the width of 1 m, or 1.2w/m^2.

The pressure is the lowest at the crest; the difference from the pressure at the trough is 70 Newton/m^2; this is about two-fifths of the velocity head (measured at a height of 6 m).

It is possible to make an evaluation of the dimension y_0 in the logarithmic formula for the velocity at a distance y from the boundary $v = (v_*/x) \log (y/y_0)$.

Using the velocity of the air measured in the wind flume (ranging from 8.8 m/sec at 0.08 m over mean water level to 10.5 m/sec at 0.20 m over mean water level and subtracting 1.3 m/sec for the speed of the wave) we find $y_0 = 1.6 \times 10^{-3}$m. So Nikuradse's roughness length, about 33 y_0, is 0.05 m, that is, half the height of the wave.

The slope of the water in the wind flume is 0.011 m in a distance of 30 m. Intermediate points have also been measured; the water level is slightly hollow. This means that the mean tangential stress $\bar{\tau}$ increases with the size of the waves, which are only ripples at the upper end of the flume.

There must be some stress along the bottom too, caused by the return flow of water in the lower layers. We know (by other observations) that this stress is between 5 and 10 percent of that along the surface. Taking this stress and the horizontal component of the normal pressure into account, we find for $\bar{\tau}$ about 0.8 N/m^2. It is concentrated near the crests of the waves.

We may assume that the stress is proportional to the local velocity of the wind, which may be calculated from our pressure observations by means of Bernoulli's law. The orbital movement is known at each point of the wave, and so the work done by the tangential stress may be calculated. We shall not give the whole calculation but mention that the work R_T is about 0.1 w per wave length and per meter in width.

So $$R_N + R_T = 1.4 + 0.1 = 1.5 \text{ w}.$$

What happens with this energy? The part that is stored in the wave, causing it to grow, is readily deduced from Sverdrup's diagram. In unit time

$$\Delta E = \Delta\left(\frac{1}{8}\rho g \lambda H^2\right) = \frac{1}{8}\rho g H (H\Delta\lambda + 2\lambda\Delta H).$$

$\Delta\lambda$ and ΔH are found by reading the increase of λ and H per unit length and multiplying by the velocity of propagation c. The result is 0.4 w.

$$W_I + W_B = 1.5 - 0.4 = 1.1 \text{ w}.$$

By means of Sverdrup's diagram a rough evaluation of W_B may also be arrived at. We may read from it the growth of our wave in deep water. This gives $\Delta E = 0.7$w. In this case there is no friction along the bottom, and if we assume that W_I, as well as R_N and R_T, are the same in both cases, $W_B = 0.3$ w. The balance, 0.8 w, must be equal to W_I. So the result is (per wave length and per meter in width) $R_N = 1.4$ w; $R_T = 0.1$ w; $W_I = 0.8$ w; $W_B = 0.3$ w; $\Delta E = 0.4$ w.

The result cannot be more than a very rough approximation.

Observations of the normal pressure have been made with several speeds of the water flowing over the paraffin wave. The pressure line is always the same in respect to the velocity head. The "shoulder" is always present and always at the same place. So is the little bump in the line in section 20; here the pressure is always slightly higher than just upstream and downstream of this spot.

Observations on a trochoid showed pressures that are nearly symmetrical in respect to the crest. So R_N is very small in this case, and this leads to the conclusion that the growth of the wave is mostly caused by its asymmetric shape.

We intend to go on with this investigation. In the first place, better observations have still to be made. The frictional force exerted on the wind blowing over the waves and by the water flowing over the paraffin has been measured. By means of observations in the empty wave flume effort was made to calculate the stress along the fixed walls and roofs. The balance should agree with the shear measured on the waves, but the result is not satisfactory.

Other shapes of waves should be measured, especially steeper ones.

Direct observations of tangential stress at the bottom should be made. Prior work of Bagnold [3], of Putnam and Johnson [4], and others should be taken into consideration.

On the other hand, theoretical studies must complete the work.

The observations have been made by various engineers of the hydraulic laboratory at Delft. Mr. J. G. Faber has taken great pains in measuring with comparatively primitive means the data described in the second part of this paper.

4. References

[1] Sverdrup, H. U., and Munk, W. H., Empirical and theoretical relations between wind, sea, and swell. Trans. Am. Geophys. Union **27**, pp. 823–827, 1946.

[2] Sverdrup, H. U., and Munk, W. H., Wind, sea, and swell: theory of relations for forecasting. Hydrographic Office, U. S. Navy, H. O. Pub. No. 601, 1947.

[3] Bagnold, R. A., Sand movement by waves; some small-scale experiments with sand of very low density. J. Inst. Civ. Eng. **27**, pp. 447–469, 1947.

[4] Putnam, J. A., and Johnson, J. W., The dissipation of wave energy by bottom friction. Trans. Am. Geophys. Union **30**, pp. 67–74, 1949.

☆ U. S. GOVERNMENT PRINTING OFFICE: 1952 — 209574